Investment Costs Reduction of Marine Energy Storage using Smart Power Generation Control

P. Spruijt

Delft University of Technology

Allseas

TU Delft

Investment Costs Reduction of Marine Energy Storage using Smart Power Generation Control

by

P. Spruijt

to obtain the degree of Master of Science in Marine Technology, specialisation *Marine Engineering*
at the Delft University of Technology,
to be defended publicly on Tuesday August 21, 2018 at 2.00 PM.

SDPO.18.026.m

Student number:	4144376	
Project duration:	November, 2017 – August, 2018	
Thesis committee:	Ir. K. Visser,	TU Delft, Chairman
	Dr. Ir. M. Godjevac,	TU Delft, Supervisor
	Ir. M. Dijk,	Allseas, Supervisor
	Prof. dr. R.R. Negenborn,	TU Delft, 3^{th} committee member

This thesis is confidential and cannot be made public until August 21, 2023.

An electronic version of this thesis is available at `http://repository.tudelft.nl/`.

TU Delft

Abstract

To reduce global warming and air pollution, the maritime industry is searching for solutions to reduce fuel consumption. This thesis focuses on the reduction of generator running hours and fuel consumption of Dynamically Positioned (DP) vessels. In this ship type, redundancy of the power generation system is regularly achieved by running on one generator more than strictly necessary in every engine room. Thereby, these vessels make superfluous running hours and unnecessary fuel consumption. Previous research in this field focused on installing a hybrid system in every separate engine room to replace this redundant running generator and achieve the power generation redundancy by a battery which is temporarily used in case of a generator failure. Since DP vessels normally operate on two separate engine rooms for safety, this results in two separate hybrid systems, i.e. a double-battery hybrid system. To reduce investment costs of a hybrid DP vessel, this thesis concentrates on finding a power management strategy that allows a single hybrid system to be installed on board, which is only connected to one of the engine room grids in case of a generator failure. A single-battery hybrid system cannot be connected to both engine room grids continuously -in contrary to the double-battery hybrid system- because this would cancel the independence of the separate engine rooms. Therefore, in the single-battery hybrid system, no back up power is present in case of an increase in power demand in one of the engine rooms. In present DP vessels, this back up power is supplied by the redundant generator. When using a double-battery hybrid system, this back up power is supplied by the continuously connected hybrid system. Therefore, for a single-battery hybrid system, the starting control decision algorithm of the power management system (PMS) should decide on starting an additional generator prior to a rise of the power demand.

Two methods for this starting decision algorithm were tested. Firstly, a mathematical-statistical method using a mathematical model for DP load forecasting and a statistical model for pipe laying load forecasting was tested. This model was found not to work properly. Secondly, a multiple linear regression model that predicts the height of power peaks based on environmental parameters like wind and waves was tested which was found to work appropriately. To assess the feasibility of using either a double-battery hybrid system in combination with a simple starting decision algorithm, or a single-battery hybrid system in combination with a smart starting decision algorithm, these two hybrid system options were compared to the current situation that uses a redundant generator in every engine room. These three system options were compared in terms of investment costs, fuel consumption, generator running hours, planned maintenance costs, and reliability. For this comparison, the DP pipelaying vessel *Pioneering Spirit* was used as a case vessel. To find the investment costs, a hybrid system was designed for this purpose. To find the fuel consumption, generator running hours, and planned maintenance costs, full year time domain simulations of the hybrid systems in operation were performed using measured power demand data from the case vessel during pipelaying. For this analysis, a mathematical model of the power generation system was used. The reliability assessment of the different systems was performed using fault tree analysis.

The single- and double-battery hybrid systems both show a significant fuel consumption reduction of 8.4 and 9.0% respectively. When also taking into account the investment costs, generator maintenance cost reduction, and battery depreciation, the payback time of these hybrid systems is 0.9 and 1.7 years respectively. The difference in payback time is mainly caused by the difference in investment costs between the single- and the double-battery hybrid system.

For a single-battery hybrid system for DP vessels, a multiple linear regression model based starting decision algorithm works appropriately. However, although the multiple linear regression model based starting decision algorithm was tested positively in simulations using the available power data, in case of an unforeseen power peak that was not related to one of the input parameters of the regression model, the power generation system lacks back up power. Therefore, the reliability of the single-battery hybrid system is insufficient when using it for DP applications. Especially when taking into account the minor absolute difference in payback time, for the replacement of the redundant generators in DP vessels, the robust and simple double-battery hybrid system is preferred over the small and smart single-battery hybrid system.

Preface

Before you lies the master thesis '*Investment Costs Reduction of Marine Energy Storage using Smart Power Generation Control*', written to obtain the degree of Master of Science in Marine Technology at Delft University of Technology. As a Marine Technology student focused on Marine Engineering, I was engaged in this project from November 2017 to August 2018. The target audience for this thesis are both academics in Marine Technology as members of industry interested in hybrid solutions for Dynamically Positioned vessels.

As current developments in society and industry are directing towards greener shipping, it has been my goal to contribute to this transition by this research topic. As engineers, I think it is our responsibility and our duty to develop solutions to limit global warming. Therefore, I hope my research is helping Allseas in particular and the maritime industry in general to reach the goals of reducing fuel consumption and therefore reducing the emission of greenhouse gasses. The research topic and the process to a suitable answer was difficult from time to time, but fortunately, a clear answer was found in the end and a contribution was made to the current scientific state of the art.

This thesis was made possible by Allseas Engineering in terms of supervision and in terms of available data and all information that was required to support my findings. Therefore I would like to thanks all people at Allseas that contributed to this thesis by answering my questions and supporting me by providing all material that was needed. Special thanks go out to dr. ir. N. Chasiotis and ir. M. Dijk for the company's supervision and feedback during the process. From university, I would like to thank dr. ir. M. Godjevac for the academical supervision that kept me on the right track and helped me to stay focused on the academical principles of this research.

Last but not least, I would like to thank my friends, family, and girlfriend for supporting me throughout the process.

P. Spruijt
Delft, August 2018

Contents

Nomenclature

Energy and Power symbols

$\dot{m}_{fuel}$	Mass flow of fuel	kg/s
E_{FW}	Stored energy in flywheel	J
J	Polar moment of inertia (flywheel)	kg· m^2
ω	Rotational speed (flywheel)	rad/s
η_{dis}	Discharge efficiency	-
C_{EOL}	Capacity at end of life compared to initial capacity	-
E_{min}	Minimum required amount of stored energy	kWh
E_{EES}	Required energy capacity of specific type of EES	kWh
R_{SOC}	Range of state of charge limits	-
fc_i	Fuel consumption in engine room i	kg
$P_{t,i}$	Total power demand in engine room i at time step t	kW
sfc	specific fuel consumption	g/kWh
$pf_{t,i}$	Power factor of total engine room i at time step t	-
$N_{t,i}^{gens}$	Number of online generators in engine room i at time step t	gens
SOC	State of Charge	-
SOC_t	State of Charge at time step t	-
SOC_{LL}	State of Charge Lower Level	-
SOC_{UL}	State of Charge Upper Level	-
$t_{start,gen}$	Starting time generator	s
EoL	End of Life	cycles
C_{left}	Left battery capacity after aging	%
P_{gen}	Power delivered by generator	kW
$E_{sp,res}$	Required energy capacity spinning reserve replacement	kWh
P_{nom}	Nominal Generator power	kW
$t_{bridging}$	Briding time	s
C	C-rate	0
C	Capacitance (supercapacitor)	F
V	Voltage	V

PMS symbols

x_t	Observation of process x at timestep t	-
ϕ_p	Weight of contribution to model of lagged observation at t-p	-
ϵ_t	Random error at time step t	-
θ_q	Weight of contribution to model of lagged error at t-q	-
$\gamma(s,t)$	Covariance between parameter s and t	-
$\rho(s,t)$	Correlation between parameter s and t	-
$\alpha(h)$	Partial autocorrelation at lag h	-
P_{n+1}^n	One step ahead variance	-
T	Period of repetitive process (time series forecasting general)	-
$T_{period,i}$	Length of pipe laying period i	-
$T_{avg,obs}$	The average pipe laying period during the observation time	-
N	Total number of observations	-
F_t	Forecast value at time step t	-
O_t	Observed value at time step t	-
$F_{env,x}$	Environmental force in x direction	N
$F_{env,y}$	Environmental force in y direction	N
$M_{env,z}$	Environmental moment around z-axis	Nm
v_{wind}	Wind speed	m/s
$c_{x,wind}$	Wind force component in x direction (dependent on direction)	-
$c_{y,wind}$	Wind force component in y direction (dependent on direction)	-
$c_{z,wind}$	Wind moment component (dependend on direction)	-
n	Propeller rotational speed	rpm
n_{nom}	Nominal propeller rotational speed	rpm
T	Thrust	N
β_x	Regression coefficient x	-
p	Peak height	kW
m	Moving mean of total power at peak p	kW
H_s	Significant wave height	m
$P_{DP,wind}$	Estimated DP load based on wind speed and direction	kW

Reliability assessment symbols

λ_t	Failure rate	failures/time
P_{fail}	Failure chance	-
IF_k	Importance factor of basic event k	-

Abbreviations

ACF	Autocorrelation Function
AR	Autoregressive
ARMA	Autoregressive Moving Average
BLP	Best Linear Predictor
CAES	Compressed Air Energy Storage
DOD	Depth of Discharge
DP	Dynamic Positioning
EDLC	Electric Double-Layer Capacitor
ER	Engine Room
FES	Flywheel Energy Storage
FT	Fault Tree
FTA	Fault Tree Analysis
LA	Lead-Acid
LCO	Lithium Cobalt Oxide
LHV	Lower Heating Value
Li-ion	Lithium-Ion
MA	Moving Average
MGO	Marine Gas Oil
MLR(A)	Multiple Linear Regression (Analysis)
NiCD	Nickel-Cadmium
NiMH	Nickel Metal-Hydride
NMC	Nickel Manganese Cobalt
PACF	Partial Autocorrelation Function
PMS	Power Management System
sfc	specific fuel consumption
SOC	State of Charge
UPS	Uninterruptible Power Supply

List of Figures

List of Tables

Main Part Use Arabic numerals for the page numbers of the chapters.

1 Introduction

In this chapter, the thesis and research is introduced. First, the background of the research is given, after which the relevant literature is shown. Thereafter, the problem statement is explained, followed by the research question and the scope of this research. The last section describes the outline of the rest of the thesis.

1.1. Background

Dynamic Positioning (DP) vessels operate in many different areas of offshore operations. In these vessels, the goal of the propulsion system is to stay at an earth fixed position or follow a preset heading and speed regardless of environmental forces like wind, waves, and currents. Examples are found in offshore supply vessels, heavy lift vessels, drilling vessels, and pipe laying vessels. In these vessels, the DP control system controls the speed and azimuth angle of all thrusters and responds to deviations from the required setpoint or to feedforward parameters like wind and wave measurements. In many offshore operations, large deviations from the setpoint are dangerous, e.g. when operating close to an offshore production platform. Therefore, for safety reasons, the systems in DP vessels are required to have a sufficient level of redundancy when used in hazardous situations. This means that in case of a failure of an active system component, no loss in position shall occur. DP vessels often use diesel-electric propulsion systems, where power is generated centrally and distributed to the different thrusters by the DP control system. For the power generation system, the redundancy requirement means that in case of a generator failure, no loss of position shall occur. Therefore, redundant DP vessels normally operate on one generator more than strictly required for the power demand. This method of fulfilling the redundancy requirement is called spinning reserve. Since a single fault in an active component shall never result in a loss of position, the power generation configuration of DP vessels is often split into two engine rooms operating as independent power islands. This results in a redundant generator in both engine rooms, meaning that for the entire vessel, two generators are running redundantly in total.

In the last decades the mindset in the maritime and offshore sector is changing towards cleaner operations. These sectors are traditionally notorious for their contribution in the global emission of greenhouse- and other polluting gasses. In the last decades, the focus in many sectors, including maritime and offshore, has become to reduce the emission of these gasses and operate in a more environmental friendly manner. Therefore, the question from industry arises if a solution to this problem of redundant generators exists by installing electrical energy storage on board that could function as uninterruptible power supply and replace this spinning reserve, which would avoid running on more generators than strictly necessary. This energy storage device would than supply power during the bridging time between a generator failure and the moment where the next generator is started and fully online. In this thesis, the focus is on the power management system that controls the hybrid power generation system.

This research project is performed in collaboration with Allseas Engineering, part of the Allseas Group S.A., a Swiss-based pipe laying and heavy lifting company. This company operates a variety of DP vessels including four pipe laying vessels, two multipurpose offshore construction vessels, and a heavy lift vessel. On these DP vessels, Allseas would like to study the possibilities of replacing spinning reserve by electrical energy storage in terms of technical and economical feasibility. For this research, Allseas offered to test the concept by using the Pioneering Spirit as case vessel.

1.2. Literature

Concerning previous research about the application of energy storage in the maritime sector, two thesis reports stand out. In 2016, Gerritsen investigated the possibilities of applying a hybrid system consisting of a battery pack together with diesel engines on board of a suction cutter dredger [27]. When dredging, a suction cutter dredger operates with a fluctuating power demand due to the inconsistencies of the soil it is dredging. This results in a very irregular time-power pattern with a lot of transient loads having a bandwidth of around 1 MW between the power peaks. To be able to run on these high powers during a power peak, the vessel is always running a big surplus of power capacity, resulting in higher fuel consumption and running hours than would be necessary when the engines could run on a more constant power.

First, Gerritsen investigated the effect of the transient loads on the efficiency of the generators. He found that the efficiency of a large medium speed diesel engine with a sufficiently large air excess ratio is not significantly influenced by transient loads. Thereafter, he modelled a hybrid system -including energy storage- that was focusing on peak shaving, attempting to reduce the running hours and optimising the system to run the engines on higher partial loads (having a lower specific fuel consumption). In this model, a lithium-ion battery was implemented as electrical energy storage. In these simulations, Gerritsen calculated the optimum battery capacity and calculated the economic feasibility of this system. It turned out that using a battery for peak shaving of a suction cutter dredger's operational profile reduces running hours but is economically not feasible. This is caused by the founding that the influence of transient loads on fuel consumption is minimal and that the battery lifetime is significantly reduced when used for peak shaving due to the high amount of charge and discharge cycles.

Also in 2016, Z. Luy did a feasibility study on applying energy storage on board of a DP crane vessel [40]. Lyu proposed to use the modelled energy storage both to replace a running generator for spinning reserve and to use for peak shaving. He modelled one hybrid system per engine room for redundancy reasons. The vessel showed an operating profile which is typical for DP operations, where the required power from the generators fluctuates very irregular with a bandwidth of around 1 MW most of the time. These fluctuations were mainly caused by the fluctuating environmental forces.

For peak shaving, Lyu focused on filtering the transient loads of the generators, but based on his models, he could not find any significant reduction in fuel consumption due to the filtering of the transient loads. The fuel savings by peak shaving the demanding loads was found to be negligible. However, replacing the spinning reserve by a battery pack resulted in significant fuel savings of 15% and a reduction in running hours of 14,000 hours per year.

In 2017, M. Godjevac described three cases for which energy storage can be used in DP operations [28]. One of them is the DP crane vessel case from Lyu [40] mentioned above. The two others are a platform supply vessel and a hypothetical vessel with 8 dual-fuel engines having a total installed power of 24 MW. The platform supply vessel was tested using two separate hybrid systems for both switchboards and the PMS used a rule based control system. By PMS, the system that controls the number of running generators is meant here. In case of the platform supply vessel, it was again shown that the reduction in running hours due to the replacement of spinning reserve gives promising results in terms of fuel consumption. It was found that on this vessel, a fuel consumption reduction of 20% could be achieved. Again, peak shaving did not show any reduction in fuel consumption. In case of the hypothetical dual-fuel engine, the vessel was again installed with two separate hybrid systems each connected to a separate switch board. In terms of peak shaving and spinning reserve benefits, the same effects occurred. A reduction in fuel consumption due to the reduction in the number of running generators, but no fuel consumption reduction due to peak shaving.

According to Godjevac, the founding that implementing energy storage for peak shaving does not have a significant influence on the fuel consumption, is caused by the introduction of losses in the charging/discharging cycle, consisting of inverting, charging, discharging and rectifying. When an efficiency of 97% is assumed for each of these components, a loss of 11.5% occurs. The aim of peak shaving is to let the engines run on higher partial loads (prefarably between 80/90% of MCR) where the engines have a lower specific fuel consumption. However, the efficiency increase that can be won by running on higher partial loads is mostly counterbalanced by the introduced losses during the charge/discharge cycle. Probably the most favourable way of using energy storage is by creating the possibility to shut down one of the engines resulting in a reduction of fuel consumption and running hours.

In [68], T.L. Vu et al used hybrid tug boats (no DP vessels) as a test case to test the benefits of using a predictive algorithm for the control of the number of online generators in a hybrid vessel. This control system was designed to minimize fuel consumption. For the load prediction, due to a lack of data, Vu et al used a simple load prediction scheme that predicts the required power based on the type of operation the vessel

is performing. In this paper it was assumed that the load profile was dominated by the operational profile rather than the environmental conditions.

1.2.1. Literature Gap

Previous research that was found on this topic focused on the economical feasibility of using energy storage in DP vessels. The economical benefits in terms of fuel consumption savings by replacing spinning reserve by a hybrid system in DP vessels was shown. No proof of reduced fuel consumption was found by using the hybrid system for peak shaving. In the previously tested cases of hybrid DP vessels, a hybrid system was continuously connected to each switchboard, so it could be used both for spinning reserve replacement as for peak shaving. However, to the author's best knowledge, no research has been performed on the power generation control systems of hybrid DP vessels that use a hybrid system only to replace spinning reserve.

Because previous research has shown that peak shaving does not significantly reduce fuel consumption, there is no necessity of installing a hybrid system for each engine room (a double-battery hybrid system). This raises the question if it is possible to install one hybrid system in total on board (a single-battery hybrid system) which is only connected to the power grid in case of a generator failure. The main difference between these two configurations is the connection of the hybrid system to the grid in standby-mode of the battery. In the previously studied double-battery system, the batteries can be connected to the grid continuously, so the battery can be used as spare capacity in case of a power demand peak. In the single-battery system, the battery can only be connected to one of the engine rooms at a time, as the engine rooms would loose their independence if the hybrid system is connected to both engine rooms simultaneously. This independence is a DP requirement to make sure the vessel does not loose position after a single failure of an active component in one of the engine rooms. Because the single-battery hybrid system is not connected continuously, no spare capacity is present in the power generation system in case of power demand peak.

For a single-battery hybrid system to be suitable in DP vessels, the PMS should be able to increase the online generator capacity prior to power demand peaks, as the power generation system cannot rely on spare capacity from a connected battery. The current standard in power management of DP vessels is the load dependent start decision algorithm, which is a conservative a posteriori[1] method that only uses the measured total power demand in the recent past. Although this starting decision algorithm is a practically proven method in DP vessels using spinning reserve, it is not applicable in hybrid vessels using a single battery which is only used in case of a generator failure. That is because only the load of the past does not tell the load in the near future. If a starting decision algorithm method can be found that controls the number of running generators such that it starts an additional generator prior to a power demand peak, a single-battery hybrid system could be feasible on DP vessels. This starting decision algorithm should also limit the amount of online generators, as the main goal of hybrid DP vessels is to reduce the spinning reserve. No research was found covering the topic of this smart starting decision algorithm.

Next to that, in previous research, no comparison between the spinning reserve option and the hybrid option was made in terms of reliability. The main goal of spinning reserve is to guarantee a save operation by running a back up generator continuously. When replacing this spinning reserve by a back up battery, the reliability of these two redundancy options should be compared for the proof-of-concept of hybrid DP vessels. No research has been found on this topic either.

1.3. Problem Statement

So far, it has been proven in previous research that replacing the spinning reserve by a hybrid system is beneficial in terms of fuel consumption and running hours. In previous research, in all engine rooms, a hybrid system was installed as back up power in case of a generator failure or in case of a power demand peak. So the battery was both used as an uninterruptible power supply (UPS) during a generator failure (spinning reserve replacement), as well as for peak shaving. However, it was was found that peak shaving does not significantly reduce operational costs, which imposes the question if it would be possible to install only one hybrid system in total that is only used as UPS during a generator failure.

The problem of this single hybrid system, or single-battery hybrid system, is that the system cannot be connected to both engine rooms simultaneously as the engine rooms would than loose their independence, which is a redundancy requirement. Therefore, in contrary to a double-battery hybrid system (as was proposed in previous research), the single-battery hybrid system cannot be connected continuously to the engine room grid. This means that if a power demand peak crosses the online generator capacity, no back-up

[1] Looking back in time or using information about the past.

power is present. In current DP vessels, this back up power is supplied by the redundant generator. In a double-battery hybrid system, this back up power is supplied by the continuously connected hybrid system. An example of this problem can be seen in Figure 1.1, which is a typical power profile of a DP vessel. In this example, two online generators are connected to the grid, creating a power capacity of 22 MW. When the power demand increases, it can be seen that a power demand peak crosses the online generator capacity between 5 and 6 hours. In a DP vessel that uses spinning reserve for the power generation redundancy, this power peak could be dealt with by an additional running generator that would have been running (as spinning reserve). In a double-battery hybrid system, this power peak can be dealt with by the continuously connected battery. However, in a single-battery hybrid system, a smart starting decison algorithm in the PMS should have started an additional generator (increasing the power capacity to 33 MW) prior to this power peak.

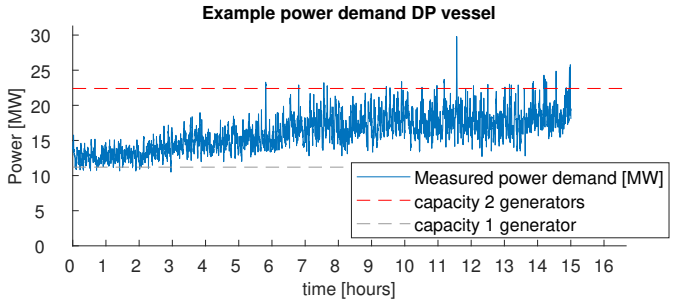

Figure 1.1: Power demand of DP vessel

It should be found what smart starting decision algorithm could be applicable in a single-battery hybrid DP vessel. If an applicable method can be found, hybrid DP vessels could be equipped with a single-battery hybrid system that is only connected to the grid in case of generator failure. This means that the investment costs are halved compared to the double-battery hybrid systems from previous research on hybrid DP vessels.

The difference in configuration between the hybrid systems of previous research and the hybrid system that would be installed on a vessel using a smart starting decision algorithm is shown in Figure 1.2. The hybrid system option that includes a smart starting decision algorithm, and would therefore only need one installed hybrid system in total, is further referred to as hybrid system option 1. The hybrid system option that was used in previous research, where a hybrid system is connected to every engine room and would use a 'backlooking' load dependent starting decision algorithm, is further referred to as hybrid system option 2. The old system which uses spinning reserve is further referred to as the 'no hybrid' system. In hybrid system option 1, the hybrid system is not connected in stand-by mode and will only be connected to an engine room when a generator failure occurs in that engine room. In hybrid system option 2, in each engine room the battery is connected continuously so it can be used as spare capacity in case of a power demand peak or in case of a generator failure.

1.4. Research Question and Objectives

To solve the above mentioned problem, the research question that will be answered in this thesis is:

"What starting decision algorithm is applicable to a single-battery hybrid DP-II vessel to guarantee sufficient power capacity to supply the power demand?"

This research question specifically mentiones DP-II class vessels, because DP vessels can be grouped in DP-I, DP-II or DP-III class vessels. DP-I class vessels do not require any redundancy in position keeping, which means that a single point of failure could result in the loss of position. In DP-II class vessels, a single point of failure of an active component may never result in the loss of position. This means that redundancy is required in this type of vessel, which is commonly achieved by the configuration of two engine rooms, where a redundant generator is online in every engine room. DP-III class vessels are required to keep position even when one engine room is flooded or on fire. When this thesis refers to DP vessels, DP-II vessels are meant.

To answer the question, the research objectives are:

- To calculate the potential benefits of using a hybrid system in the case vessel: to assess the economical and technical feasibility of using electrical energy storage in the case vessel, a preliminary estimation on the benefits of replacing the spinning reserve should be made for the case vessel;

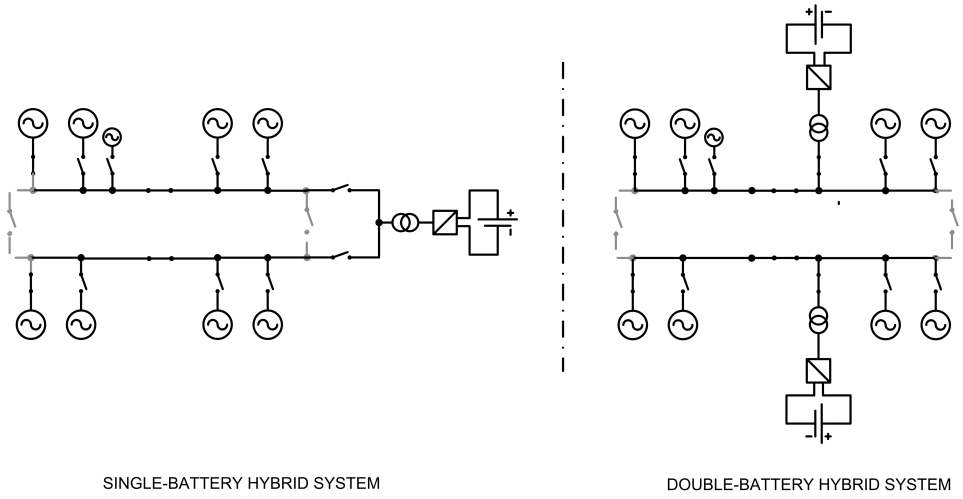

Figure 1.2: Difference configuration hybrid system option 1 (one battery) and hybrid system option 2 (two batteries). Chapter 2 and 3 will elaborate on the vessel's configuration and installation of hybrid systems.

- To select the appropriate type of electrical energy storage and determine the required size of the hybrid system;
- To find different options of the starting decision algorithm for the single-battery hybrid system option;
- To find the optimal starting decision algorithm from these potential options;
- To design an online power management system using this starting decision algorithm and test the found strategy using real measured power data from the case vessel;
- To assess the fuel consumption reduction and maintenance costs reduction of the single-battery hybrid system using a simulation of this online power management strategy, and to compare this reduction to the double-battery hybrid system and the 'no hybrid' system;
- To compare the reliability of the single-battery hybrid system (using the found smart power management strategy) to the reliability of the double-battery hybrid system and the 'no hybrid' system.

1.5. Outline of Thesis

In the next chapter, the background of the problem and the focus on the type of operation will be explained. In the same chapter, the case vessel and corresponding power profile will be explained. Chapter 3 focuses on the selection of the type of electrical energy storage and the sizing of the hybrid system for this purpose. Next to that, a hybrid system for the case vessel is described here to proof the technical feasibility and to estimate the investment costs. In chapter 4, two different methods for the starting decision algorithm are discussed and one of these is selected as the best solution to the problem. The following chapter, chapter 5, explains the reliability assessment of the three different system options (current system of case vessel, single-battery hybrid system, double-battery hybrid system). In chapter 6, the simulation and results of the two different hybrid system options in operation is explained. Next to that, it is briefly described here how the battery degradation and reduction in maintenance costs are estimated. After discussing these results in chapter 7, chapter 8 ends with the conclusion and final recommendations.

2

Background

After introducing this research in the previous chapter, the background of the company, case vessel, and operations are discussed in this chapter. Besides, the scope of the research will further be defined here. Firstly, the company that cooperated in this research is briefly described, followed by a general explanation of pipe laying. In Section 2.3, the case vessel that is used for testing the system is described, after which the next section elaborates on the power distribution on board. The following section briefly discusses the on board measurements that are used for the data in this analysis, where the last section describes the operational profile and the focus on deep water pipe laying.

2.1. Allseas

Allseas is a globally operating pipe laying and offshore heavy lift company. The company is known for their DP pipe laying capabilities and since 2015 for their offshore single lift capabilities. Allseas operates three DP pipe-laying vessels, one pipe-laying barge, two DP support vessel and one heavy lift vessel that also has DP pipe-laying capability. Since the company was founded, their core business has been pipe-laying, but since the Pioneering Spirit (previously Pieter Schelte) has been in operation, the company is also active in offshore heavy lifting. In contrast to crane vessels, the Pioneering Spirit is able to lift a topside in one piece, reducing expensive and dangerous offshore construction work. In the near future, the vessel will also be capable of transporting and launching or removing the jacket. Next to the heavy lift capability of the Pioneering Spirit, pipe laying equipment is installed on board.

2.2. Pipe-laying

Offshore pipe-laying can be performed using two different methods: the J-lay or S-lay method. During the J-lay method, the pipe is released from the vessel vertically or near vertically. In Figure 2.1, the S-lay method is schematically displayed [1]. In this method, the pipe is horizontally released from the vessel. In the overbend region, at the waterline, the pipe is guided by the stinger, making sure the pipe follows a minimum required curvature to prevent buckling. On board, tensioners clamp the pipe to hold it inside. Inside the vessel, pipe joints of 12 or 24 meter are welded onto the already installed pipe line. Before it is released into the water, the weld is checked on quality and the weld is coated. During the release, also called a pipe-pull, the tensioners keep the tension on the pipe while releasing it into the water.

As said, at the overbend region, the pipe is guided by the stinger to prevent buckling. At the sagbend region, the pipe is not supported by any structure, so to prevent buckling, a minimum required tension is kept on the pipe. The required thrust for this tension is equal to the horizontal component of the pipe-load, also called the bottom tension.

The main advantage of the S-lay method is its high production rate due to the long horizontal production facility. This production facility, also called the firing line, runs through the entire length of the vessel creating a long assembly line. This creates the possibility of working in different stations simultaneously. With this high production rate, a daily production of 4 to 5 km can be accomplished. Therefore, in this thesis, only S-lay pipe laying will be considered, but the methodology of this thesis can also be applied to other DP vessels,

[1] obtained from: https://aninditashafira.wordpress.com/2016/02/16/53/ on 04-12-2017

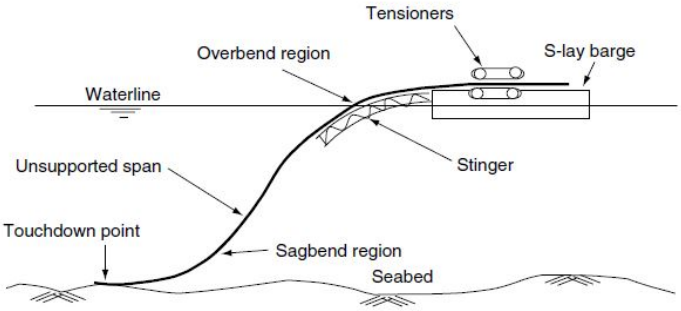

Figure 2.1: S-lay method

including J-lay DP pipe laying vessels.

2.3. Case Vessel

For this thesis, the Pioneering Spirit is selected as a case vessel. This vessel uses eight generators for the power generation and is therefore relatively flexible in the online generator capacity. Therefore, the potential in running hours reduction and fuel savings could be large. Besides, this vessel is equipped with a data logging system, so the required data for this analysis is likely to be available.

In 2016, the Pioneering Spirit started her first offshore operation with the removal of a platform in the Norwegian North Sea. The vessel has a heavy lift capacity of 48,000 ton, creating the possibility to remove or install entire platforms in a single lift. Next to the heavy lift capabilities, the Pioneering Spirit is also equipped with pipe-laying equipment and due to its size and corresponding size of the stinger, the vessel has a maximum pipe-load of 2000 T. This makes pipe-laying possible in water depths of more than 2 km. The vessel is used for pipe-laying and heavy lifting alternately. Table 2.1 shows the specifications of the vessel.

Table 2.1: Specifications Pioneering Spirit

Length overall (incl. tilting lift beams and stinger)	477 m
Length overall (excl. tilting lift beams and stinger)	382 m
Length between perpendiculars	370 m
Breadth	124 m
Depth to main deck	30 m
Topsides lift capacity	48,000 t
Operating draught	10-27 m
Maximum speed	14 knots
Displacement	1,000,000 t (at maximum draught)
Total installed power	95,000 kW
Thrusters	12 x 6050 kW azimuth
Accomodation	571 persons
Installed tension capacity	4 x 500 t
Port of registry	Valletta

2.3.1. DP system

The DP system is a fully redundant, class 3 Kongsberg system. A DP 2 system is redundant until the level where no single fault can lead to a system failure. In DP 3 class, the system should be able to hold position when there is a fire or flood in one watertight compartment. The DP system is operating with eight main diesel generators having a nominal power of 11,200 kW each, divided over four engine rooms. The vessel is propelled by 12 azimuth thrusters with a nominal power of 5000 kW each. The configuration of the thrusters is shown in Figure 2.2.

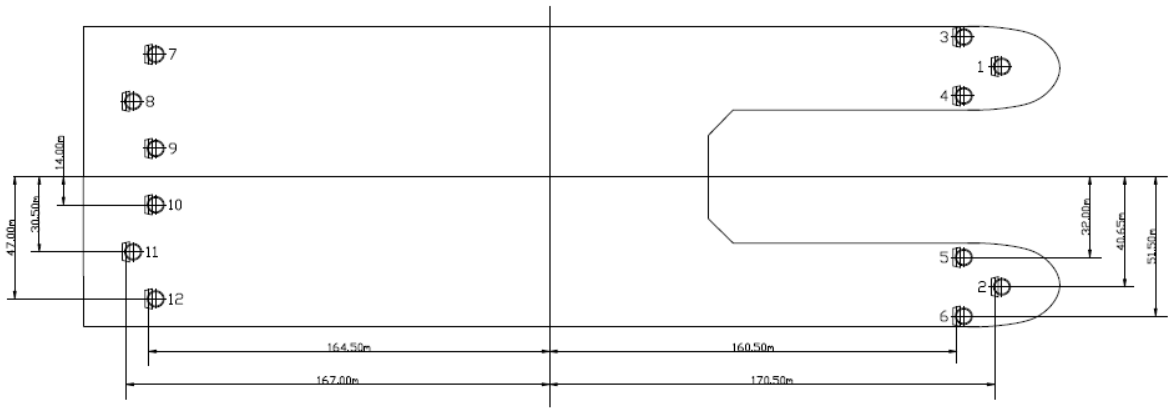

Figure 2.2: Thruster configuration Pioneering Spirit

The generators are divided over four different engine rooms, where all four engine rooms have an independent switchboard. To every switchboard, three thrusters are connected of which at least two are purposely located at opposite side of the vessel, at bow/stern or port side/starboard side. In this configuration, in case of failure of one engine room, not all thrust at one corner of the vessel is lost. Figure 2.3 shows the distribution of the power from the engine rooms. When comparing the configuration in Figure 2.2 to the power distribution lines in Figure 2.3, it can be seen that the the failure of one engine room never results in the power failure of all thrusters at one corner of the vessel.

2.4. Power Distribution

Next to the DP system, other significant consumers are the pipe-laying equipment, the ballast system, the topside lifting system (for heavy lifting operations) and the hotel facilities. However, during pipe-laying operations, the ballast system and topside lifting system are not in operation at all or do not use significant power. The hotel load is assumed to be constant.

Figure 2.4 shows the energy flow diagram of the Pioneering Spirit. The energy flow diagram is used to give insight in the power flow on board [75]. The power generation system consists of eight identical diesel generators divided over four engine rooms housing two generators each. Next to the main generators, one harbour generator of 5000 kW is installed and connected to main switchboard 3. The energy flow diagram displays one of these engine rooms, where energy follows the following paths:

- Energy Source: the energy source can either be MDO or HFO.
- C/M (chemical to mechanical): MAN dual fuel Diesel Engines.
- M/E (mechanical to electrical): Generators: 3-phase synchronous generators powering the 60 Hz grid, at a rated power of 11,200 kW.
- Main Switchboard: every engine room is equipped with a high voltage (11 kV) switchboard. In coupled bus bar configuration, the system can be considered as one system and in split bus bar configuration, the engine rooms can be considered as four independent power systems for redundancy reasons.
- E/E (electrical to electrical): Transformers: between the main switchboard and the frequency drive of the thruster, the high voltage is transformed to lower voltage (11kv/4x1850V). Next to the thruster transformers, the high voltage is transformed to 440V for a lower voltage grid and to 690V for another lower voltage grid. From the secondary switchboards at 440V the voltage is reduced to 230V for a low voltage grid.
- E/E (electrical to electrical): Frequency drives: the frequency drives regulate the rotational speed of the thruster motors by controlling the frequency input of the motors. The drives have a frequency range between 0 and 60Hz.
- E/M (electrical to mechanical): Thruster motor: the thrusters are driven by 3-phase squirrel cage induction motors. The nominal speed of the motor is 765 rpm.

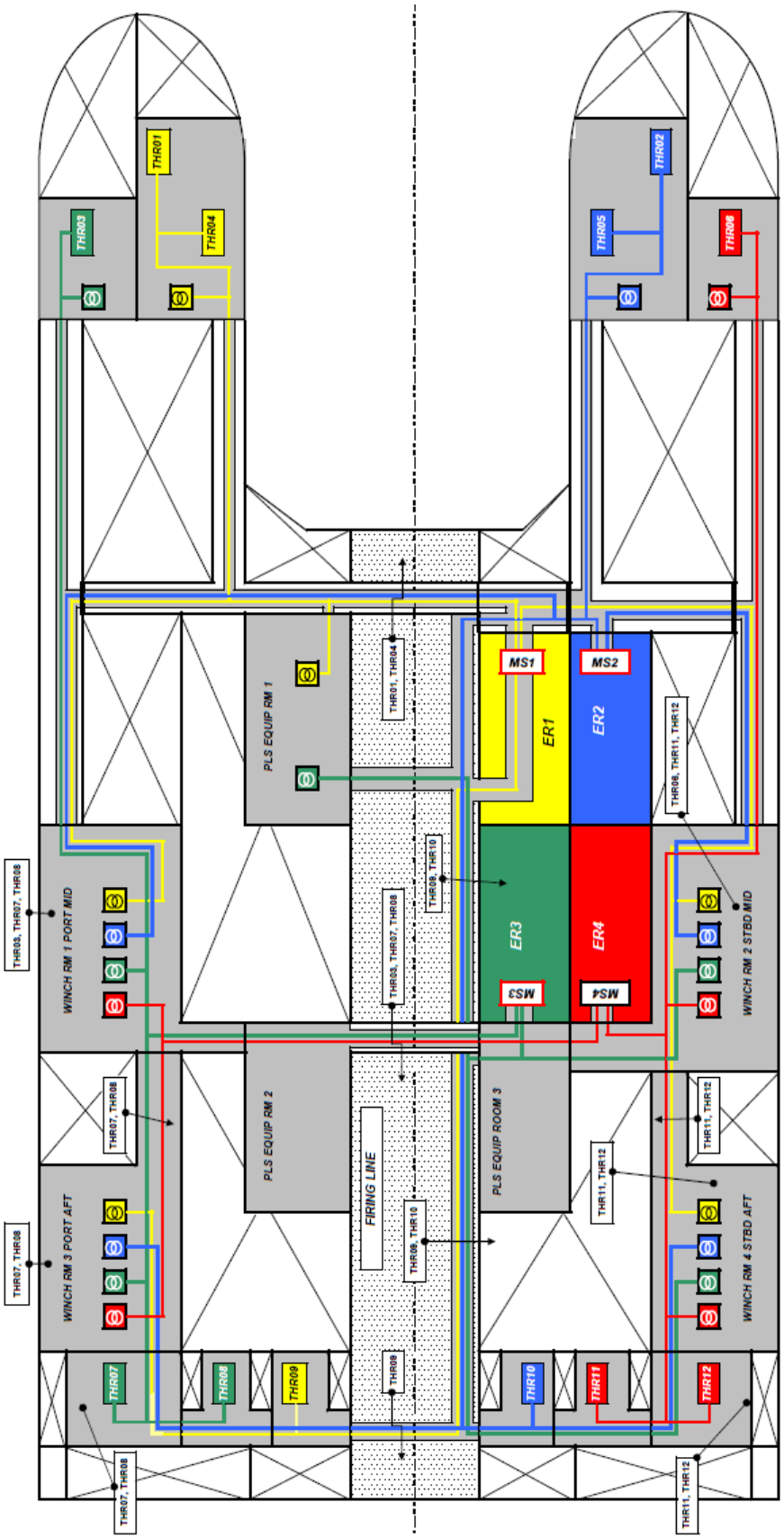

Figure 2.3: Power distribution Pioneering Spirit

- M/M (mechanical/mechanical): Gearbox: between the thruster motor and the propeller, a gearbox is installed to reduce the rotational speed.

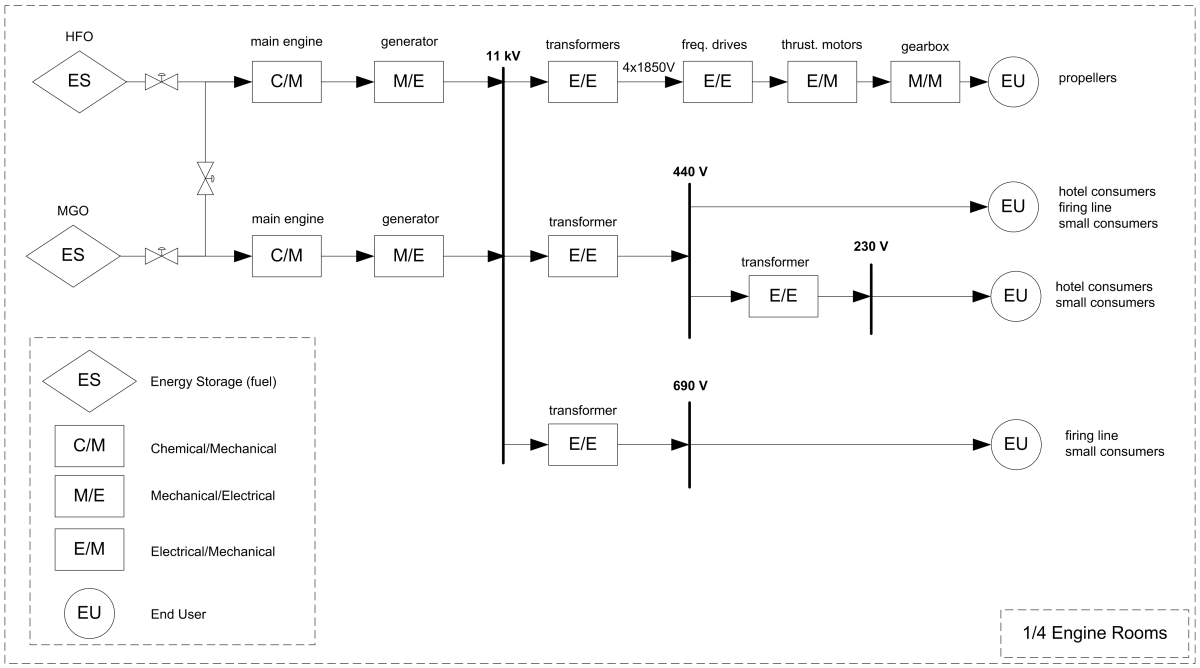

Figure 2.4: Energy Flow Diagram of case vessel

The load of the pipe-laying process is a sum of all the loads in the firingline from the equipment used for the production of the pipe line. Consumers are: the pre-heaters, the double joint factory, the transportation between different stations, the bevelling stations, the welding stations and the tensioners. The Pioneering Spirit has accommodation for 570 people, so the hotel load can be significant during pipe laying operations where a lot of crew members are on board.

2.4.1. Power Management System

The power management system (PMS) controls the power distribution of the vessel by monitoring the load and splitting the load equally over the running generators. This system guarantees that the electrical load is supplied by a sufficient amount of generators and starts an additional generator when necessary.

In the current situation without EES, the PMS guarantees that the actual load is supplied by a sufficient amount of generators and that the load does not exceed the capacity of the online generators, even after the potential failure of one of the generators. In the current situation, a decision algorithm based on the measured load in the past decides when an additional generator is started. This is known as the load-dependent start which is a decision algorithm which is based on knowledge about the load in the last thirty seconds. If the load in the last thirty seconds was above the lower limit (which depends on the number of online generators) constantly, or if the load in the last five seconds was above the higher limit (which depends on the number of online generators) constantly, an additional generator is started by the PMS. An overview of this decision algorithm, based on the 30 seconds rule, is shown in Figure 2.5. The limits for starting a next generator depend on the number of running generators. These limits are based on experience and are shown in Table 2.2. When the vessel is operating in split bus bar mode, the load dependent start of every independent system will operate as if it would be controlled by an independent PMS.

This decision algorithm is best explained by an example, see Figure 2.6. In this example, during the first ten seconds, the total load was above the third limit but below the fourth limit, so four generators were running, resulting in a total online capacity of 44,800 kW. After twelve seconds, the load increased and passed the fourth limit of 32704 kW. After being above the fourth starting limit for more than thirty seconds, the PMS decides to start an additional generator, increasing the online capacity to 56,000 kW (5 generators). If a generator would fail now, the power generation system would still have sufficient capacity to continue the operation. In practice, the capacity has not increased immediately after a starting signal, because starting a

generator takes time, as will be discussed in the next chapter.

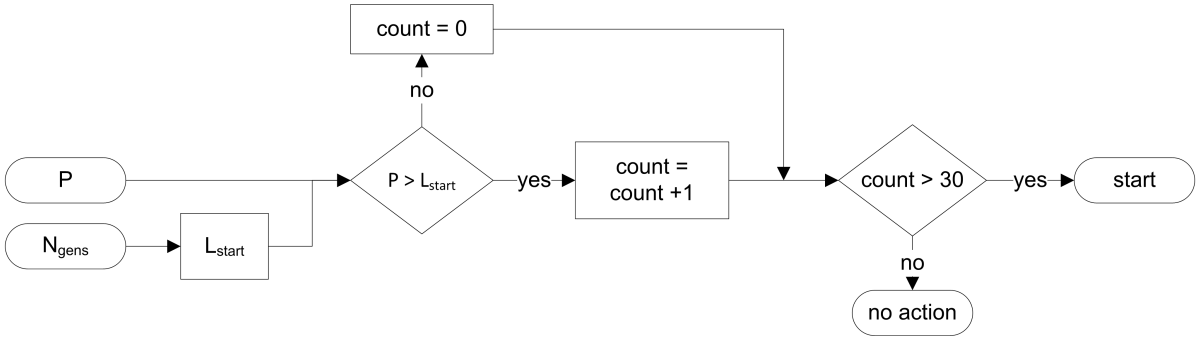

Figure 2.5: Overview load dependent start decision algorithm for lower starting limit (hence the 30 second limit). If the higher limit is exceeded for more than 5 seconds, the PMS also gives a starting signal.

Table 2.2: Load dependent start limits

#online	P_{nom}	Lower start limit	P lower limit [kW]	Delay time	Higher start limit	P higher limit [kW]	Delay time
1	11200	0.5	5600	30s	0.9	10080	5s
2	22400	0.55	12320	30s	0.9	20160	5s
3	33600	0.65	21840	30s	0.9	30240	5s
4	44800	0.73	32704	30s	0.9	40320	5s
5	56000	0.78	43680	30s	0.9	50400	5s
6	67200	0.82	55104	30s	0.9	60480	5s
7	78400	0.85	66640	30s	0.9	70560	5s
8	89600	0.88	78848	30s	0.9	80640	5s

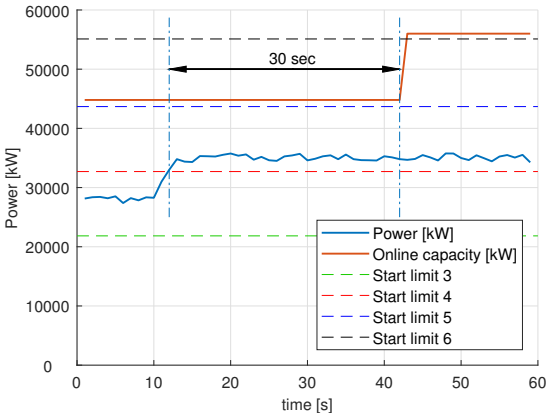

Figure 2.6: Example Load Dependent Start

2.5. On board measurements

For the analysis of the problem and to use as input for the EES system that will be examined, on board measurements were executed on the case vessel. Different time-frames were selected to compare deep and shallow water and to find a pattern in the pipe laying process. During these time-frames, the signals listed in Table 2.3 were measured. All the power signals were measured at the 11kV breakers of the main switchboards within the engine rooms, represented by MS1 to MS4 in Figure 2.3. In total, the real power at 51 breakers was measured to find the generator power, DP power and the power flowing to the other consumers. The vessel's speed was measured by the dGPS system and stored by the DP computer. The pipe speed is the speed measured by the tensioner drives and the pipe load is sum of the tension that is measured by all tensioner

drives. The wind sensors are located at different locations on the vessel, where the most accurate wind sensor is selected depending on the wind direction, because the wind measurements can be influenced by superstructures on board.

Table 2.3: Measured signals of on board measurements

	Signal	**Unit**	**Measurement location**
Generator 1-9	Real power (t)	[kW]	Switch board breakers
Thruster 1-12	Real power (t)	[kW]	Switch board breakers
Vessel's speed	Speed (t)	[m/s]	dGPS input from DP system
Pipe speed	Speed (t)	[m/s]	Tensioner drives
Consumers	Real power(t)	[kW]	Switch board breakers
Wind speed	Speed(t)	[m/s]	Multiple sensors distributed around vessel
Wind direction	Relative direction to vessel(t)	[deg]	Multiple sensors distributed around vessel

2.6. Load Profile

To find benefits the of an energy storage system, first the load profile for the case vessel should be known. A representative load profile for the pipe-laying process should be found to use as an input for the initial EES benefits estimation. The load profile is different for shallow water as it is for deeper water, so a distinction is made between these two cases. To create a representative load profile, on board measurements were executed during shallow water pipe laying and during deep water pipe laying.

2.6.1. Shallow Water

In shallow water, the speed of a pipe-laying vessel using the S-lay method is zero while station-keeping during the welding process and increases and decreases rapidly during a pipe-pull. A pipe-pull is the procedure where the pipe is released from the vessel while the vessel is moving forward. During an optimal pipe-pull, the velocity of the releasing pipe with respect to the vessel is equal to the velocity of the vessel with respect to the earth.

The pipe-pull procedure should be as quick as possible for a high daily pipe-laying rate. This results in the rapid accelerations and decelerations, causing high power peaks for a short amount of time. This profile of distinct power pulls, moving forward a 12 or 24 meter distance, is especially occurring when laying pipe in shallow water. Due to the large length of the pipe compared to its diameter, the pipe can be seen as a long straw. When the water is shallow, the pipe cannot be released into the water without moving the vessel, because it would cause the pipe to buckle at the sagbend. Therefore, during shallow water operations, the position of the vessel is very critical and the relative movement of the pipe with respect to the vessel should match the relative movement of the vessel with respect to the earth.

During a pipe-laying project of the Pioneering Spirit, time-data was gathered of the vessel's speed and the corresponding power asked by different consumers. This data belongs to a water depth of 130m, of which an impression can be seen in Figure 2.7.

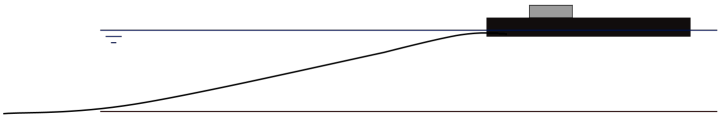

Figure 2.7: Impression of water depth compared to vessel size

In Figure 2.8, the vessel's speed, the total generated power, and the total delivered DP power during a 1-hour time-interval are shown. For the generated power, the real power delivered to the switchboards is shown. For the DP power, the real power delivered to the thrusters is shown, which was also measured at the main switchboard.

In this figure, the pipe pulls (the moments where the pipe is released into the water) are marked by the grey dotted lines. As explained, in shallow water, the vessel moves to her new position while releasing the pipe, which can be seen in the figure. It shows that together with a pipe release moment, the ground speed

of the vessel increases to move forward, after which the speed decreases again to 0 m/s for station keeping. This process repeats itself five times in the recorded hour. In the same figure, the power of the thrusters and the power of the generators is plotted. It is clear that during a pipe-pull, the thrusters require extra power to move the vessel. This results in the power peaks of the total DP power during the ground speed peaks. When decelerating, the DP power shows a small trough, after which the power returns back to the constant load. This constant thruster load is the load required for station keeping, both caused by the required pipe tension and by external forces like waves, wind and current.

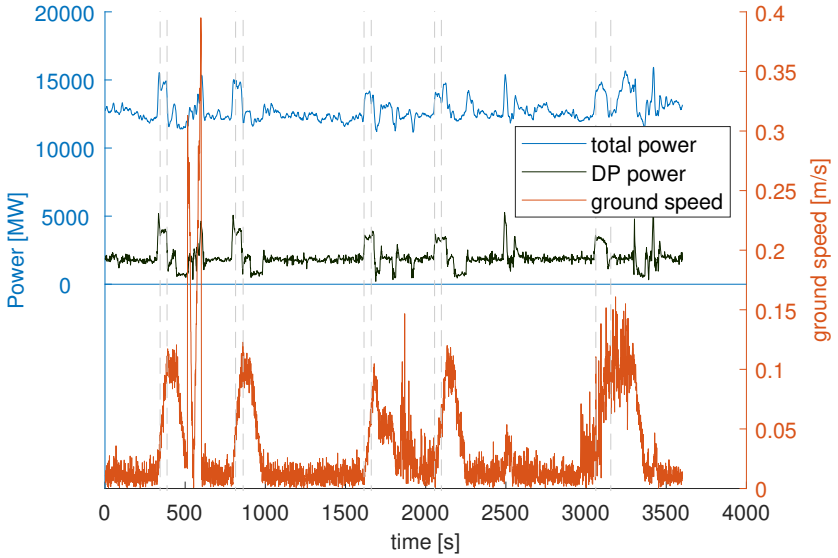

Figure 2.8: Total generator power and DP power compared to ground speed of the vessel in shallow water. Notice here that this time frame is observed during very calm weather conditions, resulting in low and relatively constant DP load. This figure is only to show the difference in power profile between shallow and deep water and should not be seen as a general load profile for shallow water pipelaying.

2.6.2. Deep Water

In deeper water, the system is less stiff and the position of the vessel is less critical. Using the analogy to the big straw again, when the pipe is in deeper water, the curvature of the pipe at the sagbend is easier to maintain and the system is more flexible. In Figure 2.9a, an impression of pipe laying in deep water is shown. The pipe is released between situation I and II without changing the velocity of the vessel. The curvature of the pipe at the sagbend decreases a little due to the pipe release, but is still within the acceptable range.

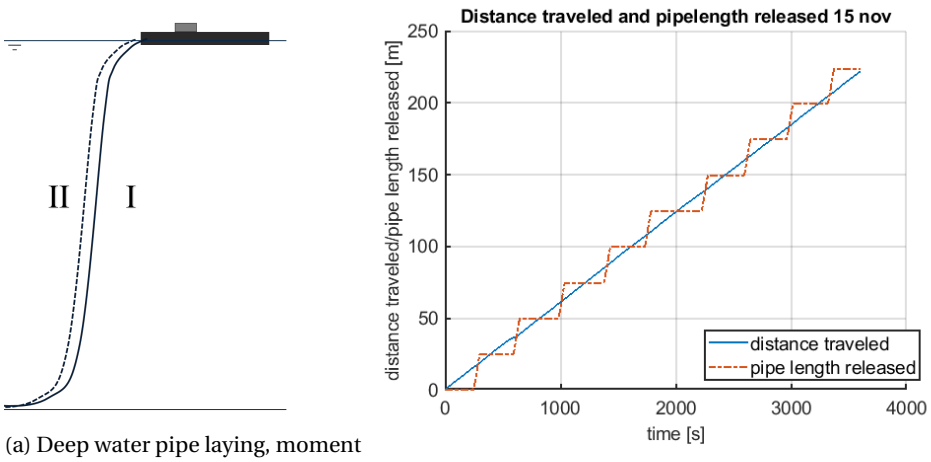

(a) Deep water pipe laying, moment of releasing pipe

(b) Distance traveled by vessel and length of released pipe

Figure 2.9: Impression water depth and consant forward speed during deep water pipe laying

Therefore, during operation in deeper water, the speed profile of the vessel shows less distinct pipe-pulls. The vessel is moving at a more constant pace forward, releasing the pipe every time a new joint of 12 or 24 meter is finished, but is less dependent on the alignment between the pipe's speed w.r.t. the vessel on the one side, and the vessel's speed w.r.t. the earth on the other side. This process can be seen in Figure 2.9b, where the movement of the vessel and the length of the released pipe are plotted. It can be seen that the vessels moves forward at constant speed and the pipe is released every 10 minutes. The total length of released pipe and the total distance travelled by the vessel is equal, but the speed of pipe and vessel are not aligned. Therefore, in the power profile of the DP system, there are no clear power peaks visible during the pipe release moment. This is shown in Figure 2.10.

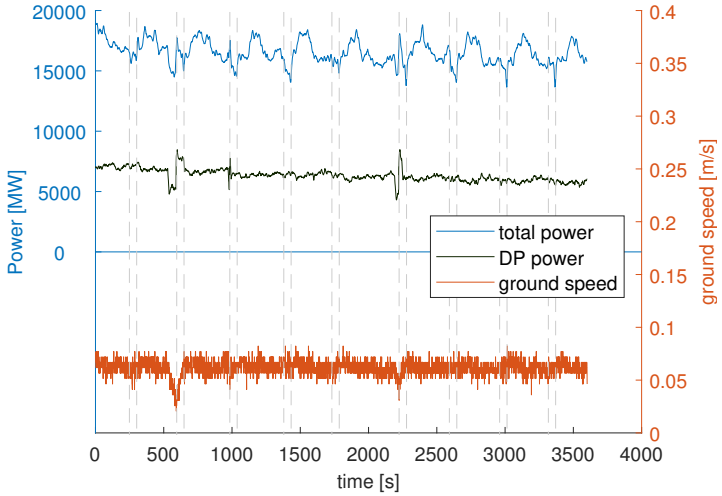

Figure 2.10: Total generator power and DP power compared to ground speed of the vessel in deep water

Again, the power asked from the generators, the power delivered to the thrusters, and the ground speed are displayed. The grey dashed lines represent the pipe release moments. In contrary to the process in shallow water, the ground speed of the vessel shows a more stable speed fluctuating around its average. The minor fluctuations are caused by disturbances like wind, waves, and current. This reflects in the DP power which also shows a more stable profile around its average.

For this thesis, it is decided to focus on deep water pipe laying because the only project for which data is available was a deep water pipe laying project. The shallow water data shown above was the first day of pipe laying for this vessel, after which the water depth increased rapidly. Since this was the first time the case vessel was used, the data measured at that day might not be representative. Besides, although the power profile is different for deep water than for shallow water, in both cases, the PMS would run one generator redundantly. This means that the savings in fuel consumption and running hours are expected not to be much affected by the focus on deep water vs. shallow water. Besides, also during heavy lifting, the PMS would run a redundant generator in every engine room, so also during heavy lifting, replacing the spinning reserve is expected to be beneficial. So the focus on deep water pipe laying is not expected to influence the end results substantially, but this will be discussed after finding the results.

2.6.3. Power Balance

For a clear understanding of the main consumers on board, the energy flow during pipe-laying was measured and analysed. The day that was examined was a day of deep water pipe-laying. During this day, the real power at all 51 breakers of the switchboards was measured. Based on the single line diagram with list of breakers, which is shown in Appendix A, the measured breakers are divided into three main categories:

- Pipe laying equipment: this is all the power that is used in the firing line during operation. Twenty-two breakers of the switchboards are directly or indirectly connected to the pipe-laying process.
- DP system: the thrusters are directly connected to the main switchboard on an 11 kV line. The auxiliary load of the thrusters is connected to a different breaker and distributed inside the thruster room by a secondary switch board.

- Hotel load: the sum of al load not related to pipe laying equipment or the DP system.

Besides, four breakers are directed both to the hotel load and to the pipelaying load, so these are a combination of two groups. These breakers are connected to a secondary 440V switchboard with lines going to the firing line and lines going to 230V switchboards. For simplicity, it assumed that half of the power on these secondary switchboards can be considered hotel load and half of the power can be considered pipe laying load. This assumption only influences the ratio of the energy distribution between the consumer groups and does not influence the total generated load.

The distribution between the three main consumers during this time frame can be seen in Table 2.4. As a check, the total generated energy delivered to the switchboard by the diesel generators was compared to the total consumed energy. The difference between generated and consumed energy was 0.7% and is assigned to the error introduced by the linearizing of the power signal (between two time-steps of one second) and to the trapezoidal integration of both the consumed- and generated power over time. This difference is considered to be acceptable. What is interesting to notice is that at most vessels, the propulsion system is the biggest contributor to the total load, but here it can be seen that during this time frame, the DP system contributed to one third of the total load. It should be noticed here that this data was captured during relatively calm weather, so the contribution of the DP load to the total consumed energy is expected to be higher during more rough sea states. The power distribution described here is mainly for the understanding of the power profile and to give insight in the contribution of the main consumers to the total power consumption.

Table 2.4: Power distribution during 11 hours of operation

Group	Average power [MW]	Total energy 11hrs [MWh]	Portion [%]
Pipe-laying equipment	5.42	59.6	37.6
DP system	5.29	58.2	36.7
Hotel load	3.72	40.9	25.7

In Appendix A, the power distribution of this 11 hour time-frame is shown. When zoomed in on one hour, as in Figure 2.11, it can be seen that the pipe laying load shows a repeating pattern. During this time-frame, the DP load fluctuates little due to the favourable wind and wave conditions on this day. Therefore, the pattern of the pipe-laying load reflects almost directly to the pattern in the total load (which is not necessarily a given fact for deep water pipelaying). The power used for the hotel load, which is the purple line in the figure, is relatively constant in time as expected. The pipe laying load follows a pattern of three repeating patterns:

1. In phase 1, the pipe is released by the tensioners into the water. The pipe-laying processes on board are paused for around 60 seconds causing a power drop during the pipe release. Next to the pausing of the processes, the tensioners deliver some power back into the network while releasing the pipe. The power fed back into the grid should be in the order of 2MW, based on a pipe load of 600 ton and the release of 24 m of pipe in 60 seconds. In the figure, these power drops during the pipe release are indeed in the order of 2 MW.

2. In phase 2, the power asked by the pipe-laying equipment starts with a high peak followed by a decreasing load. This increase in pipe-laying equipment power is caused by all the processes in the vessel combined that make the next pipe section ready for release into the water. These processes together are part of a big production line with multiple stations like transport from pipe storage, bevelling pipe ends (preparing for welding), double joining, transport to firing line, bevelling double joint ends, weld to existing pipe, coating etc. Especially the inductive preheating of the weld ends consumes a large amount of energy in this phase. All these stations have their power peak just after the pipe release, first for transporting from station to station, and then for the process itself at every station.

3. In phase 3, after the peak in phase 2, the power decreases again until all processes are finished and the pipe will be released again.

The pipelaying power pattern corresponding to the phases described above, which is repeated every 6-8 minutes is as follows:

1. A power trough of around 2 MW during the pipe release, lasting around 1 minute;

2. A power peak of 2 MW during all pipe-laying processes at the stations, lasting around 2 minutes;

3. A decrease in power during the finishing of all the pipe-laying processes at the stations, lasting around 3 minutes.

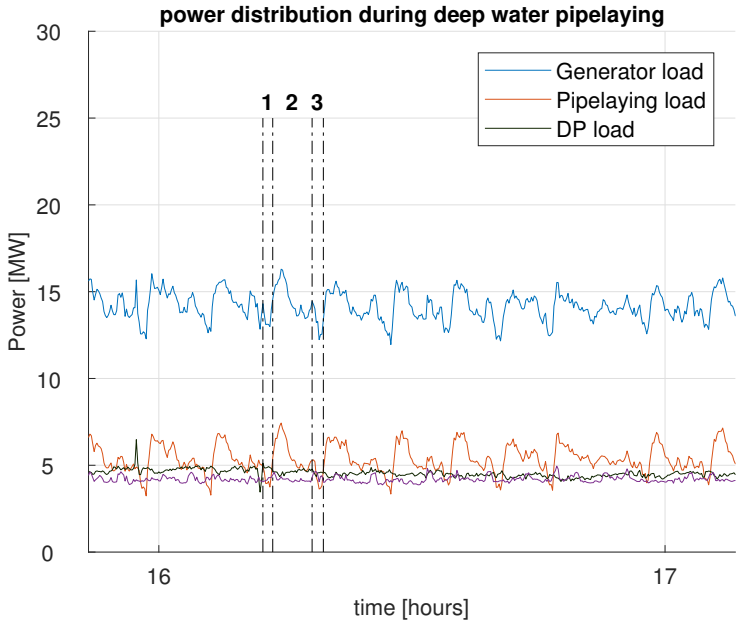

Figure 2.11: Power distribution in deep water pipelaying zoomed in on 1 hour. This power distribution in mainly to show the different stages in the pipelaying process that influence the power profile. Therefore, for clarity, a time frame is taken during calm weather to limit the influence of the DP power fluctuations on the total generator power. During less calm weather, the DP load is higher in general and fluctuates faster.

2.6.4. Operational Modes

The engine rooms of the Pioneering Spirit can be connected in three different modes of operation: no split mode, 2-split mode, or 4-split mode. When no split is made between the engine rooms, the main switchboards of all four engine rooms are connected in line, creating one equivalent switchboard where all running generators are connected to. In this mode, in the worst case scenario, a single failure might lead to the total failure of the power generation system, resulting in a black-out. Therefore, the no-split mode is not used during the DP operations of pipelaying or heavy lifting and is therefore not considered here.

During operations where the maximum redundancy is required, for example when lifting a topside, the 4-split mode is used. In this mode, in case of a fault in one engine room, in the worst case scenario, the maximum loss of power is 25%. However, a drawback of the 4-split mode is that all generators should be online, because in every engine room, one redundant generator is running as spinning reserve. Therefore, during pipe-laying, to have sufficient redundancy but not to let all generators be in operation, the vessel is operating in 2-split mode, meaning that the four engine rooms are connected such that they can be considered as two engine rooms[2].

The engine rooms can be connected in port side/starboard side 2-split mode or in forward/aft 2-split mode. In the port side/starboard 2-split mode, Engine Room 1 (ER1) and ER3 are connected to each other and ER4 and ER2 are connected to each other, see Figure 2.12. This port side/starboard side 2-split mode is used during pipe-laying. Using this split, the system can be considered as one starboard engine room and one port side engine room. Using the port side/starboard side 2-split is preferred over using the forward/aft 2-split because of the redundancy in the fuel oil system. The fuel oil system is designed such that it can

[2]During unfavourable conditions (like heavy weather, current, wind or swells), the engine rooms are connected in 4-split, creating four independent systems. In this mode, in case of a fault in one engine room, in the worst case scenario, the maximum lose of power is 25%. In 2-split mode, in the worst case scenario, a fault in one engine room could lead to a failure of two engine rooms, meaning a loss of power of 50%, which should be avoided by all means during these conditions. Therefore, the system runs on 4-split mode during less favourable conditions.

either be used to supply the four engine rooms separately when needed (for example during 4-split mode for maximum redundancy) or it can be used to supply the two port side and two starboard side engine rooms separately.

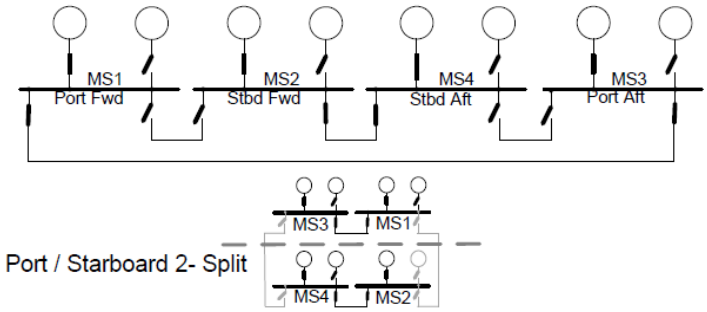

Figure 2.12: Portside/Starboard side 2-split mode

On both engine room sides, one generator is always running redundantly as spinning reserve. In case of a failure in one generator, the other generators can still deliver all the required load immediately and a new generator can be started to fulfil this redundancy requirement again. The function of EES on board of the Pioneering Spirit is to replace this spinning reserve. When using EES, in case of a generator failure, the EES delivers power during the bridging time while an additional generator is started.

3

Electrical Energy Storage

Having discussed the background of the company and case vessel, and after defining the focus on deep water pipe laying, in this chapter the electrical energy storage is discussed. Before focusing on the PMS of a single-battery hybrid DP vessel, it should first be proven that using electrical energy storage (EES) on board of the case vessel is beneficial in terms of fuel consumption and running hours savings. Besides, for a proof-of-concept, a suitable EES device should be selected and sized to be able to proof the technical feasibility. Therefore, in Section 3.1, a preliminary estimate on the fuel consumption and running hours reduction is made using the power data discussed in the previous chapter. The next section describes the required size and connection to the power grid of the EES, followed by the section where the most suitable type of energy storage is selected. After selecting an appropriate type of EES, the next section elaborates on a potential hybrid system design for the case vessel. This is followed by an introduction to the required starting decision algorithm, distinguishing between a single battery hybrid system and a double battery hybrid system. The last part concludes on all findings of this chapter.

3.1. Potential Energy Storage Benefits

Before an EES device is chosen and the starting decision algorithm method is studied, it is first calculated if it is beneficial for the case vessel to replace the spinning reserve and if it would be beneficial to shave peaks. Therefore, a preliminary assessment on potential fuel consumption and running hours savings is made before focusing on the type of EES and the starting decision algorithm of the hybrid system.

3.1.1. Spinning reserve replacement

During operation, the power asked from the generators is divided over all running generators using load droop sharing[1]. For redundancy reasons, the vessel runs on one redundant generator per engine room side. For the load profile used here, this means that the vessel has been operating on four generators, where it could have run on only two. This causes the four running generators to run on low power factor, resulting in a low efficiency.

During the factory acceptance test (FAT), the specific fuel consumption (*sfc*) of all generators was measured on different load factors. For every load factor, the average *sfc* of the eight generators is calculated, which is shown in Table 3.1. These tests are performed by the engine manufacturer and are approved by the class society [50].

If the power generation redundancy is achieved by a hybrid system instead of the spinning reserve, during pipe-laying, two generators could be switched off since these generators are running redundantly. Switching

[1]Load droop sharing is a method where the reference frequency of a synchronous generator can be adjusted to be able to increase or decrease the fuel flow to that generator in order to increase or decrease the power supply from that synchronous generator. Every generator has a governor which adjusts the fuel inflow to keep a steady synchronous speed to maintain the grid frequency of 60Hz. This governor is controlling the fuel inflow by a feedback controller that compares the measured frequency to a setpoint frequency (of 60Hz in this case). The power management system monitors the load and speed of all generators connected to the grid. When one generator tends to supply more power than the other generators connected to the same grid, the governor's frequency setpoint of this generator can be adjusted temporary to lower that power again and give chance to the other generators to increase their power. This way, the contribution to the power demand is controlled and equally shared by all online generators, creating a stable equally shared power distribution.

Table 3.1: Average specific fuel consumption of all 8 generators

load [%]	10	25	50	75	100
sfc [g/kWh]	288.9	220.2	196.3	192.8	188.8

these generators off halves the number of generator running hours reducing the maintenance costs significantly. Next to that, the two running generators would then be operating at a higher power factors resulting in a higher efficiency. To prove this effect, the load profile that is earlier discussed and which is shown in Figure 2.10 is used to calculate the difference in fuel consumption between two and four running generators.

The power management system uses droop load sharing to symmetrically share the active load [kW] over the online generators. For this preliminary estimation, it is assumed that the power management system performs this task perfectly and divides the total load equally over the running number of generators. To calculate the fuel consumption of the vessel, the following equation is used:

$$\dot{m}_{fuel}(t) = sfc(p.f.(t)) \cdot P_{gen}(t) \tag{3.1}$$

	$\dot{m}_{fuel}$:	The fuel consumption based on the power factor: $P_{gen}/P_{nominal}$	[g/h]
Where:	sfc:	Specific fuel consumption	[g/kWh]
	P_{gen}:	Power asked from the generator	[kW]

For every timestep of the load profile, the power asked per generator is calculated by dividing the total asked power by the number of generators. So when all four generators are in operation, these generators all account for 25% of the generated power at moment *t*. When only 2 generators are running, these generators account for 50% of the generated power at moment *t*. At every moment *t*, the *sfc* is calculated based on the power and using a fit through the measured *sfc* for these generators from Table 3.1. This fit is shown by the red line in Figure 3.1. To calculate the total fuel consumption per hour, the mass flow of fuel is translated to the mass flow per second, which is then integrated over the full hour. The mass flow per second is calculated for every time step *t* and is based on the power factor at that time step:

$$fc = \int_{t_0}^{t_1} sfc(p.f.(t)) \cdot P_{gen}(t)\,dt \tag{3.2}$$

	fc:	The fuel consumption during time span $t_0 : t_1$	[kg]
Where:	sfc:	Specific fuel consumption	[kg/kWs]
	P_{gen}:	Power asked from the generator	[kW]

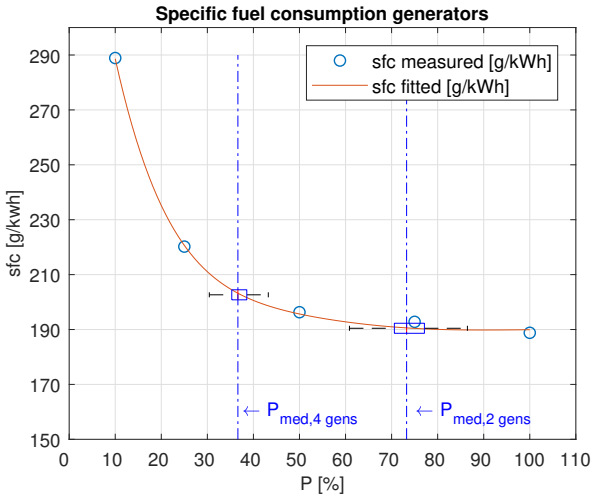

Figure 3.1: Fuel consumption using preliminary power profile

In Figure 3.1, the median of the power per generator during 1hr time interval of Figure 2.10 is indicated by the blue dotted line. This P_{med} is indicated for two situations:

1. The current situation where four generators are running. Around the median power, a boxplot is plotted to show the variations around this power. In this situation, the median of the power is at 36.6% of the nominal generator power. The *sfc* at this position is 203.2 g/kWh. The box shows the 25th and 75th percentile which are located at 35.30% and 38.56% of the nominal power. Within this power range, the *sfc* fluctuates between 201.6 and 204.5 g/kWh. The whiskers of the boxplot show the 99% range of the measured power.

2. The fictive situation where redundancy is supplied by EES, so two generators are turned off and the other two generators are used for the total power generation. When only two generators are running, they both run with a median power of 73.26% of the nominal generator power. In this situation, the 25th and 75th percentile are located at 70.60% and 77.12% of the nominal power. In the figure, it is visible that within this range, the *sfc* only fluctuates between 190.2 and 190.9 g/kWh because of the low *sfc* gradient at higher power factors.

During the one-hour time-frame, the expected fuel consumption based on this calculation is presented in Table 3.2. The potential benefits of using EES to replace the spinning reserve are the running hour reduction and the fuel consumption by only running on two generators. When comparing the fuel consumption between two and four running generators, the saved fuel is 200 kg/hour which is 6.1% of the total fuel consumption. Chapter 4 will elaborate on the saved fuel consumption and running hours using a wide variety of power data in a full year simulation.

To put this into perspective, using a fuel price of low sulphur HFO[2] of \$546/ton[3] is used, this would result in yearly fuel savings of \$1.0 Million.

Table 3.2: Comparison fuel consumption per hour for 2 or 4 running generators

Number of running generators	fuel consumption [ton/hr]	sfc_{med} [g/kWh]
4	3.355	203.2
2	3.149	190.6

Next to the saved fuel, the saved running hours are relevant for the potential benefits of replacing the spinning reserve by EES. When turning off half of the running generators, the running hour reduction obviously is 50%, resulting in a potential reduction in maintenance costs.

3.1.2. Load levelling

Previous research also focused on the benefits of EES to use for peak shaving or load levelling [27], [40], [28]. Although no proof of load levelling benefits for the fuel consumption was found in these sutdies, it is examined if load levelling would be beneficial for this specific vessel. The benefits of load levelling for hybrid maritime systems would lie in making the diesel generators operate in a more efficient operating point. As can be seen in Figure 3.1, the most efficient region of the engine envelope is at around 70 - 100% of the nominal generator power. If the required power is fluctuating a lot, a hybrid system with EES could make the engines operate in a more efficient point and could reduce the fuel consumption that way. Besides, if the power peaks would force the PMS to run an addition generator, by shaving the peaks, it would become unnecessary to run this additional generator, reducing the number of running hours.

To estimate the reduction in fuel consumption due to load levelling, the same power profile as was used before is used as a test case. The effect of load levelling is calculated by comparing the expected fuel consumption of the fluctuating load with the expected fuel consumption of a perfectly levelled load. This perfectly levelled constant load is the average of the fluctuating load. In this calculation, an ideal EES device (no losses) is used to supply power when the required power exceeds the average power and to use power when the required power drops below the average power. So after one hour of operation, the total consumed energy

[2] From 2020, global IMO regulations will set the maximum sulphur emissions to 0.50% m/m, which means that either the exhaust gasses need after treatment or the fuel that will be used from 2020 would need to have a low sulphur content. Since the Pioneering Spirit does not have scrubbers on board for exhaust gas after treatment, Low Sulphur HFO should be used used from 2020 onward. Therefore, in this thesis, the fuel that will be used for calculations is Low Sulphur HFO to make sure the calculations are representative for the near future.

[3] This is the 10 days average of Low Sulphur HFO in the port of Rotterdam at 09/03/2018. At this moment, low sulphur HFO is not yet available in many other ports than ports located in current ECA's, because the global sulphur cap is not yet in place. Therefore, the Low Sulphur HFO price of Rotterdam is used in this analysis. This number is obtained from https://shipandbunker.com/prices/emea/nwe/nl-rtm-rotterdam#ULSFO at 09/03/2018.

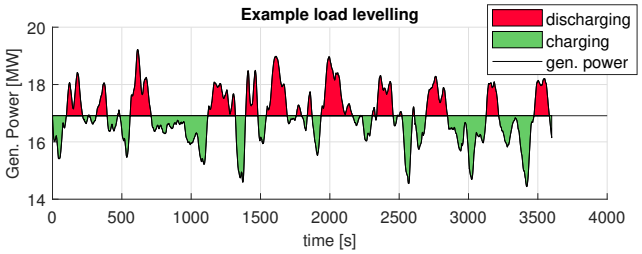

Figure 3.2: Ideal load levelling by using EES

is equal for the fluctuating and levelled load. The ideal load levelling for the test case would look like Figure 3.2. In Table 3.3, the expected fuel consumption at a levelled load can be compared to a non-levelled load.

Table 3.3: Comparison fuel consumption per hour levelled and non-levelled load

Number of running generators	fuel consumption non-levelled power [ton/hr]	fuel consumption levelled power [ton/hr]
4	3.3547	3.3573
2	3.1488	3.1487

For four running generators, the difference in fuel consumption between a levelled load and non-levelled load is 0.078%. For two running generators, the difference between levelled and non-levelled load is 0.0032%. These differences are considered to be negligible as could be expected when examining the power fluctuations which are also plotted in Figure 3.1 by the boxplots. The whiskers of the boxplots show the range covering 99% of the measured power, where it can be seen that the variation in power is small. Therefore, the variation in sfc is also small, creating only minor benefits from load levelling. When two generators would be switched off, the 99% range of the required power becomes bigger, but the range in sfc becomes even smaller because of the flat characteristic of the sfc at high power factors. In short, using EES just to level the load, would not reduce fuel consumption significantly, both for two as for four operating generators.

It would be more beneficial to not only level the load to its average load, but to fluctuate the number of running generators to force them to always operate at a load factor between 70% and 100%. In such a system, the generators are only running at high power factor to charge the battery and are turned off when the EES is fully charged. However, Gerritsen [27] already showed that the economical benefits from such a hybrid system do not cover the costs of the system. This can be explained by the fact that the benefits from the reduced fuel consumption are counterbalanced by the introduced losses. These losses apply to the round trip efficiency of the storage system, the transformer and the converter/inverter. If an efficiency of 97% is assumed for these components, the round trip efficiency would already be $0.97^5 = 85.9\%$, so the savings in fuel consumption would be nullified. Next to that, it is also questionable whether it is realistic to repeatedly start and stop the generators multiple times an hour [28]. Starting and stopping the engines excessively could cause extra wear of the engine and could probably increase maintenance costs.

Besides, by replacing the spinning reserve for an EES system, the range of required power is already at high power factors, so the efficiency would already be enlarged by only using the EES for spinning reserve replacement and can hardly be increased further by levelling the load, because of the flat *sfc* curve at higher partial loads. Taking these considerations into account, it is decided to only focus on using the EES for replacing the spinning reserve.

3.2. Energy Storage System

Because the benefits of replacing the spinning reserve by EES are shown in the previous section, a suitable size and grid connection should be found. As explained, the EES system on board of the Pioneering Spirit will be used to supply backup power in case of an unexpected shut down of one of the generators, the spinning reserve function. The time between the unexpected shut down of a generator until the moment where the next generator is fully online will further be referred to as the *bridging time*. This section describes the sizing of the EES system and the grid connection.

3.2.1. Sizing

To calculate the required size of the EES system, the length of the bridging time should be known. The bridging time starts at the moment a generator fails and ends at the moment when another generator is fully online, which is the moment from when the generator is equally contributing to the shared load.

To calculate the minimum required capacity of the EES, the diesel engine start-up time should be known. To find the start-up time, an on board starting test of a stand-by generator was performed during operation. The starting process of a generator follows a pre-set sequence, which can be found in Table 3.4.

1	Starting signal from PMS
2	Acceleration of engine until synchronous speed, no load is applied
3	Closing of circuit breaker
4	Ramping up of load in 10 seconds
5	Fully contributing to power generation

Table 3.4: Starting sequence diesel generators

The result of this starting test is shown in Figure 3.3, where the starting signal, the rotational speed, the circuit breaker closing signal and the delivered generator power are plotted. After the starting signal was given, the the rotational speed increases steadily towards the synchronous speed. When the synchronous speed is reached, the circuit breaker between the generator and the main switchboard is closed, so from this moment on, the generator is delivering power to the grid. The load on the generator is slowly increased in 10 seconds until the generator is fully contributing to the power generation. The full starting sequence takes 57 seconds from starting signal to fully contributing to the power generation. For safety, a bridging time of 90 seconds will be used in the further analysis. This means that the required capacity of the EES device for spinning reserve replacement should be at least:

$$E_{sp,res} = P_{nom} \cdot t_{bridging} = 11200[kW] \cdot \frac{1.5}{60}[h] = 280 kWh. \tag{3.3}$$

Where:

$E_{sp,res}$:	Spinning reserve replacement capacity	[kWh]
P_{nom}:	Nominal generator power	[kW]
$t_{bridging}$:	Bridging time	[h]

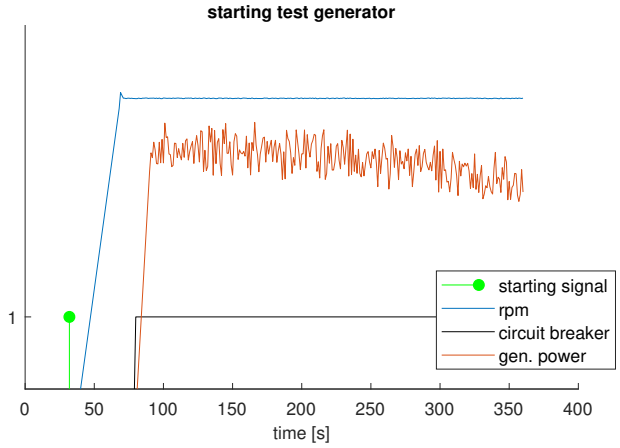

Figure 3.3: Diesel engine start up time from stand-by

3.2.2. Grid Connection

The EES device can either be connected to the main switchboards at a voltage of 11 kV or directly to the consumers at secondary switchboards of 440V. As can be seen in the single line diagram in Appendix A, the four engine rooms all contain one high voltage main switchboard. From these main switchboards, the power is distributed around the vessel over 11kV lines to high voltage consumers and to transformers connected to the secondary switchboards. In these transformers, the voltage is transformed from 11 kV to 440V. An

advantage of connecting the EES directly to the consumers or secondary switchboards is that the voltage from the EES does not have to be transformed from lower voltage to 11 kV, saving transformers.

However, in Appendix A, it is clear that every main switchboard contains multiple connections to 11kV consumers and to secondary switchboards. These consumers and secondary switchboards are located all around the vessel. In Figure 2.3, it can be seen that the high voltage lines are directed to the thrusters at all four corners of the vessel, the two whinch rooms at starboard side, the two whinch rooms at port side and to the PLS (pipe laying systems) equipment rooms next to the firing line. If the EES device would have to be connected to all these consumers and switchboards separately, this would either mean that the EES would have to be split into a large number of independent EES devices, or that new 440V lines should be installed from a central EES room to rooms throughout the vessel.

Table 3.5 summarises the advantages and disadvantages of connecting the EES to 11 kV grid compared to a direct connection to the 440V consumers. Although the 440V connection looks promising due to the lack of a transformer, installing cabling from a centralised EES point to all 440V consumers is costly and most of all unrealistic. Therefore, it is decided to connect the EES device to the 11 kV main switchboards, close to the engine rooms.

440V	11kV
No transformer needed	Transformer needed
Multiple connections around the vessel	One connection per main switchboard
Cabling throughout the vessel	Little cabling when installed close to the main switchboards

Table 3.5: Comparison 440V and 11kV connection

3.3. Types of Energy Storage

In this section, the type of energy storage device is selected. Appendix B shows the relevant characteristics that describe the performance of the types of EES which are discussed below. These characteristics are found in literature.

3.3.1. Super Capacitors

A super capacitor is an electronic component that stores electrical energy in an electric field. Instead of consuming or producing electrons, like a battery does, a capacitor stores the electrons until they are released.

Working Principle The main advantage of storing energy in capacitors is its lack of moving parts, noise and electrochemical reactions [62]. Super capacitors, also called ultra capacitors or supercaps are a widely used name for Electric Double-Layer Capacitors (EDLC). In contrary to an ordinary capacitor, the EDLC does not have a dielectric, a material that is a very poor conductor, like air. The working principle of a regular capacitor is the storage of electrical energy in an electric field, for example between two parallel plates with a small gap filled with dielectric material in between. The construction of EDLC's is different from ordinary capacitors, but the advantages of no moving parts, no noise and no electrochemical reactions remain.

An EDLC consists of two electrodes that are connected to the power source/consumer, having an electrolyte in between. This electrolyte is a fluid filled with a solvent consisting of positively and negatively charged ions. In the electrolyte, a separator prevents the electrodes from making contact. This separator functions as a membrane that is able to let the ions pass.

During charging, a voltage is applied to the electrodes causing the positively charged ions in the electrolyte to move to the negative electrode, and the negatively charged ions to move to the positive electrode. Between the ions and the electrode, a single layer of solvent is still present, creating a double layer of solvent and charged ions. During this process, electrons run from the positive electrode through the power source to the negative electrode. While discharging, the electrons run from the negative electrode through the power consumer to the positive electrode. The ions that were attached to the electrodes return back to the electrolyte and mix again [9]. With this process, EDLC differs from batteries in the theoretical absence of chemical reactions in EDLC's. Instead, the driving factor is the electrostatical reaction.

The energy stored in an ideal capacitor is equal to:

$$E_{cap} = \frac{1}{2} C V^2 \tag{3.4}$$

Where: C: Capacitance [F]
V: Voltage across the capacitor [V]

The capacitance of the capacitor is inversely proportional to the thickness of the capacitor plate. In an ordinary plate capacitor, the thickness of these plates are in the order of micrometers, but in the EDLC, the thickness of the capacitor plate is the thickness of the double layer, which is in the order of nanometers. This results in a capacitance per electrolyte surface of the EDLC that is multiple orders higher than the capacitance of an ordinary plate capacitor. Next to that, the capacitance is proportional to the surface of the electrodes. The electrodes are normally made of very porous activated carbon creating a high electrode surface, which is increasing the capacitance even higher.

Overview and Remarks Super Capacitor In Appendix B, the performance characteristics of the super capacitor are shown. The following advantages apply for the application of super capacitors as an energy storage device:

- No noise and moving parts;
- Long life-time: the working principle of the super capacitor does not require any chemical reactions. Only physical electro-statical reactions take place in the super capacitor. Due to this, the super capacitor degrades only very slowly with the number of charge/discharge cycles. This makes the life time of the super capacitor high.
- High specific power and power density: the specific power of the super capacitor is 4350 ±557 W/kg and the power density is 4293 ± 626 W/L;
- High cycle efficiency: the efficiency of a charge/discharge cycle is found to be 95%;
- Low power costs: because of the high power density, the power costs are relatively low for the super capacitor: 225 $/kW.

However, the super capacitor also faces some disadvantages:

- Low specific energy and low energy density: the specific energy of the super capacitor is only 3.9 ± 0.5 Wh/kg and the energy density is only 3.1 ± 0.3 W/L;
- High energy costs: because of the low energy density and specific energy, the energy costs are relatively high, being 9000 $/kWh;
- Self discharging: super capacitors have a relatively high self-discharge rate of around 25%/day.

Another remark should be made on the performances of the super capacitor. When a super capacitor is discharged, the voltage follows a near linear discharge curve. This means that the voltage of the super capacitor declines with the state of charge. When the power output of the super capacitor should be constant, a DC/DC converter is necessary to increase the current that would be withdrawn from the super capacitor at constant power. For a fair costs comparison, this converter should be taken into account when the super capacitor would be selected as the EES device.

3.3.2. Flywheels

Although the principle of flywheels has been known and used for a long time, using flywheels as a UPS have only been suggested in the last few years due to the rapid developments of high-tech materials and magnetic bearings.

Working Principle The principle for Flywheel Energy Storage (FES) is the storage of kinetic energy. The energy is stored in rotating disks at high speed that are driven by an electrical motor/generator. When charging, the electrical machines function as motor to accelerate the flywheel and when discharging, the electrical machines functions as a generator to retract energy from the rotating wheels.

The energy that is stored is proportional to the inertia of the disk and to the rotational speed squared according to:

$$E_{FW} = \frac{1}{2} J\omega^2 \tag{3.5}$$

	E_{FW}:	Stored energy in flywheel	[J]
Where:	J:	Polar moment of inertia	[kg $\cdot$ m^2]
	ω:	rotational speed	[rad/s]

When all mass of the flywheel is considered to be located in a thin ring, the maximum stored energy per mass of a flywheel is given by equation 3.6 [30]. A derivation for this equation can be found in Appendix D.1.

$$E_{FW,max}/m = \frac{1}{2}\sigma_{max}/\rho \tag{3.6}$$

This relation between the maximum stored energy and tensile strength over density is the reason for selecting very low dense materials with a high tensile strength. Therefore, current state-of-the-art flywheels are most often made from a composite fibre material. These machines run in a vacuum chamber to reduce the viscous friction. Because these machines are running at very high speeds and to reduce the self-discharge, in modern flywheels, the shafts are often supported by magnetic bearings. In magnetic bearings, there is no material contact, resulting in no friction. This way, the losses inside a flywheel are reduced and almost no wear occurs.

The rotor of the motor/generator can be integrated in the flywheel, or it can be connected to a shaft. When the rotor is integrated into the flywheel, it is operating in a vacuum, making it difficult to dissipate heat. When the flywheel is used as a UPS and is only used in case of power loss, this is not a main issue, but when the flywheel is used regularly, the rotor is designed to have minimum losses. Most often, this requires a permanent magnet machine [15].

3.3.3. Overview and remarks Flywheel Energy Storage

In Appendix B, the performance characteristics of flywheels are shown. As an overview, the advantages and disadvantage of FES are shown below. The advantages are:

- Long life-time: the flywheel in FES systems are equipped with magnetic bearings resulting in no contact between moving and stationary parts. Therefore, the lifetime of a FES system can be up to 1,000,000 cycles regardless of the depth of discharge and the charge- or discharge rate;
- High charge- and discharge rate: the FES system could be charged or discharged at very high rates up to a fully charging or discharging the system in the order of milliseconds. The ratio between charge- and discharge rate is equal to one.
- High cycle efficiency: the round-trip efficiency of FES is as high as 90%;
- Power density: FES has a relatively high specific power and a high power density. The specific power of FES is 1423 $\pm$760.5 kW/kg and the power density is 9.8 $\pm$2.6 Wh/L.
- Low power costs: FES is relatively cheap concerning the costs per power. With a price of $310/kW this EES principle is able to compete with super capacitors.

However, FES also faces a few disadvantages:

- A high self-discharge rate: the biggest drawback of FES is the self-discharge of 100% per day. If this type of energy storage would be used as a UPS, where the energy is only used a couple of times per year, a lot of energy would be wasted in keeping this EES device fully charged;
- Relatively low energy density and specific energy: FES is able to store around 5.2 $\pm$1.4 Wh/kg and 9.8 $\pm$2.6 Wh/L. These numbers are considered to be relatively low for an energy storage system.
- Relatively high costs for energy: in parallel with the energy density and specific energy, the costs per amount of stored energy are also relatively high for FES with estimated costs of $4000/kWh.

What should further be noticed about FES are the safety concerns of these high speed rotating masses. Especially when used for many cycles, or in case of a manufacturing fault, a flywheel could fail during operation. If the flywheel fails while rotating at 30,000 rpm, it would cause serious damage and could potentially be dangerous for crew on board. These dangerous situations could be reduced by constructing the system such that it can withstand an unexpected failure of the rotating mass, but it should be noted that maritime safety regulations may not be prepared for FES yet.

3.3.4. Batteries

Battery types The batteries that are examined in this thesis are the Lead-Acid battery, the Lithium-Ion battery (Li-ion), the Nickel-Cadmium battery and the Nickel Metal-Hydride battery.

The Lead-Acid battery is the most widely used battery having small response times and a low self-discharge rate. Besides, Lead-Acid batteries are most often the cheapest solution concerning the costs per energy [39]. In Lead-Acid batteries, the cathode is made of PbO_2, the annode is made of Pb and the electrolyde consist of sulfuric acid.

The Li-ion battery is a relatively new type of battery compared to the LA battery. Before, in hybrid vehicles, the Nickel Metal-Hydride battery was the most preferred choice, but recently more and more hybrid vehicles are equipped with a Li-ion battery [1]. In a Li-ion battery, the cathode is made of a lithium metal oxide and the anode is made of graphitic carbon [39]. The electrolyte is normally an organic liquid with dissolved lithium salts.

Nickel-Cadmium batteries were widely used in portable power applications like leaf blowers, drilling machines and portable radios. The electrodes of the Nickel-Cadmium battery are made out of nickel hydroxide and metallic cadmium. The electrolyde is water based solution with dissolved alkale [39]. Last decades, Nickel-Cadmium lost ground to Li-ion and NiMH batteries because of the higher energy density of these other chemicals and because cadmium is a toxic heavy metal, which is not present in other comparable batteries.

Nickel Metal-Hydride batteries are comparable to the Nickel-Cadmium batteries, but these batteries do not contain any toxic heavy metal. Nickel Metal-Hydride batteries are mostly used in portable devices, in hybrid vehicles and as UPS systems. In Nickel Metal-Hydride batteries, instead of cadmium electrodes, the electrodes are made from an hydrogen-absorbing alloy.

Battery Comparison In Appendix B, the relevant characteristics of the different batteries are discussed. For the comparison of batteries against super capacitors and flywheels, one of these battery types is selected. As explained in Appendix B, the nickel-cadmium battery suffers from a memory effect which could become problematic in this application, since the battery is either always fully charged, or fully charged most of the time. Therefore, it is decided not to use the nickel-cadmium battery in this comparison.

The EES used for this application should be able to deliver all the energy in a very short time, so the maximum allowed C-rate[4] should be taken into account. To deliver the required 280 kWh in 1.5 minutes, due to the different maximum C-rates, different reduced capacity at high discharge current, and due to the efficiency differences, the different battery types would need a bigger size to deliver 280 kWh in 1.5 minutes. Besides, the battery should still be able to deliver this amount of energy at the end-of-lifetime of the battery, which is usually defined as the moment where the left capacity of the battery is 80% of the initial capacity due to battery aging [66]. The minimum size of every battery to be able to supply the nominal generator power (so to stay under the maximum defined C-rate), based on the maximum C-rate, discharge efficiency, and end-of-life capacity is calculated as follows:

$$E_{min}[kWh] = \frac{\frac{1}{C}\,60\,[min]}{60\,[min/hr]} P_{nom}\,[kW] \frac{1}{\eta_{dis}} \frac{1}{C_{EOL}} \tag{3.7}$$

Where:

C:	The maximum C-rate	[-]
P_{nom}:	The nominal generator power, the maximum required power from the batteries.	[kW]
η_{dis}:	Discharge efficiency	[-]
C_{EOL}:	Ratio of capacity at end-of-life compared to initial capacity, being 0.8 here	[-]

The preliminary costs are calculated for all three battery types, using:

$$CAPEX = Cost_{energy} \cdot E_{min} \tag{3.8}$$

Where:

$Cost_{energy}$:	The cost per energy	[$/kWh]
E_{min}:	Minimum amount of energy from Equation 3.7	[kWh]

[4] The C-rate is a measure of the discharge or charge speed of an EES device. It is defined as the ratio between the charge/discharge power and the charge/discharge power that would charge/discharge the device in exactly one hour. For example, when a battery having 20 kWh of capacity would be charged at a power of 10 kW, it is charged at 0.5C. When the same battery would be discharged at 40 kW, it is being discharged at 2C.

Using Equation 3.7 and 3.8, the costs for each battery type are calculated and shown in Table 3.6.

Table 3.6: Economical comparison battery types. The cost per energy was found in literature, see Appendix B.

	Lead-Acid	Li-ion	Nickel Metal-Hydride
P_{nom} [kW]	11200	11200	11200
required energy [kWh]	280	280	280
maximum C-rate	2	20	10
Discharge efficiency	0.81	0.88	0.88
E_{min} [kWh]	8613	795	1591
$Cost_{energy}$ [$/kWh]	189	1085	750
CAPEX [$]	**$ 1,600,000.00**	**$ 860,000.00**	**$1,200,000.00**
left capacity at max C-rate [-]	0.4	0.8	0.56
required capacity [kWh]	700	350	500

As a check, it is calculated what should be the minimum amount of stored energy when the reduced capacity at high C-rates is taken into account, which is shown in the last row of Table 3.6. For all three battery types, the battery's reduced capacity is sufficient at high C-rates.

As can be seen in Table 3.6, the Li-ion battery is economically the best solution to be used in the comparison against super capacitors and flywheels. Besides, the Li-ion battery performs well at high discharge rates, has no memory effect and a relatively long lifetime. Therefore, Li-ion battery is used in the EES comparison to compare to flywheels and super capacitors. In Appendix C, for completeness, other less conventional EES mechanisms are discussed, including the reason for not using it in the EES comparison.

3.3.5. Energy Storage Selection and Size

In the previous paragraphs, the important parameters of super capacitors, flywheels and batteries were listed. To make a comparison between these three EES options, the required capacities of these options should be known. This capacity is different for batteries compared to super capacitors or flywheels due to the difference in the effect of the state-of-charge[5] on the lifetime of these devices. For super capacitors and flywheels, the state of charge of the device does not influence the lifetime of the system, both in terms of calendar lifetime and cyclic lifetime. Calendar lifetime is the lifetime of the EES device regardless of the usage of the device and it is expressed in years. The cyclic lifetime of the EES device represents the number of charge- and discharge cycles before the battery is at the end of lifetime. For Li-ion batteries, the state of charge has a big influence on both the calendar lifetime and the cyclic lifetime.

Although it is widely accepted that the average state of charge of the battery influences the calendar and cyclic aging, it is difficult to find a general correlation between the state of charge and the aging of the battery. Different cell types respond differently to the average state of charge and even the aging rate of different batteries made from the same cell type can respond differently to the average state of charge. However, different previous studies do contain the similarity that for lifetime optimisation, the average state of charge should be between 20% and 70%. Above and under these limits, the stresses in the electrodes of the battery increase. The exact state of charge where batteries degrade the least depends very much on the specific battery that is used [66].

To compare different EES systems, a state-of-charge range for the Li-ion battery should be selected to calculate its required capacity. As said, it is hard to point an optimal state of charge limit at which Li-ion batteries degrade the least -since this can differ between specific batteries- but in this analysis, the above mentioned range between 20% and 70% will be used, since this is the range that is found as the optimal life time range in different studies [66]. However, it is important to notice that these are not hard limits and more research into this topic is needed to formulate a general relation between the average state of charge and the battery aging. Besides, the capacity of the battery system should be tested regularly on board, to evaluate and possibly adjust this range.

In Table 3.7, the different EES options are compared based on the most important parameters. The capacity of these EES options are calculated using the state of charge range and the discharge efficiency. Chapter

[5]The state-of-charge of a battery is defined as the capacity that is left in the battery compared to the maximum capacity. For example, if 30% of the battery's capacity is used to supply a consumer and the battery was fully charged, the state-of-charge is 70%.

6 will elaborate more on the final size of the EES system when the failure chances of the different system options are included in the assessment.

The required capacity of the EES options are calculated by:

$$E_{EES} = \frac{1}{R_{SOC}} \frac{E_{sp,res}}{\eta_{dis}} \tag{3.9}$$

	R_{SOC}:	State of charge range	[%]
Where:	$E_{sp,res}$:	Spinning reserve replacement capacity from Equation 3.3	[kWh]
	η_{dis}:	Discharge efficiency	[%]

For the battery, the state of charge range will be between 20% and 70%. When the battery size calculated in Table 3.6 is used, this range contains 400 kWh of energy, see Figure 3.4. Using the discharge efficiency of 88%, this means that 350 kWh of energy can be recovered from this range, which is sufficient for required the spinning reserve replacement capacity of 280 kWh.

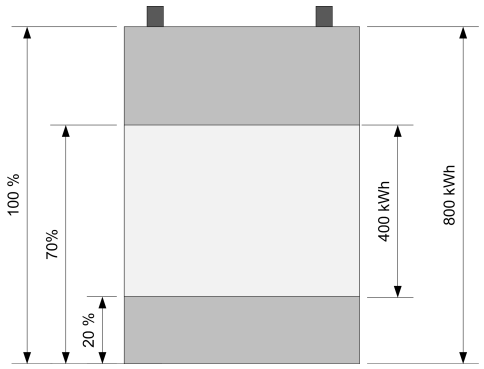

Figure 3.4: Schematic representation of state of charge of battery

For the case vessel, the size and weight are not the most dominant criteria in the EES selection as long as these characteristics are within reasonable limits. Although the size of 84 m^3 (corresponding to three TEU) for the super capacitors is relatively big, an installation of this size could be plausible on the case vessel. The investment costs are more important for the comparison, and it is clear that the super capacitors are by far the most expensive option. The CAPEX of flywheels is lower than for super capacitors, but the Li-ion battery is the best option when focusing on the CAPEX. When the self-discharge of the flywheels is also taken into account, the Li-ion batteries perform even better compared to the flywheels. When considering all these parameters in the comparison, it is decided to use the Li-ion batteries as the EES device for this application.

Table 3.7: EES comparison

		Lithium Ion	**Super Capacitor**	**Flywheels**
Capacity	[kWh]	795	327	319
Size	[m3]	3.6	106	33
Weight	[tons]	6.7	84	61
self-discharge	[%/day]	0.1	25	100
CAPEX	[$]	**$ 860,000.00**	**$ 2,900,000.00**	**$ 1,300,000.00**

3.4. Hybrid System Design

To prove the feasibility of this system, a battery design example that could be used on the case vessel is shown in this section. A detailed battery design optimisation lies outside of the scope of this project, so the design shown in this section is not necessarily the best solution, but the aim of this section is to prove the technical and economical feasibility of a battery system for this purpose. For this design, existing components are used to show the practical feasibility.

Battery The battery that is used is a high power Lithium-Ion battery manufactured by KoKam[6] which has a maximum discharge rate of 20C. This battery module contains 14 Li-NMC cells, having an average voltage of 3.7V each, creating a battery module with a voltage of 52V.

To connect the batteries to the high voltage grid on board, the voltage has to be transformed to 11kV. Existing transformers available on the market usually transform the voltage from a standard low voltage level to a standard high voltage level, like 440V/11kV or 690V/11kV. To feed the transformer, a 3-phase alternating current is required, which is provided by active front end converters. Active frond end converters are required because these devices should be used both for charging and for discharging. The limiting factor in converters is the maximum current allowed through the thyristors, so for a given power, the converters are supplied by a relatively high DC voltage from the batteries to reduce the current. Creating a relatively high voltage DC from relatively low voltage batteries is done by connecting the battery modules in series. However, more batteries in series reduces the reliability of the system, since one broken battery in the series results in the complete dis-functioning of the string. Therefore, there is maximum amount of batteries placed in series, resulting in a maximum voltage. Industry standard is to create around 1000V DC from the batteries, which can be converted to maximally $1000 * \sqrt{2/3} = 816V$ AC. This way, the cut-off voltage of battery system could be at 845V, which is the minimum required voltage to convert to 690V AC to feed the standard 690V/11kV transformer.

To obtain a voltage of around 1000V, 18 modules of 52V are placed in series, creating an average voltage of 936V. The minimum required voltage to prevent battery damage of the KoKam Lithium-Ion battery module is at 37.8V, meaning that the 18 batteries in series can safely be operated until 680V. This minimum required battery voltage is far below the 845V DC limit which is the minimum required input voltage for creating 690V AC. So when placing 18 modules in series, the battery can be operated safely between the maximum voltage and the cut-off voltage of 845V. The firing frequency of the converter's thryristors is adjusted dependent on the input voltage to always create an output voltage of 690V.

Converter The converter is that is selected for this hybrid system is a Danfoss Vacon converter[7], having a rated current of 3100 A on the input side. This means that on 1000 V, these converters have a rated power of around 3,1 MW. Therefore, four converters are needed to supply the power demand of 11,200 kW. This means that seven strings of 18 battery modules can be placed in parellel to this converter. According to the manufacturer, one of these converters costs around $190,000.00 including cooling, filtering, and housing, which means that the four converters combined cost $760,000.00 in total.

Transformer The transformer should be able to transform 690V AC to 11 kV AC on a rated power of 11,200 kW. As an example, a transformer of HTT[8] is used, estimated by HTT on $230,000.00.

Total Four blocks of batteries are connected in parellel to the transformer. These blocks consist of one converter, being supplied by 7 strings of 18 battery modules. An overview of this hybrid system design can be seen in Figure 3.5. The total investment costs of this system are shown in Table 3.8.

Battery	$ 860,000.00
Transformer	$ 230,000.00
Four converters	$760,000.00
Total	**$ 1,850,000.00**

Table 3.8: Total CAPEX hybrid system

3.5. Power Management of Hybrid System Options

In the previous sections, the most suitable storage type, the sizing, and the design of the hybrid system are explained. Chapter 2 explains the current starting decision algorithm and the 2-split operational mode. For redundancy reasons, the battery connection to the vessel's power grid should not cause the two independent engine rooms to be connected to each other, because the engine rooms would than loose their independence.

[6] Kokam Co. is a South Korean company specialised in Lithium-Ion batteries.
[7] Danfoss is a global company focused on production and services in cooling, heating, electric motors and drives.
[8] Hochspannungstechnik und Transformatorbau is a German transformator manufacturer.

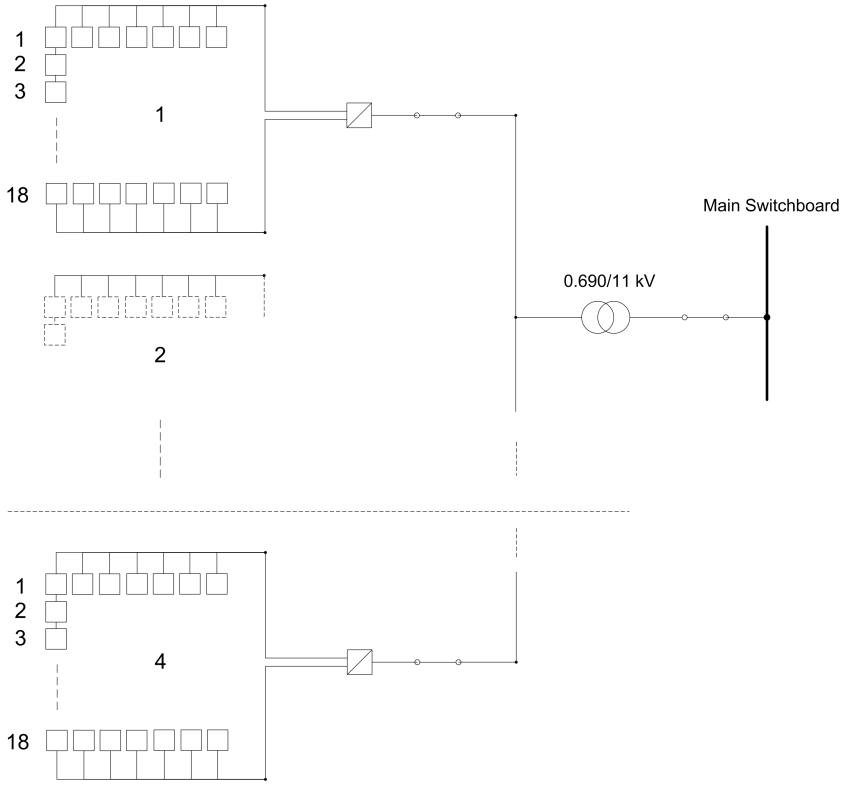

Figure 3.5: Battery Design

Therefore, in any vessel operating in DP-II mode, at least two options exist for connecting the EES to the power grid without loosing the redundancy requirement (see Figure 3.6):

1. The battery is only connected to one of the engine rooms in case of a generator failure in that specific engine room. In this situation, the biggest advantage is that only one EES device is needed in total.

2. Both engine rooms are constantly connected to an independent hybrid system separately. In this situation, two hybrid system are needed in total.

For the PMS, the fundamental difference between these two options is the starting decision principle that should be used. For option 1, no peak shaving is allowed, because the battery is only connected to the grid in case of a generator failure. This means that a PMS that is looking back in time at the measured power is not applicable, because the past generator load is not specifically telling the chance that the total running generator capacity will be exceeded in the near future. Because there is no spare generator capacity when using EES instead of spinning reserve, an exceedance of the online generator capity should be prevented in case of system option 1. In system option 2, since the battery is always connected, a back-looking starting decision algorithm -like the load dependent start- is still possible, because an exceedance of the online generator capacity can be dealt with by the continuously connected batteries.

This difference between option 1, option 2, and the old PMS of the case vessel results in different requirements of the starting decision algorithm. As explained in Section 2.4.1, the old PMS of the case vessel uses load dependent start. These new two system options require a different starting decision algorithm:

1. This system option should have started an additional generator prior to an online generator capacity exceedance.

2. This system option can still use a back-looking starting decision algorithm, where an additional generator is started when the online generator capacity is exceeded or when the battery's state-of-charge is below a set threshold.

The starting decision algorithm of system option 2 is straightforward, since it only uses one measured parameter and a simple rule of starting an additional generator when the battery has been used. The starting

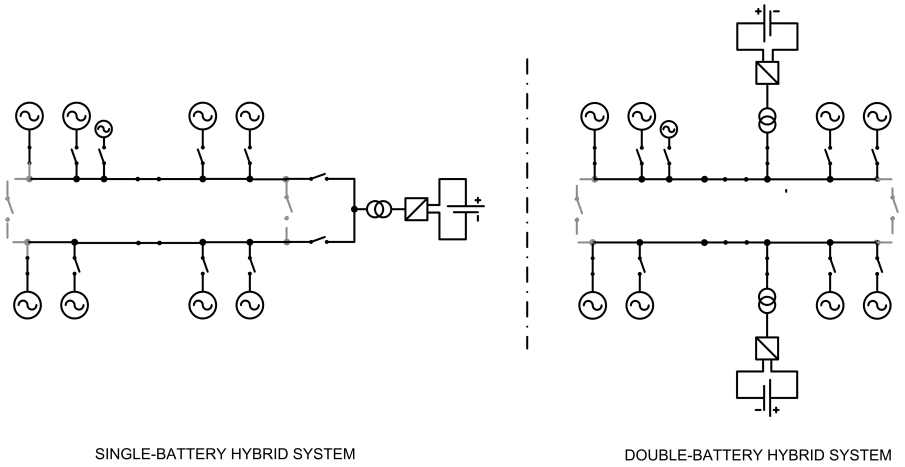

Figure 3.6: Configuration of hybrid system option 1 and 2. As can be seen in this figure, for hybrid system option 1, the battery is not connected to either of the grids in battery standby mode. For hybrid system option 2, the batteries are continuously connected to the grid. The thyristors of the converter function as switch between the battery and the power grid.

decision algorithm for system option 1 requires a sophisticated approach, since the chance of exceeding the online generator capacity in the near future given the current situation should be calculated ahead, because a starting signal should be given prior to a capacity exceedance. As shown in section 3.2.1, the starting time of a generator is 57 seconds, so when there is chance of exceeding the capacity, a starting signal should already have been given ahead, without waiting for an exceedance to happen. The differences between these two hybrid system options are summarized in Table 3.9. The next chapter compares two different approaches for this sophisticated starting decision algorithm of hybrid system option 1.

Table 3.9: Differences between hybrid system options

	Hybrid system option 1	**Hybrid system option 2**
Number of hybrid systems	1	2
Total installed energy [kWh]	800	1600
Estimated CAPEX	$1,850,000.00	$ 3,700,000.00
Starting control in PMS	Smart system	Backlooking principle, rule based
Connected to the grid	In case of a generator failure	Continuously
Occasional peak shaving	Not possible	Possible
Maturity	New technology	Used in previous research

3.6. Conclusion Electrical Energy Storage

In short, it is found that using electrical energy storage to replace the spinning reserve would potentially save 6.1% of fuel and 50% of running hours as a preliminary estimation. The potential savings are calculated here to show the feasibility and relevance of this study. If an applicable starting decision algorithm is found in Chapter 4, the fuel savings and running hours reduction will be calculated in Chapter 6 for the two different hybrid system options discussed in the previous section. In that chapter, the final fuel consumption and running hours reduction will be calculated in a full year simulation using the PMS's corresponding to the different hybrid system options.

The type of energy storage that is found to be most applicable is the lithium-ion battery, due its capabilities at high discharge rates, the lowest investment costs, smallest size, and smallest discharge rate. The estimated size of the battery is 800 kWh, which is based on the minimum amount of stored energy to supply the system with the nominal generator power for 90 seconds, taking into account the maximum discharge rate, the end-of-life capacity, and battery efficiency. The CAPEX of one hybrid system is expected to be $1,850,000.00 or €1,500,000.00[9].

[9]Using a euro/dollar exchange rate of 1.206, which is the 3 months average between 12 March and 12 June 2018.

4

Power Generation Control Methods

Because the economical and practical feasibility of using EES to replace spinning reserve in the case vessel is shown in the previous chapter, the relevance of finding a smart starting decision algorithm for hybrid system option 1 is demonstrated. As explained in the previous chapter and the problem statement, hybrid system option 1 (one battery, only to be used in case of a generator failure) requires a PMS that uses a sophisticated starting decision algorithm. This system option cannot rely on the measured power in the past, so it should use a different method for the decision of starting an additional generator. This chapter describes the assessment of the possibility of using two different PMS starting decision algorithms for a single-battery hybrid DP vessel.

First, optional starting decision methods are discussed and two of these methods which are expected to be applicable are selected for the assessment. The first mathematical-statistical method is discussed in the next section, after which a multiple linear regression approach is discussed. The following section describes the tests of the chosen starting decision algorithm in simulations using measured power data. In the last section, the conclusions on the chosen starting decision algorithm and the conclusions of that method are discussed.

4.1. Methods

For the new PMS, a method should be found that can calculate the chance of a capacity exceedance in the near future. In literature, different methods are described for the purpose of predicting power demand. These methods can roughly be divided into three different methods: mathematical methods, statistical methods and artificial intelligence methods. In literature, the mostly referred statistical methods are multiple linear regression models, semi-parametric additive models and autoregressive moving average models (ARMA) [32]. Artificial intelligence models often used for load forecasting include artificial neural networks, fuzzy regression, support vector machines and gradient boosting machines. These methods are all described briefly below.

4.1.1. Method Options

Mathematical models are models that describes the physics of a real system by mathematics, making it possible to predict the effects of real parameters on the behaviour of the real system, without physically measuring this influence. When future input parameters for the model are known, the required predictions can be made on the output of the model corresponding to this future input. For example, a mathematical model of a car can be built to predict the influence of the speed on the fuel consumption.

Multiple linear regression models use linear relations between multiple independent predictor variables and a dependent variable e.g. the relation between the domestic power consumption versus the temperature and the day of the week.

Semi-parametric additive models use parametric and non-parametric models that are combined for prediction. The parametric model is often equivalent to a linear regression model, where the future predictions based on the (finite number of) model parameters are independent of the future observations. In a

non-parameteric model, it is assumed that the predictions cannot be defined in a finite set of parameters (opposite to a regression model). A non-parametric model can grow in complexity as the amount of data grows and can change when new observations are added to the model.

ARMA modelling is a univariate method based on time series analysis. This method relies on an autoregressive part that uses a linear regression of the own lagged values and a moving average part using a linear combination of the lagged model errors. ARMA models depend on a single variable observed in time, which is also the variable it is forecasting, hence the classification univariate. In this method, linear trends and seasonal trends can also be incorporated in the forecast. For this type of modelling, it is important to make the assumption that the pattern observed in the past can be extrapolated to the future. An example is the forecast of the domestic power consumption based on the pattern of this domestic power observed before.

An artificial neural network is a black-box model having a number of input variables, some hidden layers of artificial neurons, and a number of output variables, see Figure 4.1[1]. These neurons receive an input from a predecessor and compute this to the output using an activation function of the input times a weight. A commonly used activation function is a sigmoidal function[2]. This model is trained by optimizing the weights to fit the neural network to an extensive set of training data. The trained neural network can than be used to predict future observations and is used for load forecasting.

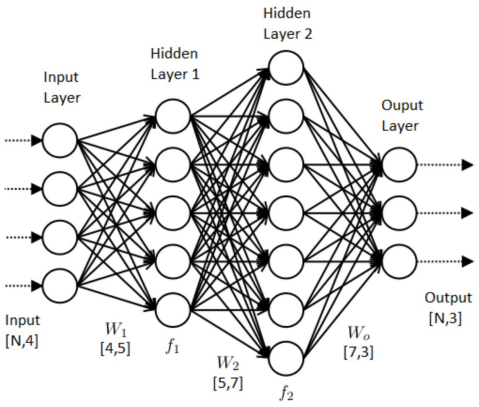

Figure 4.1: Artificial Neural Network

Fuzzy logic models make use of a set of if-then rules that compute a fuzzy forecast from a set of fuzzy input variables. The term 'fuzzy' relates to the field of fuzzy logic, where the truth of a variable can have a value between 0 and 1, in contradiction to boolean logic, where a variable can only have a truth value of 0 or 1. The input variables could either be a linguistic input, like 'very warm' as an indication of a high outside temperature, or it could be a numeric value that should be fuzzified by a fuzzy membership function. For example, an outside temperature of 30 degrees could be fuzzified to 'very warm' by the membership function, where a temperature of 20 degrees is fuzzified to 'normal temperature'. In load forecasting, a fuzzy rule could be: IF 'Previous days peak load' is 'low', AND 'forecasted maximum temperature' is 'normal', AND 'forecasted minimum temperature' is 'low', THEN 'forecasted peak load' is 'high' [53]. In a fuzzy logic model, a set of these rules is constructed based on experience and engineering knowledge. These rules combined compute a list of fuzzy outputs from the fuzzy inputs. This list of fuzzy forecasts can than be defuzzified by a defuzzification method that computes a point output from the set of fuzzy forecasts.

Support vector machines are often used in classification problems, where a user wants to define to which group a data point can be assigned. This method divides a set of data into two or more clusters separated by a hyperplane. For example, data in a 3D space is separated by a plane. For higher dimensions, hyperplanes are used up till the required amount of dimensions.

A Gradient Boosting Machine is a method of improving a classification or a regression method. This artificial intelligence method starts from a simple model and adds models to describe the residuals of the last model fit, creating a more complex model in every next step. Regularly, decision trees are used where one tree that decreases the loss function is added in every step.

[1] Obtained from: https://techblog.viasat.com/using-artificial-neural-networks-to-analyze-trends-of-a-global-aircraft-fleet/ on 13/03/2018.

[2] A sigmoidal function is an S-shaped function in order to have a continuous smooth transition from input to output. An example of a sigmoidal function is $f(x) = e^x/(e^x + 1)$.

4.1.2. Selection of Methods

When selecting a method, it should be known what data is available to the user of the system. For the case vessel, the following data is available (both real-life to be used in the PMS as historical for testing the method in this analysis): power distribution between different power groups (as explained in Section 2.4), wind speed (both measured and forecasted by weather stations), wind direction (both measured and forecasted by weather stations), significant wave height (forecasted by weather station), pipe tension, and ground speed. Given the available data, for two of the above mentioned methods, it is described below why it is expected by the author that these methods could be applicable to be used in the PMS of a single-battery hybrid DP vessel:

Mathematical-Statistical As explained in Section 2.6.3, the total load of the vessel can be split into the hotel load, DP load, and pipe laying load. The hotel load is relatively constant, so it can directly be extended to the future as a prediction. The DP load is caused by environmental forces induced by wind, waves, and current. So it is expected that the DP load can be forecasted using up-to-date weather forecasts, which the case vessel receives at a fixed time interval from different weather stations. The hypothesis is that the weather forecasts can be used in a mathematical DP model, which calculates the expected DP load based on the environmental forces. The pipe laying load shows a repetitive pattern, so it is expected that this pattern can be described by a statistical model that can recognise this pattern and forecast the load based on the found historical pattern. Therefore, it will be examined if it is possible to use a combination of a mathematical DP load model and a statistical pipe laying load model in the PMS for the starting decision algorithm. In this mathematical-statistical model, the mathematical DP model uses the weather predictions and the statistical model uses one of the statistical methods described above to find a pattern and to extrapolate this into the future. This method is further described in Section 4.2. In that section, it will also be discussed if it was found to be possible to use this method in the PMS.

Multiple Linear Regression Analysis Next to the mathematical-statistical method, recorded power- and environmental data could be used in a statistical data analysis method. If a relation can be found between the total power parameter as dependent variable and different independent parameters, the chance of exceeding the capacity can be calculated while recording these independent parameters. For this purpose, Artificial Neural Networks, fuzzy logic, or multiple linear regression analysis are expected to be useful. In the artificial neural network, several independent parameters (wind speed, vessel speed, etc.) could be the input of the first layer, where the maximum power of the coming minutes could be the output of the last layer. However, an artificial neural network requires a big amount of training data, which is not available during this research. An artificial neural network could work if it could be trained online on board for a long time, but for this analysis, a method should be found that requires less data. Fuzzy logic is a method that can translate human experience into a control system, which is not the main goal of the controller being developed in this analysis. The main advantage of fuzzy logic controllers is that these can be fed with imprecise data, which is also not the case for the controller being developed for this purpose.

Just like in an artificial neural network, a multiple linear regression model could use independent input parameters (wind speed, vessel speed, etc.) to estimate the power demand. However, a multiple linear regression model needs less data to find strong relations between the dependent parameter and the predictor parameters. Therefore, the Multiple Linear Regression Analysis (MLRA) is expected to be both a well working method as a method which is relatively easy to understand and implement. When the conditions occur where a significant chance of capacity exceedance exists (according to the Multiple Linear Regression (MLR) model), an additional generator can be started in advance. For the MLRA, it should be found which parameters influence the total power, where it is expected that environmental parameters (wind, waves, current), pipe tension, and vessel's speed might have a big correlation to the total power. Section 4.3 elaborates on the methodology and on the possibility of using a MLR model in the PMS. If it is found that the MLR method works well, further research could focus on improving this method by a semi-parametric additive model or use a different method like a gradient boosting machine.

4.2. Mathematical-Statistical (ARMA) Method

Terminology Forecasting	
Forecasting origin:	*The current moment t_0: the moment when the forecast is created.*
Prediction horizon:	*The time from the forecasting origin to the end of the forecast*
Observation time:	*The historical data where the forecast is based on up to the forecasting origin*
Univariate model:	*A model that is based on a single parameter*

Table 4.1: Terminology Forecasting

4.2.1. Method

In the mathematical-statistical approach, the goal is to forecast the load in the coming few minutes. When it is predicted that the load will pass the online generator capacity, an additional generator will be started ahead. As explained in section 2.6.3, the total load of the case vessel is split into three groups: the hotel load, the pipe laying load, and the DP load. To forecast the load, these load groups are forecasted separately, because the observed load from these three different groups have a different background and show different profiles. After forecasting the three groups seperately, the sum of these loads is the total power necessary during the forecast horizon.

Firstly, the hotel load is assumed to be constant in time, which is supported by Section 2.6.3 and Appendix A. Secondly, the DP load is a result of the environmental forces, the vessel's speed, the pipe's bottom tension and the thruster allocation of the DP system. The pipe's bottom tension and the vessel's speed are relatively constant in deep water pipe laying, so the fluctuations in the DP load are mostly dominated by the environmental forces. These are the wind, waves, and current forces. The DP load is the power needed for the vessel to move ahead slowly with a fixed heading regardless of the environmental forces and pipe tension. Thirdly, the pipe laying load, consumed by all equipment related to pipe laying, shows a repetitive character as explained in Figure 2.11 in Section 2.6.3. This load fluctuates around a constant mean and corresponds to the pattern of pipe laying having a relatively constant period. In the paragraphs below, the prediction methods of the different load groups will be explained.

Hotel Load The prediction of the hotel load is a constant extrapolation of the average of the hotel load during the observation time. The observation time is the time prior to the forecasting origin. The length of the observation time is equal to the length of the observation time of the pipe laying load forecasting method, which is discussed below.

DP Load The mathematical DP model will use the weather forecast received by the vessel, containing wind, waves, and current forecasts. From this weather forecasts, it calculates the resulting forces on the vessel and uses a simplified model of the DP system to calculate the effect of this resulting force on the power consumption. Section 4.2.7 elaborates more on the possibility of using this type of modelling for short term load forecasting of the DP load.

Pipelaying Load The pipelaying load follows a repeating pattern fluctuating around a constant average. When the bottom pipe tension is kept constant, this load is only influenced by the on board processes. In general, the bottom tension increases with decreasing water depth, but this effect is very minor during deep water pipe laying because of the flexible pipe system. Therefore, it is assumed that the average pipe laying load is only very slowly affected by the water depth so the pattern around the mean is only influenced by the on board processes during deep water pipe laying. This means that environmental forces do not influence the pipelaying load pattern.

The total consumed pipe laying load is a sum of the load of a large number of machines and equipment, including machines controlled by humans, creating unpredictable behaviour. This makes it hard to find a model for the pipe laying load based on multiple parameters like in the model of the DP load. However, when visually inspecting the pipelaying load, it is expected that it can be approximated by a reoccurring pattern that can be extrapolated into the future to forecast the load. This means that it is expected that the pipe laying load can be forecasted using only the measurements of the pipe laying load itself, which is a univariate method.

The method that will be used for the pipelaying load forecasting should satisfy the following criteria:

1. The method should be able to be used online. Because the prediction model is used for the decision of starting the next generator, it should be able to compute the forecast multiple times per minute during operation. This means that the computational time is limited to the level where an online computer is able to continuously predict the load for the coming minutes.

2. The model should be adaptive to the operation where it is used on. Different pipelaying projects can result in different welding techniques, different pipe diameters, different water depths and different laying rates, causing variations in the load pattern. Therefore, the model should be able to adapt the model paramaters to adjust to the changing load patterns.

3. Since the pipelaying load is influenced by many unknown, unpredictable variables like human handling or welding quality, it is hard to select the variables which can be measured that influence the load. However, from the pipe laying load plots, a clear pattern is recognized. That means that the model should be able to find a pattern in the previous load, without taking into account other variables than the load itself, being univariate.

Considering above three criteria, it is decided to use ARMA modelling to predict the pipe laying load in this statistical model. ARMA models are efficient predictors requiring limited computational time when the order of the model is within a reasonable limit. This holds for the computational time to set up the model, and also for the computational time to use the model for the prediction. This characteristic supports both criterion 1 and criterion 2. A limited computational time for using the model to predict the future load means that an online version is able to predict the load continuously, satisfying criterion 1. Because of the limited computational time for setting up the model itself, the model can continuously adapt to the current situation [36]. Next to that, ARMA models rely on univariata data only, where a pattern is found in the data which is extrapolated to the near future without using other variables. Fuzzy logic models, multi linear regression models, and semi-parametric additive models lack this characteristic and usually use multiple independent variables to forecast the dependent variable that is needed.

Besides, ARMA models can rely on a limited amount of data, for example, a model can be fitted to the monthly electricity demand in the last five years to forecast the electricity demand in the next year. Especially artificial neural networks lack this characteristic, because this method needs a lot of training data to train the model. This also makes this model less suitable for criterion 2, since ANN models would than be trained for a specific operational profile that could change per pipe laying project.

ARMA modelling in time series analysis is a method introduced by Box and Jenkins, who combined the properties of autoregressive and moving average models. Later, Box and Jenkins introduced the seasonal ARMA models, mostly referred to as SARMA models. The method is widely used in economics, marketing and social sciences forecasting. Also in short-term load forecasting of electric load meant for national or local power grids, ARMA is a intensively studied and well proven method [36]. In the maritime sector, ARMA modelling has been used for forecasting fish production [52] and for financial forecasting of the baltic dry index [74], but no literature was found on using it in forecasting the electric load of a DP vessel. The next section will elaborate further on using this statistical modelling method for the pipe laying load forecasting.

Total Load After forecasting the three separate load groups, the sum of these load groups is the total forecast, which is used for the starting decision algorithm. An overview of this forecasting method can be seen in Figure 4.2.

4.2.2. ARMA Modelling

Autoregressive moving average (ARMA) models are models used to extrapolate trend and patterns of time series. Time series are sets of data of a process that are sampled at equally spaced time steps. Examples are the daily maximum stock exchange rate or the monthly amount of air traffic passengers. In this thesis, the power asked by the pipe laying equipment is the time series that is analysed. The time series used in these models are assumed to be stochastic processes where every data point in time represents a random variable of which the mathematical process is not well understood, hence the use of a statistical model. The observed time series is considered as a realization of this stochastic process and is realized by the probabilistic laws covering the specific process. For this model to be used for forecasting, a strong belief of some correlation between the future observations and the current and past observation should exist. The ARMA modelling

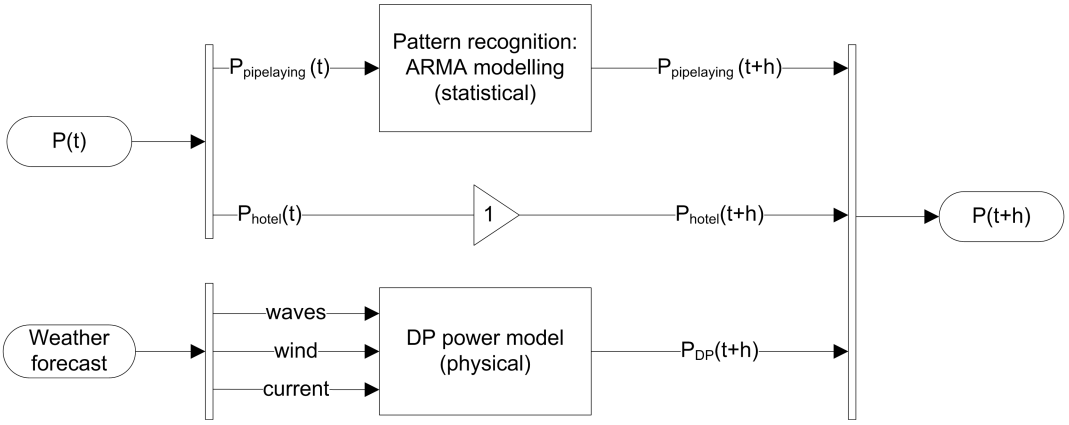

Figure 4.2: Overview mathematical-statistical load forecasting, where h is the length of the prediction horizon

method and description used in this thesis is constructed based on Montgomery et al. [42], Shumway and Stoffer [58], Box and Jenkins [17] and Neusser [47]. For an elaborated explanation of ARMA modelling in general, the reader is referred to Appendix E. This appendix also explains the process of using ARMA models for time series forecasting.

In an autoregressive AR(p) model, every observation of a process is described as a linear extrapolation of lagged observations of that same process. This can be written as:

$$x_t = \phi_1 x_{t-1} + \phi_2 x_{t-2} + ... + \phi_p x_{t-p} + \epsilon_t \tag{4.1}$$

Where:

x_t: The observation of the process at t

$x_{t-p} - x_{t-1}$: The lagged observations of the process at $\{t-p, ..., t-1\}$

$\phi_1 ... \phi_p$: The weights of the contribution of every lagged value

ϵ_t: A random error, which is an independent and identically distributed white noise signal*, having zero mean and variance σ^2. For these models, a Gaussian white noise is used, so the error terms are normally distributed.

*A white noise signal is a signal where all random values of a series are uncorrelated and have a constant mean. Here, the white noise is independent and identically distributed white noise, which means that the values are uncorrelated but drawn from the same probability density function.

In a moving average MA(q) model, the process is written as a linear extrapolation of the previous errors between observation and model. Because these errors depend on the model itself, the parameter estimation of this model is done recursively[3]. For a detailed explanation, the reader is referred to Appendix E. The MA model follows the following equation:

$$x_t = \theta_1 \epsilon_{t-1} + \theta_2 \epsilon_{t-2} + ... + \theta_q \epsilon_{t-q} + \epsilon_t \tag{4.2}$$

Where:

x_t: The observation of the process at t

$\epsilon_{t-1} ... \epsilon_{t-q}$: The error at the lagged time steps from *t-1* to *t-q*. With $\epsilon \sim N(0, \sigma^2)$.

$\theta_1 ... \theta_q$: The weights of the contribution of every lagged error

An autoregressive moving average model combines these two model types to join the strengths of both model types, so an ARMA(p,q) model is written as:

$$x_t = \phi_1 x_{t-1} + ... + \phi_p x_{t-p} + \theta_1 \epsilon_{t-1} + ... + \theta_q \epsilon_{t-q} + \epsilon_t \tag{4.3}$$

When a process has a repetitive character, it shows strong correlation between observations that are a period apart from each other. The pipe laying load is an example of such a process, because the load shows a

[3]Recursion is the phenomena where an equation is based on itself. In this case, the outcome of the error of the next time step depends on errors of the previous time steps meaning that the errors of the model are introduced by the lagged errors themselves. For the MA model, this means that the algorithm starts with an error and than calculates the next value step-by-step. "To understand recursion, you must understand recursion" David Hunter, 2011.

reocurring pattern having a relatively constant period. For these processes, a seasonal ARMA (SARMA) model can be used. In these models, a seasonal part is added to Equation 4.3. The ARMA(p,q) model than changes to a SARMA(p,q)(P,Q)$_T$ model:

$$x_t = \phi_1 x_{t-1} + ... + \phi_p x_{t-p} + \theta_1 \epsilon_{t-1} + ... + \theta_q \epsilon_{t-q} + \underbrace{\phi_P x_{t-T} + \theta_Q \epsilon_{t-T}}_{seasonal} + \epsilon_t \tag{4.4}$$

Where: T: Period of repetitive process

The paramaters are estimated by maximizing the likelihood that the observed data has been originated from the model, as explained in Appendix E.

4.2.3. Nature and Order of the Pipe Laying Load

For the online load predictor, the estimation of the model parameters changes at every time step, but the order p and q of the ARMA(p,q) model is fixed. To select the model order, the autocorrelation plot and partial autocorrelation plot of the pipelaying load of a full day are examined to find the underlaying process. According to [17], by visually inspecting these two plots of seasonally differenced[4] observed process, the process nature can be found by using Table 4.2.

	AR(p)	MA(q)	ARMA(p,q)
ACF	gradually tails off	cuts off after lag q	gradually tails off
PACF	cuts off after lag p	gradually tails off	gradually tails off

Table 4.2: Behaviour of PACF and ACF for different underlying processes [17]

The autocorrelation plot and partial autocorrelation plot of a full day pipe laying load are shown in Figure 4.3. Both the autocorrelation plot and the partial autocorrelation plot gradually tail off, indicating an ARMA process. This also means that the order of the process should be found iteratively. This iterative process is done by increasing the model order step by step, until the residuals between the observations and the model do not show significant correlation anymore. This way, the minimal required order is used, without over dimensioning the model. This iterative process is schematically displayed in 4.4. Although the order p and q cannot be found directly from the autocorrelation plot and the partial autocorrelation plot, these plots do indicate a strong seasonal component around lag 490, which would indicate the pipe laying period.

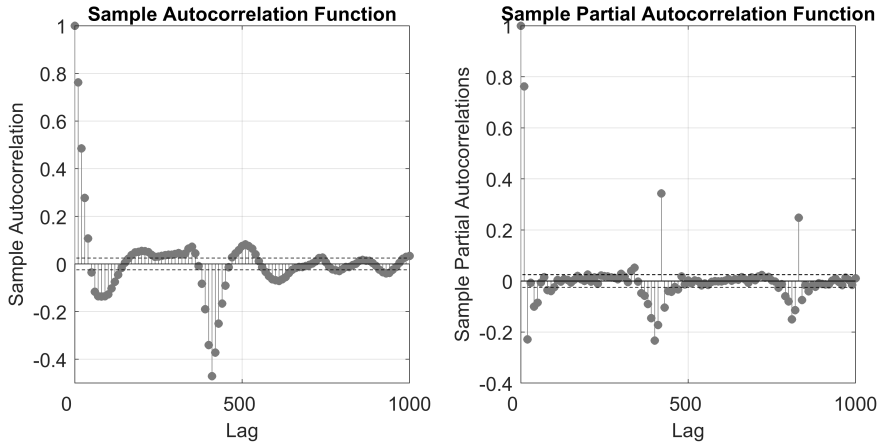

Figure 4.3: Autocorrelation and Partial Autocorrelation of pipe laying load

After seven iteration steps, the model that showed little significant correlation is defined by the SARMA(3,3)(2,3) model. The autocorrelation and partial autocorrelation of the residuals between model and observations is

[4] The observations of the pipe laying load should first be seasonally adjusted before examining the (partial) autocorrelation plot. Because the process shows a very repetitive character, the correlation of observations with the observations around them is very strong. These correlations are trivially strong and do not show the underlying process. Therefore, the observed pipe laying load is seasonally adjusted first, before plotting the autocorrelation and partial autocorrelation. For more details, the reader is referred again to Appendix E.

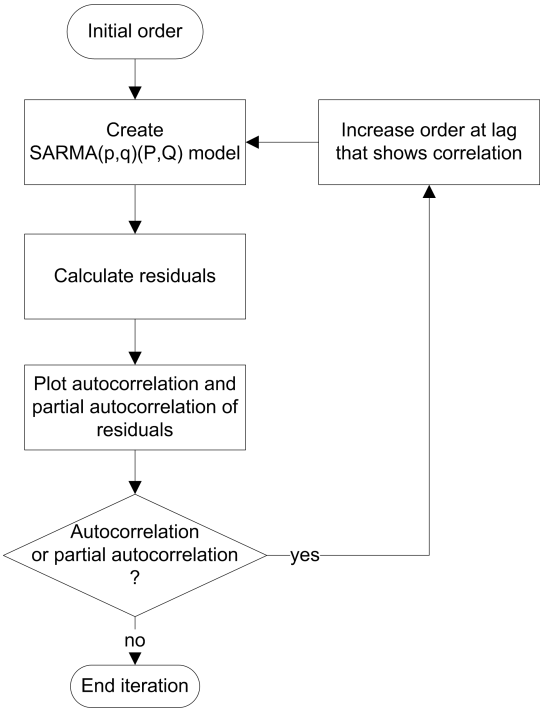

Figure 4.4: Iteration of model order

shown in Figure 4.5, where it can be seen that the residuals show little significant correlation. Increasing the order further did not reduce the correlations more, so this model is used for the pipe laying forecasting algorithm.

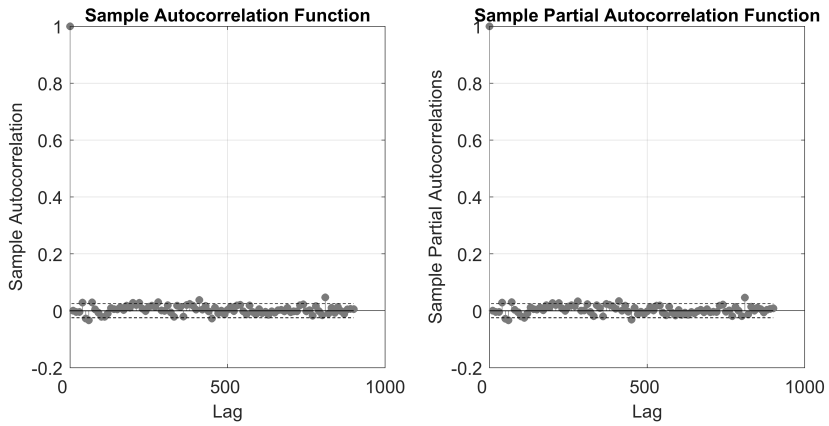

Figure 4.5: Autocorrelation and partial autocorrelation of residuals

4.2.4. Input Data

The repetitive character of the pipe laying load is well explained by Figure E.1b in Appendix E, where it is clear that a one-hour sample of the pipe laying pattern shows big autocorrelation at lags equal to the pipelaying period (390 seconds in this case). For SARMA modelling, the assumption of a constant period is an important assumption because in these models, the output of the model relies on observations and errors that are at a constant time period apart from the current time step, see Equation 4.4. In practice, it shows that the period of the pipe laying load is not exactly constant but fluctuates between five and eight minutes. Therefore, instead of using the pipe laying load directly, a temporary copy of the load is made which shows the pipe laying load at ratio's of every period, which is explained below. The model that is based on this temporary copy is used to forecast the load, where it is assumed that the pipe laying load continues at a constant period, equal to the

average period during the observation time.

The lengths of the pipe laying periods are found by finding the zero crossings of the filtered pipe laying load. These zero crossings are marked in Figure 4.6a by the black dots. In this figure -which is a twenty-minutes sample of a full day pipe load measurement- the blue line represents the measured load, where the smooth orange line is the filtered load, created by a centered moving average filter[5]. To find the periods, every length between two upcrossings of the filtered load is considered to be a pipe laying period. The filtered load is used here because it is less sensible to small peaks that cross the reference line. To find the relevant period lengths, it is required that outliers do not influence the model too much. An upper outlier in period length can be caused by a temporary stop of the pipe laying process, for example when a weld is of poor quality and has to be cut. A lower outlier can be caused by a misinterpretation of the load profile where a random fluctuation that crosses the average is considered as a pipe laying load period although it is just a minor peak. Such a misinterpretation is shown in Figure 4.6b at 850 minutes. Here, the filtered load crosses the reference line twice although obviously the length between these crossing is not considered to be a pipe laying period. In a full day measurement, this misinterpretation was found only once and filtered out as explained.

The outliers are removed from the input data to make sure the model is only fit to representative pipe laying periods. This is done to make sure that the model is actually based on the pipe laying pattern instead of random disturbances of the process or on misinterpretations of the pattern. The outliers that are removed are periods that are outside the range $[q_1-1.5(q_3-q_1),\ q_3+1.5(q_3-q_1)]$, where q_1 is the first quantile of the period lenghts and q_3 is the third quantile of the period lengths. This range is known as the Tukey range [24] and is commonly used to detect outliers. An automatic method for removing outliers is sometimes controversial to statisticians in data analysis, because the outliers are removed without knowing where they originate from. However, in this situation, the outliers are only removed to make the model robust to misinterpretations or to power fluctuations that are not representative for the pipe laying load period. The cleaned data is not used to draw any other conclusions about the load, and it is therefore considered to be acceptable to use automatic outlier detection here.

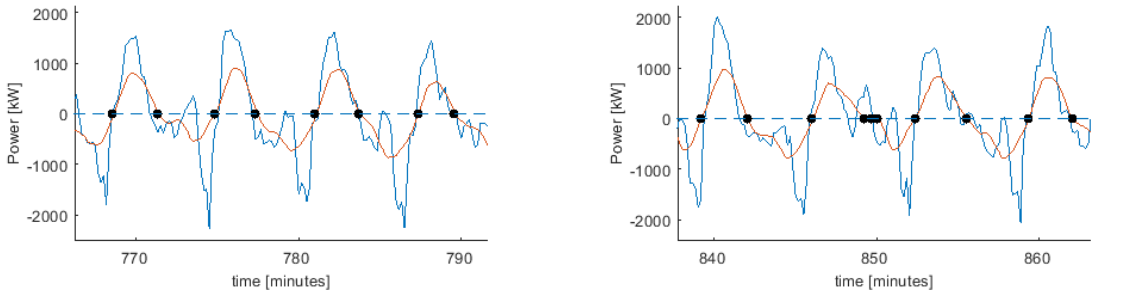

(a) Zero crossings of filtered pipe laying load

(b) Example of misinterpretation load period

Figure 4.6: Period lengths pipe laying load

After removing the outliers, the temporary load copy is created that will be used to fit a model to. This copy is generated by sampling every load period such that all temporary copies of the periods have an equal length. So instead of using the load at absolute time steps, the load at relative parts of the periods are used. For a given observation time, the average pipe laying period of that observation time is used for the forecasting, so every pipe laying period is sampled at sample time t_{sample}, which is calculated by Equation 4.5 and is visualised in Figure 4.7.

$$t_{sample} = \frac{T_{period,i}}{T_{avg,obs}} \tag{4.5}$$

Where:

T_{period} : The length of pipe laying period i

$T_{avg,obs}$: The average pipe laying period during the observation time

When there is no observation available at a sampling point, it is computed by linear interpolation between the two nearest points. During this process, i pipe laying periods having the same length of $T_{avg,obs}$ are

[5] A centered moving average filter is used for smoothening, where the filtered load at t is the average of the load across the sliding window around t. For example, when the sliding window has a length of 11, at $t = 50$, the moving average is $\hat{x}_{50} = (x_{45} + x_{44} + \ldots + x_{54} + x_{55})/11$.

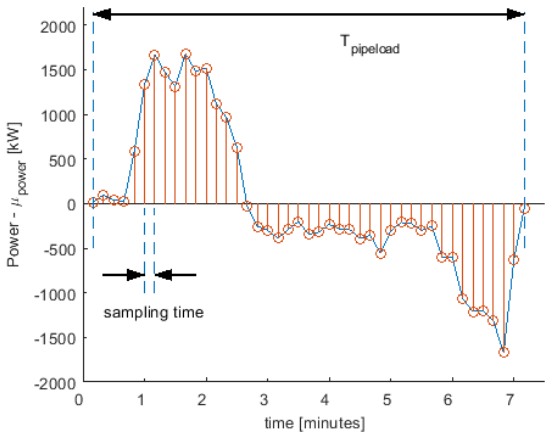

Figure 4.7: Sampling of pipelaying period i

created. These periods in line represent the temporary pipe load copy which is used to fit the model to.

4.2.5. Online ARMA Pipe Laying Load Forecasting

The order of the model is determined beforehand and is fixed in time, but because the model should be adaptive to new situations, the parameters are re-estimated at every time step. The previous subsection explained the input data that is used to fit the model to. In the online version of the PMS, this input data is reproduced at every new time step, which is then used as the input data for the re-estimation of the parameters (making the online version adaptive). So in the online version, at every new forecast origin, the parameters are estimated based on the observation time, which travels with the forecast origin, see Figure 4.8. So at time t_a, the forecast is made where the parameters are estimated based on the observations in interval $\{t_a - t_{observation}, ..., t_a - 1\}$. One time step later, at time $t_a + 1$, the parameters are re-estimated based on the observations in interval $\{t_a - t_{observation} + 1, ..., t_a\}$. This is visualised in Figure 4.8.

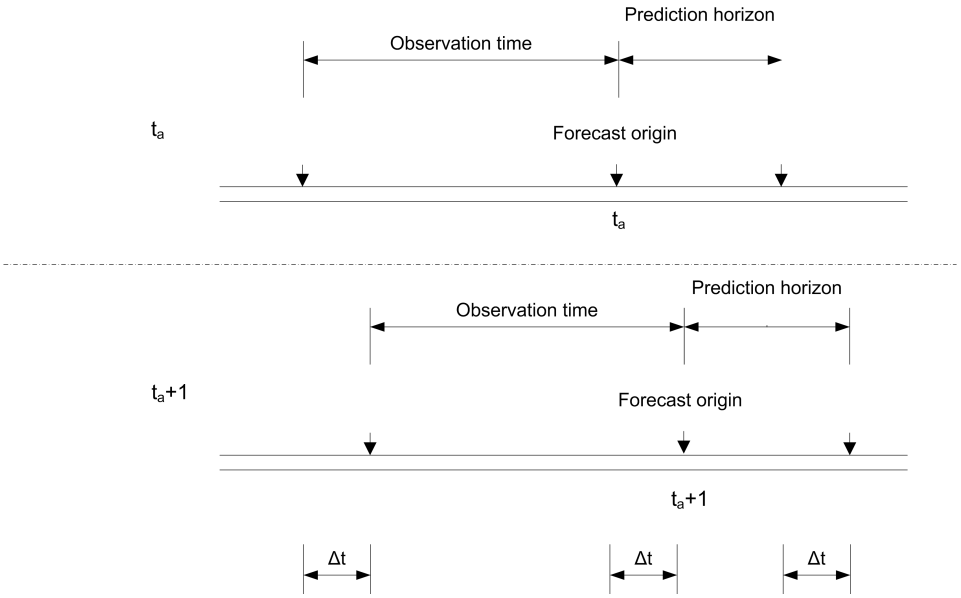

Figure 4.8: Travelling observation time and prediction horizon

The prediction horizon that is used is 90 seconds, corresponding to a save margin for the generator starting time, which is 57 seconds as tested in Section 3.2.1. The observation time is set at one hour, being a compromise between a long observation time to be statistically more certain about the average pipe laying load, and a short observation time which is better adapting to changing situations. When the parameters

are estimated, the model is used to forecast the load during the prediction horizon. This is done by substituting the estimated parameters into Equation 4.4. The load during the complete prediction horizon is than forecasted recursively for every time step.

4.2.6. Results of ARMA pipe laying load forecasting

The SARMA pipe laying forecast method is simulated for five different days. In Figure 4.9, a small window of 45 minutes is selected where the forecasted and measured pipe laying power can be compared. This figure shows that the ARMA method is functioning properly when the period of the pipe laying load is constant. However, in the same figure, the limitation of this method is shown. The last pipe laying period in this figure (between 39300 and 39650 seconds) is longer than the previous periods, causing a significant prediction error. In this case, the error is relatively large, because the forecast seems to be in anti phase compared to the measured load.

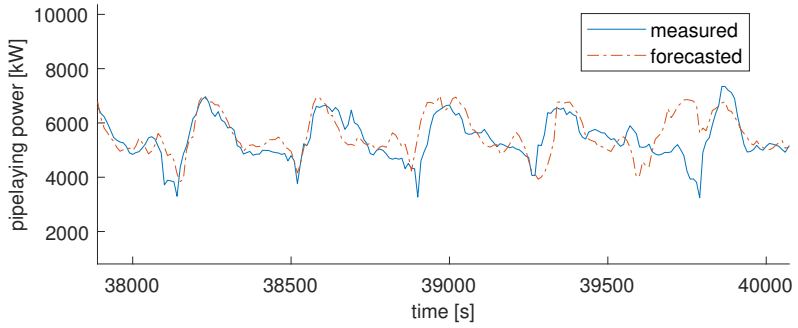

Figure 4.9: Comparison forecast vs. measured pipe laying power

A summary of the performance of these days is made in Table 4.3, showing the 95% bounds of the forecast errors and the mean absolute percentage error (MAPE). The MAPE is a method of representing the average error between the forecasted and measured time series [18]. It is calculated by Equation 4.6. The table shows that the MAPE on these five days is between 9.1% and 10.6%, indicating that the pipe laying load prediction of this method is on average 10% off. To interpret these numbers, the MAPE of a constant model is shown in the right column of the table. The constant model uses the last measured value of the observation time as the constant forecast for the entire prediction horizon. As can be seen, the SARMA pipe laying forecast is only a minor improvement compared to this simple constant model[6].

$$MAPE = \frac{1}{N}\sum_{t=1}^{N}\left|\frac{F_t - O_t}{O_t}\right| \tag{4.6}$$

Where:

N:	Total numer of observations	[observations]
F_t	Forecast value at t	[kW]
O_t	Observation value (measurement) at t	[kW]

Table 4.3: Error analysis of ARMA pipe laying load forecasting

day	5% lower bound of errors [kW]	95% upper bound of errors [kW]	MAPE [%]	MAPE constant model [%]
1	-1319	1130	10.4	10.6
2	-1464	1203	10.2	10.3
3	-1340	1161	10.6	11.2
4	-1277	1055	9.24	9.28
5	-1267	1053	9.10	10.4

In Figure 4.10a, the kernel density of the errors on day 4 is shown as an example. A kernel density plot is a computational method of estimating the probability density plot of a discrete data set. It is a subtitution of the

[6]This 'constant model' is only used to evaluate the SARMA model and find if it is of added value compared to using the last measured value of the load to forecast the load in the prediction horizon. This is done because the MAPE on its own is hard to interpret.

histogram, where the kernel density is much smoother, making it easier to recognise the probability density function [21]. From this distribution, it can be seen that the average error is 1.0% and the 95% confidence bounds are between an under-prediction of 1055 kW and an over-prediction of 1277 kW. When compared to the kernel density of the constant model forecast, it can be seen that the SARMA forecast is less biased than the constant model forecast, as the density plot of the SARMA forecast is symmetrical around the mean error. So although the SARMA model is of little added value based on the MAPE, it is an improvement compared to the constant model in terms of unbiasedness.

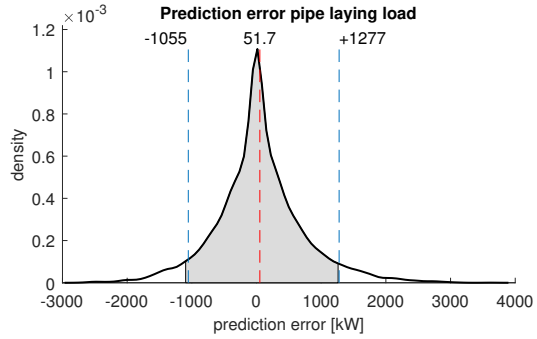

(a) Kernel density of pipe laying load prediction error using SARMA forecasting

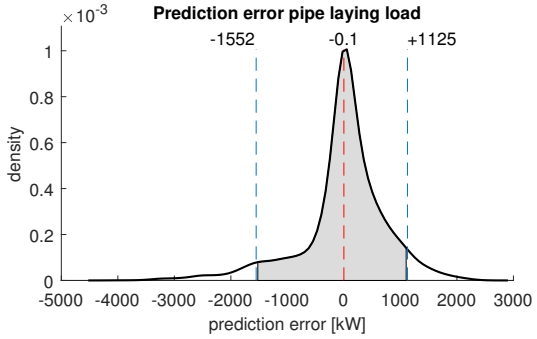

(b) Kernel density of pipe laying load predicition using constant model forecasting

Figure 4.10: Comparison density plot of SARMA pipe laying load forecasting versus constant model pipe laying load forecasting

4.2.7. DP load model

The statistical method of forecasting the pipelaying load is described in the previous sections, the mathematical method of forecasting the DP load relies on the weather data. Every three hours, the vessel receives updated weather data for the coming days. At the moment, this weather data is used on board for long-term decision making during pipe laying or heavy lift operations. For example, when it is encountered that the vessel will not be able to stay in position the next day due to heavy weather, an abandon procedure will be started, where the pipe will be abandoned in a controlled manner. The pipe is then left on the sea bed and is recovered later. In this section, it will be discussed if it is possible to use this weather data to forecast the DP load in the coming minutes.

Weather Data The data that is sent to the vessel are the 1-hour average forecasts of the:

- Wind speed;
- Wind direction;
- Wave primary peak direction;
- Wave period of spectral primary peak;
- Significant wave height.

Unfortunately, only the wind speed and the wind direction are measured on board. So before a complicated dynamic DP model is created and before additional measurements on other parameters are performed, the effect of the accuracy in wind speed and direction forecasts on the accuracy in the DP load forecast is investigated. When it is found that the errors in wind speed and direction forecasts already cause the DP load forecast to be too inaccurate, the mathematical-statistical method is rejected. Only if it is expected that the accuracy of the wind speed and direction is sufficient to calculate an accurate DP load estimation, the research into the mathematical-statistical method will be pursued and a method should be found to investigate the effect of the other environmental parameters.

Because the wind speed is accurately measured on board, the difference between forecasted and measured wind speed can be calculated. This difference is caused by two different effects:

1. The 1-hr moving average of the actual wind speed differs from the forecast;

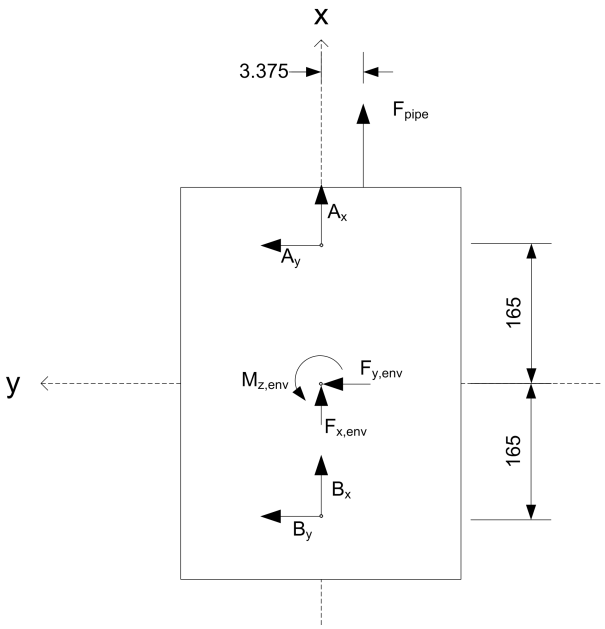

Figure 4.11: Forces on vessel

2. The actual measured wind speed is fluctuating around the 1-hr moving average.

To find difference 1, the same five days that were previously used for the pipe laying pattern, are used to compare the wind speed forecasts to the 1-hr moving average of the measured wind speed. On these five days, the variance of the error between forecast and measured 1hr average wind speed, Var_1, is found. For difference 2, the variance of the error between the measured wind speed and the 1-hr moving average of the wind speed Var_2 is calculated by subtracting the 1-hr moving average of the wind speed from the actual wind speed. When a normal distribution $N(0,\sigma^2)$ is assumed for the wind speed prediction error, the variance of this distribution is the sum of Var_1 and Var_2, since $Var(X+Y) = Var(X)+Var(Y)$ [21]. These variances can be found in Table 4.4. A variance of 6.86 means the wind speed forecast error has a standard deviation of 2.62 m/s.

Difference cause	Variance σ^2
1: weather forecast error	6.41
2: deviation from 1-hr moving average	0.45 +
	6.86

Table 4.4: Variance of wind speed forecast error

DP model To assess the effect of the variance in the wind speed forecast on the variance in the DP load, a simplified quasi-static DP model is created. The goal of this model is to do a sensitivity analysis of the DP load vs. the wind speed. It should be noted here that this model is not able to calculate the exact DP load because this would require a dynamic model of the vessel and DP system in a time-domain simulation. However, to do a sensitivity analysis on the effect of the wind speed on the DP load only, this model can be used to give insight in the effect of the wind speed error on the DP load error.

In this model, the six thrusters in the front and the six thrusters in the aft are centralized as one front azimuth thruster and one aft azimuth thruster having equivalent characteristics to all six thrusters combined. The thruster and environmental forces are shown in Figure 4.11. By solving the sum of forces and moments on the vessel the required thrust of the DP system to keep position can be calculated.

To estimate the required thrust the DP system should deliver, the least-squared solution of the following system of equations of all forces is solved:

$$\begin{bmatrix} 1 & 0 & 1 & 0 \\ 0 & 1 & 0 & 1 \\ 0 & L_a & 0 & -L_b \end{bmatrix} \begin{pmatrix} A_x \\ A_y \\ B_x \\ B_y \end{pmatrix} = - \begin{pmatrix} F_{env,x} + F_{pipe} \\ F_{env,y} \\ M_{env} + 3.375 F_{pipe} \end{pmatrix} \tag{4.7}$$

In which:

$$\begin{aligned} F_{env,x} &= c_{x,wind} \cdot v_{wind}^2 \\ F_{env,y} &= c_{y,wind} \cdot v_{wind}^2 \\ M_{env} &= c_{z,wind} \cdot v_{wind}^2 \end{aligned} \tag{4.8}$$

The coefficients $\{c_{x,wind}, c_{y,wind}, c_{z,wind}\}$ are determined by model tests at Marin and depend on the relative direction of the wind with respect to the vessel.

From the force components of the azimuth thrusters, the required thrust is calculated by Equation 4.9, where it is assumed that the azimuth thrusters can rotate freely.

$$\begin{aligned} |T_A| &= \sqrt{A_x^2 + A_y^2} \\ |T_B| &= \sqrt{B_x^2 + B_y^2} \end{aligned} \tag{4.9}$$

It is assumed that the relation between thrust and rpm is quadratic[7] and it is assumed that the relation between power and rpm is cubic[8] [75]. This means that the relation between the required thrust and required power can be derived by:

$$\begin{aligned} T(n) = T_{nom} \left(\frac{n}{n_{nom}} \right)^2, \quad P(n) = P_{nom} \left(\frac{n}{n_{nom}} \right)^3 \\ \sqrt{\frac{T}{T_{nom}}} = \frac{n}{n_{nom}}, \quad \Rightarrow \quad P(T) = P_{nom} \left[\left(\frac{T}{T_{nom}} \right)^{0.5} \right]^3 \\ P(T) = P_{nom} \left(\frac{T}{T_{nom}} \right)^{1.5} \end{aligned} \tag{4.10}$$

Where: P_{nom}: $6 \cdot P_{nom,1thruster}$: the nominal power of the thruster at n_{nom}
T_{nom}: $6 \cdot T_{nom,1thruster}$: the nominal thrust of the thruster at n_{nom}

The model is tested for different wind speeds at a full range of relative directions. The results are shown in Figure 4.12, where it can be seen that wind from port side results in the highest required power. Wind from the front results in the least amount of required power, as was expected.

Sensitivity analysis of DP load vs. wind speed The mean of the wind speed of the five days that were previously analysed was 10.1 m/s. As said, the variance of error in wind speed forecasts was 6.86. Therefore, for the sensitivity analysis of the DP load accuracy vs. the wind speed forecast accuracy, a Gaussian $N(\mu, \sigma^2) = N(10.1, 6.86)$ distribution is used for the wind speed forecast. To assess the maximum impact of the wind speed inaccuracy, the relative direction of the wind is fixed to 90 degrees. The goal here is to find the distribution of the DP-load forecast when the distribution of the wind speed forecast is known. Using this wind speed prediction distribution (see Figure 4.13 a) and the method of estimating the DP load described above, the distribution of the DP load estimation can be seen in Figure 4.13 b.

[7] During pipe laying, the propellers have zero to nearly zero advance speed because the forward speed of the vessel is almost zero (on the five days previously used, 99% of the time, the ground speed is below 0.53 m/s, or 0.27 kn). Besides, the inflow of most thrusters is not parallel to the forward speed of the vessel, since most force should be directed opposite to the forces induced by the environment (wind, waves, current). Therefore, bollard pull conditions are used here, having zero to nearly zero advance speed. In bollard pull conditions, K_T should be constant and the thrust can be assumed to have a quadratic relation to the rotational speed of the propeller according to: $T(n) = K_T \rho n^2 D^4$ [75]. When varying the rotational speed between 10 and 680 rpm and varying the advanced speed between 0 and 0.53 m/s, the range of K_T is between 0.49 and 0.44, see appendix F for the propeller open water diagram. Therefore, this assumption seems reasonable.

[8] When following the same reasoning for the power curve with respect to the rotational speed, the power follows the relation: $P(n) = K_Q \rho n^3 D^5$. The range of K_Q is between 0.435 and 0.432, so the assumption of a cubic relation between power and rotational speed seems reasonable. This is supported by full scale measurements during sea trials, which can be seen in Figure F.2 in Appendix F.

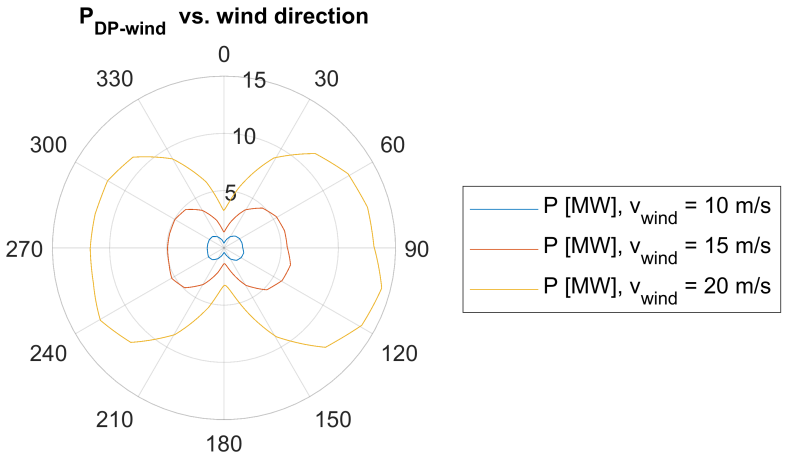

Figure 4.12: Static DP power vs. wind direction ($v_{current} = 0, H_s = 0$)

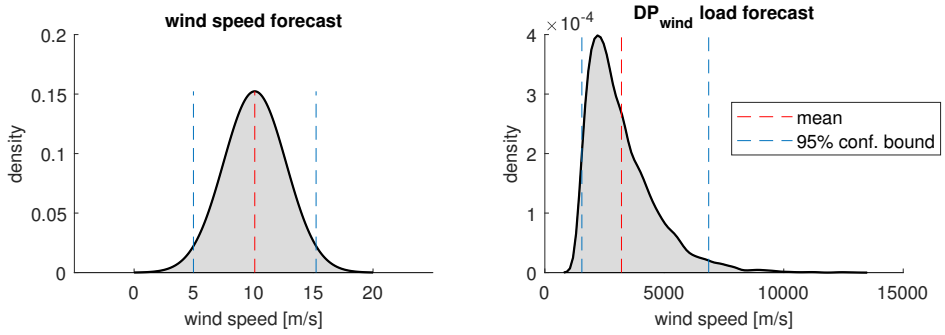

Figure 4.13: Sensitivity of DP load forecast to wind speed forecast at wind direction of 90 degrees. The variance of the DP load forecast is $1.96 \cdot 10^6$, so the standard deviation is 1.40 MW.

From this figure it can be seen that the forecast error of the wind speed causes a wide spread in DP load forecasts. Because of the high variance of the wind speed forecast, the forecast in DP load caused by this wind speed also has a high variance of $1.96 \cdot 10^6$, corresponding to a standard deviation of 1.40 MW. The probability density function of the estimated DP load due to the wind is skewed to the left because of the cubic relation between wind speed and DP load, see relation 4.11.

$$P_{DP,wind} \sim c \cdot T^{1.5} \sim c \cdot (v_{wind}^2)^{1.5} = c \cdot v_{wind}^3 \tag{4.11}$$

When the probability density function of the wind speed forecast of Figure 4.13 is used, the 95% confidence bound of the DP load forecast is: {1500; 6800} kW. This suggest that the range of the wind speed forecast causes a DP load forecast to have a range of 5.3 MW, which is only caused by the error in wind speed forecast already. When this is compared to the forecasting method where the last measured value of the DP load is taken as the forecast for the entire prediction horizon, the forecast using the last measured value is more accurate, see Table 4.5. This means that using the weather forecasts for DP load forecasting is not of added value compared to the DP load measurements. The error introduced by this method of DP load forecasting would only be higher than the change in DP load during the prediction horizon. When there is an error introduced by the current speed and by the wave height as well, the error in DP load forecast using these environmental forecasts could even be higher.

4.2.8. Conclusion Mathematical-Statistical (ARMA) method

The goal of this method was to assess the possibility of using a mathematical-statistical method to forecast the total generator load in the observation time accurately enough to be used in the PMS as starting decision algorithm. When referring back to the starting decision algorithm overview of Figure 4.2 at page 38, the total forecasted generator load was a sum of the pipe laying load, the hotel load, and the DP load. The mea-

Table 4.5: Comparing variance of DP load by wind speed forecast and by last measured DP load value

	Variance
DP load forecast using wind speed forecasts	1.96E+06
DP load forecast using last measured DP load value extended into prediction horizon	1.00E+06

sured hotel load in the observation time could directly be extended into the prediction horizon due to the constant character, which works properly. A seasonal autogressive moving average model (ARMA) was found to work properly when the pattern of the pipe laying load has a constant period. However, the limitation of this method is a changing pipe laying period, for example due to a human error in the pipe laying process. It was found that extending the pattern found in the observation time could cause a big forecast error when the forecasted and true pipe laying load are in anti phase. During a simulation of this method for five days of pipe laying, the mean absolute percentage error (MAPE) of the forecasts was 9.91%, which is only a minor improvement compared to the MAPE of a (relatively simple) constant model. This constant model uses the last measured pipe laying load as a constant forecast resulting in a MAPE of 10.4%. When comparing the probability density function of the prediction error, the ARMA model did show an improvement in unbiasedness of the forecast compared to the constant model. In short, because the period of the pipe laying process is not perfectly constant, forecasting the pipe laying load using a seasonal ARMA model causes problems when the pipe laying period is changing.

Although the results of the hotel load forecast look promising and the the pipe laying load forecasts are at least an improvement compared to using the last measured value, forecasting the DP load by a mathematical method using the weather forecasts is not of added value compared to the last measured value of the DP load at the forecast origin. Since it is believed that the current measurement of the DP load does not give enough information about the DP load in the prediction horizon and since the seasonal ARMA method of pipe laying load forecasting is also limited, using the mathematical-statistical method in the PMS is rejected. Therefore, another method should be found to use as starting decision algorithm in the PMS of a single-battery hybrid DP vessel. The next section elaborates on the possibility of using Multiple Linear Regression Analysis (MLRA) in the starting decision algorithm.

4.3. Multiple Linear Regression Analysis Method

The second method that is tested is a Multiple Linear Regression Analysis (MLRA) on the generator power and different parameters that influence the generator power. In MLRA, it is is examined how different independent parameters influence one dependent parameter. In the following parts, the relevant literature, the method, parameter selection, input data, and model discussion are described.

4.3.1. Literature Review Multiple Linear Regression Analysis

In [25], MLRA was used to improve the estimation of the fuel consumption based on the on board navigation data. In this paper, the goal was to improve this estimation compared to the regular method of using speed-power curves. In this analysis, the dependent variable was the fuel consumption per mile, and the predictor variables used for the regressions where: mean speed over ground, mean head wind, mean side wind, mean displacement, stabilizer fin usage, the cumulative docking time, and engine operation mode. A linear model of the dependent variable, based on the predictor variables was constructed as:

$$Q = \beta_0 + \beta_1 X_1 + ... + \beta_q X_q + \epsilon \tag{4.12}$$

Where:
- $\beta_0..\beta_q$: Regression coefficients
- $X_1..X_q$: The predictor variables
- ϵ : The error between the model and observations

The regression coefficients where found by a least-square estimation based on the observations of the fuel consumption at different trips, where the predictor variables where measured. In this article, the strength of the model was analysed by examining the residuals between the model and the observations. It was stated that when the residuals are normally distributed with constant variance σ^2 the model could be considered as accurate.

In [44], MLRA was used to predict the effect of the shape of a building on the heating or cooling energy consumption of that building in two different climate conditions. The energy data was created by a Monte-Carlo simulation where the energy consumption for cooling or heating was calculated based on a set of building paramaters. The goal was to be able to make a preliminary heating or cooling estimation in an early design stage, based on a set of building parameters. In the simulation, seventeen different paramaters like floor insulation, ground floor construction, and roof absorbance were varied to estimate the energy consumption. From the data obtained by the simulation, the linear regression model was created by least-square-estimates. In this paper, the accuracy of the model was tested by the coefficient of determination (R^2), the F-test, and by calculating the root mean squared error (RMSE). However, only the coefficient of determination of the linear models was presented in this article.

In [48], MLRA was used to estimate the state of health of a car's battery based on several parameters that are measured by the car's monitoring system. First, for 27 different parameters, a scatter plot was used to visually find the relation between a parameter and the state of health of the battery. After that, the parameters that were not well measured were removed from the analysis. The residual parameters were used to find the correlation coefficient between these parameters and the state of health of the battery. From this table of correlation coefficients, the redundant parameters and the parameters having a very low correlation coefficient to the state of health, were removed. Three parameters remained for the multiple linear regression, which were used in an alarming system of an approaching battery failure.

4.3.2. Method

For the PMS, the goal is to find a starting decision algorithm that starts an additional generator when the chance arises that the online generator capacity will be exceeded. The total generator load is a sum of the slowly changing moving average and the rapidly fluctuating power peaks compared to this moving average, see Figure 4.14.

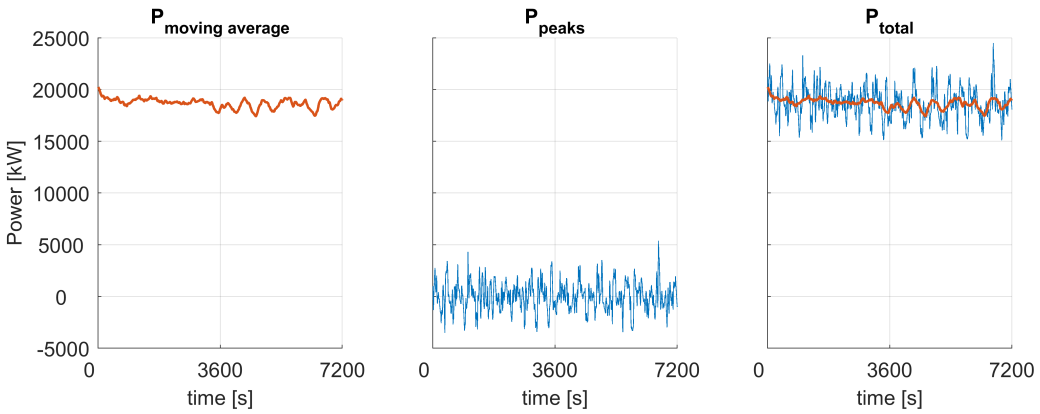

Figure 4.14: Sum of moving average and power peaks in 2-hr time frame. A moving average window of 4 minutes is used here, which is explained below.

The moving average of the total generator power of the last minutes can be measured and it is believed that the ratio between the power peaks and the moving average depend on different independent parameters like wind, waves, current, the vessel's speed, and the pipe tension. If the ratio between the moving average and the power peaks could be found, a generator could be started when there is a chance of an online generator exceedance, given the moving average of the measured load and the peak-to-mean ratio of the load (predicted by the predictor paramaters of the MLR model). The peak-to-mean ratio is found by the linear regression model, using the relevant input parameters. Section 4.3.3 will elaborate on how the relevant parameters are found. When the conditions arise where the measured moving average of the power times the peak-to-mean ratio (estimated by the MLR model) have a chance of exceeding the online generator capacity, an additional generator is started, see Figure 4.18. In Figure 4.15, the definition of the peak-to-mean (ptm) ratio is shown. The peak-to-mean ratio is defined as:

$$ptm = \frac{p}{m} \tag{4.13}$$

Where:

p: Peak height w.r.t. the moving average, see Figure 4.15 [kW]

m: The moving average of the measured load in the sliding window $\{t_{now} - W_{mov.avg} : t_{now}\}$ where $W_{mov.avg}$ is the moving average window length. So this is the time prior to the current moment which is used to calculate the moving average of the measured power. See Figure 4.15. [kW]

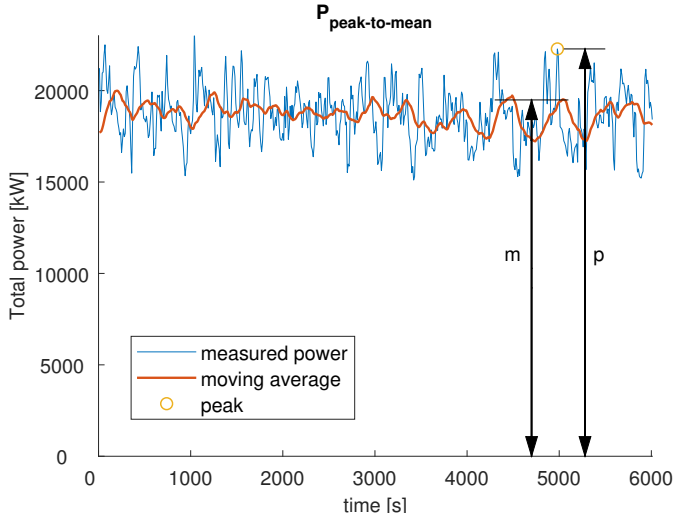

Figure 4.15: Definition of peak-to-mean ratio. The moving average of the generator power that is shown here at every time step t is the moving average of the 4 minutes prior to time t. So the sliding window of the moving average is 4 minutes shifted to the left. In the online version that would be used on board, the moving average that is used in the starting decision algorithm is also the moving average of the 4 minutes prior to the current moment, because only the power of the past can be measured. The specific length of 4 minutes is explained below.

The length of the moving average window is a compromise between a short window to only use the relevant measured load and a long window to effectively filter the power peaks. It is desired to have a short moving average window because the load measured more recently is more relevant for the load of the coming minutes than the load measured further in the past. However, when the moving average window is chosen too short, peaks are not filtered out, and no peak-to-mean ratio can be calculated. Therefore, the moving average window is chosen iteratively to fulfil both criteria.

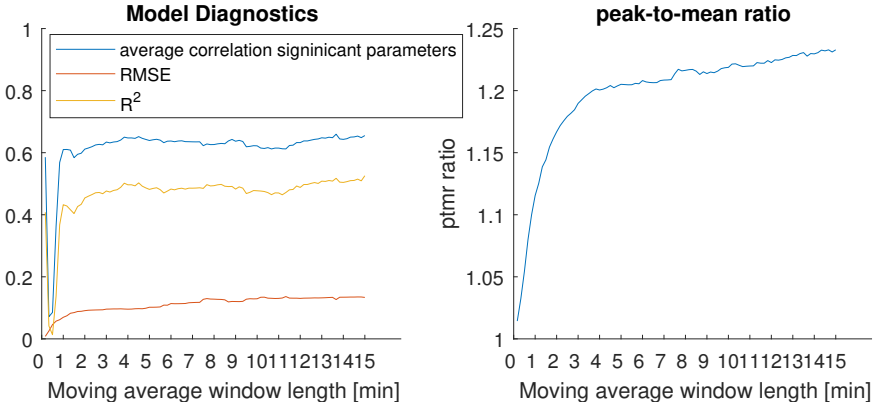

Figure 4.16: Left: effect of moving average window length on model diagnostics. Right: Effect of moving average window length on average peak-to-mean ratio of the power.

First, a moving average window of six minutes was chosen based on the visual inspection of the load profile, where it was found that typical load peaks last around one to two minutes. Using this moving average window, the multiple linear regression analysis was performed, and the useful model parameters were chosen, using the method that will be described in Section 4.3.3. Using these relevant parameters, the effect of

the moving average window on the model diagnostic parameters was found. The effect of the moving average window length on the model diagnostics and on the average peak-to-mean ratio of the power can be seen in Figure 4.16. From the effect of the window length on the peak-to-mean ratio (Figure 4.17 b), it can indeed be seen that when using a short moving average window, the peaks are not filtered out, and no peak-to-mean ratio exists. When extending the moving average window length, the peak-to-mean ratio increases, because the filtered load will be less likely to follow the same path as the unfiltered load (the difference between filtered and unfiltered peaks increases). After four minutes, the rate of the increasing peak-to-mean ratio declines, after which it only increases moderately. From the left graph of this figure, it can be seen that the diagnostics of the model (which will be explained in Section 4.3.6) are relatively constant from a moving average window of three minutes or higher. As said before, it is desired to have a short moving average window because the load closer to the current moment is more relevant to the next minutes than the load further in the past. However, a minimum window length is needed to actually measure the peak-to-mean ratio. In Figure 4.16, it can be seen that both conditions are met when using a moving average window of four minutes. After using this moving average window, the parameters that were selected as the relevant parameters for the MLR model were unchanged compared to the initial six minutes moving average window. Therefore, the moving average window length of four minutes is used in the MLR model, and no further iteration steps were needed. An overview of this iteration is shown in Figure 4.17.

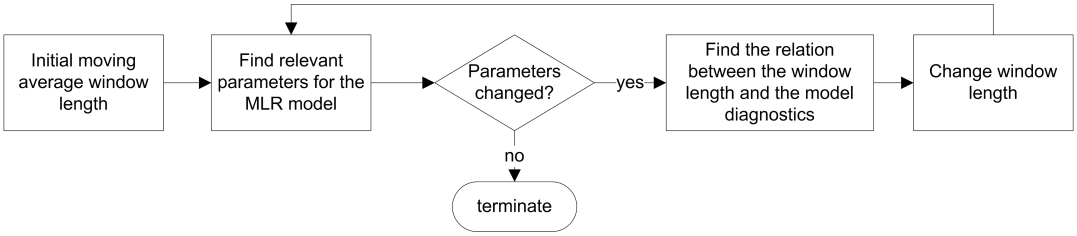

Figure 4.17: Iteration steps of finding moving average window length

For an overview of the starting decision algorithm using MLRA, see Figure 4.18. In the coming sections, the goal is to find the linear model that can predict a confidence interval of the peak-to-mean ratio when the model input parameters are measured on board.

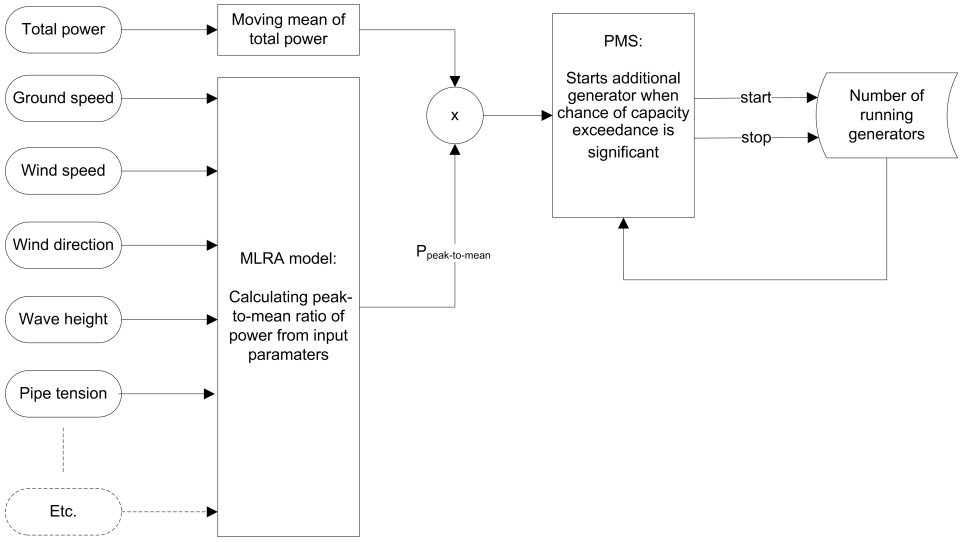

Figure 4.18: Overview of starting decision algorithm using MLR model

4.3.3. Selection of Parameters

On board, a number of parameters are measured continuously and stored in a data logging system. For the regression model, the parameters that are relevant for the peak-to-mean ratio should be found. From the data logging system, the measured paramaters that are expected to be relevant for the MLRA are listed in

Table 4.6. In this list of parameters, the significant wave height is the only parameter that is not measured directly, because there is no system on board that is accurately measuring the wave height. This parameter is therefore used from the weather forecasts that are send to the vessel every hour. Although this might be different from the actual wave height because of a forecast error, it is believed that a relation could be found between the wave height forecasts and the peak-to-mean ratio of the power, because of an expected high correlation between forecasted and actual wave height. That means that the peak-to-mean ratio of the power would have an indirect correlation to the forecasted wave height through the correlation between peak-to-mean ratio and the actual wave height and the correlation between the forecasted and the actual wave height. Section 4.3.5 elaborates more on the correlations found for all parameters.

Table 4.6: Measurements used in MLRA

Parameters	**Unit**	**Sensor**
Wind speed	[m/s]	Wind monitors at different locations of the vessel
Relative wind direction	[deg]	Wind monitors at different locations of the vessel
Pipe laying load	[kW]	Sum of all breaker sensors at main switchboards that supply power to the firing line
DP load	[kW]	Sum of all breaker sensors at main switchboards that supply power to the thrusters
Ground speed	[m/s]	dGPS
Pipe tension	[tons]	Sum of tension in tensioner drives
Significant wave height	[m]	*From weather forecasters*

From this list of potentially relevant parameters, a list of eight potentially relevant features is made. These features can be found in Table 4.7. One of these features is the estimated DP_{wind} load, which is calculated using both the wind speed and direction. In Figure 4.12, it was shown that the load on the DP system due to the wind depends very much on the direction of this wind. Therefore, next to using the wind speed and instead of using the wind direction directly in the MLRA, the estimated DP load due to this wind speed and direction is also used in the MLRA. The DP_{wind} load is estimated by using the DP model described in Section 4.2.7. The features peak-to-mean DP_{wind} load, peak-to-mean ground speed, and peak-to-mean pipe laying load are calculated using the same methodology as the peak-to-mean of the power, as was explained by Figure 4.15.

Table 4.7: Features for MLRA

	Features	**Unit**	**From**
1	Estimated DP wind load due to wind speed and direction	[kW]	Calculated by DP model
2	Significant wave height	[m]	Weather forecasters
3	ptm estimated DP wind load	[kW/kW]	Calculated
4	Pipe laying load	[kW]	Measured at switchboard breakers
5	ptm pipe laying load	[kW/kW]	Calculated
6	Wind speed	[m/s]	Wind sensors
7	Ground speed	[m/s]	dGPS
8	ptm ground speed	[(m/s)/(m/s)]	Calculated

In the next section, the power data that is used for the MLRA is discussed. After that, for the eight features mentioned before, it will be examined which features show a significant correlation to the peak-to-mean ratio of the power.

4.3.4. Power Data

To train the model, it is desired to use all power data available in the data logging system on board of the case vessel. However, there is a practical limitation to the amount of data that can be used in this analysis, because the data on board is sent to shore via a satellite connection, which has a limited bandwidth. Therefore, weather data during the last full year of operation is inspected and it is endeavoured to find power data that covers the total range of sea states[9] the vessel encountered during this year. The distribution of sea states

[9]For sea states, the World Metereological Organization (WMO) coding is used [64].

can be found in Figure 4.19. As can be seen in this table, a wide range of sea states are covered using this list of days. However, further research could improve the model by using more different days in the regression analysis, e.g. by continuously training the model online during operations.

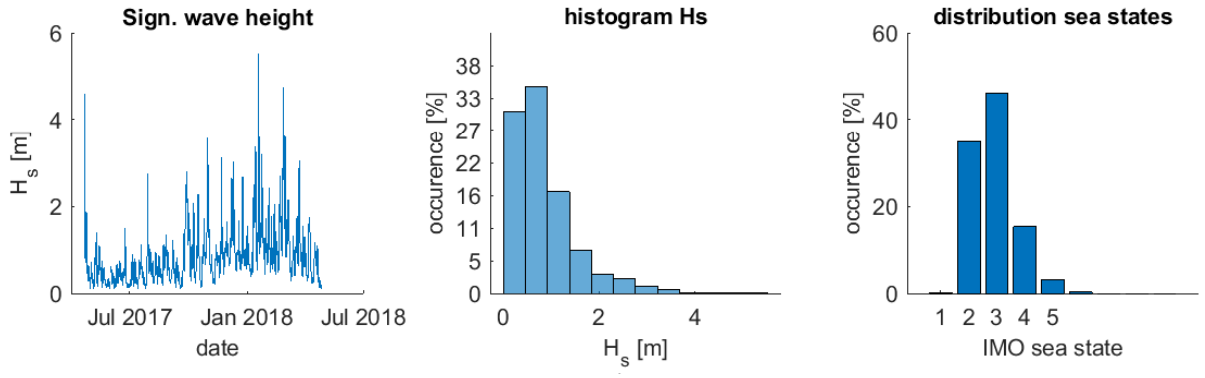

Figure 4.19: Distribution of significant wave height and sea states throughout last operational year

From this sea state distribution, power data is selected to be used in the MLRA. The data that was already available for the mathematical-statistical analysis is used for the MLRA, and seven extra days are added to cover the light and the rough sea states. The days that are used in the MLRA are listed in Table 4.8.

Table 4.8: Model Training and Testing Data

date	**average Hs [m]**	**maximum Hs [m]**	**sea state**
Training data			
11/10/2017	0.3	0.5	2
26/10/2017	1.0	1.6	3
25/12/2017	2.1	2.3	4
26/12/2017	0.9	1.6	3
10/01/2018	1.6	2.3	4
13/01/2018	2.6	3.0	5
15/01/2018	1.2	1.9	3
18/01/2018	3.2	5.4	4-6
02/02/2018	1.1	1.8	3
21/02/2018	2.3	2.7	4 -5
Testing data			
09/28/2017	2.5	2.7	5
26/02/2018	3.7	4.7	5 - 6

From all available power data, 10 days are selected to train the model and two days are left for testing the PMS later on, which is a common practice in model testing [44]. The days that are left for testing the PMS are two days having rough to very rough sea states, because these are the days where the starting decision algorithm is really in use. In calm sea states, the requested power is relatively constant, so there is little action required from the PMS. The testing data will be used in the online PMS tests in Section 4.4.

4.3.5. Correlations and Model Formulation

To find which features influence the peak-to-mean ratio of the power, the linear correlation between all features is found. The features that show significant correlation to the peak-to-mean ratio of the power are used to set up the regression model. As a measure of the linear dependence between two parameters, the correlation coefficient is often used. The correlation coefficient that is used in this analysis is the Pearson sample correlation coefficient [7]:

$$r_{xy} = \frac{cov(x,y)}{\sigma_x \sigma_y} = \frac{1}{N-1} \sum_{i=1}^{N} \left[\left(\frac{x_i - \bar{x}}{\sigma_x} \right) \left(\frac{y_i - \bar{y}}{\sigma_y} \right) \right] \tag{4.14}$$

Where:
- N : Length of series x and y
- x_i : Observation of parameter x at time step i
- y_i : Observation of parameter y at time step i
- $\bar{x}$: Sample mean of parameter x
- $\bar{y}$: Sample mean of parameter y
- σ_x : Sample standard deviation of parameter x
- σ_y : Sample standard deviation of parameter y

The Pearson correlation coefficient between all parameters is shown in the correlation matrix in Table 4.9. On the diagonal of this matrix, all correlations are equal to one, because a correlation of a parameter with itself is equal to one by definition.

Table 4.9: Correlation matrix of all features

		ptm power	DP_{wind} load	H_s	ptm DP_{wind} load	pipe load	ptm pipe load	v_{wind}	ground speed	ptm ground speed
	ptm power	1.00	**0.70**	**0.61**	**0.67**	-0.20	-0.18	**0.59**	0.36	0.36
1	DP_{wind} load		1.00	**0.80**	**0.84**	-0.36	-0.32	**0.90**	0.28	0.37
2	H_s			1.00	0.78	-0.46	-0.52	**0.77**	0.14	0.40
3	ptm DP_{wind} load				1.00	-0.43	-0.45	**0.74**	0.19	0.30
4	pipe load					1.00	0.67	-0.33	0.31	-0.08
5	ptm pipe load						1.00	-0.30	0.21	-0.09
6	v_{wind}							1.00	0.18	0.29
7	ground speed								1.00	0.29
8	ptm ground speed									1.00

In the correlation matrix, it can be seen that four features show a significant correlation to the peak-to-mean ratio of the power:

- DP_{wind} load;
- Significant wave height;
- Peak-to-mean of DP_{wind} load;
- Wind speed.

The estimated DP_{wind} load shows a strong correlation to the wind speed because the wind speed is directly used to calculate this estimated DP_{wind} load, as was explained in Section 4.3.3. Since the wind speed is already included in the estimated DP_{wind} load, and because this feature shows a stronger correlation to the peak-to-mean ratio of the power than only the wind speed itself, it is decided to only use the estimated DP_{wind} load. Using the wind speed itself as well would be redundant for the regression model and would result in an over-fitted model. The same applies for the peak-to-mean ratio of the DP_{wind} load vs. DP_{wind} load itself. Therefore, it is decided to only use the significant wave height and the DP_{wind} load in the MLR model. This decision is supported by evaluating the difference in root-mean-squared error for a MLR model that used the peak-to-mean ratio of the DP_{wind} load vs. a MLR model that does not use the peak-to-mean ratio of the DP_{wind} load. The difference in RMSE between these two options is only 1.1%, which indicates that the MLR model is hardly improved by adding this parameter. What is further interesting to notice from this correlation matrix, is the strong correlation between the significant wave height and the wind speed, as could have been expected, because heavy wave heights could be a result of rough weather.

Using the significant wave height and the estimated DP_{wind} load as predictors and the peak-to-mean ratio of the power as the response variable, the multiple linear regression model is written as:

$$ptm(P_{DP,wind}, H_s) = \beta_0 + \beta_1 P_{DP,wind} + \beta_2 H_s \tag{4.15}$$

The model parameters are estimated by QR decomposition[10], and can be found in Table 4.10. Figure 4.20 shows a visualisation of the linear model, using these parameter estimates.

$\hat{\beta}_0$	0.97
$\hat{\beta}_1$	$1.24 \cdot 10^{-5}$
$\hat{\beta}_2$	0,079

Table 4.10: Linear regression model parameter estimates

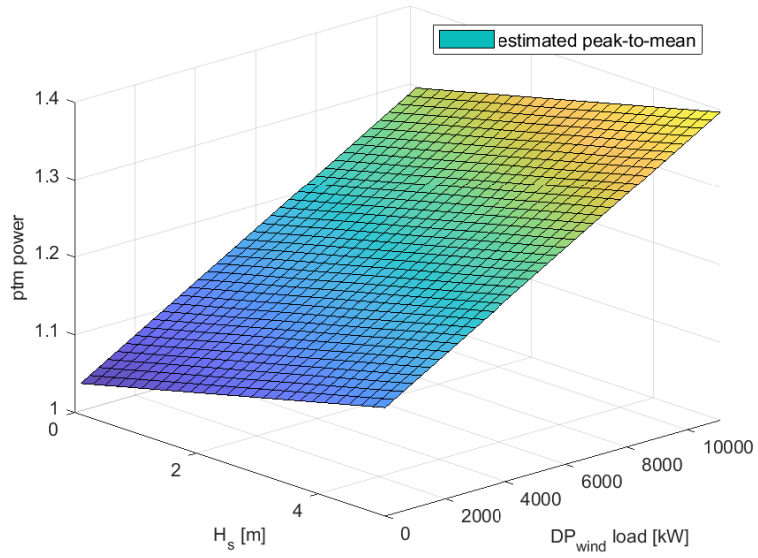

Figure 4.20: 3D visualisation of MLR model

4.3.6. Discussion of Multiple Linear Regression Model

In [25], the model is evaluated by examining the density plot of the residuals. It was stated that a well-fit model shows a normal distribution of the residuals with constant variance. When the kernel density plot is constructed from the model residuals, it indeed shows a normal distribution having zero mean, as can be seen in Figure 4.21, indicating a well-fit model.

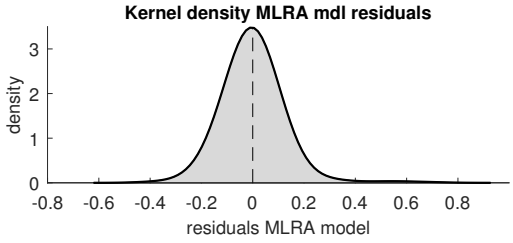

Figure 4.21: Kernel density of MLR model residuals

In [44], the model was evaluated by the root mean squared error (RMSE) and the coefficient of determination (R^2). The RMSE is calculated by Equation 4.16

$$RMSE = \sqrt{\frac{\sum_{i=1}^{N} (\hat{x}_i - x_i)^2}{N}} \tag{4.16}$$

[10] In this thesis, the Matlab - Statistics and Machine Learning Toolbox is used for the regression analysis.

Where:
N : Length of time series of parameter x
$\hat{x}_i$: Estimation of parameter x at timestep i by using the MLR model
x_i : The observation of parameter x at timestep i

The RMSE is a measure of the standard deviation of the model error and the R^2 is a measure of the amount of variation in the response that is explained by the model. For the model found above, the RMSE is 0.095 and R^2 is 0.53. These numbers at least tell that the model error is within reasonable limits and that half of the response's variance is explained by the model, but on their own, these values do not say much, so instead the prediction interval of the peak-to-mean ratio of the power is studied. When the linear regression model is used to predict the peak-to-mean ratio of the power, the 95% prediction interval is maximally ±0.19 around the estimated peak-to-mean ratio for all $H_s \in \{0:5\}$ [m] and $P_{DP,wind} \in \{0:11000\}$ [kW] [11]. This prediction interval is visualised in Figure 4.22. In this DP_{wind} load and wave height range, the upper limit in the prediction interval is maximally 18% higher than the expected peak-to-mean ratio (when the wave height and the DP_{wind} load are maximal). This is considered to be an acceptable range as long as the upper prediction interval limit is used in the starting decision algorithm to be on the conservative side.

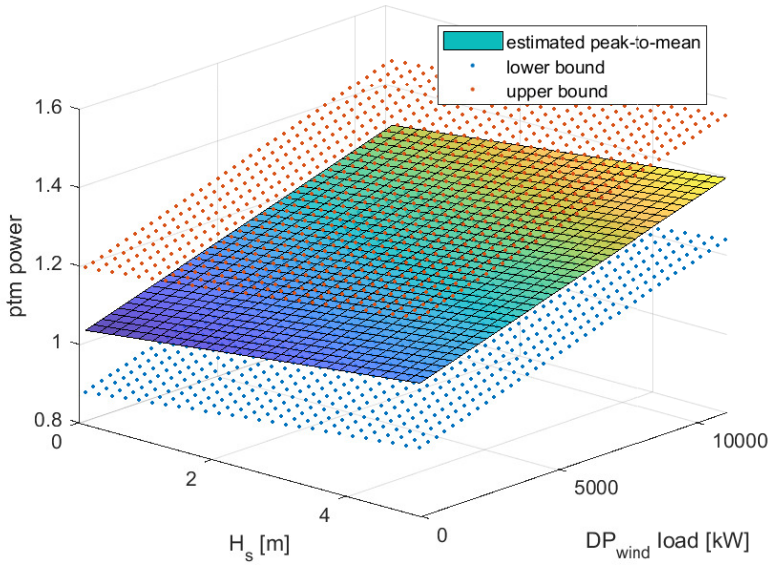

Figure 4.22: 3D visualisation of MLR model including confidence bounds

The results of the MLR model are promissing for implementation as the starting decision in the PMS. After having created the MLR model of the peak-to-mean ratio of the power, it will be tested as input for the starting decision algorithm of the PMS. Referring back to the method described in Section 4.3.2, after selecting the appropriate input parameters, the starting decision algorithm overview is reduced to Figure 4.23. This PMS will be tested in the next section, where an online version of the PMS is simulated using the power data that was left as test data.

4.4. PMS simulation using the Multiple Linear Regression Model

To test the PMS, the online version is simulated using the power and environmental data (H_s, DP_{wind} load) of the two days that were not used for training the model. These days have relatively rough sea states to test the PMS at extreme conditions. Besides, during calm sea states, there is little action required from the starting decision algorithm due to the relatively constant power demand. The input and output parameters for the simulation at every time step are listed in Table 6.3. Both engine rooms are simulated separately, because the engine rooms are independent islands as required for DP vessels.

From the wind speed, wind direction and significant wave height, the MLR model is used to calculate

[11] In the examined weather data used for this model, the wave height was always below 5.2 [m] and the wind load was always below 10900 [kW]

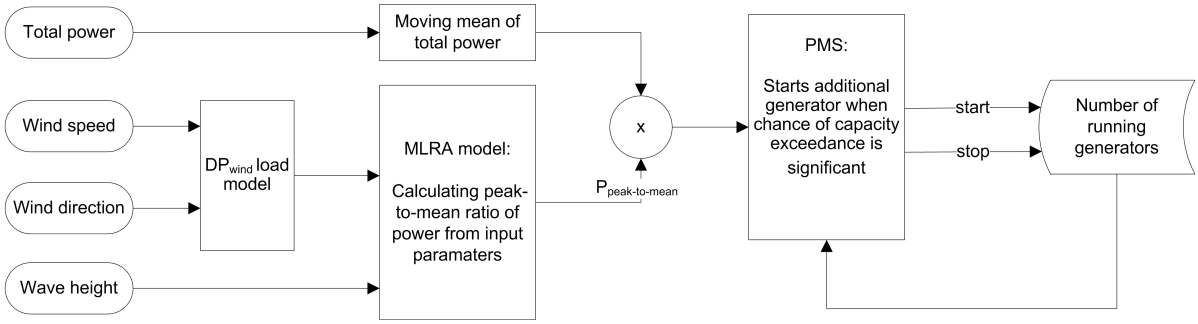

Figure 4.23: Final MLRA based starting decision algorithm

Table 4.11: Input/output PMS simulation

Input parameters		**Unit**	**Output parameters**		**Unit**
Measured total generator power per engine room	$P(t)$	[kW]	Number of running generators	$N^{gens}(t)$	[generators]
Wind speed	$v_{wind}(t)$	[m/s]	Startsignal	$start(t)$	[0/1]
Relative wind direction	$\theta_{wind}(t)$	[deg]	Stopsignal	$stop(t)$	[0/1]
Significant wave height	$H_s(t)$	[m]			

the expected peak-to-mean ratio of the power with corresponding prediction intervals. As explained before, when the PMS detects a significant chance of generator capacity exceedance, it will give a starting signal. Therefore, the prediction interval that is chosen for the peak-to-mean ratio is the 98% prediction interval. This means that given the training data, there is a 1 % chance that the peak-to-mean ratio is lower and a 1% chance that the peak-to-mean ratio is higher during the conditions (H_s and DP_{wind} load) measured. So the starting decision algorithm starts an additional generator if the chance of capacity exceedance -given the measured moving average of the power demand and the environmental conditions- is 1%. A conservative limit is chosen here because the starting decision algorithm is a critical system for the system that uses only one battery. If an online MLR model would have been trained more by continuous learning online or by adding more data afterwards, this limit could be set wider after testing the system on board for a wide range of sea states. For the PMS test in this thesis, this conservative limit is used.

An overview of the simulation steps including starting decision algorithm is shown in Figure 4.25. In every new timestep, the MLR model calculates the upper prediction limit of the peak-to-mean ratio of the power, given the environmental input. The PMS then decides if an additional generator should be started, which is the case if there exists a chance of a capacity exceedance. After a starting signal, 60 seconds later, the generator is fully online and the online generator capacity is increased by 11,200 kW (the nominal generator capacity). In the old PMS, a stop signal could only be given manually by the engine room crew to prevent too many starts and stops. In the new PMS, a manual stopping decision will still be used, but for the simulation, a time based stopping delay is used to simulate this human effect. This stopping delay is chosen such that the number of stops in the measured power data when using the new PMS is equal to the number of stops in the old PMS, to imitate the human experience of the engine room crew about the required stopping frequency. In the 12 examined days, the number of stops in the observed power data was 74. In Figure 4.24, it can be seen that a stopping time of 1260 seconds (21 minutes) is needed in the simulation to have the same amount of stops when simulating the new PMS.

In the simulation overview, the following steps are performed each second (see layers in Figure 4.25):

A This layer tests if at the current timestep, a manual start signal is given. Manual start signals are given prior to switching on DP bias mode[12].

B If decision in layer A is:

[12] Bias mode is a DP setting where two thrusters are set to puch against each other. This mode is turned on in very calm environmental conditions to prevent too much azimuth rotation. During calm weather, there are little environmental forces to push against. The direction in which the DP system should push is fluctuating a lot, because little disturbances are always present but vary a lot in direction. This means that the azimuth angles of the thrusters have to adjust frequently, which is undesired. Therefore, the DP operator switches on bias mode where the direction of the force can be adjusted by changing the rotational speed of the thrusters that are pushing against each other. To prevent wear in the thruster motors, the wash is directed outside.

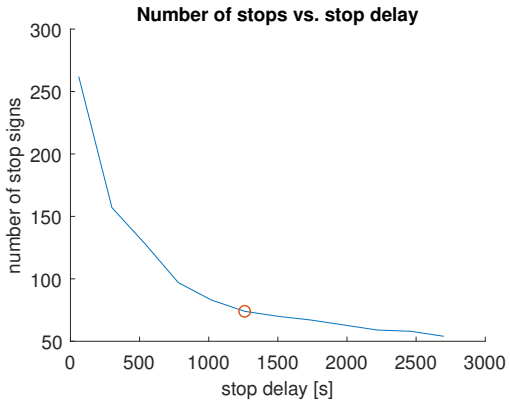

Figure 4.24: Number of stops vs. the stop delay when simulating the PMS using the MLR model. This relation is caused by the fact that a longer stop delay results in a system responding slowly to decreasing power, resulting in less generator starts and stops.

- no: It is checked if the peak-to-mean ratio times the measured average power of the last four minutes is higher than the online generator capacity.
- yes: A start signal is given; the number of running generators in the coming 59 seconds is set to be unchanged (due to the start delay); the number of running generators at one minute from now is increased by one; the simulation is forced one minute forward.

C If decision in layer B is:

- no: It is checked if the peak-to-mean ratio times the measured average power of the last four minutes is lower than the online generator capacity - if one generator less would be running. So it is checked that if one generator would be turned off, there would still be no chance of exceeding the online capacity.
- yes: A start signal is given; the number of running generators in the coming 59 seconds is set to be unchanged (due to the start delay); the number of running generators at one minute from now is increased by one; the simulation is forced one minute forward; the stop signal counter is reset.

D If decision in layer C is:

- no: The stop signal counter is reset.
- yes: The stop signal counter is increased by one.

E Here it checked of the stop signal counter is above the limit of 21 minutes, which can only be the case if the path was followed through a 'yes' from layer C.

F If decision layer E is:

- no: The starting decision algorithm does not act and the number of running generators stays constant.
- yes: A stop signal is given and one generator is switched off. No time is needed to switch off a generator so the online capacity is decreased instantly.

G If the next time step is higher than the simulation time, the simulation is terminated.

The measured total power demand, significant wave height, estimated DP_{wind} load and the corresponding peak-to-mean ratio of the test data can be found in Figure 4.26. The peak-to-mean ratio is calculated using the MLR model as described in Equation 4.15. This peak-to-mean ratio of the power is used in the simulation in layer B and C as explained above. The result of the simulation of the PMS is shown in Figure 4.26. This figure shows the difference between the number of running generators as was measured in the old 'no hybrid' system and the new PMS using a hybrid system including the MLR model. This figure only shows the port side engine room in operation, but in Appendix G, the starboard engine room is also shown. It should be noted again that the PMS is tested on these days in relatively rough conditions (sea state 4 to 5). In average

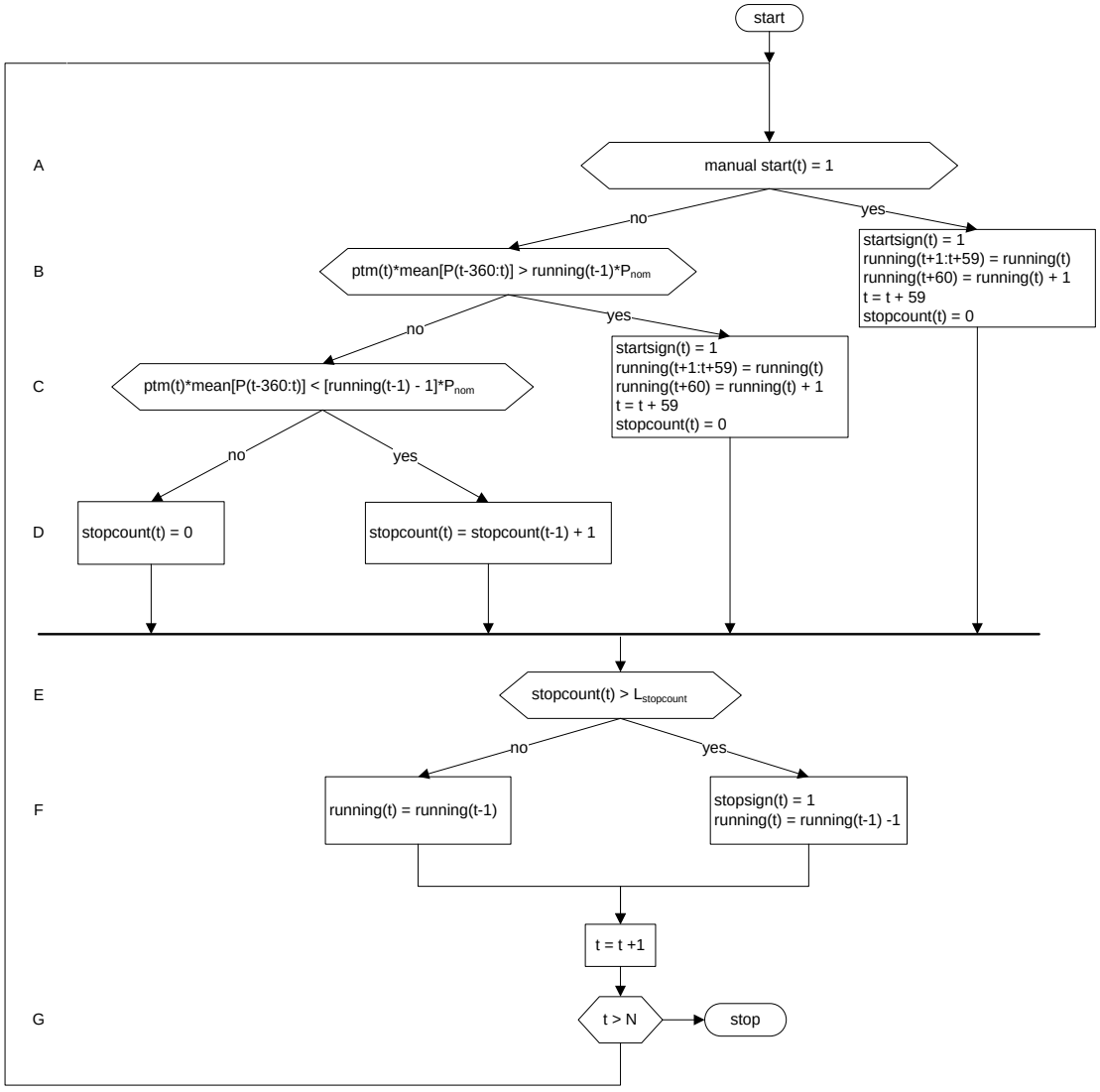

Figure 4.25: Simulation of PMS using MLR model

weather conditions, the power demand is under the nominal power of one generator most of the time and the PMS is acting less. An example of a calm weather day is also shown in Appendix G.

The PMS using the MLR model works as required as can be seen in the tests. It can immediately be seen that the number of running generators fits better to the amount of running generators that is minimally required for the power demand. This reduces the running hours significantly and it is expected that is also reduces the fuel consumption significantly, which will be calculated in a full year simulation in Chapter 6. Besides, the main task of the MLR model based starting decision algorithm is performed well, as the starting decision algorithm starts generators in time to make sure the online generator capacity is sufficient for the power demand.

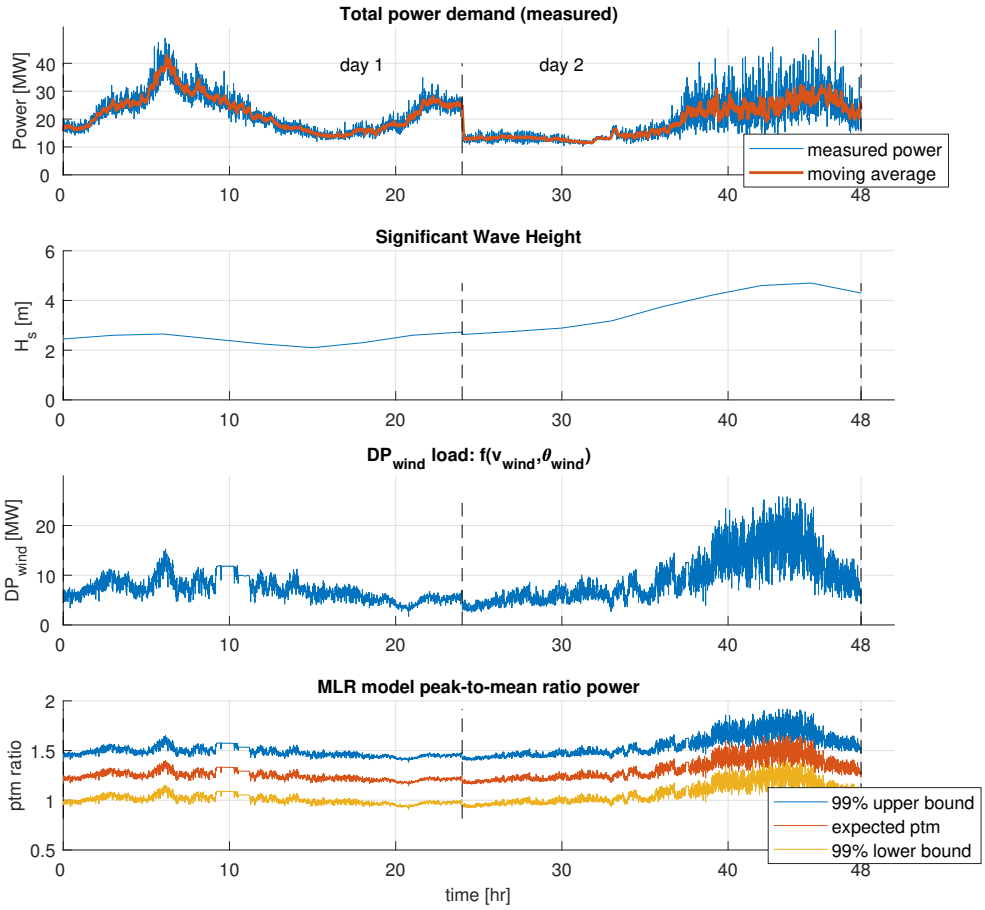

Figure 4.26: The measured power, significant wave height, estimated DP_{wind} load and corresponding peak-to-mean ratio. The peak-to-mean ratio is calculated by the MLR model using the significant wave height and the DP_{wind} load.

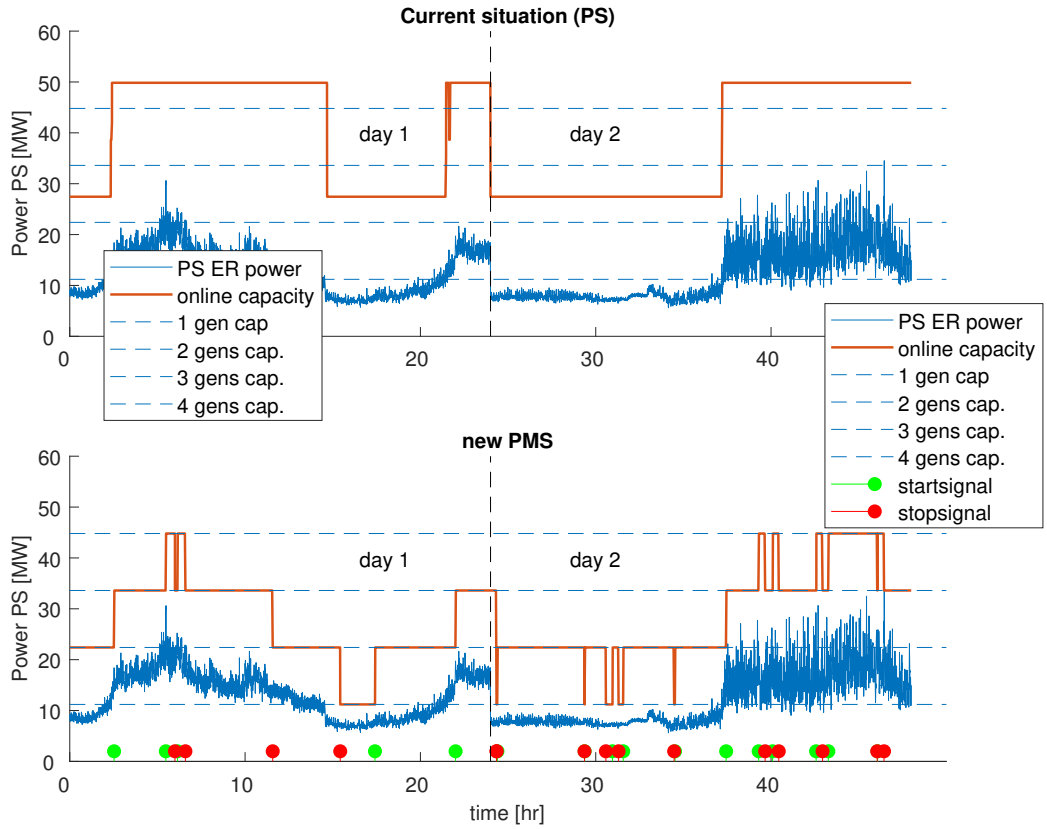

Figure 4.27: PMS test using the MLR model. In the old PMS (noted as 'Current situation'), the small harbour generator was also running on port side. This results in the online generator capacity laying in between two nominal power limits. Note here that the PMS is tested for the two roughest sea states the vessel encountered in the analysed year. For typical power data, see Appendix G.

4.5. Conclusion Starting Decision Algorithm

In this chapter, the goal was to find a suitable starting control algorithm for the PMS that controls the hybrid system of a DP vessel using only one hybrid system for both engine rooms. A mathematical-statistical method using a DP model and environmental parameters as mathematical part and an autoregressive moving average model as statistical part turned out to lack accuracy especially in forecasting the DP load. The uncertainties in weather forecasts turned out the be too high for the mathematical-statistical approach to be applicable in the PMS. For the pipe laying load, a seasonal ARMA model was used, which turned out to be of small added value compared to a simple model using the last measured value of the pipe laying load as forecast. This is mainly caused by the variety in pipe laying period length. This forecasting method works properly when the pipe laying pattern has a constant period, but is limited when the pattern is disturbed. For these reasons, the mathematical-statistical starting decision algorithm was rejected.

The multiple linear regression based PMS shows better results. The relevant parameters for the MLR model are the significant wave height and the estimated DP_{wind} load, which is calculated using the wind speed and wind direction. These environmental parameters are used to estimate the peak-to-mean ratio of the total power demand peaks compared to the moving average of the power demand, given the environment $(H_s, v_{wind}, \theta_{wind})$. This peak-to-mean ratio is used to calculate if there is a chance of generator capacity exceedance, which is the condition for starting an additional generator. For this regression analysis, data of ten days were used to train the model, and two days were left to test the PMS. The PMS that uses the MLR model was tested on days of rough weather and it was found that it works as required and that it significantly reduces running hours. The results of the PMS for the fuel consumption reduction will be discussed in Chapter 6. The next chapter elaborates on the reliability assessment of this PMS compared to the old 'no hybrid' system and compared to the double-battery hybrid system, as was proposed in previous research.

5

Reliability Analysis

As discussed before, two different hybrid system configurations are compared to the old 'no hybrid' system. In hybrid system option 1, only one battery is installed where the PMS uses a multiple linear regression model as discussed in the previous chapter. In hybrid system option 2, two batteries are installed which are connected to both engine rooms separately (as was proposed in previous research) where the PMS makes use of a simple rule that an additional generator is started when the battery has been used. The configuration of these different systems was presented in Figure 3.6 in Chapter 3. The fundamental difference between these hybrid options is the number of hybrid systems installed, where system option 1 only uses one hybrid system in total and system option 2 uses two hybrid systems in total, doubling the investment costs. However, although the previous chapter indicated a well working MLR based starting decision algorithm, the hypothesis is that the single-battery hybrid system is less robust than the double-battery hybrid system and is therefore less reliable. Therefore, in this chapter, the reliability of hybrid system option 1 is compared to hybrid system option 2 and the old 'no hybrid' system. This reliability study is performed by a Fault Tree Analysis quantified by an expert's opinion on the failure rate of the different components. The confidence bounds of the reliability are calculated using a Monte Carlo Simulation.

The fault tree analysis is shown in Section 5.1, followed by the quantification of the fault trees and the calculations of the reliability in the following section. The last section discusses the method of finding the confidence bounds of the reliability using a Monte Carlo simulation.

5.1. Fault Tree Analysis

Fault Tree Analysis (FTA) is a widely used tool in reliability assessments of physical systems in many industries [10]. A fault tree translates physical systems into logical trees, where the user creates an overview of which system component failures or which combination of system component failures could result in a main failure. In the analysis, the user defines an undesirable main event and splits up the physical system into smaller basic events that could occur when the system is in use. In this thesis, the main event is 'insufficient power capacity', which means that the system cannot supply the power demand. The fault tree itself is a qualitative tool but it can be quantified by the probabilities of occurrence of the basic events and using boolean logic to calculate the corresponding probability of the top event.

In the fault tree used for this system, five fault tree symbols have been used, which can be seen in Figure 5.1:

- The top event is the event that is undesired. In this case, the top event is 'insufficient power capacity', which means that total the power demand cannot be supplied by the power generation system, on either side of the engine rooms.
- A basic event is the lowest degree of the fault tree. This is represents the failure of one component of the physical system. An example for the case vessel is the failure of a transformer.
- An intermediate event describes the part of the fault tree under that symbol. An intermediate event does not change the probability of that part of the fault tree and is only descriptive.
- An AND gate propagates the failure if all the inputs of this gate occur at the same time.

- An OR gate propagates the failure if one of the inputs of this gate occurs.
- House Event: an event that is normally expected to occur as part of the operation. This is not seen as a failure.

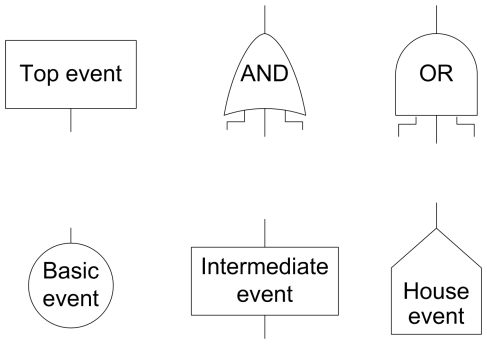

Figure 5.1: FTA symbols

The fault trees for the 'no hybrid', hybrid option 1, and hybrid option 2 are discussed below. In all three systems, the undesired top event is the event where the power capacity is insufficient to supply the power demand, because in all three cases the main goal of the power generation system is to supply the power demanded by all the vessel's systems connected to that engine room.

5.1.1. Fault Tree No Hybrid System

In the old system, where the redundancy is reached by spinning reserve, the main event occurs if two generators fail at the same time, or if a generator fails while the left capacity is insufficient to supply the power demand. The fault tree for this hybrid system option is shown in Figure 5.2.

Basic events

1. Power train failure: an unexpected failure of a part of the power train (fuel supply, diesel engine, generator, etc.).
2. Power is higher than the online capacity minus P_{nom}: the power demand is higher than the online generator capacity if a generator would fail at this moment. For example, during an operation, the power demand has been 12,500 kW for the last 20 seconds, so the PMS has not started an additional generator yet, as the start delay is 30 seconds in the load dependent start system of the old PMS. If a generator would fail at that specific moment, the power capacity is too low and the main event would occur.
3. Power train failure: see event 1.

5.1.2. Fault Tree Hybrid System Option 1: MLR based PMS

For hybrid system option 1, where one battery is installed in total, the fault tree is shown in Figure 5.3. This fault tree is split into a short-term failure and a long-term failure. In the short-term failure, a single power peak crossing the online generator capacity directly results in the main event to occur, because no back up power is present since the battery is only connected in case of a generator failure. The battery cannot be connected continuously to both engine rooms at the same time because the engine rooms should operate independently for the redundancy requirements of DP-II vessels. The long term failure occurs when the hybrid system is used as back up power e.g. when a generator fails. For a long-term failure, a combination between a power demand which is higher than the generator capacity on the one side and no power from the hybrid system on the other side, would result in the main event to occur.

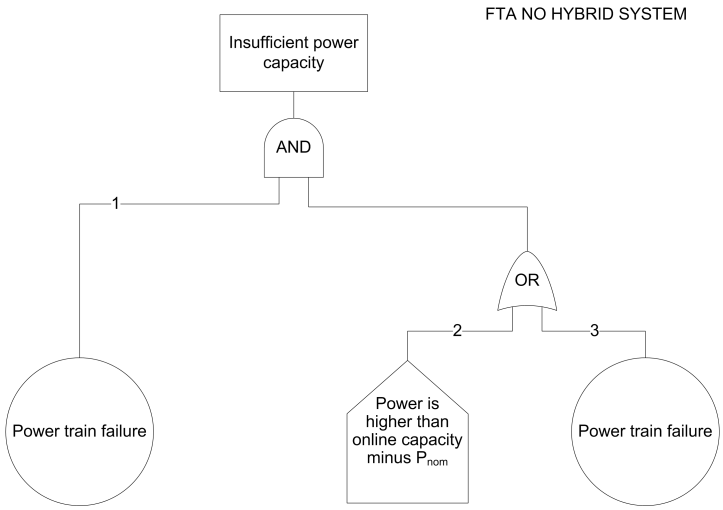

Figure 5.2: Fault Tree for the old 'no hybrid' system

Basic events

1. Power train failure: an unexpected failure of a part of the power train (fuel supply, diesel engine, generator, etc.).

2. No power from battery: a failure of the hybrid system. The fault tree of the hybrid system is presented in a sub-fault-tree, which can be seen in Figure 5.4 and is split into:

   A Circuit breaker closing failure battery/grid: a failure in closing the circuit breaker between the hybrid system and the vessel's power grid in case of a generator failure. This basic event is only of influence in hybrid system option 1, because in hybrid system option 2, the circuit breaker is always closed as the battery is connected continuously.

   B Transformer hybrid system failure: a failure of the transformer between the battery's converters and the vessel's power grid.

   C False positive health status from battery monitoring system: the event where the battery's monitoring system falsely claims a healthy battery system.

   D Unhealthy batteries: no power from the batteries.

   E Battery auxiliary system failure: failure of battery auxiliary system e.g. the battery cooling.

3. Power peak crossing online generator capacity: this event occurs when a small power peak crosses the online generator capacity. Theoretically, by applying the MLR model in the starting decision algorithm, the chance of occurence of this event should be eliminated. In the next chapter, the starting decision algorithm using MLR will be simulated for 100 days in a row, where it will be measured how many times this event occurs altough the MLR model based starting decision algorithm is active. When using hybrid system option 1, no backup power is available in case this event occurs, so this will directly result in the main event to occur, which is undesired.

4. Unexpected rise of power: this event implies that even when using the MLR model, there still exists a chance of an unexpected power peak, for example caused by a malfunctioning tensioner or a sudden change in heading which was not foreseen by the MLR model.

5. Circuit breaker additional generator/grid failure: after starting an additional generator while using the battery, it should be connected to the grid. This event occurs when the circuit breaker between the generator and the power grid fails.

6. Additional stand-by generator starting failure: this event occurs when the additional generator fails to start, while using the hybrid system.

7. Requested power close to maximum capacity: the intermediate event 'battery SOC insufficient' occurs when a combination of two out of three basic events occur. This means that if two or more of the battery inverters fail (leaving only half of the energy available) or if the generator starting time is longer than 90 seconds (requiring the battery for a longer time), that this would only cause a problem if the power demand was close to the maximum generator capacity. If this is the case, the battery would need all available energy during a generator failure.

8. Two or more battery inverters fail: when one of the inverters fail, the hybrid system only looses $1/4^{th}$ of the stored energy due to the hybrid system design (see Chapter 3), which would not cause a problem directly. However, when multiple inverters fail, the hybrid system looses a bigger part of the stored energy, which would result in an energy shortage.

9. Generator starting time longer than 90 seconds: when a generator unexpectedly takes more time than 90 seconds to start (which is 1.5 times the tested starting time).

5.1.3. Fault Tree Hybrid System Option 2: Rule Based PMS

The fault tree of hybrid system option 2 is comparable to hybrid option 1. The main difference is that in the short time failure side of the fault tree, hybrid system option 2 relies on the back-up power from the battery when the power demand is higher than the online generator capacity. Therefore, the short term failure only occurs if next to the event where the power demand is higher than the generator capacity, the hybrid system would fail. The other difference is that due to the backlooking starting decision algorithm, the event could occur where the batteries have been used for occasional peak shaving, resulting in insufficient state-of-charge. The fault tree is shown in Figure 5.5.

Basic Events Only the events that are not discussed above are discussed here.

2. In hybrid system option 2, the battery is used for occasional peak shaving during the starting time of an additional generator. This is due to the backlooking principle of the starting decision algorithm that is rule based and only starts an additional generator if the battery has been used. Therefore, this event occurs occasionally and could result in a short term failure of the main event if the hybrid system fails at the same moment. The occurrence of this event will be found by simulating hybrid system option 2 as will be explained in the next chapter.

3. No power from battery: in the sub-fault-tree for hybrid system option 2, the basic event 'circuit breaker closing failure' is eliminated because the hybrid system is continuously connected.

4. No power from battery: see event 3.

7. SOC (state-of-charge) insufficient due to peak shaving: due to the rule based starting decision algorithm, where an additional generator is only started when the battery has been used, the battery is sometimes used for peak shaving before the online capacity is increased. Therefore, it could be possible that the state-of-charge is too low to supply power during a generator failure. The probability of occurrence of this event will be found by simulating hybrid system option 2.

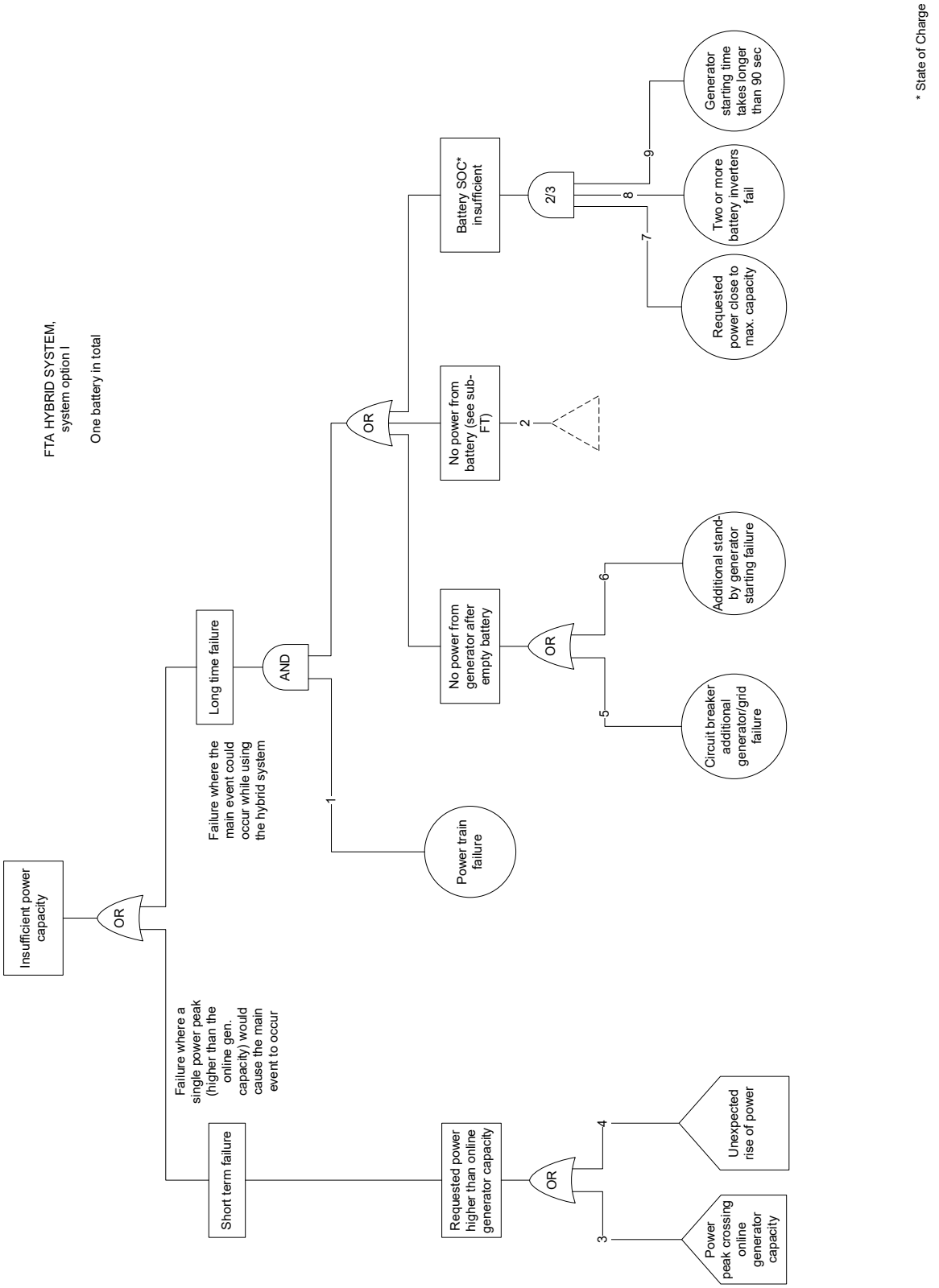

Figure 5.3: Fault Tree of hybrid system option 1: One battery in total

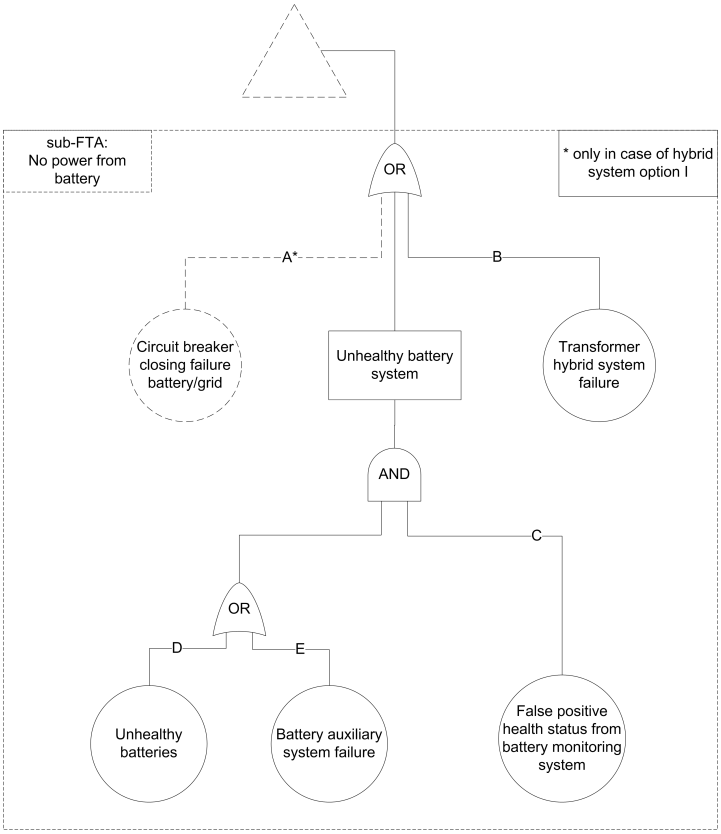

Figure 5.4: Sub-fault-tree of hybrid system

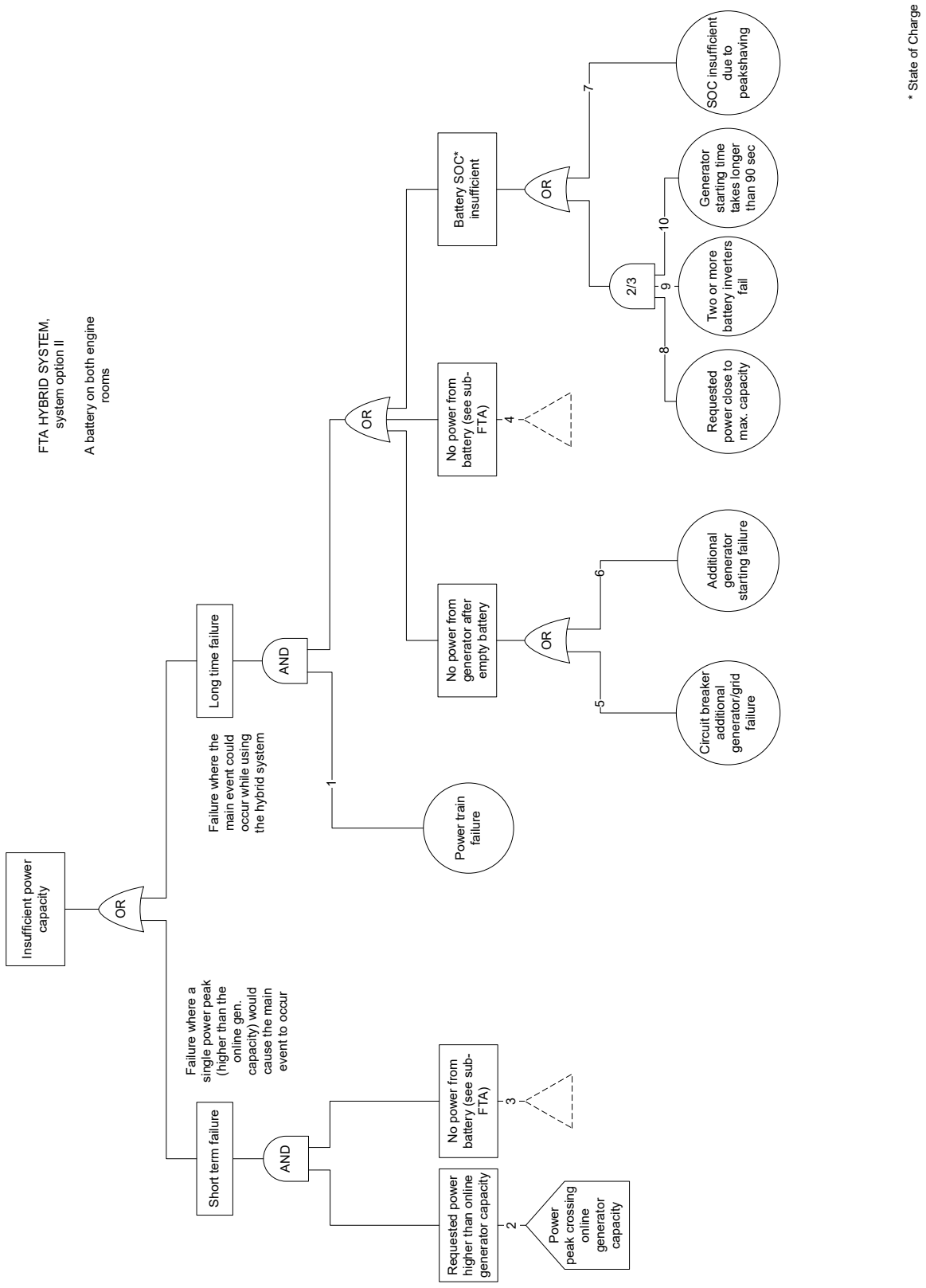

Figure 5.5: Fault Tree of hybrid system option 2: two batteries in total

5.2. Quantification of Fault Tree

To quantify the probability of the main event to occur, the probability of the basic events to occur should be found. Using boolean logic, the probability of occurrence of the main event, or the failure rate, can be calculated when the probabilities of the basic events are known. A component failure probability, or unreliability, is calculated using the failure rate, defined as the number of failures per unit of time e.g. a component failure rate could be: $\lambda = 2$ [failures/year]. The failure probability of a component during a certain time interval is than calculated by [63]:

$$P_{fail}(t) = 1 - e^{-\lambda t} \tag{5.1}$$

Where:
λ : The failure rate [failures/time]
t : The examined time interval [time]

For small values of λt ($\lambda t < 0.1$), the failure probability can be approximated by λt [63], which is explained by the the Taylor series expansion of $e^{-\lambda t}$:

$$P_{fail}(t) = 1 - e^{-\lambda t} = 1 - (1 - \frac{\lambda t}{1!} + \frac{\lambda^2 t^2}{2!} - \frac{\lambda^3 t^3}{3!} ...) \approx \lambda t \tag{5.2}$$

So the failure rate of $\lambda = 2$ [failures/year] can be used to calculate the probability of failure of component in a certain minute, $\lambda t = 2 \cdot 1/(365 \cdot 24 \cdot 60) = 3.8 \cdot 10^{-6} < 0.1$. So the failure chance of that component to fail in a certain minute is $3.8 \cdot 10^{-6}$. Next to failure rates of components that can fail while in use, components could have a failure per demand, also called a pure event probability. In this case, the probability of failure is not defined per unit of time, but per unit of times demanded. An example of such a failure is the basic event 'circuit breaker closing failure'.

When all failure rates or pure event probabilities of the basic events are known, the probability of occurrence of the top event can be calculated using the fault tree. This is done by calculating the probability of occurrence of every subset of the fault tree and adding these to calculate the probability of occurrence of the top event, because:

$$P(A \cup B) = P(A) + P(B) - P(A \cap B) = P(A) + P(B) - P(A)P(B) \tag{5.3}$$

Where it is assumed that A and B are independent events. However, since the probabilities of occurrence of every basic event is a lot smaller than 1, $P(A)P(B) \ll P(A) + P(B)$, so $P(A)P(B)$ is neglected in Equation 5.3, leaving:

$$P(A \cup B) \approx P(A) + P(B) \tag{5.4}$$

This means that for an OR-gate, the probability of occurrence of the fault tree part below this gate is a sum of the probabilities of occurrence of all inputs. For an AND gate, when it is again assumed that the input events are independent events, the probability of occurence of the fault tree part below this gate is:

$$P(A \cap B) = P(A)P(B) \tag{5.5}$$

Using Equation 5.4 and Equation 5.5, the total fault tree can be calculated bottom up, resulting in the probability of occurrence or the failure rate of the main event.

Failure rates or probabilities of occurrence To estimate the failure rate of every basic event, an expert's opinion is used from the technical department of Allseas. However, for the hybrid system, little experience is present within Allseas. Therefore, a preliminary conservative estimation is made for the failure rates of these components, of which the influence on the end result will be evaluated in the next chapter. In the next section, it is explained how the importance of every basic event for the probability of occurrence of the top event can be evaluated. When the importance of every basic event is known, it is evaluated if the estimation of the failure rate of the hybrid system should be more accurate using a different method.

For all basic events, the failure rate or probability of occurrence per year, or the failure chance per demand is known and given in Table 5.1, including the confidence margins.

For the long-term failure in hybrid system option 1 and 2, the failure rate of every component is calculated per 60 seconds, corresponding to the start time of a generator. That means that for example that when a generator fails and there is no power from the battery in the same 60 seconds, the main event occurs. To

be able to add the long- and the short term-failure, the short-term failure is also expressed in probability of occurrence per 60 seconds. In hybrid system 2, the short-term failure rate is first calculated per second before is multiplied by 60, because the basic events of the short-term failure would have to occur at the exact same time to propagate the failure. In the 'no hybrid' option, the probability of occurrence is also presented per 60 seconds for an easy comparison.

The probability of occurrence of the basic event 'SOC insufficient due to peak shaving' and the basic event 'requested power close to generator capacity' are not found by an experts opinion but are found in the PMS simulation of the different system options in the next chapter.

Table 5.1: Experts opinion on probability of occurrence or failure probability on demand per basic event

Event	Occurrence	Estimated λ_{year}	lower bound	upper bound	P_{demand}	lower bound	upper bound
Generator failure	Once - twice per year	1.50	1.00	2.00			
Generator does not start when asked	once per 400 - 600 times				$2.00 \cdot 10^{-3}$	$1.67 \cdot 10^{-3}$	$2.50 \cdot 10^{-3}$
It takes longer to start a generator than 90 seconds	once per 300 - 400 times				$2.86 \cdot 10^{-3}$	$2.50 \cdot 10^{-3}$	$3.33 \cdot 10^{-3}$
Transformer failure	Once per 18-22 years	0.05	0.05	0.06			
Converter failure	Once per 4 - 7 years	0.14	0.10	0.25			
Circuit breaker to grid closing failure	once per 150 - 200 times				$5.71 \cdot 10^{-3}$	$5.00 \cdot 10^{-3}$	$.67 \cdot 10^{-3}$
Unexpected rise of power	6-20 times per year	12.00	6.00	20.00			
Unhealthy batteries	Once per 5 -7 years	0.17	0.14	0.20			
Battery auxiliary system failure	Once per 3 - 6 years	0.25	0.17	0.33			
False positive health status from battery monitoring	Once per 5 - 10 years	0.13	0.10	0.20			

For all components, a constant failure rate is assumed, because it is assumed that the infant mortality phase has been passed, and the aging phase is prevented by closely monitoring and planned maintenance, see Figure 5.6 [76]. This is common practice in reliability assessments if little failure data is available [63].

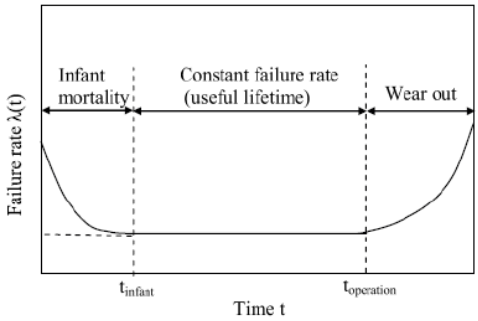

Figure 5.6: Bathtub curve failure rate during life time [76]

Importance Factor To understand which events influence the probability of occurrence of the top event the most, the importance factor is used [65]. The importance factor of every basic event represents the influence of that basic event on the ocurrence probability of the top event by calculating the difference in probability between the fault tree with and without that specific basic event. The importance factor (IF) is calculated by:

$$IF_k = \frac{P(N) - P(N_k)}{P(N)} \tag{5.6}$$

Where:

IF_k : The importance factor of basic event k

$P(N)$: Probability of occurrence of the top event when all basic events are present

$P(N_k)$: Probability of occurrence of the top event when basic event k is not present

The importance factor will be used to evaluate if the conservative estimation of the failure rates of the hybrid system (in the sub-fault-tree) should be more accurate by using a different method. Besides, it can be used to find which risks have to be mitigated to increase the reliability of the system.

Reliability From the failure rate or probability of occurrence of the top event, the reliability of the system can be calculated and the reliability of the different system options can be compared. The reliability of a system is defined as the probability that it will not fail during the time interval that is studied. So the reliability can be written as:

$$R(t) = 1 - P_{fail}(t) = 1 - (1 - e^{-\lambda t}) = e^{-\lambda t} \tag{5.7}$$

For the comparison of the different system options ('no hybrid', hybrid system option 1, hybrid system option 2), the 10 years reliability and the length of the time span before 95% reliability is reached will be compared. The results of this comparison can be found in Chapter 6.

5.3. Monte Carlo Simulation of Reliability

In reliability assessments using fault tree analysis, the confidence interval of the reliability is often found using a Monte Carlo Simulation [63], [65]. In this simulation, in every simulation step, for all the basic events, a random number is drawn from a uniform distribution between the confidence bounds of that basic event. Using these random probabilities of occurrence of every basic event, the probability of occurrence of the top event is calculated using boolean logic and the fault tree. The probability of occurrence of the top event in every simulation step is saved. From this range of generated data, the 95% confidence bounds of the probability of occurrence of the top even can be found. An overview of the simulation steps is shown in Figure 5.7.

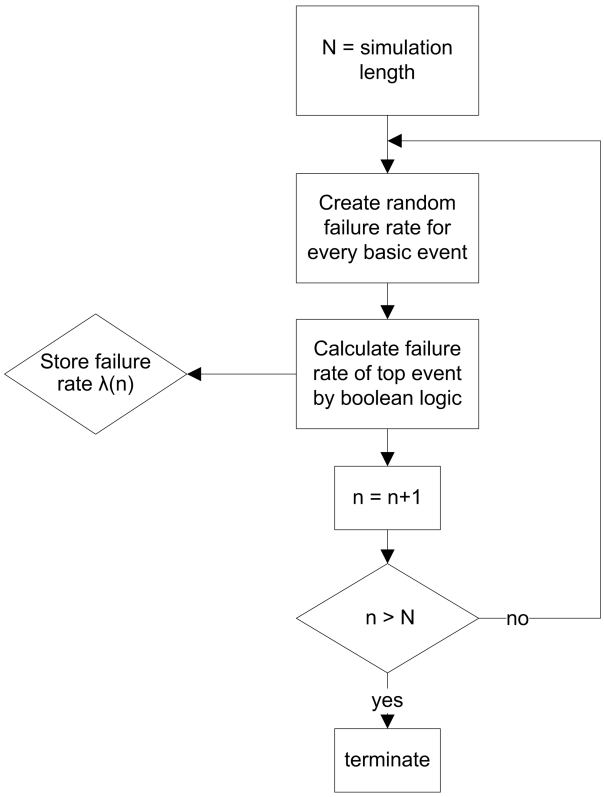

Figure 5.7: Monte Carlo simulation for failure rate of top event

The simulation length is found by calculating the confidence bound of the failure rate for different simulation lengths and inspect where the upper and lower limit converge to a constant limit [11]. For all three system options, the 95% confidence bounds of the failure rate λ are shown in Figure 5.8 for different Monte Carlo simulation lengths. It can be seen that for all three systems, the confidence bounds rapidly converge to a constant width, so a simulation length of 1000 is considered to be sufficient.

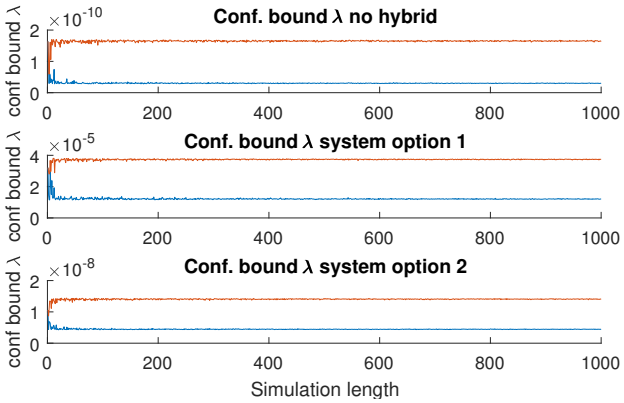

Figure 5.8: 95% confidence bounds of failure rate at different simulation lengths

6

Simulation and Results

The EES is selected and sized in Chapter 3 and a well working starting decision algorithm for the single-battery hybrid system option is found in Chapter 4. The old 'no hybrid' system on board of the case vessel uses spinning reserve and previous research focused on using two separate hybrid systems. In this chapter, these different system options -'no hybrid', hybrid system option 1 (single-battery), and hybrid system option 2 (double-battery)- are simulated to compare the fuel consumption, the generator running hours, and the reliability of functioning as the power generation system. Next to that, in this chapter is explained how these simulations can be used to estimate the battery degradation and the maintenance costs.

In the first section, the input data that is used for the simulations is described, followed by the explanation of the fuel consumption and running hours estimation in Section 6.1.2. The reliability estimation from these simulation is explained in Section 6.1.3, after which the battery aging calculations will be discussed in Section 6.1.4. The final Section about the simulations explains the estimation of the maintenance costs.

After discussing the simulations, the results of these paragraphs are discussed in the same order in Section 6.2. The last subsection gives a summary of all results.

6.1. Simulation

6.1.1. Input Data

In Chapter 4, the PMS using a MLR model is tested for two days of rough weather. In reality, the vessel encountered little of these days in the analyzed year of operation. Therefore, for a more representative estimation of the fuel consumption reduction, the running hours reduction, and the reliability analysis, the different system options will be simulated using a representative ratio of sea states as power data input. The distribution of sea states the vessel encountered in the analyzed year was shown before in Section 4.3.4 and the occurrence ratios of these sea states are shown in Table 6.1.

Table 6.1: Ratio of sea states during last year of operation

Sea State	1	2	3	4	5	6	7	8	9
Occurrence [%]	0.0	34.9	46.1	15.3	3.2	0.3	0.0	0.0	0.0

Using this ratio, a 100 day simulation of the different system options is performed using 35 days of sea state 2 data, 46 days of sea state 3 data, 15 days of sea state 4 data, 3 days of sea state 5 data, and 1 day of sea state 6 data in a row. To resemble 100 operational days, the power data that was available for the MLRA is used as power demand data (for the data, see Table 4.8). This method is chosen here because of the limited access to measured power data, as the data was sent to shore from the case vessel by satellite connection. The available data is represented as 100 consecutive days, where the ratio between the sea states of the power data resembles the real sea state ratio the vessel encountered in the analyzed year. This ratio can be seen Table 6.2.

6.1.2. Fuel Consumption and Running Hours

Fuel Consumption The fuel consumption is calculated using the same methodology as for the preliminary check on potential fuel consumption savings using EES in Section 3.1. However, in that section, for the pre-

Table 6.2: Contribution of specific days to the total 100 days simulation

Date	09-28-2017	11-10-2017	26-10-2017	25-12-2017	26-12-2017	10-01-2018	13-01-2018	15-01-2018	18-01-2018	02-02-2018	21-02-2018	26-02-2018
Sea State	5	2	3	4	3	4	5	3	4	4	5	6
Contribution to 100 days simulation	1	35	16	4	15	4	1	15	4	3	1	1

liminary assessment, it was assumed that the total power demand was split equally between all running generators in both engine rooms. In this simulation, more information is available about the power demand per engine room. So the fuel consumption of the port side engine room and the starboard side engine room are calculated separately. This fuel consumption is calculated using the factory acceptance test for the specific fuel consumption at different partial loads. The total fuel consumption is calculated by:

$$fc_i = \sum_{t=1}^{T} sfc_t(pf_{t,i}) \cdot P_{t,i} \Delta t \tag{6.1}$$

Where:

fc_i:	The fuel consumption in engine room i during time span $t = \{1 : T\}$	[kg]
$sfc_{t,i}(pf_{t,i})$:	The specific fuel consumption given the power factor at time step t in engine room i. The $sfc(pf)$ is obtained from the curve fit through the measurements of the factory acceptance test.	[kg/kWs]
$P_{t,i}$:	Total power demand at timestep t in engine room i	[kW]
Δt:	Time step of simulation (1 second)	[s]

Here it assumed that the efficiency of the generators is not influenced by transient loads as was shown by [27] and [40]. The power factor at every time step is calculated by the total power demand for that specific engine room divided by the online capacity in that engine room:

$$pf_{t,i} = \frac{P_{t,i}}{N_{t,i}^{gens} P_{nom}} \tag{6.2}$$

Where:

$P_{t,i}$:	Total power demand in engine room i at time step t	[kW]
$N_{t,i}^{gens}$:	Number of online generators in engine room i at time step t	[gens]
P_{nom}:	Nominal generator power (11200 kW)	[kW/gen]

The difference in fuel consumption and running hours between the three different system options is caused by the difference in the number of online generators. The simulation of the number of online generators at every time step is described below.

Number of Online Generators For the old 'no hybrid' system, the number of running generators is measured. For hybrid system option 1 that uses the MLR model in the starting decision algorithm, the number of running generators at every time step is found by the simulation method that is explained in Section 4.4, but than using the 100 day data input as described above. For hybrid system option 2, the starting decision algorithm is load dependent which starts an additional generator as soon as the online generator capacity is insufficient, so when the battery has been used. The simulation of this hybrid system, using the load dependent start will be described below.

For hybrid option 2, the simulation steps in every time step can be seen in Figure 6.1. In the top of this overview (block 'SOC battery'), the state-of-charge (in the Figure noted as SOC) for every time step is calculated as follows:

$$SOC_t = SOC_{t-1} - [P_t - N_t^{gens} P_{nom}] \Delta t \tag{6.3}$$

	SOC_{t-1} :	The SOC of the battery in the previous time step	[kWs]
	P_t :	The measured power demand at time step t	[kW]
Where:	N_t^{gens}:	Number of online generators in time step t	[gens]
	Δt:	The length of time step t, in this simulation 1 second	[s]
	P_{nom}:	Nominal generator power (11200 kW)	[kW/gen]

Besides, for every time step, a fictive state-of-charge is calculated which is used as input for the stopping decision. The fictive state-of-charge of the battery is defined as the state-of-charge the battery would fictively have if the engine room would be running on one generator less than is actually online. If the fictive state-of-charge would be sufficient for longer than the stopping delay, one generator is switched off. So the fictive state-of-charge $SOC_{fictive}$ is calculated as follows:

$$SOC_{fictive,t} = SOC_{fictive,t-1} - [P_t - (N_t^{gens} - 1)P_{nom}]\Delta t \tag{6.4}$$

	$SOC_{fictive,t-1}$:	The fictive SOC of the battery in the previous time step	[kWs]
	P_t :	The measured power demand at time step t	[kW]
Where:	N_t^{gens}:	Number of online generators in time step t	[gens]
	Δt:	The length of time step t, in this simulation 1 second	[s]
	P_{nom}:	Nominal generator power (11200 kW)	[kW/gen]

Both for the actual state-of-charge as for the fictive state-of-charge, the lower and upper limit are set at 20% and 70% of the battery's capacity as was explained in Chapter 3.

In the simulation steps in Figure 6.1, the following steps are performed each second for hybrid system option 2:

A This layer tests if at the current timestep, a manual start signal is given. Manual start signals are given prior to switching on DP bias mode.

B If decision in layer A is:

- no: It is checked if the state-of-charge of the battery in the current time step is lower than the lower limit of the state-of-charge (SOC_{LL}). This lower limit is set to 1% under the nominal limit of 70% state-of-charge, which in practice means that if the power demand is higher than the online generator capacity, this decision block is answered with 'yes' and a starting signal is given in the next layer.
- yes: A start signal is given; the number of running generators in the coming 59 seconds is set to be unchanged (due to the start delay); the number of running generators at one minute from now is increased by one; the simulation is forced one minute forward. In this minute, the state-of-charge of the battery is still calculated and saved, because although a starting signal is given, no additional generator is started yet, so the battery can be used in this minute.

C If decision in layer B is:

- no: It is checked if fictive state-of-charge of the battery in the current time step is higher than the lower limit of the state-of-charge (SOC_{LL}). If the fictive state-of-charge is higher than (SOC_{LL}), the system could have been running on one generator less.
- yes: A start signal is given; the number of running generators in the coming 59 seconds is set to be unchanged (due to the start delay); the number of running generators at one minute from now is increased by one; the simulation is forced one minute forward. Here the state-of-charge of the battery is also still calculated and saved in this minute.

D If decision in layer C is:

- no: The stopcount is reset to zero.
- yes: the stopcount is started, or the stopcount is increased by one.

E Here it checked of the stop signal counter is above the limit of 21 minutes, which can only be the case if the path was followed through a 'yes' from layer C.

F If decision layer E is:

- no: The PMS does not act and the number of running generators stays constant.
- yes: A stop signal is given and one generator is switched off immediately.

G If the next time step is higher than the simulation time, the simulation is terminated.

Summary of simulation In Table 6.3, a summary is given of the input and output of the simulation of hybrid system option 1 and hybrid system option 2. The number of online generators in the old 'no hybrid' system option is not simulated but measured from on board data.

Table 6.3: Simulation input and output for hybrid system option 1 and 2

System option	Simulation input	PMS principle	Simulation output
option 1 (one battery)	P(t) demand per engine room	MLR model	N_t^{gens} per engine room
option 2 (two batteries)	P(t) demand per engine room	Rule based (backlooking)	N_t^{gens} per engine room

Using the number of online generators per engine room (N_t^{gens}) the fuel consumption per engine room is estimated using Equation 6.1. The number of running hours is calculated using the number of online generators at every time step.

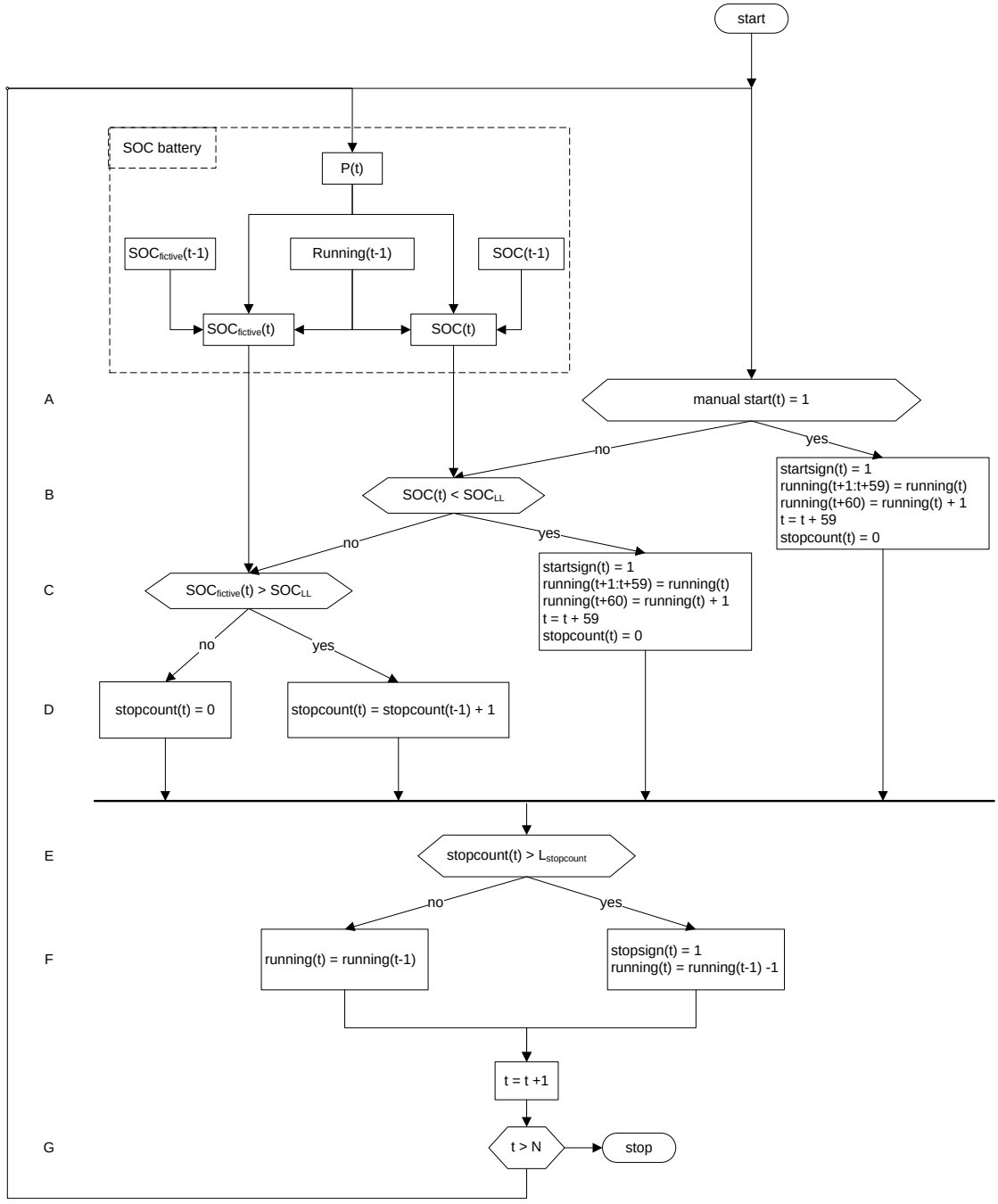

Figure 6.1: Simulation steps in every time step for hybrid option 2

6.1.3. Reliability

In the fault trees, the following basic events should be found using the simulations of the PMS's:

- 'No hybrid' option: basic event 'power demand is higher than online generator capacity minus P_{nom}'.
- Hybrid option 1: basic event 'requested power close to maximum capacity'.
- Hybrid system option 2:
  - basic event 'SOC insufficient due to peakshaving'
  - basic event 'requested power close to maximum capacity';

Hybrid systems For the two hybrid systems, these basic events are related to the intermediate event 'battery SOC insufficient', see the fault trees in Figure 5.2, 5.3, and 5.5. As was explained, for the intermediate event 'battery SOC insufficient' of the hybrid system options to occur, two of the following three events have to occur: 'requested power close to maximum capacity', 'two or more battery inverters fail', 'generator starting time takes longer than 90 seconds'. The event 'power close to maximum capacity' is obtained from the simulation by comparing the online generator capacity at every time step to the power demand. In combination with one of these other two events, this event causes problems during a generator failure if the power demand is continuously close to the online capacity, because this would require the maximum available energy from the battery. So this event is defined to occur when the difference between the 60 seconds moving average of power demand and the online generator capacity is smaller than 10% of the nominal generator capacity. The moving average is chosen here because it should be found where this event would cause problems to the amount of stored energy, which means that the power demand should be close to the online capacity for the full minute of using the battery during a generator failure. This 10% limit is assumed to be a reasonable limit for the definition of close to the online generator capacity, but the effect of this limit to be 10% instead of for example 5% or 20% should be examined. Therefore, it is examined what the effect is on the result if this limit is set at 5% and at 20%. It was found that for none of the system options, the importance factors, nor the reliabilities changed significantly by changing the definition of close to the online generator capacity between 5% and 20%. So from this simulation, the probability of occurrence or failure rate of this event is:

$$\lambda_{100days} = \sum_{t=1}^{T} \left(\left[N_t^{gens} \, P_{nom} - \overline{P_{t-30:t+30}} \right] < 0.1 \, P_{nom} \right) \Delta t \tag{6.5}$$

Where:

N_t^{gens}:	Number of online generators at time step t	[gens]
P_{nom}:	The nomininal generator power	[kW/gen]
$\overline{P_{t-30:t+30}}$:	The 60 seconds moving average of the power demand at time step t	[kW]
Δt:	The simulation time step, 1 second in this simulation	[s]

For hybrid system option 2, the same basic event 'requested power close to maximum capacity' is calculated using the same method. The other basic event of hybrid system option 2, 'SOC insufficient due to peak shaving' is also found in the simulation and is defined as the time the battery's state-of-charge is below the amount of energy that is required in case of generator failure. So the probability of occurrence is defined by:

$$\lambda_{100days} = \sum_{t=1}^{T} (SOC_t < P_{nom} \, t_{start,gen}) \Delta t \tag{6.6}$$

Where:

SOC_t:	The state-of-charge of the battery at time step t	[kWs]
P_{nom}:	The nomininal generator power	[kW]
$t_{start,gen}$	Generator starting time (60 seconds, see Section 3.2.1)	[s]
Δt:	The simulation time step, 1 second in this simulation	[s]

'No hybrid' system option For the 'no hybrid' system option, the basic event 'power demand is higher than online generator capacity minus P_{nom}' is calculated using the measurements of the number of online generators and the power demand at every time step:

$$\lambda_{100days} = \sum_{t=1}^{T} (P_t > [N_t^{gens} - 1]\ P_{nom})\Delta t \tag{6.7}$$

Where:

P_t:	The power demand at time step t	[kW]
N_t^{gens}:	Number of online generators at time step t	[gens]
P_{nom}:	The nomininal generator power	[kW]
Δt:	The simulation time step, 1 second in this simulation	[s]

From these 100-day failure rates, the 60 seconds failure rates are calculated by $\lambda_{60s} = \lambda_{100days}/(100 \cdot 24 \cdot 60)$, which are used in the reliability analysis.

6.1.4. Battery Aging

Because of the electro-chemical reaction in lithium-ion batteries, the battery degrades over time due to cycle aging and battery aging. These aging mechanisms are caused by different phenomena inside the battery that reduce the capacity of the battery. Cycle aging is defined as the reduction in capacity caused by charging and discharging the battery while using the battery. Calendar aging is defined as the reduction in capacity that occurs irrespective of the usage of the battery. For the estimation of the aging of the lithium-ion battery used in for this hybrid system, the aging model of ten Cate Hoedemaker [66] is used, which was specifically developed for maritime hybrid systems using a lithium-ion battery. For an elaborate explanation of battery aging and the model used in this analysis, the reader is referred to [66]. This section describes the relevant equations and parameters that are used from this model.

Calendar Aging In this model, the calendar aging depends on the cell temperature compared to the optimal temperature and on the state-of-charge compared to the reference state of charge according to:

$$Q_{cal} = \left(\alpha \cdot \beta^{\Delta T} + \kappa \cdot (SOC - SOC_0)\right) \cdot t^{-0.5} \tag{6.8}$$

Where:

Q_{cal}:	Capacity loss per day	[%/day]
α:	Temperature factor parameter	
β:	Temperature base parameter	
ΔT:	The difference between the battery's temperature and the optimal storage temperature	
κ:	SOC effect parameter	
SOC:	Storage state-of-charge of the battery	
SOC_0:	Reference state-of-charge of the battery at which the parameters α, β, and κ were established	
t:	The number of days	

So it can be seen that the capacity loss per day (or aging rate) reduces in time because of the negative exponent in this equation. To assess the total capacity loss due to calendar aging at a specific day, the sum of the capacity loss of all passed days is calculated. Equation 6.8 was found using aging data of lithium-ion tests ranging to 800 days (2.2 years), so no data was available for calendar aging after this limit. Therefore, it is unknown how the calendar aging proceeds after two years, so for this analysis it is assumed that this power relation can be used between 0 and 800 days and that the daily calendar aging does not decline further and is constant after this limit. This means that the battery's capacity declines linear after this limit. The calendar aging parameters were found by fitting Equation 6.8 to data from different battery tests and can be found in Table 6.4. As stated in Chapter 3, the storage state-of-charge is at 70%. Further, it is assumed that for the majority of the time, the battery room is kept at the optimal storage temperature, meaning that ΔT is 0 in general. Only when charging or discharging the battery, the cell temperature changes, but because the charging and discharging time together is only 0.22% of the time for hybrid system option 2 (found by the simulation described in Section 6.1.2), the influence of this temperature change on the total calender aging is neglected. The charging and discharging time for hybrid system option 1 is even less, because the battery is only used for testing, generator failures, and human errors.

α	0.07
β	1.061
κ	0.003
SOC_0	50%

Table 6.4: Calendar aging parameters [66]

Cycle Aging Cycle aging is affected by the depth-of-discharge[1] of a cycle and the C-rate during the charging or discharging of the battery. The aging per cycle due to the depth-of-discharge is given by a Woehler curve, which is set up by ten Cate Hoedemaker using a collection of different battery tests. A Woehler curve shows the amount of full cycles until the end-of-life of the battery, dependend on the depth-of-discharge of each cycle. The Woehler curve used in the model is shown in Figure 6.2a and the effect of the depth-of-discharge on the capacity loss per cycle is shown in Figure 6.2b, which is based on Figure 6.2a.

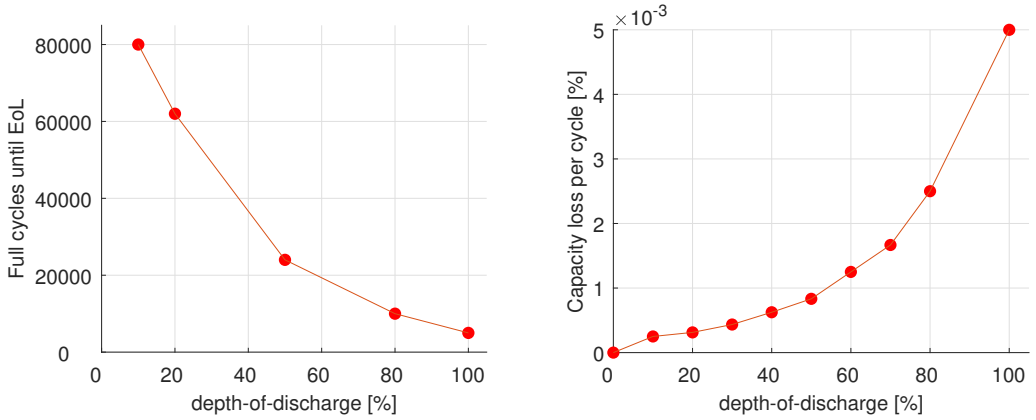

(a) Woehler curve showing number of full cycles until end of life (EoL) depending on depth-of-discharge

(b) Inverted Woehler curve showing the capacity loss per cycle depending on the depth-of-discharge

Figure 6.2: The Woehler curve and inverted Woehler curve used in the cycle aging model [66]

Next to the depth-of-discharge, cycle aging is also affected by the charge and discharge rate during the cycles. This effect is taken into account by an amplification factor depending on the C-rate. The amplification factor is different for charge cycles than for discharge cycles. Using the amplification factor and the Woehler curve, the cycle aging for the discharging and for the charging part of the cycle are calculated by:

$$Q_{cyc,d} = Q_{DOD,d} \cdot AF_d = \frac{Q_{Woeh}}{2} \cdot \left(1 + (\gamma_1 \cdot C_{rate})^2 - \gamma_2\right) \tag{6.9}$$

$$Q_{cyc,c} = Q_{DOD,c} \cdot AF_c = \frac{Q_{Woeh}}{2} \cdot \left(1 + (\gamma_3 \cdot C_{rate})^2 - \gamma_4\right) \tag{6.10}$$

Where:

$Q_{DOD,d}$:	The capacity loss due to the discharge part of the cycle	[%]
$Q_{DOD,c}$:	The capacity loss due to the charge part of the cycle	[%]
AF_d:	The amplification factor based on the C-rate during discharging	[-]
AF_c:	The amplification factor based on the C-rate during charging	[-]
Q_{Woeh}:	The capacity loss found in the Woehler curve based on the depth-of-discharge	[%]
γ_1:	C-rate effect discharging coefficient	
γ_2:	C-rate effect discharging constant	
γ_3:	C-rate effect charging coefficient	
γ_4:	C-rate effect charging constant	

[1] Here the depth-of-discharge is defined as the maximum difference between the state of charge at the beginning of the discharging cycle and the state of charge during the discharging cycle.

From the simulation of the hybrid systems, the charge/discharge cycles are found from the battery's state-of-charge that is saved in every timestep. Next to that, a number of manual cycles are added in the battery aging calculations to represent both generator failures and battery testing cycles. In hybrid system option 1, these manual cycles are the only cycles the battery is subjected to because the battery is never used to back up the power generation from the generators. In hybrid system option 2, the batteries are used more often because the PMS only starts an additional generator when the battery has been used, meaning that a rise in power demand that crosses the online generator capacity results in a discharge cycle of the batteries. The yearly manual cycles that are added are:

- Two generator failure cycles which are caused by a generator failure in one of the engine rooms. For a conservative aging estimation, in these cycles, it is assumed that the full battery range between 70% and 20% is used during a generator failure;

- Six testing cycles (one full cycle testing every two months). To make sure the batteries function as supposed, the battery is tested every two months for the full range between 70% and 20% state-of-charge;

- Two human error cycles. It is assumed that the back-up battery sometimes needs to be used to back-up a human error like the accidental shut down of a generator. For conservative reasons, these cycles are also assumed to require the full range of 70% to 20% state-of-charge.

In these manual cycles, the maximum power of one generator is used to calculate the C-rate, which is maximally 14C given the size of the battery and the power of 11,200 kW.

6.1.5. Maintenance Costs

Due to the reduction in running hours, it is expected that the maintenance costs will also reduce for the following reasons:

1. The reduction in running hours reduces the material costs of planned maintenance because the planned maintenance schedule is directly based on the amount of running hours of the generators. An example of a planned maintenance job is to replace all piston rings after 12,000 running hours. The planned maintenance schedule is recommended by the generator manufacturer and directly used on the case vessel.

2. The reduction in running hours reduces the amount of corrective maintenance because the chance of failures reduces when the generators are running less.

The reduction in material costs of the planned maintenance (reason 1) can be calculated using the planned maintenance schedule of the generators. In Table 6.5, a part of the planned maintenance schedule of the case vessel is shown, where it can be seen how the total maintenance costs for 24,000 running hours are calculated. Different vessels would have different maintenance schedules, so this calculation could differ per assessment, but to get a feeling of the effect of the reduction in maintenance cost due to the reduction in running hours, the maintenance schedule of this specific case vessel is used here. Further research could focus on a more general approach to find the relation between running hours and maintenance costs of diesel generators.

In this Table 6.5, for different maintenance jobs, the quantity of parts that are needed at every maintenance interval (between 6,000 and 24,000) are shown. By calculating the total amount of parts needed in the full 24,000 hours of operation, the total costs per job can be calculated when the part price is known. Since the information in this table is classified, no specific jobs and part prices are mentioned here, but the total material costs after 24,000 running hours of $930,000.00 are the real costs based on the MAN spare parts prices [35]. Unfortunately, no data is available on the material costs of the planned maintenance schedule after 24,000 running hours, so this estimation is based on the first 24,000 generator running hours. In the results, it will be shown how much time passes before an average generator reaches this 24,000 running hours limit. Using these figures, the average material costs for planned maintenance are $38.50 per running hour. When the costs per running hour are known, the reduction in maintenance costs is calculated by multiplying the reduction in running hours by these maintenance costs per running hour.

Table 6.5: Part of planned maintenance schedule, notice here that the prices that are used to calculate the costs of the parts are directly taken from the MAN offer, hence the exact numbers up to 2 decimals.

	nr. of parts						
Job	6000 hr	12000 hr	18000 hr	24000 hr	total in 24000 hr	part price	Job total
A	2	2	2	2	8	$ 10,000.00	$ 80,000.00
B		4		4	8	$ 150.00	$ 1,200.00
C				20	20	$ 20,000.00	$ 400,000.00
⋮							⋮
Z		3		3	6	$ 23.00	$ 138.00 +
							$927,192.16

6.2. Results

6.2.1. Fuel Consumption and Running Hours

The results from the simulation described in the previous section are summarized in Table 6.6. Since this simulation was executed for 100 days, the absolute fuel consumption and running hours are multiplied by 3.65 to the find the results per year. The reduction in fuel consumption and running hours is bigger for hybrid system option 2 than for hybrid system option 2, because in this system option, an additional generator is only started when the battery has been in use. System option 1 operates more conservatively because no back up power is present in case the power demand is higher than the online generator capacity. Therefore, on average, in hybrid system option 1, more generators are online than in hybrid system option 2. This difference is made clear when the PMS of hybrid system option 2 is shown in operation, as can be seen in Figure 6.3. As is shown in this figure, in hybrid system option 2, the online generator capacity is lower on average than in hybrid system option 1, of which the operation was tested and shown in Figure 4.27 in Section 4.4. This operating difference directly translates into the running hour reduction and indirectly translates into the fuel consumption reduction through Equation 6.1, because when running on more generators, the power factor is lower, so the specific fuel consumption is higher. The result for the specific fuel consumption by running on higher partial load is shown for hybrid system option 1 in Figure 6.4 and for hybrid system option 2 in Figure H.1 in Appendix H. In these figures, the blue box represents the 25^{th} and 75^{th} percentile of the operating load, and the black dotted boxplot whiskers represent the 99% bound of the operating partial load.

Table 6.6: Results fuel consumption and running hours reduction, an HFO price of 546$/ton is use here, like in Chapter 2.

System option	**Running hours [hr/yr]**	**reduction**	**Fuel consumption [ton/yr]**	**reduction**	**fuel consumption reduction [$/year]**
'no hybrid'	4.1E+04	-	2.9E+04	-	-
system option 1 (one battery)	2.1E+04	-50.1%	2.6E+04	-8.4%	1.3E+06
system option 2 (two batteries)	1.9E+04	-53.1%	2.6E+04	-9.0%	1.4E+06

6.2.2. Reliability

Simulation Results In the old 'no hybrid' system, the power generator system consisted of two engine rooms housing a number of running generators of which one generator was redundant most of the time. In hybrid system option 1, the power generation system consists of a minimum amount of online generators per engine room, where one battery can supply power in case of a generator failure. In hybrid system option 2, the power generation system also consists of a minimum amount of online generators per engine room, but a battery is installed in each engine room.

From the simulations, the failure rates of the basic events that were not known from the experts experience are listed in Table 6.7. It can be seen that although the relatively conservative method of load dependent start is used in the old 'no hybrid' system, the chance that the power is above the online generator capacity in case a generator would fail is still significant, in the order of 5% during 60 seconds. This is caused by load dependent start having a start delay of 30 seconds, as explained in Chapter 2. This means that power peaks lasting shorter than 30 seconds will not cause a starting decision and corresponding increasing online gener-

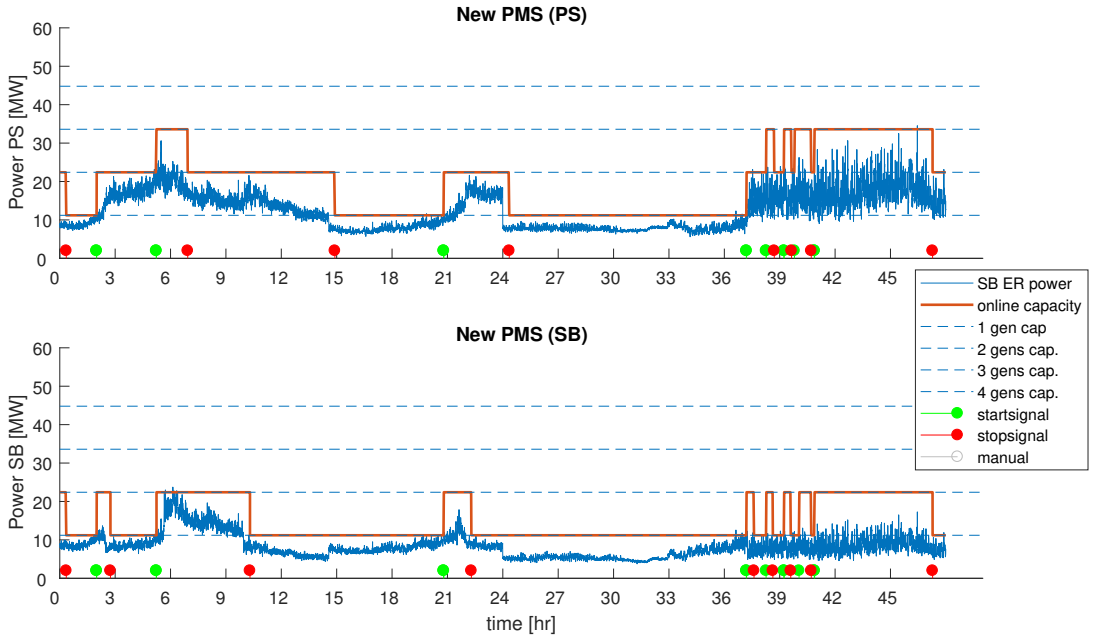

Figure 6.3: PMS test using load dependent start for hybrid system option 2 (two batteries). Both port side engine room as starboard side engine room.

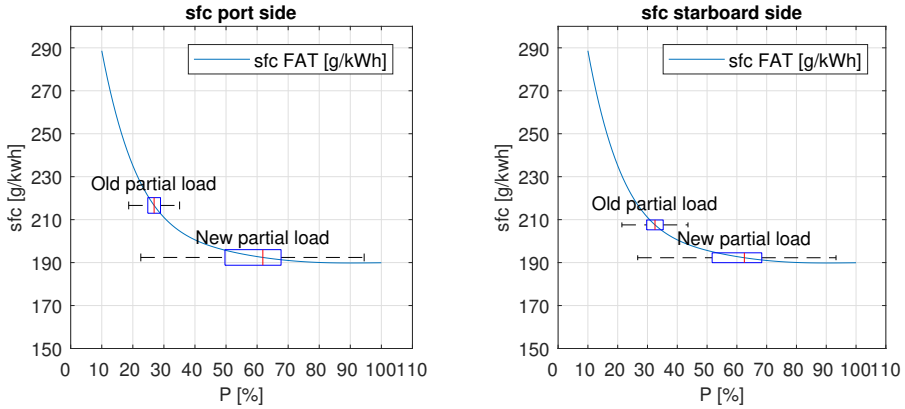

Figure 6.4: Hybrid system option 1: Difference in specific fuel consumption by running on lower partial load in the fuel consumption simulation of the portside engine room and the starboard side engine room.

ator capacity. An example of a situation where this event occurs can be seen in Appendix G, where the PMS of hybrid system option 1 is compared to the old PMS. In Figure G.1 the old PMS is shown in operation. On day 2, from 38 hours until the end, the power demand is fluctuating a lot and numerous short power peaks are above the online generator capacity minus P_{nom}, so the basic event 'Power demand is higher than online generator capacity minus P_{nom}' is occurring frequently in this time span.

The difference between the probability of occurrence of the event 'requested power close to generator capacity' of hybrid system option 1 and hybrid system option 2 is caused by the conservative principle of the starting decision algorithm using the MLR model in hybrid system option 1. Because hybrid system option 1 does not have any back up power in case the power demand is higher than the online generator capacity, the decision of starting an additional generator is relatively conservative compared to hybrid system option 2. The result of this difference on the fuel consumption and running hours was explained in the previous section. For this basic event 'requested power close to generator capacity', the same explanation results in this difference in probability of occurrence between the different hybrid system options.

The basic event 'SOC insufficient due to peak shaving' in hybrid system option 2 did not occur in the 100

days simulation. This is caused by the spare capacity of the battery, which is sized based on supplying the nominal generator capacity for 90 seconds, although the starting time of a generator is tested at 60 seconds as was explained in Chapter 3. This results in the battery's state-of-charge to not have been below the minimum required amount of energy that is needed to supply the system with the nominal generator power for 60 seconds.

Table 6.7: Results of probabilities of occurrence from PMS simulations. For the fault trees, see Figure 5.2, 5.3, and 5.5

System option	Basic event FT	Description	λ_{60}
no hybrid	2	Power demand is higher than online generator capacity minus P_{nom}	4.60E-02
hybrid option 1	7	Requested power close to maximum capacity	5.79E-05
hybrid option 2	7	SOC insufficient due to peak shaving	0.00
hybrid option 2	8	Requested power close to maximum capacity	1.03E-02

Significance of basic events For all three system options, the importance factor of every basic event is calculated using the failure rates from the expert's opinion and the simulation as described above. These importance factors can be seen in Figure 6.5. The importance factors tell the contribution of each basic event to the probability of occurrence of the top event. From these important factors, the following can be seen:

- For the 'no hybrid' option, a combination between a power train failure and the power demand being above the online generator capacity is dominant. This result is well explained by the fault tree of this system option (Figure 5.2). For the main event to occur, a combination of one of the events on left and one of the events on the right side of this fault tree should happen at the same time. On the left side of this fault tree, the only event is the event of a generator failure. On the right side, the probability of occurrence of the event of the power demand being above the online generator capacity is completely dominating (being a factor 16,000 higher than the probability of a generator failure).
- For hybrid system option 1, the event of an unexpected rise of power is dominating the chance of the top event to occur. As can be seen in the fault tree of this hybrid system option (Figure 5.3), this event directly results in a short-term failure, making the chance of this short-term failure around 36,000 times higher than the long-term failure side of the fault tree.
- In hybrid system option 2, the top event probability of occurrence is dominated by the long term failure side of the fault tree through a combination of a power train failure combined with either the failure of the to be started additional generator, or a circuit breaker failure of that additional generator. The fault tree of this hybrid system option was shown in Figure 5.5.

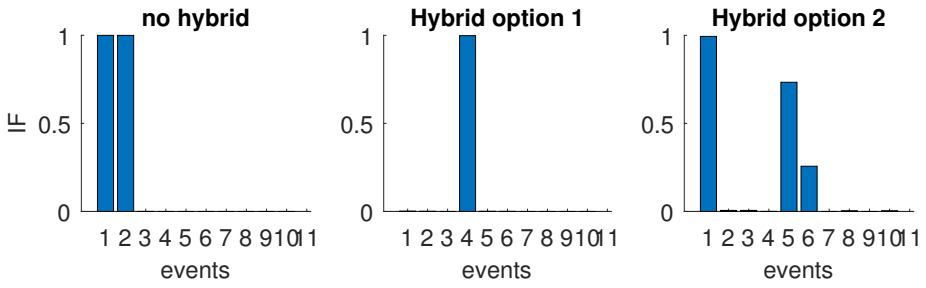

Figure 6.5: Importance Factors of different basic events of 'no hybrid option', hybrid option 1, hybrid option 2. For the legend of these importance events, see Table 6.8

For the hybrid system itself, the importance factors of every component are shown in Figure 6.6. For the sub-fault-tree of the hybrid system, refer back to Figure 5.4. The difference between hybrid system option 1 and hybrid system option 2 is the failure on demand of the circuit breaker to close (basic event A). In system option 1, the battery is only connected to the power grid in case of generator failure, so if the circuit breaker fails to close when needed, the sub-fault-tree of the hybrid system propagetes a failure. Therefore, the closing of the circuit breaker is dominant in this sub-fault-tree, as the probability of occurrence of this event is

Table 6.8: Overview of significant basic events for the probability of occurrence of the top event. For reference, see the fault trees of the different system options in Figure 5.2, 5.3, and 5.5

system option		**Significant basic events**
no hybrid	(old system)	1: Generator failure 2: Power demand is higher than online generator capacity
hybrid option 1	(1 battery system)	4: Unexpected rise of power demand
hybrid option 2	(2 batteries system)	1: Generator failure 5: Circuit breaker closing failure 6: Additional generator starting failure

significantly higher than the probabilities of occurrences of other subsets of this fault tree. For hybrid system option 2, the hybrid system is continuously connected to the power grid, so there is no chance of a circuit breaker closing failure. Therefore, in this sub-fault-tree, the transformer failure (basic event B) is dominant, as the probability of occurrence of this event is significantly higher than other subsets of the fault-tree when the circuit breaker is not included.

From these importance factors of this sub-fault-tree, it can be seen that the conservative estimates of the battery related components of the hybrid system (unhealthy batteries, battery auxiliary failure, false positive health status from battery monitoring system) are not significantly contributing to the failure chance of the hybrid system. As explained in Chapter 5, for these components, no expert's opinion was available, so conservative estimates were used. From the analysis of the importance factors, it can be seen that even these conservative estimates have no significant influence on the end result[2], so it is concluded that in this reliability analysis there is no need for a more accurate estimation of the failure chance of the hybrid system basic events using a different method.

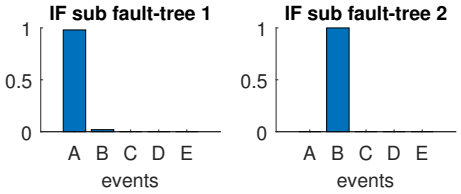

Figure 6.6: Importance Factors of components in sub-fault-tree of hybrid system option 1 and hybrid system option 2

Reliability Using the probabilities of occurrence from the expert's opinion and the simulation as described above, the reliability of the three different system options is assessed by the method described in Chapter 5. The confidence bounds of these reliabilities are calculated using a Monte Carlo simulation using a uniform distribution of every basic event. For all three system options, the 10 years reliability is calculated, representing the chance that the power generation system has been able to supply the power demand in the given time interval. Next to that, the expected time needed to reach 95% reliability is calculated. The reliability $R(t)$ of all three systems is shown in Figure 6.7 on different axis scales for readability. It can be seen that the 10 years reliability of the 'no hybrid' system is expected to be between 0.40 and 0.63. The 10 years reliability of hybrid system 1 is expected to be 0. The 10 years reliability of hybrid system option 2 is expected to be between 0.83 and 0.93. The time to reach 95% reliability is between 205 and 397 days for the 'no hybrid option', between 1 and 3 days for hybrid system option 1, and between 1000 and 2700 days for hybrid system option 2. These numbers are summarized in Table 6.9.

For the 'no hybrid' system option, because the chance of the power demand being above the online generator capacity minus P_{nom} is significant (around 5% during 60 seconds), the expected probability of occurrence of the main event is 7% each year. This results in the reliability to decrease to around 50% in ten years. For hybrid system option 1, the reliability is totally dominated by the chance of an unexpected rise of power because no back up power is present to cope with an unexpected power peak in this system option. This

[2]When multiplying the probabilities of these three battery related events by a factor 1000 to assess the effect of even more conservative estimates, these events do still not significantly contribute to the failure probability of the sub-fault-tree of the hybrid system. This is caused by the fact that these events have to occur simultaneously for the hybrid system to fail, so the probabilities of occurrences are multiplied.

results in the low reliability as can be seen in the comparison. Hybrid system option 2 shows a relatively high reliability as the probability of the main event to occur is dominated by combinations of events that show a relatively low probability of occurrence. The main difference between the 'no hybrid' and hybrid system option 2 is the ability of the system to supply power when a generator fails. For the 'no hybrid' option, there is a chance that the power demand is higher than the generator capacity that is left after a generator failure resulting in insufficient power capacity. For hybrid system option 2, if a generator fails while the power demand is higher than the online generator capacity, the battery is discharged faster than if the power would have been under the online generator capacity, but it is still able to supply the power demand and the top event would not occur directly.

The reader should pay attention here to the definition of the main event: insufficient power capacity. This means that the main event occurs if the power generation system cannot supply the power demand. However, further research is needed to assess the consequences of this main event. For the case vessel, when this event occurs, the first consumer that is cut is the DP system, which means that less power is directed to the DP system than it requests. This could result in a loss of position, which should be avoided at all times, but a loss of position is not necessarily the case during every shortage of power. However, the goal of the power generation system is to supply the power that is requested by all systems combined, so the reliability of fulfilling this goal is a strong measure to compare the effectiveness of these different system options relative to each other in functioning as the power generation system and is therefore used in this analysis.

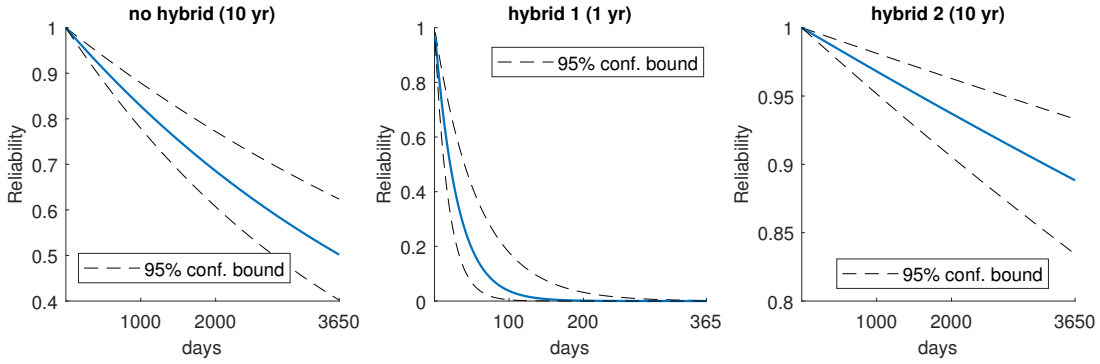

Figure 6.7: Reliability of different system options. For the 'no hybrid' and hybrid system option 2, the 10 years realiability is shown. For hybrid system option 1, the 1 year reliability is shown. The graphs are shown in different scales for readability.

Table 6.9: Overview of reliability results

	$\mathbf{R}_{10years}$ [-]		$\mathbf{t}_{R=0.95}$ **[days]**	
	lower bound	upper bound	lower bound	upper bound
no hybrid	0.40	0.62	200	400
hybrid system option 1	0.00	0.00	1	3
hybrid system option 2	0.83	0.93	1000	2700

6.2.3. Battery Aging

In case of hybrid system option 1, the battery is only in use during one of the full cycles caused by a generator failure, a battery test, or a human failure as described in Section 6.1.4. This means that the battery goes through ten full discharge cycles between 70% and 20% state-of-charge per year. In case of hybrid system option 2, the battery goes through the same ten full discharge cycles as well, but is also subjected to the smaller cycles when the power demand exceeds the generator capacity. In Figure 6.8a, the depth-of-discharge and C-rate of an example day is shown for hybrid system option 1. As can be seen, the battery is hardly used because the battery should only be used as back up power during a generator failure. Only at the end of the day, an example is shown of a battery test, where the battery is fully discharged from the initial 70% to 20%, creating a cycle having a depth-of-discharge of 50%. For hybrid system option 2, during the example day, 19 regular cycles occurred (the power data of Figure 6.3 is used for this example) and in this example also a manual cycle is added presenting a battery test. From these cycles, the cycle aging is calculated using the depth-of-discharge and C-rate of every cycle in Equation 6.9 and Equation 6.10. Again, the 100 day simulation

-as explained in Section 6.1.1- is used to find all charge/discharge cycles that occur each 100 days for hybrid system option 2. For hybrid system option 1, the battery is only subjected to the yearly manual cycles.

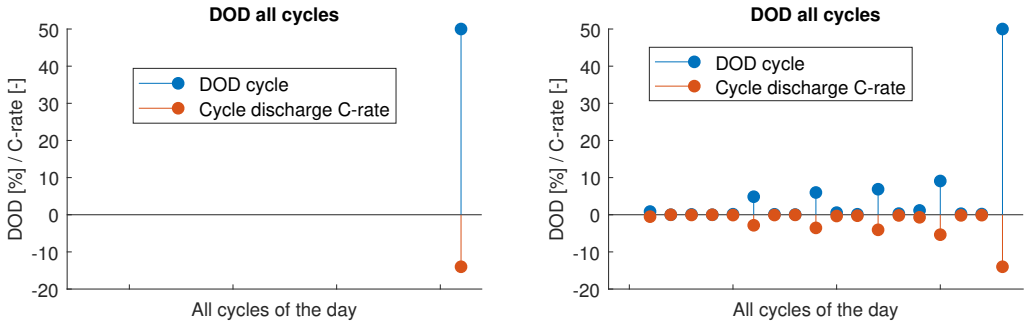

(a) DOD and C-rate of all charge/discharge cycles during the day of Figure 6.3 using hybrid system option 1

(b) DOD and C-rate of all charge/discharge cycles during the day of Figure 6.3 using hybrid system option 2

Figure 6.8: Examples of the depth-of-discharge during charge/discharge cycles using either hybrid system option 1 or hybrid system option 2. At the end of the day, a battery test is performed, so the battery is discharged from 70% to 20% state-of-charge at maximum C-rate of 14C.

When all cycles are used to estimate the yearly aging using the simulations of the two different hybrid system options, the loss in capacity due to cycle aging of hybrid system option 1 is 0.015% per year and of hybrid system option 2 is 0.063% per year for the portside battery and 0.031% for the starboard side battery.

In Figure 6.9, the cumulative capacity loss due to calendar and cycle aging is shown during the first 5 years of operation by the blue solid line. In this figure, the aging of hybrid system option 2 is shown in order to show the effect of the cycle aging by using the battery also to support the power generation system during power demand peaks. In hybrid system option 1, the only cycles the battery is subjected to are the cycles for testing, generator failures, and human error. However, the total cumulative battery degradation (blue solid line) would be almost equal, because the total battery degradation is dominated by the calendar aging. In this figure, the cycle aging is shown by the black solid line at the bottom of the figure, where it can indeed be seen that the cycle aging has only a small contribution to the total battery aging. This is caused by the fact that the battery is only cycled little, which is a result of the load dependent start that starts an additional generator immediately after the battery has been used. In further research, an optimization strategy could be used to find the economical optimal limit for this load dependent start limit taking into account the fuel costs, maintenance costs, and battery degradation.

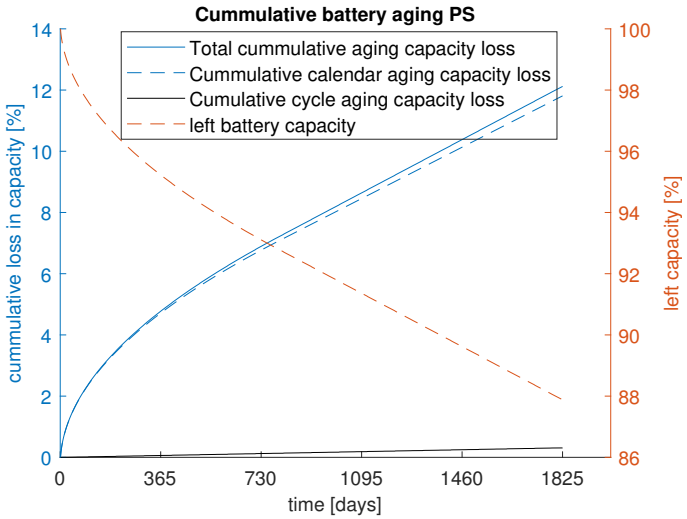

Figure 6.9: Cumulative battery aging

If the linear relation (from 800 days onward) would be extended, which would imply that the calendar

aging stays constant and that the cycle aging does not change in time, the time to end-of-life can be calculated. The linear relation between time and battery degradation (from 800 days onward) follows the following equation:

$$C_{left}(t) = 96.64 - 0.0048 \cdot t \tag{6.11}$$

Where:
C_{left}: The left battery capacity after t days [%]
t: Time [days]

Solving this equation for the end-of-life capacity of 80%, the battery would have to be replaced after 9.5 years of operation, making the depreciation of the battery $90,000.00 each year for the portside battery of hybrid system option 2, of which the degradation was shown in Figure 6.9 and explained above. When the same methodology is used to calculate the depreciation of the starboard side battery of hybrid system option 2, this also results in $90,000.00 per year (as could have been expected, since only the cycle aging is different for the starboard side engine room, but the cycle aging is only a small portion of the total battery aging). Therefore, the total depreciation costs of the batteries of hybrid system option 2 are $180,000.00 per year.

The same methodology is used to calculate the yearly depreciation of hybrid system option 1, which is $87,000.00 per year. The difference between hybrid system option 1 and 2 is caused by the difference in charge/discharge cycles, because in hybrid system option 1, the battery is only used for generator failures, battery testing, and human errors, where the batteries of hybrid system option 2 are also used for dealing with power demands that are higher than the online generator capacity. Again, it should be noted here that it is assumed that the linear relation between time and battery aging can be extended up till 10 years of operation. However, more battery aging test data is needed to support this assumption.

6.2.4. Maintenance Costs

As was explained in Section 6.1.5, the total material costs for planned maintenance are $930,000.00 for 24,000 running hours, which can be translated to an average of $38.50 per running hour. This means that based on the running hour reduction of hybrid system option 1, the reduced material costs for planned maintenance are $760,000.00 per year, and of hybrid system option 2, the reduced material costs for planned maintenance are $850,000.00 per year. The results of the planned maintenance material costs reduction is summarized in Table 6.10.

Table 6.10: Summary of material costs reduction of planned maintenance

System option	**Running hours**	**PM material costs** [$/year]	**Reduction** [$/year]
'no hybrid'	4.12E+04	$ 1,600,00.00	-
hybrid system option 1	2.14E+04	$ 820,000.00	$ 760,000.00
hybrid system option 2	1.94E+04	$ 750,000.00	$ 850,000.00

As said, only for the first 24,000 hours, data of the planned maintenance schedule is available. When using one of the hybrid systems, the time that is needed for an average generator to reach these 24,000 running hours is 9.1 years for hybrid system option 1 and 10.1 years for hybrid system option 2. Therefore, it is concluded that the planned maintenance schedule until 24,000 running hours is sufficient to use in the analysis on the first 10 years of operation of the hybrid system.

To find the effect of the corrective maintenance reduction, further research is required into the relation between engine wear and running hours. Using the planned maintenance schedule to estimate the material costs reduction of planned maintenance is a relatively straight forward method using predetermined prices for engine parts and a deterministic planned maintenance schedule. However, corrective maintenance requires a more general approach and a more statistical method, which could be a research topic on it own and is therefore left out in this analysis.

6.2.5. Summary of Results

In Table 6.11, an overview of all results is shown. The difference in configuration between hybrid system option 1 and hybrid system option 2 is shown again here in Figure 6.10. Both hybrid system options show significant running hours and fuel consumption reduction compared to the 'no hybrid' system. The amount of required hybrid systems (batteries, converters, transformers) of hybrid system option 1 is half the amount of hybrid system option 2. This means that the investment costs of hybrid system option 2 are double the investment costs of hybrid system option 1. The fuel savings compared to the 'no hybrid' system are higher

for hybrid system option 2 than for hybrid system option 1, because hybrid system option 2 runs on less generators on average, meaning a higher power factor, resulting in a lower specific fuel consumption. Using hybrid system option 1, the fuel consumption costs could be reduced by $1,300,000.00 per year and using hybrid system option 2, the fuel consumption costs could be reduced by $1,400,000.00 per year during pipe laying. The reduction in running hours results in the reduction in material costs for planned maintenance of $760,000.00 for hybrid system option 1 and of $850,000.00 for hybrid system option 2.

The 10 years reliability of hybrid system option 1 to be able to supply the power demand is almost zero, because no back up power is present in case of an unexpected rise of power. In case of the 'no hybrid' system, this back up power is present as a redundant generator. In case of hybrid system option 2, this back up power is present as the continuously connected battery. So although the MLR model based starting decision algorithm results are promising for hybrid system option 1, even a small chance of an unexpected power rise (which was not expected by the MLR model) results directly in insufficient power capacity to supply the demand, hence the low reliability.

By using two separate hybrid systems, like in hybrid system option 2, the reliability to supply the power demand has significantly increased compared to the old 'no hybrid system'. This is caused by the significant chance (around 5%) that the power demand is higher than the online generator capacity in case of generator failure in the 'no hybrid' system. This chance was introduced in the 'no hybrid' system by the start delay in the load dependent start.

The depreciation costs of the battery due to battery aging is calculated using the lithium-ion battery degradation model. The battery aging is mainly caused by calendar aging, because the batteries are not used excessively and the charge/discharge cycles are relatively shallow. For hybrid system option 1, the only discharge cycles are the cycles for testing, generator failures, and human errors. For hybrid system option 2, the battery is also subjected to the cycles that are needed for back-up power in case of an increasing power demand. This results in a difference in depreciation, as the batteries of hybrid system option 2 degrade faster than the batteries of hybrid system option 1. This results in a depreciation of the batteries of $87,000.00 and $180,000.00 for hybrid system option 1 and 2 respectively.

In short, both hybrid system options show significant fuel consumption and running hours reduction. The investment costs of hybrid system option 1 are half the investment costs of hybrid system option 2. However, the fuel consumption and maintenance costs reduction are higher for hybrid system option 2. Using the investment costs, fuel consumption reduction, maintenance cost reduction, and battery depreciation, the payback time of hybrid system option 1 is 0.94 years, and the payback time of hybrid system option 2 is 1.8 years during pipe laying operations. However, the reliability of hybrid system option 1 is insufficient for this system to be practically feasible. By applying hybrid system option 2, the reliability of the system compared to the old 'no hybrid' system could be increased. In the next chapter, it will be discussed how these numbers should be interpreted and which parameters influence the results the most.

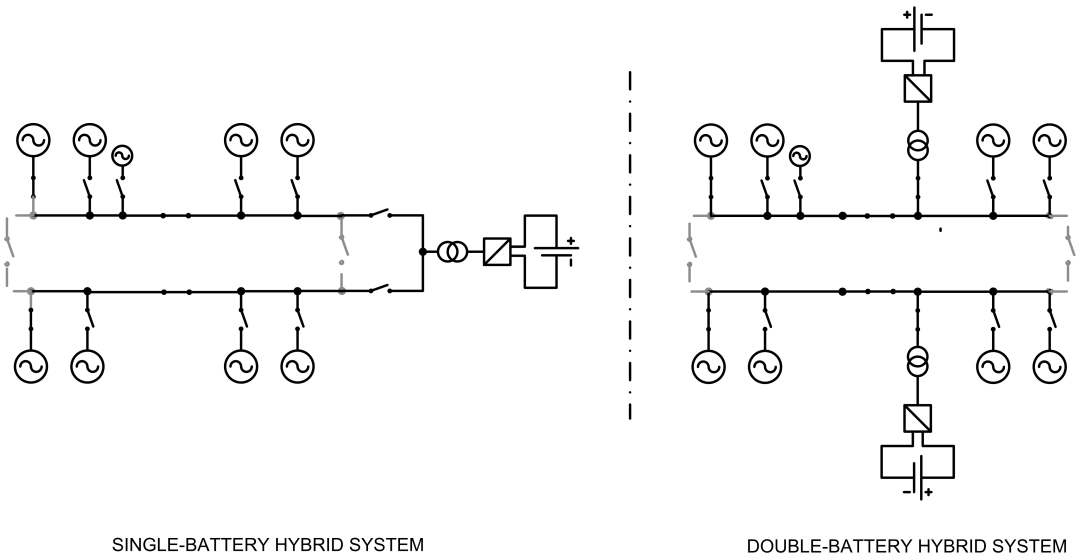

Figure 6.10: Difference in configuration of hybrid system option 1 and 2

Table 6.11: Summary of Results, *PM: Planned Maintenance

		no hybrid	**hybrid option 1**	**hybrid option 2**
EES connection to grid		-	In case of a generator failure	Continuously
Number of hybrid systems		-	1	2
Maturity		Pracitcally proven technology	New technology	Studied in previous research
PMS principle		Load dependent start	Multiple Linear Regression model	Backlooking (load dependent start)
Installed energy storage	[kWh]	-	800	1600
CAPEX	[$]	-	1,850,000.00	3,700,000.00
Fuel savings	[%]	-	8.4	9.0
	[$/year]	-	1,300,000.00	1,400,000.00
Running hours savings	[%]	-	50.1	53.1
PM* costs savings	[$/year]	-	760,000.00	850,000.00
Battery depreciation	[$/year]	-	87,000.00	180,000.00
Payback time	[years]	-	0.94	1.8
10 years reliability	[%]	40-62	0.00	83-93
time to reach 95% reliability	[days]	200-400	1-2.9	1000 - 2700

7

Discussion of Results

The previous chapter presents the simulation results for the fuel consumption, running hours, and reliability of the three system options: 'no hybrid', hybrid system option 1 (single-battery), and hybrid system option 2 (two seperate batteries). In this chapter, next to these simulation results, the results found in previous chapters are discussed. It will be discussed how the assumptions that were made influence the results and how the found results should be interpreted.

7.1. Operational

In Chapter 2, it was explained that the focus of this thesis is on pipe laying operations although operations of the case vessel include pipe laying and heavy lift projects. The decision to only focus on pipe laying was made because the critical operation during heavy lifting where maximum redundancy is required only lasts a couple of hours to days per year, where pipe laying projects are continuous operations lasting multiple months to years. However, both during pipe laying operations as during heavy lift operations, the vessel is using spinning reserve for DP redundancy. Therefore, although the method is only tested during pipe laying operations, the benefits of replacing spinning reserve by energy storage both apply to pipe laying operations as to heavy lift operations. Only during transit, the vessel is not using spinning reserve because all generators are online continuously to reach maximum speed to save working time. So during transit, the benefits of the hybrid system are not applicable. When data of more years of operation are available, a more specific operational profile could be created, but when examining the currently available data, during the first operational year of the case vessel, the vessel has been in transit for 10% of the time. This means that for the case vessel, the true benefits of the hybrid system compared to the benefits during continuous pipe laying which are presented in the results are possibly 10% lower during last year. The effect of the transit time should be studied when more information is available about the vessel's general operational profile throughout the years.

Next to that, all available power data was measured during the first pipe laying project of the case vessel, because this was the only available data measured so far. This project was completely executed in the Black Sea. It was endeavoured to use a wide variation of sea states to train the model, but the model should be trained more during operations in different waters and different sea states, because the vessel might respond differently to wave periods that are different in other waters. Besides, a data set of twelve days is used, where it could be possible that not all possible combinations of wave height, primary peak direction, wave period, wind speed, and wind directions are learned by the model. In this thesis, the concept of using a MLR model in the PMS is demonstrated, but for the practical application of this method, more training data would create a more 'experienced' model, which is more likely to predict power peaks correctly.

The same chapter explains the focus on deep water pipe laying. This focus was chosen because no data was available for shallow water pipe laying and because it was expected not to influence the result. The main difference between shallow and deep water pipe laying are the pipe pulls that are made during shallow water pipe laying. Pipe pulls are distinct moments where the vessel moves 12 or 24 meters (dependent on the pipe lengths) forward when a pipe weld is finished. In shallow water, the forward movement of the ship should be aligned with the length of pipe being released in the water. This results in high power peaks from the DP system, because the vessel is moving ahead as fast as possible for a high pipe laying rate. Therefore,

there is a difference in the power profile and corresponding peaks between shallow and deep water pipe laying projects. The MLR model is trained on a deep water pipe laying project and is therefore not applicable during shallow water projects. Before it can be used in a shallow water project, further research is needed into the power profile of these projects. However, the running hours and fuel consumption reduction are still expected to be significant when using a hybrid system instead of spinning reserve, because pipe pulls typically last longer than 30 seconds, which means that the load dependent start of the old 'no hybrid' system would make the system run on an additional -redundant- generator, creating a low power factor, so a high specific fuel consumption. In short, in the end, the decision to focus on deep water pipe laying does influence the training of this specific MLR model, but it does not influence the proof-of-concept of using this method in the PMS, and it is expected that it does not influence the benefitis in fuel consumption and running hours reduction.

7.2. Electrical energy storage

In Chapter 3, different types of EES are compared, where it is stated that flywheels typically have a self-dicharge of 100% per day. Although this was found in different papers, it is questioned if current modern flywheel systems still have a self-discharge this high. However, when the self-discharge of a flywheel system would be as low as the self-discharge of a lithium-ion battery, the lithium-ion battery would still have been selected as the EES on board of the case vessel because of the lower investment costs.

The size of the EES system is now based on supplying the nominal generator power for 90 seconds, which is the tested generator starting time of 60 seconds plus a safety margin. However, since replacing the spinning reserve of DP-II vessels is new technology that has not been proven yet, it is expected that class societies are reluctant to approve these systems for DP-II applications and require a bigger safety margin. This means that the investment costs of the battery could be higher than stated before. For the case vessel, it is expected that this would not be a problem, because of the high benefits that are gained by using a hybrid system. However, it does confirm the necessity of a single battery in combination with a smart starting decision algorithm.

7.3. Multiple Linear Regression Model

In the tests of the MLR model based starting decision algorithm, the system worked perfectly. However, some assumptions were made during the process that leave room for discussion. Firstly, the significant wave height that is used in the analysis is the forecasted significant wave height data received by the vessel from several weather stations. Although it is expected that the forecasted wave height shows a high correlation to the real wave height, no proof of this correlation exists yet, so it should be studied what the difference is between the forecasted wave height and the real wave height encountered by the vessel. This requires accurate wave measurements on board of the vessel or on buoys close to the vessel. No measurements of this kind have been performed yet during pipe laying. Next to that, only the wave height is used in the regression analysis, but it is expected that the direction of the waves also influences the peak-to-mean ratio, where waves from the side have a bigger influence than waves from the back[1].

Secondly, a linear relation between the peak-to-mean ratio and the predictor parameters is assumed in this analysis, but it could be possible that this relation is not linear. Instead of the linear relation, nonlinear relations between the dependent variable and the predictor variables can be used. Especially when considering the cubic relation between the wind speed and the estimated DP_{wind} load (as was stated in Section 4.2.7), the relation between the peak-to-mean ratio and the estimated DP_{wind} load could have a higher power. Therefore, a polynomial regression model potentially fits better.

Thirdly, the limited amount of power data that is used to train the regression model might not cover significant operational power increases that are unrelated to the wave height and the wind speed/direction. Examples of such operational power increases could be a sudden change in heading or the mooring of a pipe supply vessel to the side of the *Pioneering Spirit*. These sudden power increases are unexpected to the MLR model as these are not a result of environmental conditions that are the input to the model and could therefore be a threat to the save operation of hybrid system option 1. Therefore, before using the MLR model based starting decision algorithm, further research is needed into sudden unexpected power increases caused by other factors than the environmental conditions. In hybrid system option 2, sudden unexpected power increased are

[1] Front waves also have an exceptionally high influence on the DP power of this specific case vessel due to the unusual shape of the front ship of the Pioneering Spirit.

covered by the continuously connected batteries.

Lastly, only parameters that are well measured on board are used in the regression analysis, both due to the availability of data as to develop a working online version. However, this could result in a limited perspective on the relevant predictor parameters for the peak-to-mean ratio of the DP load, as other parameters might also influence this ratio. Parameters that potentially also influence the peak-to-mean ratio are the pipe tension, the water depth, or the current speed/direction. These parameters would have to be measured and stored to find the relation between these parameters and the peak-to-mean ratio. Further research could expand the selection of parameters by finding methods of measuring these parameters.

7.4. Reliability

The reliability of hybrid system option 1 is minor compared to hybrid system option 2 and to the old 'no hybrid' system. This is caused by the the consequence of exceeding the online generator capacity. When the online generator capacity is exceeded, no spare power capacity is available, because the battery is only connected in case of a generator failure. Therefore, the chance of exceeding the online generator capacity directly results in the unreliability of this system. Although the MLR model based starting decision algorithm of this system option shows the oparability of this PMS principle, according to expert's opinion, an unexpected rise of power could occur between 6-20 times a year, causing the reliability of this system to decrease to 95% within 1 to 3 days. To find the influence of the this expert's opinion, it is investigated what changing this occurrence rate means for the reliability of hybrid system option 1.

To reach the reliability of the old 'no hybrid' system, the probability of occurrence of an unexpected rise of power should maximally be between: $9.0 \cdot 10^{-8}$ and $1.7 \cdot 10^{-7}$ during 60 seconds, which means that an unexpected rise of power may only occur once every 21 years of operation. To reach this reliability, the MLR model should be trained with an extensive range of environmental scenarios and should apply the most extreme power peak cases encountered in a specific environment to comparable environments. Using a MLR model based starting decision algorithm this way could lead to an excessively conservative PMS and reduce the benefits from the hybrid system. Besides, the estimated reliability of these three systems is a useful tool to compare the systems to each other, but the consequence of unreliability to the operation should be further investigated, because not every case of insufficient power demand would lead to a loss of position. If the consequences of insufficient power capacity and the risks involved for the operation would be known, the smart small hybrid system option 1 could be compared to the simple but robust hybrid system option 2 in terms of risks involved and the corresponding costs of these risks.

A strong addition to hybrid system option 1 would be to install two separate fast-response-EES devices connected to both engine rooms, for example a small super capacitor in both engine rooms. The system would than also operate using the MLR model in the PMS and would still use only one back-up battery in total, to be used only in case of a generator failure. When sized well, this smaller EES device would deal with the minor power peaks crossing the online generator capacity. The advantage of only having to install one big hybrid system would than still hold, but a power peak crossing the online generator capacity would not directly result in insufficient power capacity, so it would increase the reliability significantly. Further research is needed to determine the exact size of this fast-response device, but as a preliminary impression, during the 100-day simulation of the PMS of hybrid system option 2, the battery's depth-of-discharge[2] has not been above 10.6%. So for the power data available, no unexpected power peaks could have needed more than 67 kWh of energy. Note here that in the simulation of the PMS of hybrid system option 2, the load dependent backlooking starting decision algorithm is used, so every power peak crossing the capacity was unexpected (since the PMS only responds to power peaks crossing the capacity in the past, it is an a posteriori principle). When using the a priori MLR model based starting decision algorithm, unexpected power peaks are expected to require less energy, so a fast-response EES device of 70 kWh would probably be sufficient for this application. Sizing and selection of a fast response EES to increase the reliability of a single battery hybrid DP-II vessel would be an interesting topic for a follow-up study.

Another discussion on the results of the reliability analysis is the assumption that all basic events are independent. To calculate the probability of occurrence of the top event of the fault tree, it is assumed that the basic events occur independently as was explained in Section 5.2. However, it could be possible that a basic event influences another basic event. For example, for the 'no hybrid' system, it is assumed that the chance that the power is higher than the online generator capacity after a generator failure is around 5% during 60

[2]The depth-of-discharge is defined here as 1-SOC, where SOC is the state-of-charge.

seconds. This is stated because in 5% of the time in the power data, the power demand is higher than the online generator capacity minus the nominal power of one generator. However, it could be possible that a generator failure is influenced by the power demand, so it could be possible that the chance that the power demand is higher than the left capacity after a failure is higher than 5%, because generators fail more often during increasing power. This would decrease the reliability. It could also be possible that generators fail more often during decreasing power, which means that the chance that the power demand is higher than the left capacity after a generator failure is smaller than 5%, which would increase the reliability. For this analysis, the difference in reliability between the three systems is high, so little fluctuations in the results due to this assumption are expected not to change the comparison between the three system options.

For the hybrid systems, dependent on the amount of online generators, the reliability is estimated relatively conservative because if an additional generator does not start during a generator failure, this directly leads to insufficient generator capacity according to the fault tree. However, if the power demand is relatively low compared to the left generator capacity after a generator failure, there could be time to start the next generator if one additional generator does not start and more standby generators are available in that engine room. For hybrid system option 1, this is of little influence because the probability of occurrence in this system is dominated by another basic event. For hybrid system option 2, this conservative estimate could lead to lower estimated reliability than the actual reliability. This does not influence the final conclusion, where the reliability analysis is used for the comparison between the different hybrid options, because hybrid system option 2 is the most reliable option in this analysis and could potentially only be more reliable. To prevent this conservative estimate, a dynamic fault tree could be used, which is depending on the amount of online generators and the power demand.

For the reliability analysis, it was assumed that the failure rate of every component is constant regardless of the time it has been in operation. This is common practice in reliability assessments when little reliability data is available, but this assumption could influence the result. If the failure rate increases in time, the reliability curves could decrease faster, which means that the reliability is currently over estimated. For the 'no hybrid' system, an increasing failure rate of the generators would directly influence the reliability. For hybrid option 1, this would be of little influence because the probability of occurrence of the undesired event is not dominated by the failure of a component. For hybrid system option 2, an increasing generator failure rate or an increasing probability of a generator to not start when requested would influence the reliability. If extensive failure data is available, this influence could be studied, but for this analysis where the difference between the hybrid systems is especially important, the effect on the final conclusion is expected to be minor.

A final remark can be made on the reliability using a MLR model. The MLR based starting decision algorithm is now developed for the single battery hybrid system, but it could also be applied to the current power management system to replace the load dependent start and increase the reliability of the current 'no hybrid' system. So DP-II vessels could increase the reliability of the power generation system with little investment costs. Since the input sensors for the MLR model are already available on board, only the software of the PMS would have to be updated. This would decrease the chance of the power demand being above the online generator capacity after a generator failure and would therefore improve the reliability for DP-II vessels in general that are currently using load dependent start.

7.5. Economical

The reduction of maintenance costs is currently estimated using only the materials needed in the planned maintenance schedule. However, it is also expected that corrective maintenance would be reduced significantly due to the expected reduced chance of failure when less generators are running. Therefore, it is expected that the maintenance costs reduction is potentially higher than presented in the results. It would be interesting to find a relation between running hours and corrective maintenance in following research.

The battery aging parameters that are used to estimate the battery aging are based on lithium-ion batteries that were tested for 800 days. In the first part of these 800 days, the aging rate (battery capacity loss per day [%]) declined rapidly, after which it kept declining slowly. After these 800 days, no testing data of the calendar aging is present, so no information is available on the aging rate after these 800 days. In the analysis, it assumed that the aging rate does not decline anymore after these 800 days and keeps constant. Besides, it

assumed that the cycle aging is also constant in time. This results in a linear decline in battery capacity after 800 days. However, since no aging data is available of lithium-ion batteries after this time span, the estimation of the depreciation costs could be inaccurate. If the aging rate keeps declining, the battery could have a longer life time, but if the aging rate starts increasing again after some time, the battery could have a shorter life time than estimated here.

For the complete economical analysis, it should be estimated what the engineering and installation costs of the hybrid system are. It is proven in this thesis that both the single battery hybrid system as the double battery hybrid system have a short payback time when taking into account the material costs, but before deciding on the installation of this system, ship owners should consider the total project costs.

A final economical remark on the results should be made. Because hybrid system option 1 relies on only one hybrid system in total, the investment costs are half of the investment costs of hybrid system option 2. The investment costs of the transformer and the converters are a estimation from manufacturers and therefore relatively reliable, but the battery investment costs are based on an average cost/energy found in literature. For ship owners, when deciding on using energy storage, more specific information from battery manufacturers should be collected to consider the return on investment.

8

Conclusions and Recommendations

8.1. Conclusions

Currently, in DP vessels, common practice is to use spinning reserve to achieve redundancy of the power generation system to guarantee the power capacity in case of a generator failure. As was explained in the introduction, previous research focused on replacing this spinning reserve by a separate hybrid system in every engine room. In this thesis, the goal was to find a starting decision algorithm that would be applicable to a single-battery hybrid DP vessel. In this hybrid system, the battery is only connected to one of the engine room grids in case of a generator failure in that specific engine room. When the power demand increases, the starting decision algorithm in this PMS will start an additional generator before a power demand peak crosses the online generator capacity. It should do so because no spare capacity is present since the hybrid system is only connected in case of a generator failure. Therefore, no occasional peak shaving is allowed. By finding a starting decision algorithm that is applicable to this system, the investment costs for the hybrid system are halved compared to the double battery hybrid system as was proposed in previous research. In this thesis, an applicable starting decision algorithm is found and compared to the old system using spinning reserve and to a double-battery system option using separate hybrid systems in every engine room. These system options are compared to each other in terms of fuel consumption, maintenance costs, investment costs, and reliability. The research question that is answered is:

"What starting decision algorithm is applicable to a single-battery hybrid DP vessel to guarantee sufficient power capacity to supply the power demand?"

To answer this question, a set of research objectives was formulated and studied. These research objectives are discussed below:

- *To calculate the potential benefits of using a hybrid system in the case vessel: to assess the economical and technical feasibility of using electrical energy storage in the case vessel, a preliminary estimation on the benefits of replacing the spinning reserve should be made for the case vessel:*

  As preliminary check, it was examined if using maritime energy storage on board of DP pipelaying vessels would be beneficial in terms of fuel consumption and running hours. Using a short time-frame of power demand data, it was found that using electrical energy storage to replace spinning reserve would potentially reduce fuel consumption and running hours significantly. This preliminary check indicated the necessity of the research and the economical feasibility of the solution.

- *To select the appropriate type of electrical energy storage and determine the required size of the hybrid system:*

  Three different types of energy storage were compared: flywheel energy storage, super capacitors, and four types of batteries. From the relevant characteristics of all three types of energy storage, the lithium-ion battery was selected as the most suitable type of energy storage for this purpose. The required size of the battery is established at 800 kWh, based on the generator starting time, optimal state-of-charge range, battery efficiency, and battery's end-of-life capacity. Including the investment costs for the power electronics, this battery size results in a CAPEX of $1,850,000.00 for the single-battery hybrid system option and $3,700,000.00 for the double-battery hybrid system.

- *To find different options of the starting decision algorithm for the single-battery hybrid system option:*

  The starting decision algorithm options that were expected to be suitable for the power management system of a single-battery hybrid DP vessel were a mathematical-statistical method and a multiple linear regression analysis method. The mathematical-statistical method was a load-forecasting method that splitted three load groups and forecasted the load of these these groups separately. The hotel load was considered to be constant, so the measured hotel load was extended into the prediction horizon directly. The DP load was forecasted using the weather forecasts and a mathematical DP model. The pipe laying load was forecasted using a seasonal autoregressive-moving average model which was fitted to the observed pipe load and extends the learned pattern into the prediction horizon.

  In the multiple linear regression based power management system, the moving average of the total power demand -which is a slowly changing parameter- is measured and the peak-to-mean ratio compared to that moving average is predicted by the Multiple Linear Regression (MLR) model. This prediction is based on the relevant predictor parameters which are the input to the MLR model. When the measured moving average of the total power times the predicted peak-to-mean ratio (according to the MLR model) crosses the online generator capacity, an additional generator is started by this power management system.

- *To find the optimal starting decision algorithm from these potential options:*

  It was found that the mathematical-statistical method could not forecast the power demand accurately enough to be sufficient for the power management system. Due to the uncertainty in the weather forecasts, the DP load forecast based on the weather forecasts was not of added value compared to a constant propagation of the last measured DP load value. Besides, for accurate load predctions, the seasonal autoregressive-moving average method relies on a constant pipe laying period, which causes prediction errors when the pipe laying period changes.

  The multiple linear regression model based power management system works appropiately. The relevant input parameters to this model were found to be the significant wave height and the estimated DP load calculated by the wind speed and direction. The multiple linear regression model was trained by ten days of power and environmental data and was tested by two days of data in rough sea states to test the operability of this system in heavy conditions. The power management system worked flawless in these tests.

- *To assess the fuel consumption reduction and maintenance costs reduction of the single-battery hybrid system using a simulation of this online power management strategy, and to compare this reduction to the double-battery hybrid system and the 'no hybrid' system:*

  The fuel consumption of all three system options was calculated using the specific fuel consumption at different partial loads. Compared to the old 'no hybrid system', the fuel consumption is reduced by 8.4% using the single-battery hybrid system option and by 9.0% using the double-battery hybrid system. This difference between the hybrid system options is caused by the more conservative power management system of the single-battery hybrid system compared to the double-battery hybrid system, which is required to prevent power demand peaks that would cross the online generator capacity. When using an HFO price of $546/ton, this would result in a yearly fuel consumption reduction of $1.3M and $1.4M for the single- and double-battery hybrid system respectively. The maintenance costs reduction was calculated by the reduction in material costs of planned maintenance. For the single-battery hybrid system, the reduction in maintenance costs is $760,000.00 and for the double-battery hybrid system the reduction is $850,000.00. When also taking into account the battery depreciation, the payback period is 0.9 years for the single-battery hybrid system option and 1.8 years for the hybrid configuration where a separate hybrid system is installed in both engine rooms.

- *To compare the reliability of the single-battery hybrid system (using the found smart power management strategy) to the reliability of hybrid system 2 and the 'no hybrid' system.*

  The three different system options were compared based on the reliability in functioning as the power generation system. Fault Tree Analysis was used for this reliability analysis, where the fault tree was quantified using experts opinion on the probabilities of occurrence of the basic events. The main event of the fault tree was the event where the power demand could not be fulfilled by the power generation system. For the confidence bounds of the reliability, a Monte Carlo simulation was used. To compare

the system options, the time to reach 95% reliability was compared. For the old 'no hybrid' system, this limit was reached after 200-400 days, for the single-battery hybrid system, this limit was reached after 1-3 days, for the double-battery hybrid system, this limit was reached after 1000-2700 days. In short, the reliability of the single-battery hybrid system is insufficient for this system to be used as hybrid system of a DP vessel. This poor reliability is caused by the fact that that an unexpected power peak that crosses the online generator capacity causes the main event to occur directly. In other words, when the multiple linear regression model does not predict a power peak, the situation where where the power generation system cannot fulfil the power demand directly occurs.

To reach the same reliability as the old 'no hybrid' system, the multiple linear regression model would have to be trained extensively and reach a confidence where an unexpected power peak would only occur once every 21 years of operation. Next to that, it is expected that the reliability could be increased by using a fast response electrical energy storage device in every engine room, where the single-battery system could still be used. These fast response electrical energy storage devices could than deal with the unexpected power peaks, where the main battery is installed for an unexpected generator failure. Further research is needed for this application.

Using the findings in the different research objectives, the answer to the research question was found. The Multiple Linear Regression Model based power management system is applicable to a single-battery hybrid DP vessel. It works appropriately as was tested in different sea states and it reduces the investment costs for a hybrid DP vessel by 50% compared to hybrid system configurations proposed in previous research on hybrid DP vessels.

However, the single-battery hybrid system is less robust and more sensitive to unexpected power peaks than the double-battery configuration using a separate hybrid system in both engine rooms. The reliability analysis in this thesis demonstrates the difference between a hybrid system using a smart starting decision algorithm and a hybrid system using a relatively simple starting decision algorithm. The smart and small hybrid system results in lower investment cost while having a lower reliability and the robust and bigger hybrid system results in higher investment costs but has also a higher reliability.

Both the single-battery hybrid system as the double-battery hybrid system show significant reduction in fuel consumption and maintenance costs. However, as practical application for the case vessel discussed in this thesis and for DP vessels in general, the robust and simple double-battery hybrid system is preferred over the small and smart single-battery hybrid system due to the considerable difference in reliability. This conclusion is supported by the minor absolute difference in payback time between the single- and double-battery hybrid system, which is merely 0.9 years based on the CAPEX, battery depreciation, fuel consumption and planned maintenance costs reduction.

8.2. Societal and Ethical Impact

This research faces a number of societal and ethical effects which are discussed below:

- Fuel consumption and maintenance: as positive societal effects, the obvious results of this research are the reduction in fuel consumption and the reduction in maintenance due to the reduction in generator running hours. This results in a reduction in the emissions of green house and other polluting gasses and a reduction in spare parts consumption.

- Carbon dioxide balance: to assess the impact of the hybrid system on the reduction in green house gasses, it should be assessed if the CO_2 reduction caused by the fuel consumption reduction is sufficient when taking into account the environmental impact of the production of the batteries. According to [51], the CO_2 equivalent[1] of lithium-ion batteries is 110 kg/kWh of capacity. This means that the global warming effect of the production of a lithium-ion battery having 1 kWh of capacity would be the same 110 kg of CO_2 emmissions. This means that for the hybrid system proposed in this research, the single battery hybrid system would have to save at least 88 tons of CO_2 to break even. The double battery hybrid system would have to save at least 176 tons of CO_2. When the IMO conversion factor[2] of 3.1 is

[1] CO_2 equivalent is used to express the life cycle impact of goods. The CO_2 equivalent is a measure of how big the global warming effect of the production of a product is. It is expressed in the mass of CO_2 that would have the same impact on global warming as the production of a particular good.

[2] This conversion factor is the ratio between the mass of consumed fuel and the mass of emitted CO_2. This conversion factor is an approximation and depends on the composition of the fuel. Since the exact composition of the fuel is not known here and since the these numbers are only used for a firts approximation, it is assumed that this conversion factor can be used here.

used from HFO to CO_2 [27], [2], the yearly CO_2 reduction is 8100 tons when using the fuel consumption reduction. So replacing spinning reserve using this hybrid system has a significant positive effect on global warming.

- Fire safety of lithium-ion batteries: this battery chemical can be subject to thermal run away, where a chain reaction can occur if one cell overheats. This can cause a spontaneous fire in the battery modules. This phenomenon can be mitigated by a safe design that can dissipate the heat if one of the lithium ion cells overheats. However, even when optimizing the battery module design for fire safety, it should be taken into account in the risk analysis of this system that lithium-ion batteries face this problem.

- Employment rate: when reducing the maintenance jobs in the case vessel, it could be possible that less crew is needed on board, which could potentially result in a higher unemployment rate. However, this effect is expected to be limited in this specific case because engine room engineers are on board regardless of the amount of maintenance required. However, in the bigger picture, this research implicitly also contributes to smarter maritime systems on a wider scale, so it is contributing to the automation of maritime operations. Potentially, in the longer term, this could indirectly result in a higher unemployment rate of maritime personnel, which is an ethical concern that should be taken into account when designing smart solutions in the maritime industry.

8.3. Recommendations

From this research, a number of questions and recommendations arose. And since *"No man really becomes a fool until he stops asking questions."* (Charles P. Steinmetz[3]), these questions, ideas for further research, and recommendations are listed below:

- Find the effect of shallow water pipe laying on the reduction in fuel consumption and running hours of the generators. In shallow water, the power profile is significantly different than the power profile in deep water, because the vessel is moving 24 meters (a double pipe length) ahead every 5-7 minutes and is station keeping in between these 'pipe pulls'. This results in high power peaks from the DP system because these 24 meters shall be finished as soon as possible to continue the pipe laying process;

- Find more reliable numbers on the costs of lithium-ion batteries from manufacturers. In the battery comparison, the costs per energy that are used were found in literature, but these numbers could be outdated or too general for the specific battery that is required for this purpose;

- Train the MLR model in a wider variety of seas before implementing it in the PMS. The model is currently only trained in the Black Sea, but other waters may result in different peak-to-mean ratios due to different wave spectra;

- Study other relations between the predictor parameters and the dependent parameter of the MLR model. In this analysis, only the linear relation is studied, but a different relation e.g. a polynomial relation could result in a more accurate model;

- Find the accuracy of the forecasted significant wave height vs. the real significant wave height. Because of a lack of an accurate method of measuring the significant wave height on board, the forecasted wave height is used instead, but it should be found how accurate these forecasts are;

- Include more parameters in the regression analysis, e.g. the pipe tension, water depth, or current speed/direction. These parameters are currently not taken into account due to a lack of available data or the inability of measuring these parameters online. However, the model might be improved by analysing more different predictor parameters;

- Study the possibility of using an artificial neural network that can be trained continuously online to improve the power demand peak forecasting. This artificial neural network could be fed with a wide variety of input parameters that are measured on board continuously;

[3] Charles P. Steinmetz (1865- 1923) was a mathematician and electrical engineer contributing largely to the field of alternating current. He developed mathematical theories for electrical engineering problems making it possible for electrical engineers to design better electric machines.

- Study the possibility of a combination of a small fast-response electrical energy storage (EES) device in every engine room for unexpected power peaks and a big central EES device functioning as uninterruptible power supply in case of a generator failure. If this system is feasible, the vessel can still use the (cheaper) single-battery hybrid system, but would have a comparable reliability to the double-battery hybrid system 2;
- Find the response of a single-battery hybrid system to a generator failure when only one generator was running. It should be found if a stable grid can be maintained instantly when a generator fails and the battery is connected to the grid as response to this failure;
- Study the effect of a changing failure rate of system components. It is common practice to assume a constant failure rate when little failure data is known about specific components, but it should be found if this assumption is correct and what the influence would be on the reliability assessment if the failure rate is not constant in time;
- Study long term battery aging to make a better estimation on the battery depreciation costs. In this analysis, calendar aging data from battery tests until 800 days is used, but no information is available on the aging rate after this time span;
- Find an optimization strategy that economically optimizes the load dependent start limit of the double-battery hybrid system, regarding the battery aging, fuel consumption, and maintenance costs;
- Study the general relation between generator running hours and corrective maintenance costs using a statistical approach;
- Discuss the hybrid system with class society for the practical implementation of this system;
- Analyze the engineering costs for the full picture of involved costs in the hybrid system, because only the material costs have been taken into account yet in this analysis.

A

Power Distribution

A.1. Single Line Diagram of the PS

Notes:

1. The single line diagram is only readable in the electronic version. However, the information in Table A.1 is the most relevant.

2. The power to the whinch rooms is added to the pipe laying equipment because the power is distributed from the switchboards in the whinch rooms towards the firing line. The whinches themselves are not used during pipe laying, because the vessel is moving on DP, so all power directed to the whinch rooms is used for the pipe-laying process.

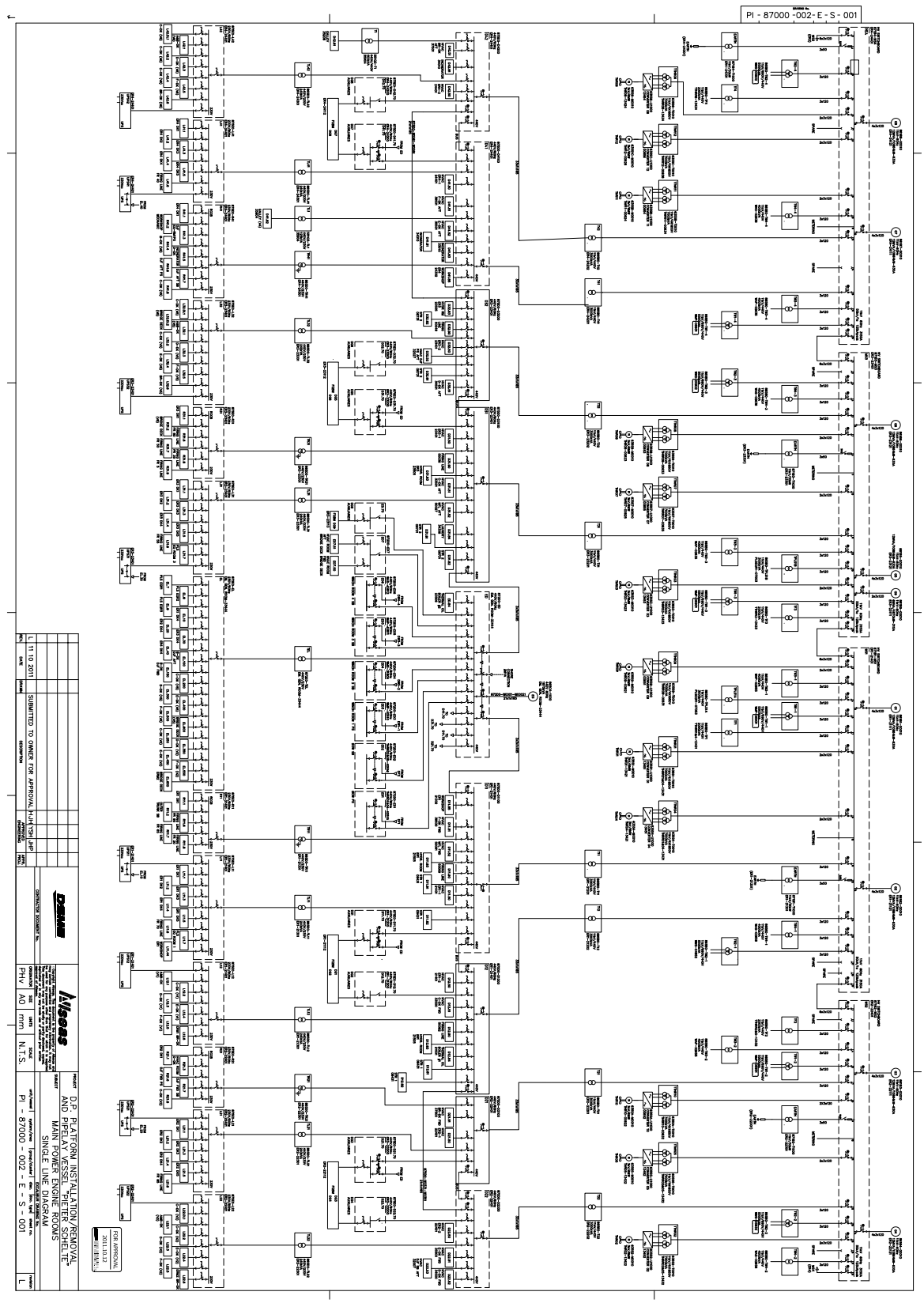

Figure A.1: Single Line Diagram of the PS

Table A.1: List of all breakers on main switchboards

Group	Breaker	Power in/out	Origin/Destination
Thrusters	TTHR01	out	thruster 1
	TTHR02	out	thruster 2
	TTHR03	out	thruster 3
	TTHR04	out	thruster 4
	TTHR05	out	thruster 5
	TTHR06	out	thruster 6
	TTHR07	out	thruster 7
	TTHR08	out	thruster 8
	TTHR09	out	thruster 9
	TTHR10	out	thruster 10
	TTHR11	out	thruster 11
	TTHR12	out	thruster 12
	TF1	out	auxiliary thr. Room
	TF2	out	auxiliary thr. Room
	TF3	out	auxiliary thr. Room
	TF4	out	auxiliary thr. Room
Hottelload	T21	out	to 230 V
	T22	out	to 230 V
	T42	out	to 230 V
	T41	out	to 230 V
Combination hotel/pipe laying	T12	out	firing line and to 230V
	T11	out	firing line and to 230V
	T32	out	firing line and to 230V
	T31	out	firing line and to 230V
Pipe laying equipment	TW3-1	out	whinch room
	TW1-1	out	whinch room
	TW4-1	out	whinch room
	TW2-1	out	whinch room
	TW3-2	out	whinch room
	TW1-2	out	whinch room
	TW2-2	out	whinch room
	TW4-2	out	whinch room
	TW2-3	out	whinch room
	TW4-3	out	whinch room
	TW3-3	out	whinch room
	TW1-3	out	whinch room
	TW2-4	out	whinch room
	TW4-4	out	whinch room
	TW3-4	out	whinch room
	TW1-4	out	whinch room
	TPLS1A	out	pipe lay systems
	TPSL1B	out	pipe lay systems
Generators	G1	in	generator 1
	G2	in	generator 2
	G3	in	generator 3
	G4	in	generator 4
	G5	in	generator 5
	G6	in	generator 6
	G7	in	generator 7
	G8	in	generator 8
	G9	in	generator 9

A.2. Power distribution 26 November

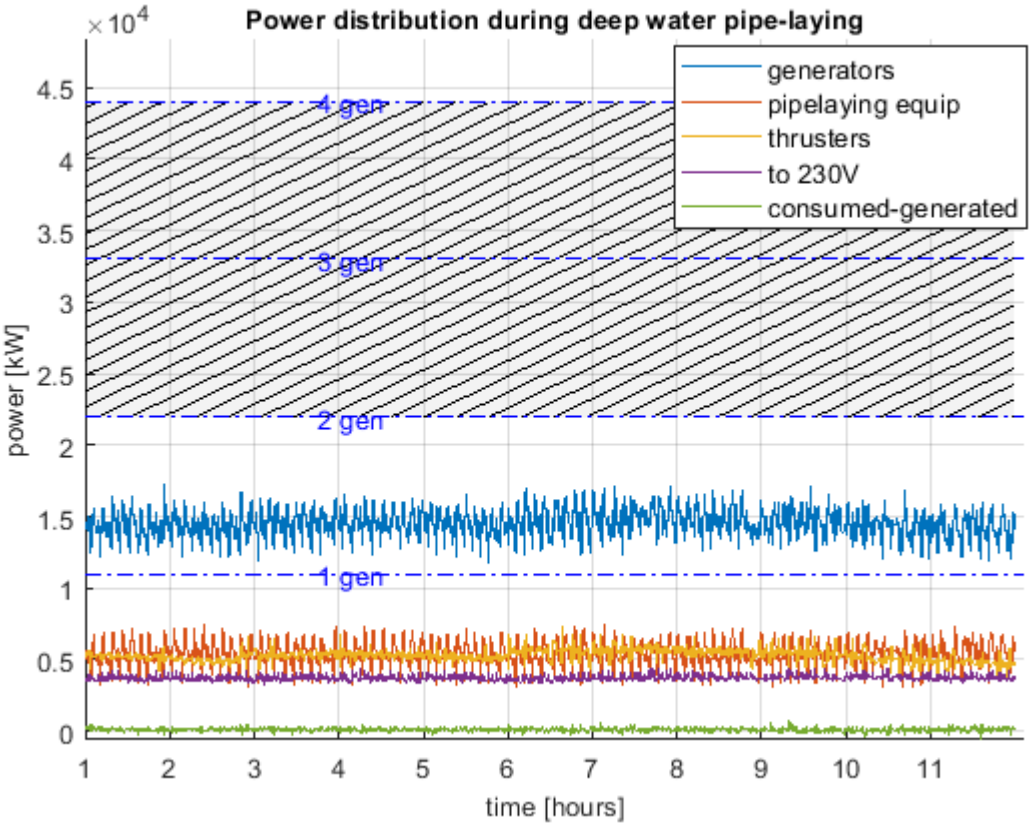

Figure A.2: Power distribution on 26 November

B

Performance Characteristics EES Types

B.1. Super Capacitors

Lifetime Due to the lack of chemical reactions in a super capacitor, the cyclic aging is relatively slow. The lifetime of a super capacitor is normally expressed in the number of cycles before the end of lifetime. Maxwell Technologies[1] considers a super capacitor to be at the end of lifetime when one of the following conditions is met [34]:

1. The capacitance is lower than 80% of the initial capacity;

2. The equivalent serial resistance has increased by 100 % of the initial resistance.

According to Maxwell Thechnologies, the super capacitor has degredation of capacitance that follows an exponential relation during the first couple of cycles. The reduction in energy storage capacity is proportional to the reduction in capacitance according to equation 3.4. During the main part of the life-time, the degradation in capacitance is linearly and at the end of life-time, the degradation is exponential again. Murray tested the degradation of capacitance and the increase of equivalent serial resistance based on the number of cycles [45]. He tested a small EDLC, but noted that in large EDLC's made for energy storage applications, the aging effects in the modules of multiple EDLC are expected to be similar. He tested the capacitance and the equivalent serial resistance for 10 million cycles at 25°C and indeed found an exponential degradation of the capacitance for the first cycles followed by a linear degradation. After 6.7 million cycles, the first condition of the end of life is met where the capacitance is 80% of the initial capacitance of this EDLC.

The increase in equivalent resistance was also tested, but the decrease in capacitance is shown to be dominant in the aging effect of the capacitor, where the second end-of-life condition of an increase of 100% of the initial equivalent resistance is not met, even after 10 million cycles.

Charge- and discharge rate Super capacitors can provide very high charge- and discharge rates. This is caused by the surface reaction of electrode materials without chemical reactions that require time [72]. Super capacitors are widely used in applications where charging and discharging occurs multiple times per seconds. For a super capacitor, the full charge or discharge time ranges from milliseconds to a few seconds [37].

Cycle efficiency Four different articles and technical reports found that the cycle efficiency of a super capacitor is 95% [5], [71], [56], [14]. According to [9], the efficiency is above 95% and in [16], the efficiency is said to be 90-98%. With this figures, it is reasonable to assume an efficiency of 95% for the super capacitor. For super capacitors, it will be assumed that half of the losses are dissipated during charging and half of the losses are dissipated during discharging. Therefore, to calculate the required capacity of the EES in the comparison, a discharge efficiency of 97.5% is used.

[1] Maxwell Technologies is a globally operating company speciallised in energy storage solutions.

Energy- and Power density and specific energy and -power For the specific power and energy of the super capacitor, different super capacitors from different manufacturers are found and listed in Table B.1. The average specific energy is 3.9 Wh/kg. The average specific power is 4350 W/kg.

Table B.1: Specific power and energy / power- and energy density super capacitors [9], [29], [41]

Manufacturer	$e_{specific}$ [Wh/kg]	$p_{specific}$ [W/kg]	ρ_{energy} [Wh/L]	ρ_{power} [W/L]
Maxwell	4.0	5294		
	3.1	3846		
	3.3	4600	3.3	3401
	3.2	5500	3.2	5837
	2.6	5600	2.6	5645
	3.1	5400	3.1	4594
	2.9	4300	2.9	3608
	2.3	3600	2.3	3150
	4.0	5100	4.0	3815
Panasonic	3.1	3505		
	4.4	2000		
Superfard	5.4	1953		
SAFT	6.0	3125		
	6.8	6923		
	3.0	3225		
Montenal	5.6	5625		
mean	3.9	4349.8	3.1	4292.9
90% conf.margin	± 0.5	± 556.7	± 0.3	± 626.4

The power and energy density are only found for Maxwell's super capacitors. The average specific energy of the super capacitor is 3.1 Wh/L and the average specific power of the super capacitor is 4293 W/L.

Self-Discharging Super capacitors are known for having a high self-discharging rate compared to batteries. That is, these devices lose a fair amount of energy over time, even when not being discharged. The discharge rate of a super capacitor is around 25% per day [19], [70].

Costs The important parameters in the cost estimation are the costs for power and the costs for energy capacity, being the costs per kW and the costs per kWh respectively. As was visible in Table B.1, the specific power of the super capacitor is relatively high and the specific energy of the super capacitor is relatively low. This also results in relatively low power costs and relatively high energy costs. Since manufacturers are reluctant to release prices of their products, power and energy costs of super capacitors are estimated by comparing different sources from literature. These numbers can be found in Table B.2.

Table B.2: Power and energy costs super capacitors according to different sources from literature

Power costs [$/kW]	Energy costs [$/kWh]	Source
250-400	9500 - 10,000	[22]
100	10,000	[70]
100- 400	5000-10,000	[33]

The costs found from different sources reach from 100 to 400 $/kW and from 5000 to 10,000 $/kWh. In order to compare the costs of the super capacitor with the costs of other EES devices, the average of these three sources will be used. That makes the power- and energy costs for the super capacitor 225 $/kW and 9000 $/kWh respectively.

B.2. Flywheels

Lifetime As explained, flywheels do have moving parts, since this is the underlying principle of storing the energy. However, due to the magnetic bearings, these moving parts hardly wear because there is no physical contact between moving and stationary parts. Therefore, flywheels have a very long lifetime up to 1,000,000 cycles, regardless of the charge- or discharge rate and regardless of the depth of discharge [31].

Charge- and discharge rate The charge and discharge rate of FES depends on the size of the motor/generator that is driving the wheel. For FES, there is no difference between the charge rate and the discharge rate [70]. The required time to discharge the flywheel can be in the order of milliseconds [19], so the charge/discharge rate of FES is considered not to be the dominating paramater in the EES selection as long as the size of the motors/generators is selected properly.

Cycle Efficiency The cycle efficiency of FES is calculated as the average of multiple numbers found in literature. These numbers are listed in Table B.3.

Table B.3: Roundtrip efficiency FES from different sources

source	[70]	[22]	[31]	[12]	[60]	[57]	[26]
efficiency [%]	95	82.5	92.5	89	82.5	91.5	90

The average of the efficiency found in these different sources is 90%, which will be taken as the number for comparison with other EES devices. For FES, it will be assumed that half of the losses are dissipated during charging and half of the losses are dissipated during discharging. Therefore, to calculate the capacity of the EES, a discharge efficiency of 95% is used.

Energy- and Power density The specific energy, specific power, energy density and power density are important numbers to use in the selection of a suitable EES device. For the comparison with other energy storage sytems, the specific energy, specific power, energy density and power density from different manufacturers are listed in Table B.4.

Table B.4: Specific power and energy/ power and energy density FES [40]

Manufacturer	$e_{specific}$ [Wh/kg]	$p_{specific}$ [W/kg]	ρ_{energy} [Wh/L]	ρ_{power} [W/L]
Flybrid	4.4	4400	6	5946
S4 Energy	1.1	-	0.8	-
Blueprint	3.3	522	10.7	1712
Tribology	7.9	317	16.9	676
Powerthru	2.43	-	7.25	2065
CCM	10.6	800	21	1575
HyKinesys	6.0	2000	7.5	2500
MagnetMotor GabH	5.0	375	10.5	788
Flywheel energy	5.0	800	6.0	960
Ricardo	-	-	12.2	3327
Williams	6.55	2182	9.47	3157
mean	5.2	1424.5	9.8	2270.6
90% conf. margin	1.4	760.5	2.6	784.8

With these numbers, the specific energy and specific power that will be used are: 5.2 ±1.4 Wh/kg and 1425 ±761 W/kg respectively. The energy- and power density for FES are 9.8 ±2.6 Wh/L and 2271 ±785 W/L.

Self-Discharge The biggest drawback of flywheels is the high self-discharge rate. As mentioned, modern flywheels operate in a near vacuum to reduce the self-discharge as much as possible, but significant rotational losses still occur in flywheel systems. According to two different sources, the daily self-discharge is 100% per day [19], [70], meaning that during one day, 100% of the stored energy would be lost even when the system is not used.

Costs Just like for the super capacitors, manufacturers are reluctant to release the prices of their systems, so the costs of the flywheels are also based on figures from literature. Table B.5 shows the numbers found in literature.

The costs for energy range from 1000 to 5000 $/kWh and the costs for power range from 250 - 500 $kWh. For the comparison, the average of these three sources will be used which are: 4000 $/kWh and 310 $/kW.

Table B.5: Power and energy costs FES according to different sources from literature

Power costs [$/kW]	Energy costs[$/kWh]	Source
250-350	1000 - 5000	[19]
250	5000	[70]
250-500	3000-5000	[33]

B.3. Batteries

In Table B.6 at page 115, the important characteristics of different batteries are listed. All information in this table is found in literature. When for one parameter, different numbers (separated by semicolons) are shown that cite only one source, this source was a paper which also contained an energy storage comparison based on different sources. The different numbers separated by semicolons are than found in that single source. The most important parameters of this table are described in the following paragraphs.

Lifetime Because the energy storage device will specifically be used for spinning reserve replacement, full charge/discharge cycles will only happen several times per year. When it is assumed that there is an unexpected shut down of one of the generators five times a year, which would already be a very conservative assumption, after ten years, the battery has only gone through fifty full charge/discharge cycles. As can be seen in the comparison table, all batteries can easily fulfil this life time requirement.

Discharge rate As explained before, flywheels and super capacitors are hardly limited in the discharge time. These EES devices could theoretically be discharged in a couple of seconds, meaning that there is no hard limit to the discharge rate and that the capacity of the EES device is not influenced by the time in which it is discharged. In contrary, batteries do have a maximum discharge rate which cannot be exceeded without damaging the battery. Besides, the capacity of batteries is very much influenced by the discharge rate. Roughly said, the capacity of a battery is maximally utilised when the discharge rate is low, being multiple hours. As explained before, the EES system on board the pioneering spirit will only be used for the replacement of spinning reserve. This means that the size of the EES device should be as big as the amount of energy that is used during a bridging situation between the shut down of a generator and the moment a new generator is online. Therefore, for batteries, the maximum discharge rate is one of the most important features of the selection.

The charge/discharge rate of a battery is commonly expressed as the C-rate. This number is expressed as the discharge current normalised by the battery capacity. It is calculated by dividing the charge/discharge current by the discharge current at which the full capacity of the battery would be utulised in one hour. Optimally, the maximum discharge rate of a battery used on board of the Pioneering Spirit would be 40C, representing a discharge time of 1.5 minutes, equal to the bridging time. When a battery is installed having a maximum discharge rate of 40C, it is not neccessary to install a surplus in capacity to force a lower C-rate. However, 40C is an unrealistically high discharge rate for a battery, so a discharge rate should be found closest to 40C.

LA batteries are known for their poor capabilities at high discharge rates. The response time of a LA battery is relatively small, but when continuous high current discharge occurs, the capacity of a LA battery decreases drastically. For quasi stationary discharge conditions (at constant current), the empirical Peukert equation estimates the capacity of a battery exposed to high current discharge [8]. The Peukert equation is given below:

$$I^n \cdot t = I_N^n \cdot t_N \tag{B.1}$$

	I:	The real discharge current of the battery	[A]
	t:	The real discharge time of the battery	[t]
Where:	n:	The Peukert constant	[-]
	I_N	The nominal current of the battery	[A]
	t_N	The nominal discharge time of the batter	[s]

So the capacity of the LA battery is reduced when the battery is discharged at a higher current than the nominal current. For LA batteries, the Peukert constant is in the order of 1.1 to 1.3. Figure B.1 shows the result of this effect for the capacity of the LA battery at different C-rates [8]. From this figure, it can be seen that for increasing C-rates, the battery's capacity decreases exponantially. Already at a discharge rate of 2C, the capacity of this specific LA battery reduces to only 41% of the rated capacity at 0.1C.

The Li-ion shows better performances at high discharge rates, as can be seen in the same figure. This figure shows the overall discharge capacity of a high power Li-ion battery at different discharge currents [4]. The measured capacities are measured at a range from 1C to 10C, corresponding to a discharge current in a range between 2.5A to 25A respectively. With a cut-off voltage of 2.5V, at 10C, the capacity of the battery is still 87% of the rated capacity measured at 1C. This shows that the high power Li-ion battery is capable of being discharged at high discharge rates up to 10C without loosing a severe amount of capacity.

A NiMH battery has somewhat less favourable capacity at high discharge rates than Li-ion and NiCd batteries. Soria et al. tested a NiMH battery on high discharge currents to find the fast discharge capabilities of this type of battery [61]. She found that capacity of this NiMH battery decreases to 55% at a discharge rate of 10C, as can also be seen in Figure B.1.

Just like the Li-ion battery the discharge rate of the NiCd battery can also be relatively high. Figure B.1 also shows the typical discharge curve of a NiCd battery. The figure shows the response of the battery in terms of capacity with respect to the discharge rate [69]. For a discharge rate of 10C, the capacity is still 96%.

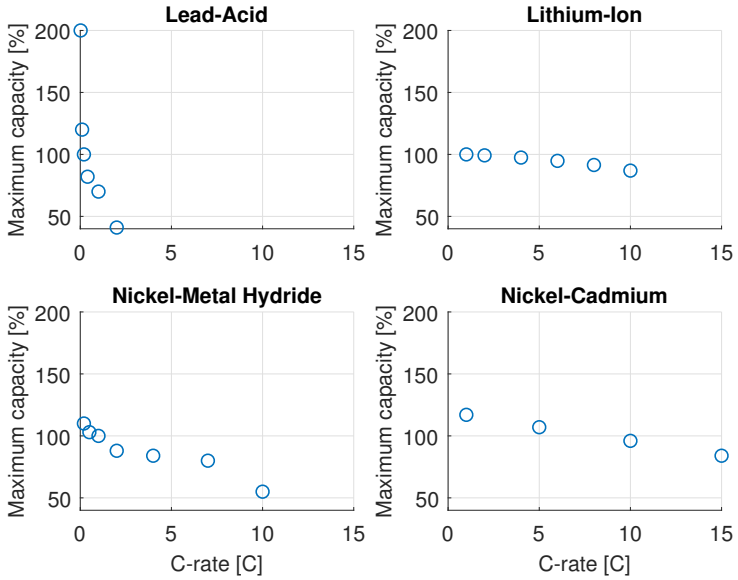

Figure B.1: Discharge characteristics different battery types

Cycle efficiency At ideal situations, the capacity of the device should be divided by the efficiency to find the capacity that should be installed. The efficiency shown in the comparison table is the cycle efficiency, so it is the amount of energy delivered by the battery while discharging divided by the amount of energy that was delivered to the battery during charging. In Elpiniki et al [6], the battery losses during charging and discharging were tested. When the battery was charged slowly and discharged rapidly, the ratio between the discharge losses and the total losses was 3:4. In this case, the battery is used as a UPS where all energy is needed during the relatively short bridging time, so fast discharge occurs. Therefore, it is assumed that 75% of the losses can be assigned to the discharge cycle, which means that if a battery will be used as the EES in this case, the capacity should be calculated by:

$$E_{EES} = \frac{t_{bridging} \cdot P_{nom}}{1 - 0.75(1 - \eta_{cycle})} \tag{B.2}$$

Therefore, the discharge efficiencies that will be used in the comparison are: 81.25% for LA, 88.75% for Li-ion, 88.75% for NiCd and 88.0 % for NiMH.

Size and weight The size and weight of the battery system is determined by the energy density, power density, specific energy and specific power. In electric vehicles, these parameters are very important, but in a vessel the size of the Pioneering Spirit, the size and weight are of less importance. For example, when the EES device that should replace a generator for 1.5 minutes on the nominal generator power, the size of the battery cells, based on the worst performing battery, would be 3 m^3 of LA battery. The weight of such a system would be in the order of 7.5 tons, which also has little influence on a vessel of this size.

Self-discharge The LA and Li-ion have very low self-discharge rates, making these batteries very suitable for long time EES. NiCd and NiMH batteries have higher self-discharge rates, being in the order of 15-30%/month.

Memory Effect NiCd batteries suffer from the so called "memory effect" if these batteries are discharged and charged in a repeating pattern. When the battery is repeatedly discharged until the same state of charge, the battery will "remember" this state of charge and at this state of charge, a voltage drop can occur in following discharge cycles. The effect reduces the capacity of the battery which can only be restored after a series of full discharges [19]. LA and Li-ion batteries do not suffer from this effect and in NiMH, this effect is very minor.

Table B.6: Characteristics of Lead-Acid, Lithium-Ion, Nickel-Cadmium and Nickel Metal-Hydride batteries

	LA	Lithium Ion	NiCd	NiMH
Lifetime $[cycles]$	2000 [70] 600 at C/3 [23]	5000 [70] 1000-10000; 20000 [39]	2000-2500;3500 [39]	Almost no capacity loss at 1000+ [55]
Max. discharge rate	35% left capacity at 5C [23] 40% left capacity at 2C [8]	87% left capacity at 10C [4] 100% left capacity at 8C [3] 80% left capacity at 20C [67]	82% left capacity at 15C [69] 95% left capacity at 10C [69]	84% left capacity at 8C [61] 56% left capacity at 10 C [61]
η_{cycle}	75% [70]	85% [70] 85 % [39]	85 % [39]	84% [77]
$e_{density}$ $[Wh/L]$	80 [70] 95 [23] 95 [49] 86 [73]	150 [70] 200-500; 200-400;150 [39] 170 [73] 210 [59]	140 [59] 60-150;15-80;80 [39]	180 [59] 170-420 [39]
$p_{density}$ $[W/L]$	128 [70] 445 [49] 240 [73]	450 [70] 1500-10000 [39]	80-600 [39]	-
spec. Power $[W/kg]$	180 [38] 320 [1] 245 [23] 215 [49]	350 [73] 1100 [1] 150-315;300;500-2000 [39] 1800 [38]	150 [38] 150-300;160;150 [39]	250-1000 [38] 690 [1]
spec. Energy $[Wh/kg]$	33 [73] 45 [23] 31 [1] 35 [38]	90 [59] 75-200;90;120-200 [39] 120 [38] 95 [1] 110 [73]	50 [59] 50-75;50;45-80 [39] 40-60 [38]	55 [59] 54 [1] 60 [38]
self-discharge	0.3%/day [70]	0.1%/day [70] 5-10%/month [59]	15-20%/month [59] 0.2-0.6;0.3; 0.03-0.6%/day [39]	20-30%/month [77]
costs/energy [$/kWh]	200 [70] 269 [38] 200 [46] 88$[73]	525 [70] 1000-2000 [38] 505 [73] 210 [46] 600-2500; 2770-3800 [39] 273 [20]	280 [38] 800-1500; 400-2400 [39] 240 [46]	500-1000 [38]
costs/power [$/kW]	125 [70]	175 [70] 1200-4000; 900-1300; 1590 [39]	500-1500 [39]	-
memory effect [39]	no	no	yes	no

C

Additional EES mechanisms

For sake of completeness, next to super capacitors, flywheels and batteries, other mechanisms of storing electrical energy are discussed below. These concepts are not included in the comparison because they are unapplicable for maritime applications. It is discussed why these EES systems are not used in the comparison.

- Compressed air energy storage (CAES): this type of energy storage is used in stabilising the power consumption or stabilizing the power generation of a local or national power grid. During a surplus of power, air is pumped into an air reservoir like an underground rock cavern at a pressure of around 40 - 60 bar. When extra power is needed, the pressurised air is use to feed a gas turbine which extracts the energy from the air [19]. The disadvantage of this type of energy storage is the system that it requires to receive the stored energy, making it expensive and voluminous. To operate this system, it needs a compressor, a pressure vessel, a low pressure turbine, a gas turbine and a generator. Normally this type of energy storage is therefore used in a system that already generates energy through a gas turbine during normal operation. Next to the costs and the big volume of this system, it also needs a relatively long time to start, in the order of 9 - 12 minutes [14]. CAES could be very useful in large grid operations, but is unlikely to be used in smaller island operations like vessels, where smaller power and energy are required and shorter starting times are asked.

  Next to the systems that store energy to supply compressed air to a gas turbine, research has been conducted to use compressed air to directly drive pneumatic motors. This way, the problem of the high response time would be solved. However, researchers keep finding the disadvantages of the low energy density, low efficiency of pneumatic motors, difficulties of no constant power output and the fact that the air temperature decreases drastically during discharging.

  As a reference, when air is stored at 30 bar and a pneumatic motor efficiency of 20% is assumed [13], an air vessel of 500 m^3 is required to store 280 kWh of energy. For the corresponding calculation, see Appendix D.2. The size of the air storage vessel is potentially even higher since it is unlikely that all energy can be recovered from the pressurised air because the pressure decreases during discharging and below a certain pressure, the required power can no longer be maintained.

  During discharging of the storage device, the pressure inside the air vessel decreases, making it hard to maintain the required power at all energy levels [54]. Theoretically, this problem could be solved by using an open accumulator system using a combination of a pneumatic system and an hydraulic system. This system uses the power density of hydraulics and the energy density of pneumatics. By controlling the ratio between the power delivered by the pneumatic versus the power delivered by the hydraulic engines, the power can be maintained constant at different energy levels. However, this energy storage mechanism is very immature, it has never been tested and little is known about the characteristics and performance of these systems.

- Pumped hydro storage: this type of energy storage is also used in large power grid operations to balance the power consumption or generation. When a surplus of power is available, water is pumped from a lower reservoir into a higher reservoir. During the extra need of power, the potential energy stored in

the higher reservoir is used to drive a turbine, which regenerates electric power. This type of energy storage is globally the most used energy storage mechanism contributing to 97% of the total energy storage capacity [33]. However, due to the required height difference and the large water volume, this type of energy storage is unsuitable for maritime applications.

- Superconducting magnetic energy storage: this type of EES stores the energy in a magnetic field generated by a superconducting coil using direct current. Although this type of energy storage has the same advantages as super capacitors having no moving parts and no electrochemical reactions, the superconducting materials are extremely expensive and this device can only release electricity for a couple of seconds [14]. Besides, the material is only superconducting at very low temperatures and this device generates a very strong magnetic field which could be harmful in this maritime environment.

D

EES derivations

D.1. Derivation of stress in flywheel ring

The following derivation is based on [30].

For a ring of mass, where all the mass is assumed to be at one distance from the center (one radius), the moment of inertia is:

$$J = mr^2 \tag{D.1}$$

So the total stored energy in the flywheel becomes:

$$E_{FW} = \frac{1}{2} mr^2 \omega^2 \tag{D.2}$$

For a ring, the stress in the outer fibre can be calculated based on the radius and rotational speed. The following figure D.1 gives the free body diagram of a infinitely small element of the ring.

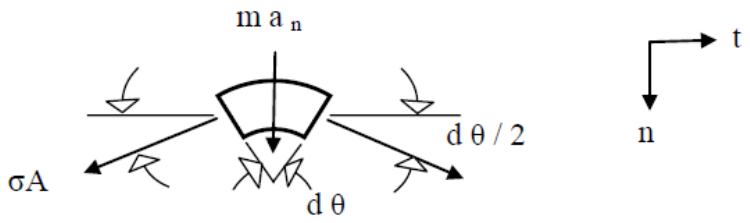

Figure D.1: Free body diagram of ring fibre

When using Newton's law of motion:

$$\sum F_n = ma_n \tag{D.3}$$

The normal force on this element is:

$$\sum F_n = 2\sigma A sin(\frac{d\theta}{2}) \tag{D.4}$$

Where:

A :	Cross sectional area	$[m^2]$
σ :	Normal stress in the ring	[Pa]

The normal acceleration of the element of the ring is:

$$a_n = r\omega^2 \tag{D.5}$$

And the mass of an element of the rotating ring is:

$$m = \rho V = \rho r d\theta A \tag{D.6}$$

Substituting results in:

$$\sigma A d\theta = \rho r d\theta A r \omega^2 \tag{D.7}$$

So:

$$\sigma = \rho r^2 \omega^2 \tag{D.8}$$

Using the equation for the stored energy in a flywheel, Equation D.2, the stored energy, based on the stress in the rotating material becomes:

$$E_{FW} = \frac{\frac{1}{2} m \sigma}{\rho} \tag{D.9}$$

So the maximum energy per mass that can be stored in a flywheel is proportional to its maximum tensile strength devided by the density of the material:

$$E_{FW,max}/m = \frac{1}{2} \frac{\sigma_{max}}{\rho} \tag{D.10}$$

D.2. Energy stored in compressed air

The work that is used to compress air from volume A to volume B is calculated using the ideal gas law:

$$pV = nRT = c \rightarrow p_A V_A = p_B V_B \rightarrow \frac{V_B}{V_A} = \frac{p_B}{p_A} \tag{D.11}$$

Where:

V_A:	initial volume	$[m^3]$
V_B:	pressure vessel volume	$[m^3]$
p_A:	ambient pressure	[Pa]
p_B:	pressure vessel pressure	[Pa]

The work used while compressing the air can be calcuted by:

$$E_{CAES} = W_{A \rightarrow B} = \int_{V_A}^{V_B} p dV = \int_{V_A}^{V_B} \frac{nRT}{V} dV = nRT \left[\ln V_B - \ln V_A\right] \tag{D.12}$$

So:

$$E_{CAES} = nRT \ln \frac{V_B}{V_A} = p_A V_A \ln \frac{V_B}{V_A} = p_B V_B \ln \frac{p_B}{p_A} \tag{D.13}$$

So the pressure vessel volume can be calculated by:

$$V_B = \frac{E_{CAES}}{p_B \ln \frac{p_B}{p_A}} \tag{D.14}$$

E

ARMA modelling

This appendix explains ARMA modelling in general and how ARMA modelling can be used in finding a pattern and forecasting the pipe laying load.

E.1. Stationarity

In order to forecast future values of a time series based on the past and current values, it is required to assume that the probabilistic characteristics of the time series are not changing. When this assumption holds, the time series is called stationary, which is a requirement for ARMA modelling. For strict stationarity, this means that the joint probability distribution of a set of observations $\{x_{t_1}, x_{t_2}, ..., x_{t_N}\}$ is equal to the joint probability distribution of a set of observations $\{x_{t_1+k}, x_{t_2+k}, ..., x_{t_N+k}\}$ for every time shift k in the time series. When a discrete time series is strictly stationary, the times series has a constant mean and a constant variance, which can be estimated by the sample mean and sample variance using [42]:

$$\hat{\mu}_x = \frac{1}{N}\sum_{t=1}^{N} x_t \tag{E.1}$$

And:

$$\sigma_x^2 = \frac{1}{N}\sum_{t=1}^{N} (x_t - \hat{\mu}_x)^2. \tag{E.2}$$

Where: N: Sample length

However, it is found that the definition of a joint probability distribution that is insensitive to the time shift is too strict for most applications and it can be sufficient for ARMA modelling to be weakly stationary [42]. For a times series to be weakly stationary (further referred to as stationary), it should comply to the following requirements:

1. The mean is fixed in time;
2. The autocovariance between two observations x_s and x_t only depends on the time difference between these observations, $|s - t|$. The definition of autocavariance is discussed in the next subsection (E.2).

Time series can also be trend-stationary meaning that the series is stationary around an increasing or decreasing mean, the trend. When the time series is found to be stationary after a fit is subtracted from the series, it is called trend-stationary. Forecasting of a trend-stationary series is done by extrapolating the trend and using an ARMA model for the de-trended series. De-trending is performed by subtracting the trend from the original data. If the trend is linear, detrending is performed by subtracting the least square linear fit from the original data:

$$y_t = x_t - [\beta_0 + \alpha_0 t] \tag{E.3}$$

In which α_0 and β_0 are the parameters of the linear trend that is fitted through the data.

When a time series shows a very strong seasonal component, meaning that the data follows a reoccurring pattern with a constant period, the series can be de-seasonalised to make it stationary. This is often done by seasonal differencing using Equation E.4. Further on in this chapter it will be explained how the de-seasonalised data can be used in finding a prediction model for the time series.

$$y_t = x_t - x_{t-T} \tag{E.4}$$

Where: T : The seasonal period

E.2. Correlation

To find the dependence between two values of a time series observed at different time steps, x_t and x_s, the linear dependence between these observations is often expressed by the covariance between these values using the autocovariance function [58]:

$$\gamma(s,t) = cov(x_s, x_t) = E[(x_s - \mu_s)(x_t - \mu_t)] \tag{E.5}$$

Where: x_s: The observed value of the time series at moment s
x_t: The observed value of the time series at moment t

Roughly said, the covariance between two random variables expresses the way these variables influence each other. A drawback of the covariance is that this expression is unit dependent, so the absolute value of the covariance depends on the unit at which the two variables are represented. To prevent the unit dependence, the covariance can be standardized, resulting in the correlation function, which is dimensionless and is always expressed in a value between -1 and 1:

$$\rho(s,t) = \frac{\gamma(s,t)}{\sqrt{\gamma(s,s)\gamma(t,t)}} \tag{E.6}$$

Since the time series that is used is assumed to be stationary, the covariance only depends on the time difference between two observations as stated in condition 2 mentioned above. This means that $cov(x_t, x_s) = cov(x_{t+h}, x_{s+h})$. Therefore $\gamma(t+h,t) = cov(x_{t+h}, x_t)$ can be written as $cov(x_h, x_0) = \gamma(h,0)$ because the covariance between x_t and x_{t+h} does not depend on t. When this is used for the autocorrelation function in Equation E.6, it mean that for a stationary time series, the autocorrelation function at lag h can be formulated as:

$$\rho(h) = \frac{\gamma(t+h,t)}{\sqrt{\gamma(t+h,t+h)\gamma(t,t)}} = \frac{\gamma(h,0)}{\gamma(0,0)} \tag{E.7}$$

Because time series are discrete data, finding the covariance and mean of the observations is impossible in terms of regular statitics. In the equations E.5 to E.7, the theoretical mean, autocovariance and autocorrelation can be calculated of the stochastic process that realizes the observations. In practice, only the discrete observations $\{x_1, x_2, ..., x_n\}$ of the stochastic process are known, making it impossible to use these equations directly. Therefore, an estimation of the autocovariance, autocorrelation and mean should be made based on an average of these values over the sample. Since the mean is constant for a stationary series, the mean is estimated by the sample mean using the same estimator as for strictly stationary series. This estimator is equal to Equation E.1. For the autocorrelation, different estimators have been suggested in literature, where it is found that the most satisfying estimator for the sample autocovariance function is [17]:

$$\hat{\gamma}(h) = \frac{1}{N}\sum_{t=1}^{N-h}(x_{t+h} - \bar{x})(x_t - \bar{x}) \tag{E.8}$$

The estimator for the sample autocorrelation function is constructed just like in Equation E.7:

$$\hat{\rho}(h) = \frac{\hat{\gamma}(h)}{\hat{\gamma}(0)} \tag{E.9}$$

For the estimation of the autocorrelation function, a sufficient amount of observations should be available. A rule of thumb for the minimum number of obervations is 50, where the the number of lags for which

the autocorrelation can be calculated should not exceed $N/4$ [47]. The autocorrelation function can be calculated for a set of lags h in a sample, resulting in a sample autocorrelation plot. The autocorrelation function of the pipe laying power profile of Figure E.1a is shown in Figure E.1b. The autocorrelation plot shows very clear that the pipelaying pattern follows a reocurring pattern, because there is strong positive correlation between lags at at a distance corresponding to the pipelaying period, $\{1T_{pipeload}, 2T_{pipeload}, ...\}$ and a strong negative correlation between lags $\{1T_{pipeload}/2, 3T_{pipeload}/2, ...\}$. If all observations at x_t are plotted versus x_{t-T} for the same sample of the pipe load, there indeed seems to be a positive correlation between observations at a time lag of T from each other, which can be seen in Figure E.2.

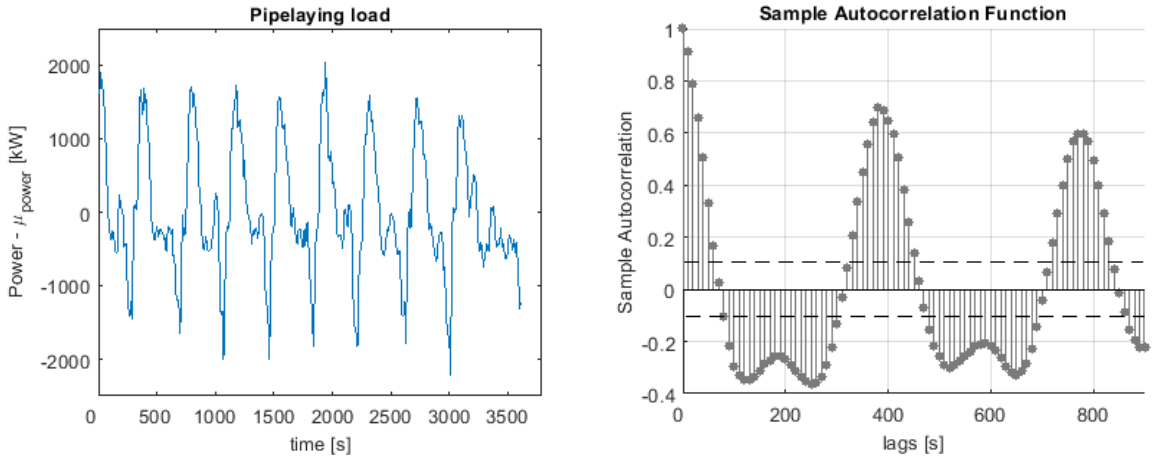

(a) Pipe laying load sample, 1 hour

(b) Sample autocorrelation function

Figure E.1: Autocorrelation function of pipelaying load sample

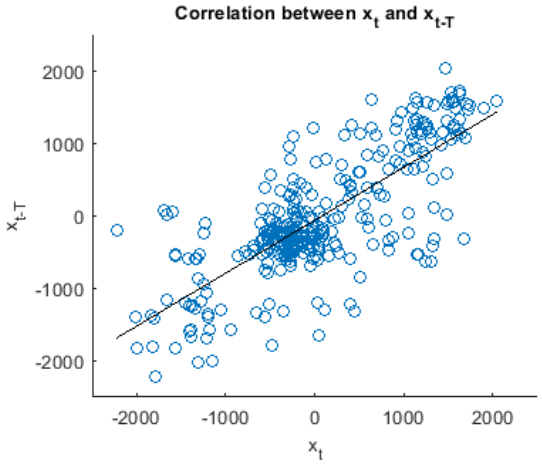

Figure E.2: Correlation between x_t and x_{t-T}

When an ACF of a white noise process[1] is plotted, theoretically, the autocorrelation between every value at different lags should be zero. However, the estimated ACF plot could show some minor correlations at different lags, so in the ACF the 95% confidence interval is plotted in which it is 95% sure that the process is white noise. So when the autocorrelation at lag h is within the confidence bounds, the correlation is considered to be insignificant.

[1] A white noise signal is a signal where all random values of a series are uncorrelated and have a constant mean. In this chapter, the white noise is independent and identically distributed white noise, which means that the values are uncorrelated but drawn from the same probability density function. Here, a normal distribution is used having zero mean and variance σ^2.

E.3. ARMA(*p,q*) Model

An ARMA model consist of an autoregressive (AR) part and a moving average (MA) part, which are described below.

Autoregressive modelling is a method that describes current values of a time series by a linear regression on lagged values of that same series. An autoregressive model of order p can be described by the following equation:

$$x_t = \phi_1 x_{t-1} + \phi_2 x_{t-2} + ... + \phi_p x_{t-p} + \epsilon_t \tag{E.10}$$

Where:
- $\phi_1 ... \phi_p$: The weights of the contribution of every lagged value
- ϵ_t: A random error, which is an independent and identically distributed white noise signal, having zero mean and variance σ^2. For these models, a Gaussian white noise is used, so the error terms are normally distributed.

Moving Average models do not use the passed observations directly, but use the error terms of preceeding values to describe the current values. The moving average model of order q is defined as:

$$x_t = \theta_1 \epsilon_{t-1} + \theta_2 \epsilon_{t-2} + ... + \theta_q \epsilon_{t-q} + \epsilon_t \tag{E.11}$$

Where:
- $\theta_1 ... \theta_q$: The weights of the contribution of every lagged error
- $\epsilon_{t-1} ... \epsilon_{t-q}$: The error at the lagged time steps from *t-1* to *t-q*. With $\epsilon \sim N(0, \sigma^2)$.

In a moving average model, it is less clear how a model could be fit to an existing time series than for an autoregressive model. In the moving average model, the error terms are unobserved terms, where in an autoregressive model, the lagged observations are actual values given by observations in the time series. It is easier to understand how moving average models work by constructing an example of one from a blank sheet. For example, when a moving average process of order 1, a MA(1) process with $\theta = 0.6$, would look like:

$$x_t = \theta_1 \epsilon_{t-1} + \epsilon_t = 0.6\epsilon_{t-1} + \epsilon_t \tag{E.12}$$

with $\epsilon_t \sim N(0,1)$ and it is given that $\epsilon_0 = 0$, than the successive values of x_t can be calculated by:

$$\begin{aligned} x_1 &= 0.6\epsilon_0 + \epsilon_1 = 0.6 \cdot 0 + 0.21 = 0.21 \\ x_2 &= 0.6\epsilon_1 + \epsilon_2 = 0.6 \cdot 0.21 - 0.78 = -0.654 \\ x_3 &= 0.6\epsilon_2 + \epsilon_3 = 0.6 \cdot 0.78 + 0.03 = 0.50 \\ x_4 &= 0.6\epsilon_3 + \epsilon_4 = 0.6 \cdot 0.03 + 1.21 = 1.23 \\ &\vdots \\ x_n &= 0.6\epsilon_{n-1} + \epsilon_n \end{aligned} \tag{E.13}$$

Where $\{\epsilon_1, \epsilon_2, \epsilon_3, \epsilon_4\} = \{0.21, -0.78, 0.03, 1.21\}$ are random variables obtained from a normal distribution having mean 0 and variance 1. Continued until *t = 100*, the MA(1) in this example model could look like Figure E.3.

Autoregressive Moving Average (ARMA) models are a combination of AR and MA models, so a ARMA(*p,q*) model is defined by:

$$x_t = \phi_1 x_{t-1} + ... + \phi_p x_{t-p} + \theta_1 \epsilon_{t-1} + ... + \theta_q \epsilon_{t-q} + \epsilon_t \tag{E.14}$$

When a process shows a seasonal component, an ARMA model can also be fitted to the process having a dependency on an observation or an error at lags with a time difference of the period T. For example, when the power consumption of a city depends on the outside temperature, the process could show a reoccurring pattern having a period of twelve months. In that case, a seasonal ARMA (SARMA) can be used to fit a model to the process. In a SARMA(*p,q*)x(*P,Q*) model, the current value of x_t does not only depend on the preceding lags

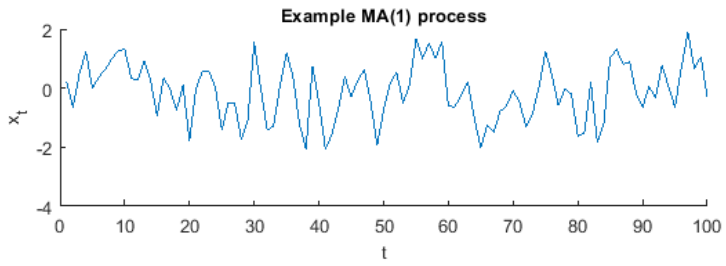

Figure E.3: Example MA(1) process

up to *t-p* or *t-q*, but also on the lags *t-P* and *t-Q*. In case of the before mentioned example, a SARMA(*1,1*)x(*1,1*) model could be fitted to the process, which results in:

$$x_t = \phi_1 x_{t-1} + ... + \phi_p x_{t-p} + \theta_1 \epsilon_{t-1} + ... + \theta_q \epsilon_{t-q} + \underbrace{\phi_{12} x_{t-12} + \theta_{12} \epsilon_{t-12}}_{seasonal} + \epsilon_t \tag{E.15}$$

Where $\{\phi_1, ..., \phi_p\} \neq 0$, $\{\theta_1, ..., \theta_q\} \neq 0$, $\theta_{12} \neq 0$ and $\phi_{12} \neq 0$, but all other values of ϕ and θ are 0.

The SARMA model will be used for fitting a model to the pipelaying load, because the process shows a clear reocurring pattern, where current observations seem to depend on observations at *t-T*.

E.4. The Nature and Order of the Process

The nature of the process (Autoregressive, Moving Average, or both) that should be modelled and the orders p and q are estimated by examining the autocorrelation function (ACF) of the process at different lags. In this section, the autocorrelation (ACF) and partial autocorrelation (PACF) plots are explained because these are needed to find the nature of the pipelaying load pattern that will be forecasted. The ACF and PACF of the pipelaying load pattern will be used for the construction of the load prediction model.

The order of an MA(q) process can be estimated from the ACF plot of that process, because in that plot it can be seen up to which lag the correlation between x_t and x_{t+h} is significant. In an MA(q) process, the correlation between x_t and x_{t+h} for lags higher than q is zero. This is caused by the fact that all ϵ_t are independent variables, meaning that there is no correlation between the errors terms themselves. Since there is no correlation between ϵ_{t+h} and ϵ_t, the only correlation between x_{t+h} and x_t is determined by the θ parameters. So when $h > q$, there is no correlation between x_t and x_{t+h}, since there exist no θ paramater for $h > q$. Therefore, the ACF plot of an MA(q) process shows no significant autocorrelation at lags higher than q. In short, this can be written as[2]:

$$\rho(h) = \frac{\gamma(h,0)}{\gamma(0,0)} \quad \begin{cases} = 1, & for\ h = 0 \\ \neq 0, & for\ h \leq\ q \\ = 0, & for\ h > q \end{cases} \tag{E.16}$$

When the ACF of the MA(1) example of Figure E.3 is used, it can indeed be seen in Figure E.4a that the autocorrelation at lag 1 is significant, where the autocorrelation at larger lags do not show a significant value. So in a MA(q) process, the order q can be estimated by examining the ACF plot and finding the last lag where the autocorrelation shows a significant value.

In an AR(p) process, it is more difficult to directly find the order p based on the ACF plot, because in an AR(p) process, even for lags higher than p, there still exists some correlation between x_t and x_{t+h} because of the linear dependence of the values $\{x_{t+1}, x_{t+2}, ..., x_{t+h-1}\}$ in between x_t and x_{t+h}. When an AR(1) process is taken as an example, it can be shown that the current value x_t still depends on the value x_{t-2} even though $h > p$ because $2 > 1$. This is shown by the following equation:

$$\begin{aligned} x_t &= \phi_1 x_{t-1} + \epsilon_t \\ x_t &= \phi_1 \left(\phi_1 x_{t-2} + \epsilon_{t-1}\right) + \epsilon_t \end{aligned} \tag{E.17}$$

[2]This only holds for an MA(q) process

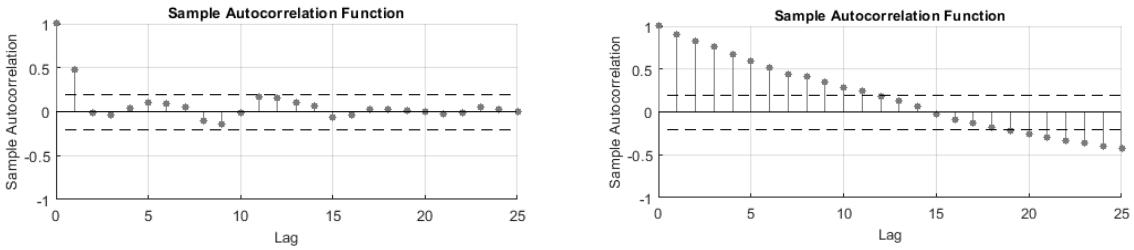

(a) ACF plot of MA(1) process of Figure E.3

(b) ACF plot of typical AR(1) process

Figure E.4: ACF plot of MA(1) process and ACF of AR(1) process

This results in an ACF of an AR(p) process that gradually decreases as can be seen in E.4b, which is an ACF plot of an AR(1) process. Only from this figure, it is not clear what the order of the AR(p) process is. Instead of using the ACF plot to find the order of an AR(p) process, the partial autocorrelation function (PACF) is used, where the correlation between x_t and x_{t+h} is calculated after the linear dependence of these values on the values in between, $\{x_{t+1}, x_{t+2}, ..., x_{t+h-1}\}$, is removed. This is done by finding a linear relation between all "in-between values" $\{x_{t+1}, x_{t+2}, ..., x_{t+h-1}\}$ and x_t and finding a linear relation between all "in-between values" and x_{t+h}. For x_t, this is done by subtracting $\hat{x}_t$ from x_t and for x_{t+h}, this is done by subtracting $\hat{x}_{t+h}$ from x_{t+h}. $\hat{x}_t$ and $\hat{x}_{t+h}$ are representations of x_t and x_{t+h} but than calculated by a linear regression on the observations in the middle:

$$\hat{x}_t = \beta_1 x_{t+h-1} + \beta_2 x_{t+h-2} + ... + \beta_{h-1} x_{t+1} \tag{E.18}$$

$$\hat{x}_{t+h} = \beta_1 x_{t+1} + \beta_2 x_{t+2} + ... + \beta_{h-1} x_{t+h-1} \tag{E.19}$$

The coefficients $\{\beta_1, \beta_2, ..., \beta_{h-1}\}$ belong to the least square sum of the error between the observed values and the linear regression. After removing this linear dependence of x_t and x_{t+h} on the "in-between values", what leaves is the clean correlation between x_t and x_{t+h} without the effect of the dependence between x_t and x_{t+h} that is caused by the dependence on all the values in between. This indirect dependence effect, that is removed in the PACF, is shown in the example in Equation E.17. The PACF at lag h is than defined as:

$$\alpha(h) = corr\,(x_{t+h} - \hat{x}_{t+h}, x_t - \hat{x}_t) \tag{E.20}$$

As said, the PACF is used for the estimation of the order p of an AR(p) process. When an AR(p) process is considered, x_{t+h} is determined by:

$$x_{t+h} = \sum_{j=1}^{p} \phi_j x_{t+h-j} + \epsilon_{t+h} \tag{E.21}$$

The least square sum estimate of a linear regression on $\{x_{t+1}, x_{t+2}, ..., x_{t+h}\}$ written in Equation E.19 of this AR(p) process can be calculated to find the value of $\hat{x}_{t+h}$. When $h > p$, the least square sum estimate should find exactly the AR(p) process itself (without the error term):

$$\hat{x}_{t+h} = \sum_{j=1}^{p} \phi_j x_{t+h-j} \tag{E.22}$$

For example, $\hat{x}_{t+5}$ of an AR(2) process will be estimated by:

$$\hat{x}_{t+5} = \beta_1 x_{t+1} + \beta_2 x_{t+2} + \beta_3 x_{t+3} + \beta_4 x_{t+4} \tag{E.23}$$

Where the least square sum of the error between the linear fit and the observed process should be obtained by $\{\beta_1, \beta_2, \beta_3, \beta_4\} = \{0, 0, \phi_2, \phi_1\}$ for an AR(2) process. This means that, by substituting Equation E.21 and Equation E.22 into Equation E.20, , the PACF for an AR(p) process when $h > p$, becomes:

$$\begin{aligned}\alpha_{h>p}(h) &= corr\,(x_{t+h} - \hat{x}_{t+h}, x_t - \hat{x}_t) \\ &= corr\left(\left\{\sum_{j=1}^{p}\phi_j x_{t+h-j} + \epsilon_{t+h} - \sum_{j=1}^{p}\phi_j x_{t+h-j}\right\}, x_t - \hat{x}_t\right) \\ &= corr\,(\epsilon_{t+h}, x_t - \hat{x}_t) \\ &= 0\end{aligned} \tag{E.24}$$

The last step in the above equation is zero because there is no correlation between an independent random error term on the one side and $(x_t - \hat{x}_t)$ on the other side. Analogous to the ACF of an MA(q) process, the PACF of an AR(p) shows the following characteristics:

$$\gamma(h) = \begin{cases} = 1, & for\ h = 0 \\ \neq 0, & for\ h \leq\ q \\ = 0, & for\ h > q \end{cases} \tag{E.25}$$

That means that the order p of an AR(p) process can be estimated by examining the PACF plot and finding the last lag where the partial autocorrelation shows a significant value. Figure E.5a shows an AR(1) process where $\phi_1 = 0.2$, with the PACF plot of this process in Figure E.5b. The PACF indeed shows no significant partial autocorrelation at other lags than lag 1. The PACF plot can also be plotted for an MA(q) process, which is shown in Figure E.6. In this figure, this can be seen that the partial autocorrelation for a MA(q) process does not cut off after the q^{th} lag, but tails off similar to characteristic that the the ACF of an AR(p) process tails off. This is caused by invertibility of an MA(q) process, which means that a MA(q) process can be written as an infinite representation of an AR like process. When the succeeding steps of the MA(1) process of Equation E.12 are written as follows:

$$\begin{aligned} x_2 &= \epsilon_2 + \theta\epsilon_1 \\ x_3 &= \epsilon_3 + \theta\epsilon_2 = \epsilon_3 + \theta[x_2 - \theta\epsilon_1] = \epsilon_3 + \theta x_2 - \theta^2\epsilon_1 \\ x_4 &= \epsilon_4 + \theta\epsilon_3 = \epsilon_4 + \theta[x_3 - \theta x_2 + \theta^2\epsilon_1)] = \epsilon_4 + \theta x_3 - \theta^2 x_2 + \theta^3\epsilon_1 \\ x_5 &= \epsilon_5 + \theta\epsilon_4 = \epsilon_5 + \theta[x_4 - \theta x_3 + \theta^2 x_2 - \theta^3\epsilon_1)] = \epsilon_5 + \theta x_4 - \theta^2 x_3 + \theta^3 x_2 - \theta^4\epsilon_1 \\ &\vdots \\ x_t &= -\sum_{j=1}^{\infty}(-\theta)^j x_{t-j} + \epsilon_i \end{aligned} \tag{E.26}$$

If $|\theta| < 1$, this representation of an MA process converges and the process is called invertible. So when considering the MA representation in Equation E.26, this reflects into the PACF of the MA(q) process, that does not cut off after a certain lag, but slowly tails off. To show this effect, in Figure E.6, the PACF plot of the MA(1) process of Figure E.3 is shown, where it indeed is visible that the PACF does not cut off, but slowly tails off to zero.

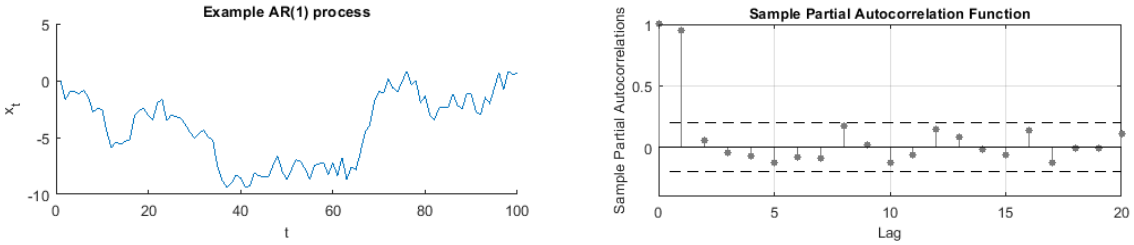

(a) Example AR(1) process

(b) PACF plot of AR(1) process

Figure E.5: Example AR(1) process and partial autocorrelation plot of this process

In short, the ACF and PACF are the estimators of the order of an MA(q) process or of an AR(p) process. Besides, from the ACF and PACF, the nature of the process can be found, where it can be seen if the process is

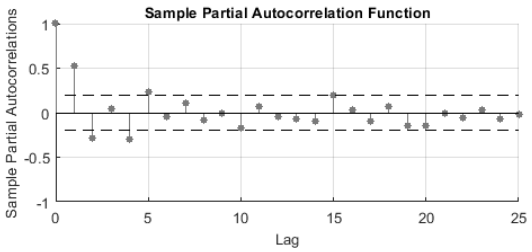

Figure E.6: PACF of the MA(1) process of Figure E.3

an MA(q) process, an AR(p) process or a combination of the two. For an MA(q) process, the ACF cuts off after the q^{th} lag, for an AR(p) process, the PACF cuts off after the p^{th} lag. The ACF of an AR(p) process does not cut off, but slowly tails down to zero at higher lags. The PACF of an MA(q) process does not cut off, but slowly tails down to zero at higher lags. So when the ACF and PACF are both not cutting off, but tailing down slowly, the process contains both an MA part and an AR part, and it is concluded that the process is an ARMA(p,q) process. Table E.1 summarises the foundings of the ACF and PACF plots behaviour for the different underlying processes. When it is found that the process is an ARMA(p,q) process, finding the order of p and q from the ACF and PACF is not as obvious as in an AR or an MA process, so the orders of the process should be found iteratively.

	AR(p)	MA(q)	ARMA(p,q)
ACF	gradually tails off	cuts off after lag q	gradually tails off
PACF	cuts off after lag p	gradually tails off	gradually tails off

Table E.1: Behaviour of PACF and ACF for different underlying processes

E.5. Estimating the Parameters

When the order of the underlying process is found, a model of the process can be constructed which is fitted to the observations by estimating the parameters $\beta = \{\phi_1, ...\phi_p, \theta_1, ..., \theta_q\}$. For the estimation of the parameters, the maximum likelihood principle is used, where the likelihood of the observed data to have been originated from the model is maximized.

For ARMA models, the following likelihood function is maximized:

$$L(\beta, \sigma_\epsilon^2) = \left(\frac{1}{\sqrt{2\pi\sigma_\epsilon^2}} \right)^n \left[r_1(\beta) r_2(\beta) \dots r_n(\beta) \right]^{-1/2} exp\left[-\frac{S(\beta)}{2\sigma_\epsilon^2} \right] \tag{E.27}$$

In which:

$$S(\beta) = \sum_{t=1}^{n} \left[\frac{(x_t - x_{t-1}^t(\beta))^2}{r_t(\beta)} \right] \tag{E.28}$$

And:

$$r_t(\beta) = \left[\sum_{j=0}^{\infty} \psi_j^2 \right] \left[\prod_{j=1}^{t-1} (1 - \phi_{jj}^2) \right] \tag{E.29}$$

Where:
- ψ_j : The weights of the causal representation of the ARMA(p,q) model, which is fixed in time and depends only on β.
- ϕ_{jj}: The best linear prediction parameters at $t = j$.

The maximization of Equation E.27 is performed by the numerical minimization of $S(\beta)$ with respect to β from Equation E.28. From this minimization, the model paramater estimator $\hat{\beta} = \{\hat{\phi}_1, ..., \hat{\phi}_p, \hat{\theta}_1, ..., \hat{\theta}_q\}$ is found, which describes the model that fits best to the observed data and will be used for forecasting the load during the prediction horizon

E.5.1. Maximum Likelihood of Parameters

The derivation of above three equations is a detailed process which is described below.

When the order p and q are found, the estimation of the parameters is performed by finding the parameters that maximize the likelihood that the error terms between the model and the observations at every time step follow a Gaussian distribution. The parameter estimation procedure that is followed here is obtained mainly from [58] and the Durbin-Levinson algorithm is used from [43].

For the ARMA model, the likelihood of the data $\{x_1,...,x_n\}$ to have been originated from the model, defined by $\beta = \{\mu, \phi_1,...,\phi_p, \theta_1,...,\theta_q, \sigma_\epsilon^2, \mu\}$ is maximimized, which is written as follows:

$$\begin{aligned} L(\beta,\sigma_\epsilon^2) &= f(x_1,...,x_n|\beta,\sigma_\epsilon^2) \\ &= f(x_1)f(x_2|x_1,\beta,\sigma_\epsilon^2)f(x_3|x_1,x_2,\beta,\sigma_\epsilon^2)\dots f(x_n|x_1,\dots,x_{n-1},\beta,\sigma_\epsilon^2) \\ &= \prod_{t=1}^{n} f(x_t|x_1,\dots,x_{t-1},\beta,\sigma_\epsilon^2) \end{aligned} \tag{E.30}$$

What is written here is the product of all the probabilities that the observations were created from the model. So the probability of observation x_1 times the probability of x_2 given observation x_1 and the model, times the probability of x_3 given x_1, x_2 and the model, and so on. The probability distribution of x_t given the preceding observations, $f(x_t|x_1,...,x_{t-1})$, should have a Gaussian distribution having a mean of the one-step-ahead prediction $x_t|x_1,...,x_{t-1}$ (from here on written as x_t^{t-1}) and a variance of the one-step-ahead variance P_t^{t-1} (the estimated variance for x_t based on $\{x_1,...,x_{t-1}\}$). Here it is important to notice that by x_t, the observed x_t from the time series data is meant. So in this case, the measured pipe laying power at *t*. When the observed values of x_t follow a Gaussian distribution around a mean which is determined by the one-step-ahead prediction of the model at every time step, the errors between the observed values and the model are known to follow a Gaussian distribution. The parameter estimation process is focused on coming as close as possible to a Gaussian distribution of the errors between model and observations. When this likelihood is maximized, the data to be originated from the model is most likely and the goal of the parameter estimation is achieved.

Any continuous Gaussian(μ,σ^2) probability density function (normal distribution) is written as Equation E.31. This is the general equation for a random variable x that is normally distributed having mean μ and variance σ^2.

$$f(x) = \frac{1}{\sigma\sqrt{2\pi}} e^{-\frac{1}{2}\left(\frac{x-\mu}{\sigma}\right)^2} = (2\pi\sigma^2)^{-1/2} exp\left[-\frac{1}{2}\left(\frac{x-\mu}{\sigma}\right)^2\right] \tag{E.31}$$

The one step ahead prediction of x_t is written as x_t^{t-1} which means: the prediction of x_t based on the preceding observations $\{x_1,...,x_{t-1}\}$. The variance of the one-step-ahead prediction is written as P_t^{t-1}, which means: the prediction of the variance at x_t based on preceding observations $\{x_1,...,x_{t-1}\}$. Using these definitions and the general probability density function of a Gaussian distribution in Equation E.31, the likelihood of Equation E.30 is written as:

$$\begin{aligned} L(\beta,\sigma_\epsilon^2) &= \prod_{t=1}^{n} f(x_t|x_1,\dots,x_{t-1},\beta,\sigma_\epsilon^2) \\ &= \prod_{t=1}^{n} \left\{ (2\pi P_t^{t-1}(\beta,\sigma_\epsilon^2))^{-1/2} exp\left[-\frac{1}{2}\frac{(x_t - x_t^{t-1}(\beta,\sigma_\epsilon^2))^2}{P_t^{t-1}(\beta,\sigma_\epsilon^2)}\right]\right\} \end{aligned} \tag{E.32}$$

Where:

$x_t^{t-1}(\beta,\sigma_\epsilon^2)$: The one-step-ahead prediction of x_t based on $\{x_1,...,x_{t-1}\}$.

$P_t^{t-1}(\beta,\sigma_\epsilon^2)$: The variance of the one-step-ahead prediction of x_t based on $\{x_1,...,x_{t-1}\}$. Finding this parameter is described below.

So the likelihood function which is maximized is *"the likelihood that the observations x_t follow a Gaussian distribution having mean x_t^{t-1} and variance P_t^{t-1}, which are determined by the model and the preceding observations $\{x_1,...,x_{t-1}\}$ "*. When this likelihood is maximized, the likelihood that the errors between the model and the observations at every time step follow a Gaussian$(0,\sigma_\epsilon^2)$ distribution is maximized.

One-step-ahead variance

In Equation E.32, the one-step-ahead variance is used, which will be described here. The one-step-ahead

variance is determined by finding the variance of the best linear prediction of x_t^{t-1}, where this prediction is based on a linear extrapolation of all preceding observations of x. For AR models, the best linear predictor is equivalent to the model, but for ARMA models, it can be complicated to find the best linear predictor. Therefore, for ARMA models, the one-step-ahead variance is found by recursion[3] using the Durbin-Levinson algorithm which will be described below. To show the necessity of a recursive algorithm for the one-step-ahead variance, it will be shown how the one-step-ahead variance can be calculated analytically when the one-step-ahead prediction is based on a linear function of the data.

When a best linear predictor of a one-step-ahead predictor is described as:

$$x_{n+1}^n = \phi_{n1}x_n + \phi_{n2}x_{n-1} + ... + \phi_{nn}x_1 \tag{E.33}$$

For example, the predictor of x_6 based on $\{x_1, ..., x_5\}$, is than written as:

$$x_6^5 = \phi_{51}x_5 + \phi_{52}x_4 + \phi_{53}x_3 + \phi_{54}x_4 + \phi_{55}x_5 \tag{E.34}$$

The best linear predictor is considered to be the best when the expectation of the mean square error between the prediction and the observation is minimized for the parameters $\phi_{j,k}$. This expectation is minimized by solving [58]:

$$E[(x_{n+m} - x_{n+m}^n)x_k)] = 0, \quad \text{for } k = 1, 2, ..., n \tag{E.35}$$

So for the linear predictor, this is written as:

$$\begin{aligned} E[(x_{n+1} - \sum_{j=1}^{n} \phi_{nj}x_{n+1-j})x_{n+1-k}] &= 0 \\ E[x_{n+1}x_{n+1-k} - \left(\sum_{j=1}^{n} \phi_{nj}x_{n+1-j}\right)x_{n+1-k}] &= 0 \end{aligned} \tag{E.36}$$

Or:

$$\begin{aligned} E[x_{n+1}x_{n+1-k}] &= E\left[\left(\sum_{j=1}^{n} \phi_{nj}x_{n+1-j}\right)x_{n+1-k}\right] \\ E[(x_{n+1} - \mu_{n+1})(x_{n+1-k} - \mu_{n+1-k})] &= \sum_{j=1}^{n} \phi_{nj}E[x_{n+1-j}x_{n+1-k}] \\ corr(x_{n+1}, x_{n+1-k}) &= \sum_{j=1}^{n} \phi_{nj}corr(x_{n+1-j}, x_{n+1-k}) \\ \gamma(k) &= \sum_{j=1}^{n} \phi_{nj}\gamma(k-j), \quad \text{for } k = 1, 2, .., n \end{aligned} \tag{E.37}$$

In matrix form, this can be written as:

$$\mathbf{\Gamma}_n\overline{\phi}_n = \overline{\gamma}_n \tag{E.38}$$

Or:

$$\begin{bmatrix} \gamma(0) & \gamma(1) & \gamma(2) & \dots & \gamma(n-1) \\ \gamma(1) & \gamma(0) & \gamma(1) & \dots & \gamma(n-2) \\ \gamma(2) & \gamma(1) & \gamma(0) & \dots & \gamma(n-3) \\ \vdots & \vdots & \vdots & & \vdots \\ \vdots & \vdots & \vdots & \ddots & \vdots \\ \gamma(n-1) & \gamma(n-2) & \gamma(n-3) & \dots & \gamma(0) \end{bmatrix} \begin{Bmatrix} \phi_{n1} \\ \phi_{n2} \\ \phi_{n3} \\ \vdots \\ \vdots \\ \phi_{nn} \end{Bmatrix} = \begin{Bmatrix} \gamma(1) \\ \gamma(2) \\ \gamma(3) \\ \vdots \\ \vdots \\ \gamma(n) \end{Bmatrix} \tag{E.39}$$

So to calculate the parameters of the best linear predictor, $\mathbf{\Gamma}_n$ can be inversed and multiplied by the covariance vector $\overline{\gamma}_n$:

[3] Recursion is the process where the next value of a sequence of values is calculated based on preceding values of that sequence. So an initial value is defined, where all succeeding values of that sequence are calculated step by step.

$$\overline{\phi}_n = \mathbf{\Gamma}_n^{-1}\overline{\gamma}_n \tag{E.40}$$

This way, the one-step-ahead prediction can be calculated using the paramaters calculated in Equation E.40:

$$x_{n+1}^n = \overline{\phi'}_n \overline{x} \tag{E.41}$$

Which is then used for the one-step-ahead variance by the regular definition of variance:

$$\begin{aligned} P_{n+1}^n &= E[(\overbrace{x_{n+1}}^{observation} - \overbrace{x_{n+1}^n}^{linear\ prediction})^2] \\ &= E[(x_{n+1} - \overline{\phi'}_n \overline{x})^2] \\ &= E[(x_{n+1} - \overline{\gamma'_n}\mathbf{\Gamma}_n^{-1}\overline{x})^2] \\ &= E[(x_{n+1}^2 - 2\overline{\gamma'_n}\mathbf{\Gamma}_n^{-1}\overline{x}\,x_{n+1} + \overline{\gamma'_n}\mathbf{\Gamma}_n^{-1}\overline{x}\,\overline{x'}\mathbf{\Gamma}_n^{-1}\overline{\gamma_n})] \end{aligned} \tag{E.42}$$

In this equation, $E[\overline{x}\,\overline{x'}]$ is actually the covariance matrix by Equation E.43 and by stationarity, which guarantees that $E[x_t x_s]$ only depends on $|t\text{-}s|$, which for example means that $E[x_2 x_1] = cov(x_2, x_1) = cov(x_1, x_0) = \gamma(1)$.

$$E[(\overline{x}\,\overline{x'})] = \begin{bmatrix} E[x_0x_0] & E[x_1x_0] & E[x_2x_0] & E[x_nx_0] \\ E[x_0x_1] & E[x_1x_1] & E[x_2x_1] & \vdots \\ E[x_0x_2] & E[x_1x_2] & & \vdots \\ \vdots & \vdots & \ddots & \vdots \\ E[x_0x_n] & \dots & \dots & E[x_nx_n] \end{bmatrix} \tag{E.43}$$

Therefore, Equation E.42 is continued as:

$$\begin{aligned} P_{n+1}^n &= \gamma(0) - 2\overline{\gamma'_n}\mathbf{\Gamma}_n^{-1}\overline{\gamma_n} + \overline{\gamma'_n}\mathbf{\Gamma}_n^{-1}\mathbf{\Gamma}_n\mathbf{\Gamma}_n^{-1}\overline{\gamma_n} \\ &= \gamma(0) - 2\overline{\gamma'_n}\mathbf{\Gamma}_n^{-1}\overline{\gamma_n} + \overline{\gamma'_n}\mathbf{\Gamma}_n^{-1}\overline{\gamma_n} \\ &= \gamma(0) - \overline{\gamma'_n}\mathbf{\Gamma}_n^{-1}\overline{\gamma_n} \end{aligned} \tag{E.44}$$

Where it is used that for an (n x n) matrix A with inverse A^{-1}, that $A^{-1}A = I_n$.

Equation E.44 is a reasonably uncomplicated method to be used for linear models like the AR(p) model, but the prediction equations can become very complicated for ARMA(p,q) models. At every new observation, the least square solution of the prediction equation has to be recomputed, which requires a big computational effort. Besides, when n is large, inverting $\mathbf{\Gamma}_n$ is also computationally intensive [47]. Therefore, instead of using Equation E.44, according to [43], a recursive method of estimating the one-step-ahead variance can be used. This method is called the Durbin-Levinson algorithm as the method was first proposed by N. Levinson in 1946 and later modified by J. Durbin in 1960. In this algorithm, the initial values of the one-step-ahead variance and the first best linear prediction parameter are set to:

$$P_1^0 = \gamma(0), \qquad \phi_{00} = 0$$

And the succeeding variances and best linear prediction parameters are calculated by the recursive procedure:

$$\phi_{nn} = \frac{\rho(n) - \sum_{k=1}^{n-1} \phi_{n-1,k}\rho(n-k)}{1 - \sum \phi_{n-1,k}\rho(k)} \tag{E.45}$$

$$\phi_{nk} = \phi_{n-1,k} - \phi_{nn}\phi_{n-1,n-k} \tag{E.46}$$

$$P_{n+1}^n = P_n^{n-1}(1-\phi_{nn}^2) \tag{E.47}$$

For n = 1, this means that:

$$\phi_{11} = \rho(1),$$

$$P_2^1 = \gamma(0)(1-\phi_{11}^2)$$

For n = 2,

$$\phi_{22} = \frac{\rho(2)-\phi_{11}\rho(1)}{1-\phi_{11}\rho(1)},$$
$$\phi_{21} = \phi_{22}\phi_{11},$$

$$P_3^2 = P_2^1(1-\phi_{22}^2) = \gamma(0)(1-\phi_{11}^2)(1-\phi_{22}^2)$$

For n = 3,

$$\phi_{33} = \frac{\rho(3)-\phi_{21}\rho(2)-\phi_{22}\rho(1)}{1-\phi 21\rho(1)-\phi_{22}\rho(2)},$$
$$\phi_{32} = \phi_{22}-\phi_{33}\phi_{21},$$
$$\phi_{31} = \phi_{21}-\phi_{33}\phi_{22},$$

$$P_4^3 = P_3^2(1-\phi_3 3^2) = \gamma(0)(1-\phi_{11}^2)(1-\phi_{22}^2)(1-\phi_{33}^2)$$

So in general, when this is continued, the recursion of the one-step-ahead variance is as follows:

$$P_{n+1}^n = \gamma(0)\prod_{j=1}^{n}(1-\phi_{nn}) \tag{E.48}$$

Determining the zero lag autocovariance

To calculate the autocovariance at lag zero, the ARMA model should be rewritten in its causal form. The causal form of an ARMA model is the opposite of the invertible form of a MA model as was described in Section E.4. Where the invertible form of an MA(q) model was an infinite representation of the model in its infinite past observations, a causal form is the notation of the model written as an infinite sequence of the past error terms. For example, the ARMA(*1,1*) model (assuming starting conditions $x_0 = 0$ and $\epsilon_0 = 0$) can be rewritten as follows:

$$\begin{aligned}
x_1 &= \epsilon_1 \\
x_2 &= \phi x_1 + \theta\epsilon_1 + \epsilon_2 \\
&= \phi\epsilon_1 + \theta\epsilon_1 + \epsilon_2 \\
x_3 &= \phi(\phi\epsilon_1 + \theta\epsilon_1 + \epsilon_2) + \theta\epsilon_2 + \epsilon_3 \\
&= (\phi^2 + \phi\theta)\epsilon_1 + (\theta+\phi)\epsilon_2 + \epsilon_3 \\
x_4 &= \phi[(\phi^2+\phi\theta)\epsilon_1 + (\theta+\phi)\epsilon + \epsilon_3] + \theta\epsilon_3 + \epsilon_4 \\
&= (\phi^3 + \phi^2\theta)\epsilon_1 + (\theta\phi+\phi^2)\epsilon_2 + (\phi+\theta)\epsilon_3 + \epsilon_4
\end{aligned} \tag{E.49}$$

So in general:

$$\begin{aligned}
x_t &= \epsilon_t + \sum_{j=1}^{\infty}(\phi^j + \theta\phi^{j-1})\epsilon_{t-j} \\
&= \sum_{j=0}^{\infty}\psi_j\epsilon_{t-j}
\end{aligned} \tag{E.50}$$

Where for the ARMA(*1,1*) process in the above example:

$$\psi_j = \begin{cases} 1, & for\ j = 0 \\ \phi^j + \theta\phi^{j-1}, & for\ j = 1,2,3,... \end{cases} \tag{E.51}$$

In general, ψ_j can be written for any ARMA(p,q) model in terms of $\{\phi_1,...,\phi_p\}$ and $\{\theta_1,...,\theta_q\}$. Equation E.50 is the general causal expression of any ARMA(p,q) model, where the weights ψ are dependend on the order p and q.

When the roots of ϕ are outside the unit circle, Equation E.51 converges to zero. For example, when the ARMA(*2,2*) model is defined by $[\phi_1\ \phi_2] = [0.3\ 0.6]$ and $[\theta_1\ \theta_2] = [-0.65\ 0.2]$ and ψ_j is plotted with respect to j, the weights converge as can be seen in Figure E.7.

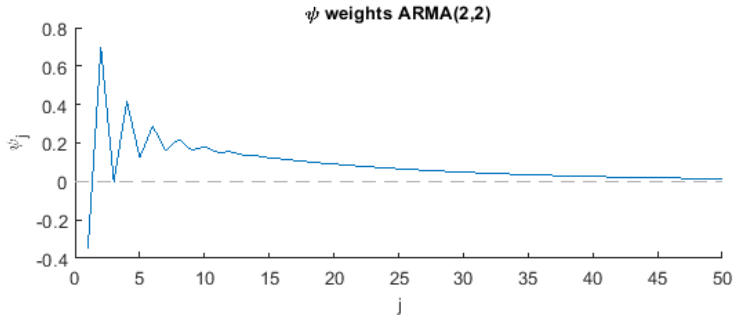

Figure E.7: Example ψ_j with respect to j for ARMA(*2,2*) model

From Equation E.50, it is clear that the expectation $E(x_t) = 0$ and the autocovariance is:

$$\gamma(h,t) = \sigma_\epsilon^2 \sum_{j=0}^{\infty} \psi_j \psi_{j+h} \tag{E.52}$$

So, at lag 0, the autocovariance is:

$$\gamma(0,0) = \gamma(0) = \sigma_\epsilon^2 \sum_{j=0}^{\infty} \psi_j \psi_j = \sigma_\epsilon^2 \sum_{j=0}^{\infty} \psi_j^2 \tag{E.53}$$

Which is used to calculate the one-step-ahead variance of Equation E.48.

Substitution in Maximum Likelihood Function

So when Equation E.53 is substituted into Equation E.48, the one-step ahead variance is written as:

$$P_t^{t-1} = \sigma_\epsilon^2 \sum_{j=0}^{\infty} (\psi_j^2) \prod_{j=1}^{n} (1 - \phi_{nn}) \stackrel{\text{def}}{=} \sigma_\epsilon^2 r_t \tag{E.54}$$

Where r_t is by definition:

$$r_t = \sum_{j=0}^{\infty} (\psi_j^2) \prod_{j=1}^{n} (1 - \phi_{nn}) \tag{E.55}$$

Substituting Equation E.54 in Equation E.32, gives:

$$\begin{aligned} L(\beta, \sigma_\epsilon^2) &= \prod_{t=1}^{n} (2\pi\sigma_\epsilon^2 r_t(\beta))^{-1/2}\ exp\left[-\frac{1}{2} \frac{(x_t - x_t^{t-1})^2}{\sigma_\epsilon^2 r_t(\beta)} \right] \\ &= (2\pi\sigma_\epsilon^2)^{-n/2} [r_1(\beta) r_2(\beta) r_3(\beta) \cdots r_n(\beta)]^{-1/2}\ exp\left[-\frac{1}{2} \sum_{t=1}^{n} \frac{(x_t - x_t^{t-1})^2}{\sigma_\epsilon^2 r_t(\beta)} \right] \\ &= (2\pi\sigma_\epsilon^2)^{-n/2} [r_1(\beta) r_2(\beta) r_3(\beta) \cdots r_n(\beta)]^{-1/2}\ exp\left[-\frac{1}{2} \frac{S(\beta)}{\sigma_\epsilon^2} \right] \end{aligned} \tag{E.56}$$

In which:

$$S(\beta) = \sum_{t=1}^{n} \frac{(x_t - x_t^{t-1})^2}{r_t(\beta)} \tag{E.57}$$

Maximizing Equation E.56 is equivalent to minimizing Equation E.57 with respect to β.

So in the end, for a given β, the following steps are followed during every iteration of the minimization process:

1. The causal weights ψ_j for $j = \{1, 2, ..., \infty\}$ are calculated by finding the general equation of these weights depending on j. This parameter only depends on β and is time independent, so only has to be calculated once per minimization iteration.

2. The best linear prediction parameters ϕ_{nn} and ϕ_{nk} are calculated recursively for every time step. This is done by Equation E.45 and Equation E.46.

3. When the best linear prediction parameters at every time step are known, the last parameters of these predictors ϕ_{nn} are used to calculate r_t in Equation E.55.

4. The best linear predictor parameters are also used to find the one-step-ahead prediction x_t^{t-1} for every time step using Equation E.33.

5. These one-step-ahead predictions and r_t for every time step are then used in Equation E.57 to calculate the value of $S(\beta)$.

For the minimization problem, sequential quadratic programming is used.

F

Propeller Curves

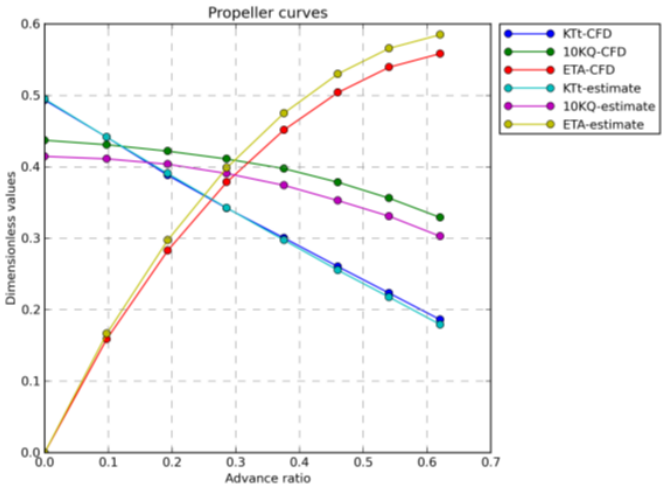

Figure F.1: Open water diagram of the propeller

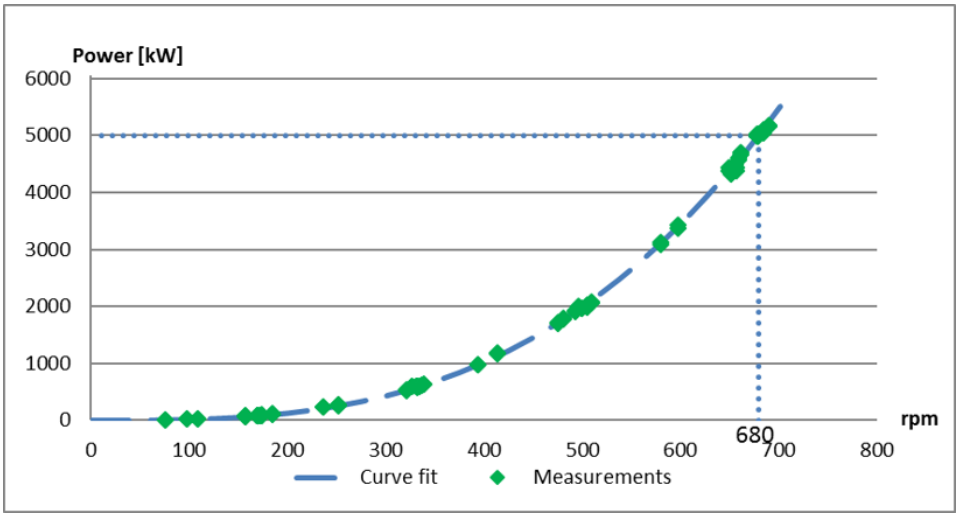

Figure F.2: Bollard pull sea trials test of power vs. rpm of the propeller. The fitted curve is a cubic curve: $P(n) = P_{nom}\left(\frac{n}{n_{nom}}\right)^3$

G

PMS Test

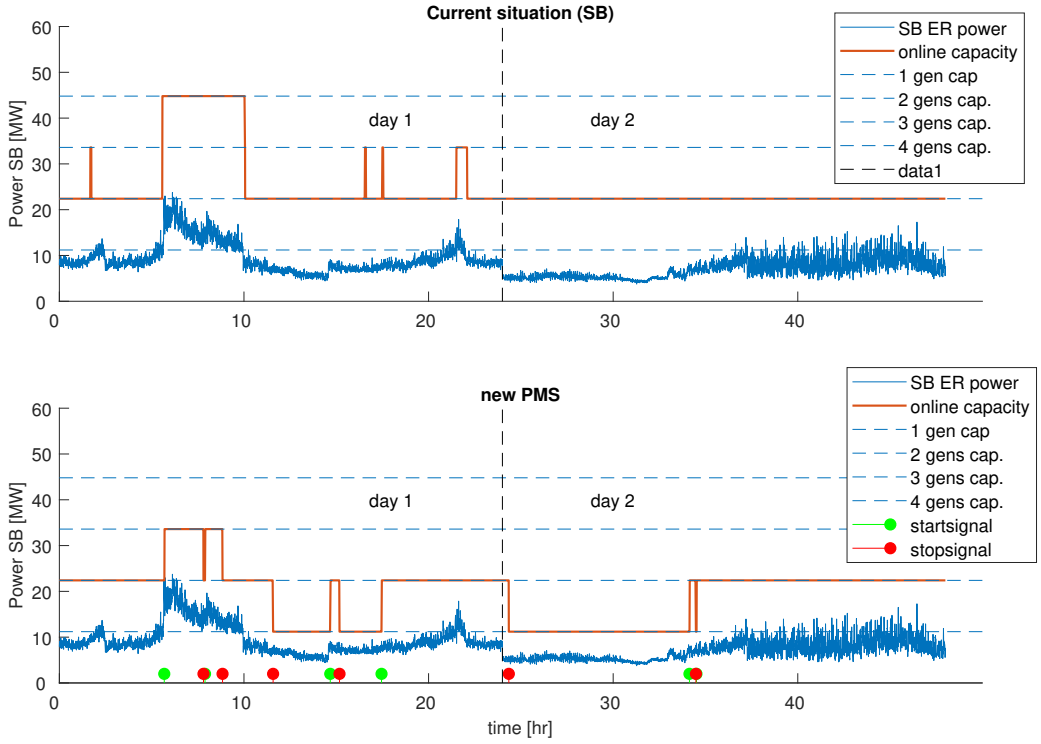

Figure G.1: PMS test using the MLR model on starboard side. The minor capacity peaks that are visible in the old PMS (noted by 'current situation') at 2, 17, and 18 hours are switching moments where the crew switched between two generators to control the distribution in running hours among the generators. During these peaks, one generator is added to the online generators before the other is switched off. This is a policy to either make sure all generators are equally used, or purposely not equally used to have different planned maintenance schedules.

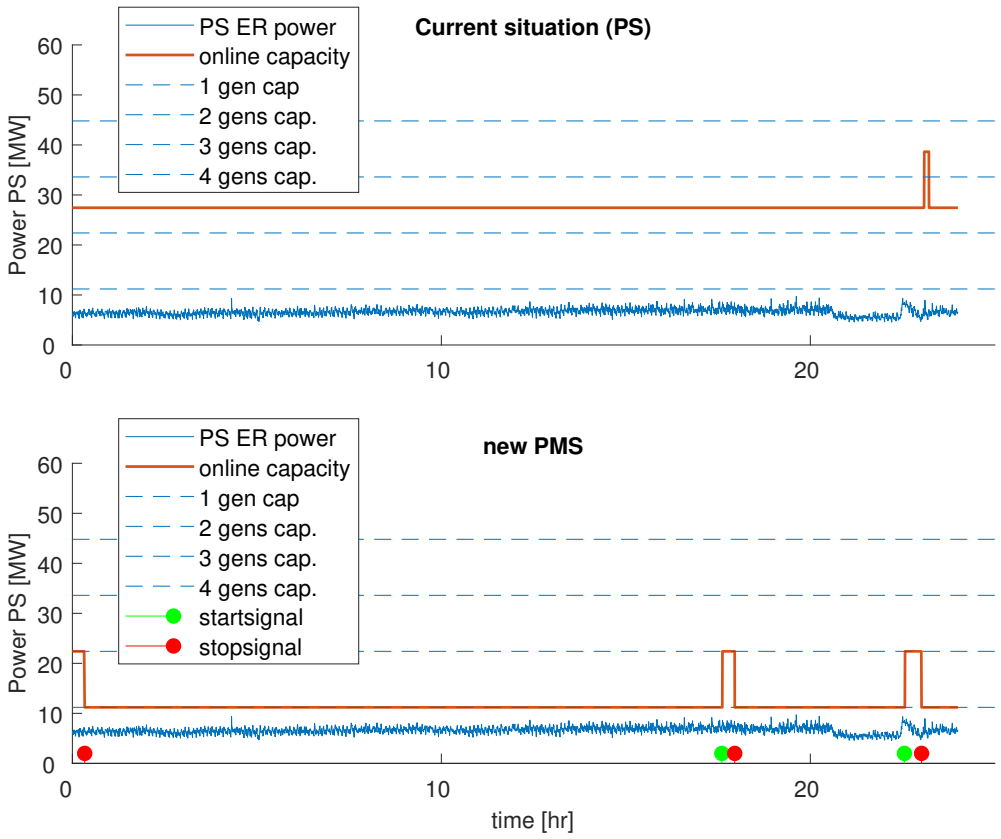

Figure G.2: PMS test using the MLR model on port side during calm weather conditions ($\bar{H}_s = 1.6$ [m])

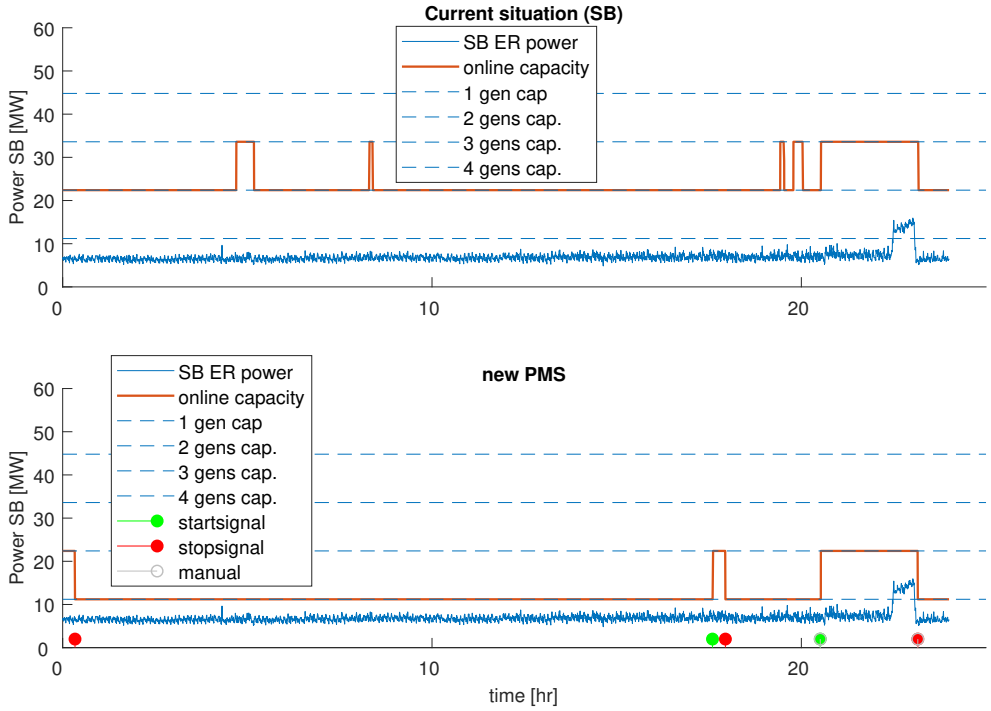

Figure G.3: PMS test using the MLR model on starboard side during calm weather conditions ($\bar{H}_s = 1.6$ [m])

H

SFC result hybrid system option 2

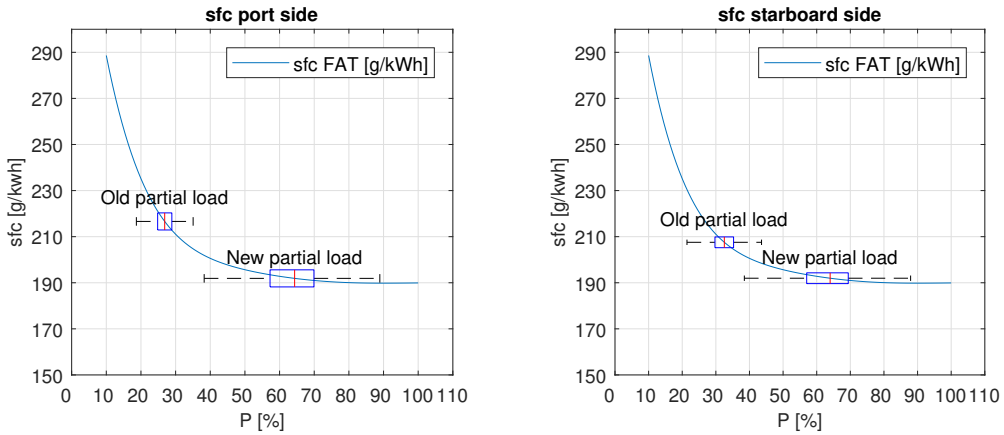

Figure H.1: Hybrid system option 2: Difference in specific fuel consumption by running on lower partial load in the fuel consumption simulation of the portside engine room and the starboard side engine room.

Bibliography

[1] *Batteries and Ultracapacitors for Electric, Hybrid, and Fuel Cell Vehicles*, volume 95, April 2007. IEEE.

[2] Prevention of air polution from ships. Minutes of meeting 58: Marine Environment Protection Committee, 2007.

[3] Lithium ion rechargeable battery technical information. presentation, August 2013. Sony Energy Devices Corporation Device Solutions Business Group / Sony Corporation.

[4] Introduction of inr18650-25r. presentation, 2013. Energy Business Division of Samsung.

[5] Hamdi Abdi, Behnam Mohammadi-ivatloo, Saeid Javadi, Amir Reza Khodaei, and Ehsan Dehnavi. *Energy Storage Systems*. 12 2017. ISBN 9780128042083.

[6] Elpiniki Apostolaki-Iosifidou, Paul Codani, and Willett Kempton. Measurement of power loss during electric vehicle charging and discharging. *Energy*, 127:730 – 742, 2017.

[7] A. G. Asuero, A. Sayago, and A. G. Gonzalez. The correlation coefficient: An overview. *Critical Reviews in Analytical Chemistry*, 2006.

[8] J. Badeda, M. Huck, D.U. Sauer, J. Kabzinski, and J. Wirth. 16 - basics of lead–acid battery modelling and simulation. In *Lead-Acid Batteries for Future Automobiles*, pages 463 – 507. Elsevier, 2017.

[9] Skundin Alexander M. Volfkovich Yurij M. Bagotsky, Vladimir S. John Wiley Sons, 2015. ISBN 978-1-118-46023-8.

[10] Ahmed Ali Baig, Risza Ruzli, and Azizul B. Buang. Reliability Analysis Using Fault Tree Analysis: A Review. *International Journal of Chemical Engineering and Applications*, 4(3):169–173, 2013.

[11] Francesco Ballio and Alberto Guadagnini. Convergence assessment of numerical monte carlo simulations in groundwater hydrology. *WATER RESOURCES RESEARCH*, 40, 11 2004.

[12] J. Barton and D. Infield. Energy storage and its use with intermittent renewable energy. *IEEE Trans. Energy Convers.*, 19:441 – 449, June 2009.

[13] Peter Beater. *Pneumatic Drives - System Design, Modelling and Control*. Springer, 1993.

[14] Marc Beaudin, Hamidreza Zareipour, Anthony Schellenberglabe, and William Rosehart. Energy storage for mitigating the variability of renewable electricity sources: An updated review. *Energy for Sustainable Development*, 14(4):302 – 314, 2010.

[15] Donald Bender. Flywheels. Technical report, Sandia National Laboratories, May 2015. Sandia is a multiprogram engineering and science laboratory operated by Sandia Corporation, a Lockheed Martin Company, for the US Department of Energy.

[16] P.N. Borza. *Application of the Energy Storage Systems*. February 2017. ISBN 9780323429771.

[17] G.E.P. Box, G.M. Jenkins, and G.C. Reinsel. *Time Series Analysis: Forecasting and Control, fourth edition*. Series in Probability and Statistics. Wiley, 2015.

[18] Ömer Özgür Bozkurt, Göksel Biricik, and Ziya Cihan Tayşi. Artificial neural network and SARIMA based models for power load forecasting in Turkish electricity market. *Plos One*, 12(4):e0175915, 2017.

[19] Haisheng Chen, Thang Ngoc Cong, Wei Yang, Chunqing Tan, Yongliang Li, and Yulong Ding. Progress in electrical energy storage system: A critical review. 19:291–312, 2009.

[20] Claire Curry. Sony energy devices corporation device solutions business group / sony corporation. Technical report, Bloomberg New Energy Finance, July 2017. Bloomberg is a financial software, data, and media company from New York.

[21] F.M. Dekking, C. Kraaikamp, H.P. Lophuhaä, and L.E. Meester. *A modern introduction to probability and statistics - understanding why and how.* Springer, 2015.

[22] Deloitte. Energy storage: Tracking the technologies that will transform the power sector, 2015. Deloitte. is a globally operating financial service and consulting company.

[23] Sandeep Dhameja. *Electric Vehicle Battery Systems.* Elsevier, 2002.

[24] R. A. Donnelly and F. Abdel-Raouf. *Statistics, Third edition, First American edition.; Idiot's Guides: As Easy As It Gets!* Alpha, July 2016.

[25] Pasquale Erto, Antonio Lepore, Biagio Palumbo, and Luigi Vitiello. A Procedure for Predicting and Controlling the Ship Fuel Consumption: Its Implementation and Test. *Quality and Reliability Engineering International*, 31(7):1177–1184, 2015.

[26] S Faias, Patrícia Santos, Jorge Sousa, and Rui Castro. An overview on short and long-term response energy storage devices for power systems applications. In *Renewable Energy and Power Quality Journal*, volume 1, 03 2008.

[27] J.L.S. Gerritsen. the hybrid cutter dredger, a study on technical and economical feasibility. Master's thesis, Delft University of Technology, October 2016.

[28] M. Godjevac, K. Visser, E.J.C. Boomen, C. Malikouti, B.T.W. Mestemaker, Z. Lyu, and F. van der Veen. Electrical energy storage for dynamic positioning operations. In *Electric Ship Technologies Symposium (ESTS)*.

[29] A Green and C. Jehoulet. The non-battery battery - the potential role of supercapacitors in standby power applications. Technical report, Saft, 2002. Saft is a company involved in the design, the development and the manufacturing of batteries used in transport, industry and defense.

[30] James G. R. Hansen and David U. O'Kain. An assessment of flywheel high power energy storage technology for hybrid vehicles. Technical report, Oak Ridge National Labaratory, December 2011. Prepared for Vehicle Technologies Program, Office of Energy Efficiency and Renewable Energy, Department of Energy USA.

[31] Magnus Hedlund, Johan Lundin, Juan de Santiago, Johan Abrahamsson, and Hans Bernhoff. Review: Flywheel energy storage for automotive applications. 8, September 2015.

[32] Tao Hong and Shu Fan. Probabilistic electric load forecasting: A tutorial review. *International Journal of Forecasting*, 32(3):914–938, 2016.

[33] H. Ibrahim, A. Ilinka, and J. Perron. Energy storage systems characteristics and comparisons renewable sustainable energy review. 12, 2008.

[34] Maxwell Technologies Inc. Maxwell technologies boostcap energy storage modules life duration estimation, 2014.

[35] Kriegenhofer. Man spare parts offer no. 20789713.

[36] Corentin Kuster, Yacine Rezgui, and Monjur Mourshed. Electrical load forecasting models: A critical systematic review. *Sustainable Cities and Society*, 35:257–270, 2017.

[37] Jingshan Li, Shiyu Zhou, and Yehui Han. *Advances in Battery Manufacturing, Service, and Management Systems.* Wiley-IEEE, 2017.

[38] Albert N. Link, Alan C. O'Connor, and Troy J. Scott. *Battery Technology for Electric Vehicles : Public science and private innovation.* Taylor and Francis, 2015.

[39] Xing Luo, Jihong Wang, Mark Dooner, and Jonathan Clarke. Overview of current development in electrical energy storage technologies and the application potential in power system operation. *Applied Energy*, 137:511 – 536, 2015.

[40] Zelan Lyu. Concept design of hybrid crane vessel, feasibility study of utilizing electric energy storage technology. Master's thesis, Delft University of Technology, April 2016.

[41] Maxwell. Product matrix super capacitors. Technical report, 2017. Maxwell is an American developer and manufacturer headquartered in California and is focussed on energy storage and power delivery solutions.

[42] Douglas C. Montgomery, Cheryl L. Jennings, and Murat Kulahci. *Introduction to Time Series Analysis and Forecasting*. Wiley, 2015.

[43] Pedro A Morettin. The levinson algorithm and its application in time series analysis. *International Statistical Review*, 52(1):83–92, 1984.

[44] Mohammad Mottahedi, Atefeh Mohammadpour, Shideh Shams Amiri, David Riley, and Somayeh Asadi. Multi-linear regression models to predict the annual energy consumption of an office building with different shapes. *Procedia Engineering*, 118:622 – 629, 2015.

[45] Donald B. Murray. Cycle testing of supercapacitors for long-life robust applications. 30, May 2014.

[46] Nirmal-Kumar C. Nair and Niraj Garimella. Battery energy storage systems: Assessment for small-scale renewable energy integration. *Energy and Buildings*, 42(11):2124 – 2130, 2010.

[47] Klaus Neusser. *Time Series Econometrics*. Texts in Business and Economics. Springer, 2016.

[48] Jim Otjens. How to estimate the state of health of an online battery by use of non-invasive measuring methods. Master's thesis, Delft University of Technology, January 2017.

[49] Detchko Pavlov. Chapter 14 - valve-regulated lead–acid (vrla) batteries. In *Lead-Acid Batteries: Science and Technology (Second Edition)*, pages 593 – 620. Elsevier, Amsterdam, second edition edition, 2017.

[50] Peter Strick (MAN Diesel Turbo) Peter Werner (Allseas). Test protocol engine 20v 32/44cr, man diesel se, mv pieter schelte.

[51] Jens F. Peters, Manuel Baumann, Benedikt Zimmermann, Jessica Braun, and Marcel Weil. The environmental impact of li-ion batteries and the role of key parameters – a review. *Renewable and Sustainable Energy Reviews*, 67:491 – 506, 2017.

[52] Rohan Kumar Raman, T. V. Sathianandan, A. P. Sharma, and B. P. Mohanty. Modelling and forecasting marine fish production in odisha using seasonal arima model. *National Academy Science Letters*, 40(6): 393–397, Dec 2017.

[53] D.K. Ranaweera, N.F. Hubele, and G.G. Karady. Fuzzy logic for short term load forecasting. *International Journal of Electrical Power & Energy Systems*, 18(4):215–222, 1996.

[54] Mohsen Saadat, Farzad A. Shirazi, and Perry Y. Li. Modeling and control of an open accumulator compressed air energy storage (caes) system for wind turbines. *Applied Energy*, 137, 2015.

[55] T. Sakai, H. Miyamura, N. Kuriyama, I. Uehara, M. Muta, A. Takagi, U. Kajiyama, K. Kinoshita, and F. Isogai. Nickel-metal hydride battery for electric vehicles. *Journal of Alloys and Compounds*, 192:158–160, 1993.

[56] Susan Schoenung. Energy storage systems cost update. Technical report, Sandia National Laboratories, April 2011. Sandia is a multiprogram engineering and science laboratory operated by Sandia Corporation, a Lockheed Martin Company, for the US Department of Energy.

[57] S.M. Shoenung. Characteristics and technologies for long- vs. short-term energy storage. Technical report, United States Department of Energy, March 2001.

[58] Robert H. Shumway and David S. Stoffer. *Time Series Analysis and Its Applications, fourth edition*. Springer, 2010.

[59] Chester Simpson. Characteristics of rechargable batteries. Technical report, Texas Instruments, 2011. Texas Instruments Inc is an American technology company that designs and manufactures semiconductors and various integrated circuits.

[60] S. Smith, P. Sen, and B. Kroposki. Advancement of energy storage devices and applications in electrical power system. In *Power and Energy Society General Meeting — Conversion and Delivery of Electrical Energy in the 21st Century*. IEEE, July 2008.

[61] M.Luisa Soria, Joaquın Chacón, J.Carlos Hernández, Daniel Moreno, and Araceli Ojeda. Nickel metal hydride batteries for high power applications. *Journal of Power Sources*, 96(1):68 – 75, 2001. Proceedings of the 22nd International Power Sources Symposium.

[62] H. Spath and K.P. Becker. Energy storage by capacitors. *ETEP*, 12(3), June 2002.

[63] Dr. Michael Stamatelatos and Dr. William Vesely. *Fault Tree Handbook with Aerospace Applications*. NASA, 1.1 edition, 2002.

[64] Jose Taboada and Hirpa Lemu. Analysis of wave energy sources in the north atlantic waters in view of design challenges. In *35th International Conference on Ocean, Offshore and Arctic*, 06 2016.

[65] Masoud Taheriyoun and Saber Moradinejad. Reliability analysis of a wastewater treatment plant using fault tree analysis and monte carlo simulation. *Environmental Monitoring and Assessment*, 187(1), 2015.

[66] S. ten Cate Hoedemaker. Battery aging in full electric ships. Master's thesis, Delft University of Technology, September 2017.

[67] Walter van der Pennen. presentation meeting, December 2017. EST-Floattech is an energy storage technology company selling lithium-polymer battery for maritime and landbased purposes.

[68] Thanh Long Vu, Aaron Alexander Ayu, Jaspreet Singh Dhupia, Louis Kennedy, and Alf Kare Adnanes. Power Management for Electric Tugboats Through Operating Load Estimation. *IEEE Transactions on Control Systems Technology*, 23(6):2375–2382, 2015.

[69] David G. Vutetakis. *Digital Avionics Handbook*, chapter 10 - Batteries. CRC Press, 2001.

[70] Di Wang, Chuangang Ren, Anand Sivasubramaniam, Bhuvan Urgaonkar, and Hosam Fathy. Energy storage in datacenters: What, where, and how much? *SIGMETRICS'12*, 40, 2012.

[71] Yonggang Wang, Yanfang Song, and Yongyao Xia. Electrochemical capacitors: mechanism, materials, systems, characterization and applications. 45:5925–5950, 2016.

[72] Yonggang Wang, Yanfang Song, and Yongyao Xia. Electrochemical capacitors: mechanism, materials, systems, characterization and applications. *Chem. Soc. Rev.*, 45:5925–5950, 2016.

[73] Jonathan X. Weinert, Andrew F. Burke, and Xuezhe Wei. Lead-acid and lithium-ion batteries for the chinese electric bike market and implications on future technology advancement. *Journal of Power Sources*, 172(2):938 – 945, 2007.

[74] Hsien-Lun Wong. Bdi forecasting based on fuzzy set theory, grey system and arima. In *Modern Advances in Applied Intelligence*, pages 140–149, 2014.

[75] Hans Klein Woud and Douwe Stapersma. *Design of Propulsion and Electric Power Generation Systems*. IMaREST, 80 Coleman Street, Londond EC2R 5BJ, 2008.

[76] Xingguo Xiong, Yu-Liang Wu, and W Jone. Reliability model for mems accelerometers. 12 2007.

[77] Wenhua H. Zhu, Ying Zhu, Zenda Davis, and Bruce J. Tatarchuk. Energy efficiency and capacity retention of ni–mh batteries for storage applications. *Applied Energy*, 106:307 – 313, 2013.